

**STATISTICAL OPTIMIZATION OF SUPERCAPACITOR PILOT
PLANT MANUFACTURING AND PROCESS SCALE -UP**

AHMIDA AJINA

**THESIS SUBMITTED TO THE UNIVERSITY OF NOTTINGHAM
FOR THE DEGREE OF DOCTOR OF PHILOSOPHY**

JULY 2015

DEDICATION

اهداء إلى والدي العزيزين

To my Parents

ABSTRACT

In recent years, electrical double layer capacitor (EDLCs) has become one of the most popular energy storage devices. This can be attributed to its high capacity, long life cycle and fast charge/discharge rates. However, it has some drawbacks – mainly it stores less amount of energy than batteries. Hence, there is a need to optimize the EDLC to increase its capacity and decrease its equivalent series resistance (ESR), resulting in a supercapacitor that is able to charge quickly and will hold a large amount of energy for a long time.

This thesis presents a design, build and setup process of a supercapacitor pilot plant in the University of Nottingham Malaysia Campus for manufacturing and optimization of EDLCs. Two packages were considered, cylindrical and coin type packages. In addition, the design of a manufacturing process flow, with details on steps for fabrication, which will meet specific standards (BS EN 62391-1:2006, BS EN 62391-2-1: 2006, BS EN 62391-2-1: 2006 and DOD-C-29501/3 NOT 1) for quality and throughput for both the packaging types is discussed. Following this, significant factors of the fabrication process were identified and optimized by adopting the Taguchi design of experiment (DOE) methodology.

Results of the optimization process show that the most significant factors that affect the EDLC capacitance are PVDF % (polyvinylidene difluoride) and mixing time; the optimum values are determined to be 5% and 3 hours respectively. In the case of ESR optimization, the most significant factors are PVDF % and carbon black %. The

optimum values are 5% for both. Using these optimized values, a final prototype EDLC was fabricated. The capacitance value obtained for the cell was 54.70mF.

The final EDLC prototypes were tested according to the international standards (ISO) and compared with the supercapacitors available in the market. Results indicated that the electrochemical performance of the prototypes has a good resemblance to the performance of the supercapacitors available in the market. A selected prototype samples were sent for benchmark testing to companies in mobile applications in Korea and the Netherlands to confirm that the prototypes meet the required standards.

Finally the research work sets the basis for integrating genetic algorithms with the Taguchi technique for future research in improving the optimization process for robust EDLC fabrication.

PUBLICATIONS

Ahmida Ajina, Dino Isa, 'Symmetrical Supercapacitor using Coconut Shell-Based Activated Carbon' *Pertanika J. Sci. & Technol.* 18 (2): 351– 363, 2010.

Ahmida Ajina, Dino Isa, 'Capacitance and Equivalent Series Resistance (ESR) Optimization using the Taguchi Technique for EDLC's', 2010 International Conference on Electronic Devices Systems and Applications, ICEDSA2010.

Ahmida Ajina, Dino Isa, 'EDLC Capacitance Optimization Using the Taguchi Technique', *International Journal of Engineering and Innovative Technology (IJEIT)*, Volume 2, Issue 3, September 2012

Chia Yen Yee, Ridhuan A. Samsuri, Dino Isa, Ahmida Ajina, 'Optimization of Process Factors in Super capacitor Fabrication Using the Genetic Algorithm to Optimize Taguchi Signal-to-Noise Ratios', *International Journal of Engineering Science and Innovative Technology (IJESIT)*, Volume 1, Issue 2, November 2012.

ACKNOWLEDGEMENTS

I would like to express my deep and sincere gratitude to the people who made this PhD thesis possible. Special thanks to my supervisor **Professor Dino Isa** for his insight resolving many of the problems encountered throughout the research and the thesis writing, for his inspiring and encouraging way to guide, and his invaluable comments during my research.

I am highly indebted to my second supervisor **Dr Khiew Poi Sim** for his support especially at the start of this PhD research.

Special thanks to supercapacitor group in Nottingham UK campus for the support and the inspiring discussions.

I also owe my loving thanks to my parents and my family; they have lost a lot due to my research abroad. Without their encouragement and understanding it would have been impossible for me to finish this work.

This project was mainly funded by MOSTI (S0001.54.01). I would like also to thank the Faculty of Engineering and Nottingham University Malaysia Campus for providing significant help in completing the project.

TABLE OF CONTENTS

| | |
|---|-------|
| DEDICATION | i |
| ABSTRACT | ii |
| PUBLICATIONS | iv |
| ACKNOWLEDGEMENTS | v |
| TABLE OF CONTENTS | vi |
| LIST OF FIGURES | xii |
| LIST OF TABLES | xxv |
| ACRONYMS | xxvii |
| | |
| 1. Introduction | 1 |
| 1.1 Introduction | 2 |
| 1.2 Problem Statement | 3 |
| 1.3 Research Objectives | 5 |
| 1.4 Research Scope | 5 |
| 1.5 Contribution of the Thesis | 6 |
| 1.6 Thesis Outline | 7 |
| 2. Literature Review | 8 |
| 2.1 Introduction | 9 |
| 2.2 Supercapacitor Classes | 13 |
| 2.2.1 Electrical Double Layer Capacitors (EDLC) | 14 |
| 2.2.1.1 Activated Carbon | 15 |
| 2.2.1.2 Carbon Aerogels | 17 |
| 2.2.1.3 Carbon Nano Tubes (CNT)..... | 18 |
| 2.2.2 Pseudocapacitors | 19 |

| | | |
|---------|---|----|
| 2.2.2.1 | Metal Oxide Supercapacitor | 20 |
| 2.2.2.2 | Conducting Polymers..... | 21 |
| 2.2.3 | Hybrid Capacitors | 22 |
| 2.2.3.1 | Composites Supercapacitor..... | 23 |
| 2.2.3.2 | Asymmetric Supercapacitor..... | 24 |
| 2.2.3.3 | Battery-Type | 24 |
| 2.3 | Taguchi Method | 25 |
| 2.4 | Pilot Plant in this research | 30 |
| 3. | Methodology | 33 |
| 3.1 | Introduction | 34 |
| 3.2 | Fabrication of the first supercapacitor prototypes | 36 |
| 3.2.1 | Supercapacitor using Carbon Nano Tubes | 36 |
| 3.2.1.1 | Supercapacitor with CNT Model Cap-1 | 37 |
| 3.2.1.2 | Supercapacitor with CNT Model Cap-2 | 39 |
| 3.2.2 | Supercapacitor prototypes using Activated Carbon | 40 |
| 3.2.2.1 | Supercapacitor with AC Model Cap-3..... | 41 |
| 3.2.2.2 | Supercapacitor with AC model Cap-4 | 42 |
| 3.2.2.3 | Supercapacitor with AC Model Cap-5..... | 44 |
| 3.3 | Fabrication Processes of Optimized Prototype using activated carbon | 45 |
| 3.3.1 | Cylindrical Supercapacitor Fabrication Process | 45 |
| 3.3.2 | Coin Supercapacitor Fabrication Process..... | 56 |
| 3.4 | Electrolyte | 64 |

| | | |
|-------|---|-----|
| 3.5 | Testing Processes | 65 |
| 3.5.1 | Cyclic Voltammetry | 65 |
| 3.5.2 | Constant-current charging | 66 |
| 3.5.3 | Impedance spectroscopy | 67 |
| 3.5.4 | Constant-power cycling..... | 68 |
| 3.5.5 | Taguchi Technique..... | 69 |
| 3.5.6 | The Pilot Plant..... | 73 |
| 4. | Results..... | 76 |
| 4.1 | Introduction | 77 |
| 4.2 | EDLC prototypes using Carbon Nano Tubes..... | 78 |
| 4.3 | EDLC prototype with flat panel geometry from CNT (Cap-1)..... | 78 |
| 4.3.1 | EDLC prototype with flat panel geometry from CNT (Cap-2)..... | 80 |
| 4.4 | Supercapacitor prototypes using Coconut shell-based Activated Carbon..... | 83 |
| 4.4.1 | Disk-shape prototype using AC (Cap-3)..... | 83 |
| 4.4.2 | Flat -shape supercapacitor prototype (Cap-4) | 88 |
| 4.4.3 | Disk-shape supercapacitor Prototype Cap-5 | 97 |
| 4.5 | Cylindrical Supercapacitor Prototypes | 102 |
| 4.5.1 | Cylindrical Prototype CY-1 | 104 |
| 4.5.2 | Cylindrical prototypes CY-2 to CY-11 | 114 |
| 4.6 | Comparison between CY-1 to CY-11 | 114 |
| 4.7 | Coin Supercapacitor prototypes | 116 |
| 4.7.1 | Coin prototype B-1..... | 117 |

| | | |
|-------|---|-----|
| 4.7.2 | Coin prototypes B-2 to B-18 | 122 |
| 4.8 | Comparison between different coin prototypes..... | 122 |
| 4.9 | Optimizing Supercapacitor using Taguchi Technique | 125 |
| 4.10 | Optimization of process factors using Taguchi technique and Genetic Algorithm | 132 |
| 5. | Conclusion | 134 |
| 5.1 | Conclusion..... | 135 |
| 5.2 | Future work | 140 |
| 6. | References | 142 |
| 7. | Appendix A | 154 |
| 7.1 | Cylindrical supercapacitor CY-2..... | 155 |
| 7.2 | Cylindrical prototype CY-3..... | 161 |
| 7.3 | Cylindrical prototype CY-4..... | 168 |
| 7.4 | Cylindrical prototype CY-5..... | 169 |
| 7.5 | Cylindrical prototype CY-6..... | 173 |
| 7.6 | Cylindrical prototype CY-7..... | 174 |
| 7.7 | Cylindrical prototype CY-8..... | 175 |
| 7.8 | Cylindrical prototype CY-9..... | 175 |
| 7.9 | Cylindrical prototype CY-10..... | 180 |
| 7.10 | Cylindrical prototype CY-11..... | 180 |
| 8. | Appendix B | 185 |
| 8.1 | Coin prototype B-2..... | 186 |

| | | |
|------|--------------------------|-----|
| 8.2 | Coin prototype B-3..... | 191 |
| 8.3 | Coin prototype B-4..... | 195 |
| 8.4 | Coin prototype B-5..... | 200 |
| 8.5 | Coin Prototype B-6..... | 204 |
| 8.6 | Coin prototype B-7..... | 209 |
| 8.7 | Coin prototype B-8..... | 213 |
| 8.8 | Coin Prototype B-9..... | 217 |
| 8.9 | Coin prototype B-10..... | 222 |
| 8.10 | Coin prototype B-11..... | 226 |
| 8.11 | Coin prototype B-12..... | 230 |
| 8.12 | Coin prototype B-13..... | 234 |
| 8.13 | Coin prototype B-14..... | 238 |
| 8.14 | Coin Prototype B-15..... | 242 |
| 8.15 | Coin prototype B-16..... | 246 |
| 8.16 | Coin prototype B-17..... | 250 |
| 8.17 | Coin prototype B-18..... | 254 |
| 9. | Appendix C..... | 258 |

List of Figures

| | |
|---|----|
| Figure 2-1 Ragone plot of energy storage devices [27] | 12 |
| Figure 2-2 Supercapacitor classes [26] | 13 |
| Figure 2-3 EDLC construction [28] | 14 |
| Figure 2-4 SEM image of entangled mat of carbon nano tubes [53]. | 19 |
| Figure 2-5 Glove box | 32 |
| Figure 3-1 Methodology steps | 35 |
| Figure 3-2 CNT supercapacitor prototype model Cap-1..... | 37 |
| Figure 3-3 Cyclic voltammetry for the supercapacitor cell (Cap-1 at 10mV/s) | 39 |
| Figure 3-4 CNT supercapacitor cell Cap-2 | 40 |
| Figure 3-5 Supercapacitor cell Cap-3 | 41 |
| Figure 3-6 Supercapacitors picture: Cap-4.1, Cap-4.2 and Cap-4.3 | 42 |
| Figure 3-7 Electrode dimensions | 43 |
| Figure 3-8 Capacitor Cap-5..... | 45 |
| Figure 3-9 Process flow chart for cylindrical supercapacitor fabrication | 46 |
| Figure 3-10 Overhead Stirrer Model (MSP-1)..... | 47 |
| Figure 3-11 The coating process | 48 |
| Figure 3-12 The dr. blade used for the coating process | 49 |
| Figure 3-13 The drying vacuum oven..... | 50 |
| Figure 3-14 The roll pressing machine | 51 |
| Figure 3-15 The slitting process..... | 52 |
| Figure 3-16 The ultrasonic welding machine..... | 52 |

| | |
|---|----|
| Figure 3-17 The winding process..... | 53 |
| Figure 3-18 The assembly process of the cell | 54 |
| Figure 3-19 The glove box | 55 |
| Figure 3-20 The final product of supercapacitor..... | 55 |
| Figure 3-21 Process flowchart for the coin supercapacitor manufacturing | 57 |
| Figure 3-22 a) mixing the powders b) the dough..... | 58 |
| Figure 3-23 Calendering machine during calendering process..... | 59 |
| Figure 3-24 Dough sheet..... | 59 |
| Figure 3-25 Punching process | 60 |
| Figure 3-26 Active material disks glued to the case and the cap | 60 |
| Figure 3-27 The cases, caps and separators | 61 |
| Figure 3-28 a) the crimper b) the hydraulic press | 62 |
| Figure 3-29 Testing equipment a) Gamry b) Autolab..... | 62 |
| Figure 3-30 Final coin supercapacitor..... | 62 |
| Figure 3-31 CR2016 casing | 63 |
| Figure 3-32 CR2016 dimensions | 63 |
| Figure 3-33 Organic electrolyte specifications | 64 |
| Figure 3-34 Voltammogram..... | 65 |
| Figure 3-35 Charge-discharge graph..... | 67 |
| Figure 3-36 Nyquist diagram [20]..... | 68 |
| Figure 3-37 Pilot plant fabrication line setup..... | 74 |
| Figure 3-38 Pilot plant room 1 | 75 |

| | |
|---|-----|
| Figure 3-39 Pilot plant room 2 | 75 |
| Figure 4-1 CNT supercapacitor Cap-1 | 79 |
| Figure 4-2 Cyclic voltammetry curve for Cap-1 (at scan rate of 10mV/s) | 80 |
| Figure 4-3 Supercapacitor cell Cap-2 | 81 |
| Figure 4-4 Cyclic voltammetry for Cap-2 supercapacitor at 10 mV/s..... | 82 |
| Figure 4-5 Picture of the supercapacitor cell Cap-3..... | 83 |
| Figure 4-6 Cyclic voltammetry for Cap-3 supercapacitor (scan rate 10 mV/s)..... | 86 |
| Figure 4-7 EIS testing for Cap-3 supercapacitor..... | 87 |
| Figure 4-8 Charge-discharge curve for Cap-3 | 88 |
| Figure 4-9 Cyclic voltammetry for Cap-4.1 supercapacitor (5mV/s) | 91 |
| Figure 4-10 EIS measurements for Cap-4.1..... | 92 |
| Figure 4-11 Charge-discharge measurements for Cap-4.1 | 92 |
| Figure 4-12 Cyclic voltammetry for Cap-4.2 at 10mV/s | 94 |
| Figure 4-13 EIS measurements for Cap-4.2..... | 94 |
| Figure 4-14 Charge-discharge measurements for Cap-4.2 | 95 |
| Figure 4-15 Cyclic voltammetry for Cap-4.3 at 10 mV/s | 96 |
| Figure 4-16 EIS measurements for Cap-4.3..... | 97 |
| Figure 4-17 Supercapacitor Cap-5 | 97 |
| Figure 4-18 Cyclic voltammetry for the Cap-5.1 | 98 |
| Figure 4-19 EIS measurements for Cap-5.1 supercapacitor | 99 |
| Figure 4-20 Charge-discharge measurements for Cap-5.1 | 99 |
| Figure 4-21 Cyclic voltammetry for Cap-5.2..... | 100 |

| | |
|--|-----|
| Figure 4-22 EIS measurements for Cap-5.2..... | 101 |
| Figure 4-23 Charge-discharge measurements for Cap-5.2 | 101 |
| Figure 4-24 Charge-discharge curve CY-1 | 104 |
| Figure 4-25 Initial capacitance measurements of CY-1 at 0.2 mA..... | 105 |
| Figure 4-26 Initial CV for CY-1 at 20mv/s..... | 106 |
| Figure 4-27 EIS for supercapacitor prototype CY-1 | 107 |
| Figure 4-28 Charge-discharge curve at 0.2mA after 10 cycles..... | 107 |
| Figure 4-29 Capacitance measurements of CY-1 at 0.2 mA after 10 cycles | 108 |
| Figure 4-30 Charge-discharge after 350 cycles | 109 |
| Figure 4-31 Capacitance measurements CY-1 after 350 cycles | 109 |
| Figure 4-32 CV for CY-1 after 350 cycles..... | 110 |
| Figure 4-33 Charge-discharge curve CY-1 after 1000 cycles..... | 111 |
| Figure 4-34 Capacitance measurements CY-1 after 1000 cycles | 111 |
| Figure 4-35 CV for CY-1 after 1000 cycle | 112 |
| Figure 4-36 Charge-discharge curve CY-1 after 2550 cycles..... | 113 |
| Figure 4-37 Capacitance measurements CY-1 after 2550 cycles | 113 |
| Figure 4-38 CV curve for CY-1 after 2550 cycles..... | 114 |
| Figure 4-39 Coin supercapacitor prototype..... | 117 |
| Figure 4-40 Charge-discharge for prototype B-1 after 10 cycles | 118 |
| Figure 4-41 Capacitance for prototype B-1 | 118 |
| Figure 4-42 CV curve for prototype B-1 after 10 cycles | 119 |
| Figure 4-43 Charge-discharge curve for B-1 after 100 cycles..... | 120 |

| | |
|--|-----|
| Figure 4-44 Capacitance for B-1 | 121 |
| Figure 4-45 CV curve for B-1 after 100 cycles..... | 122 |
| Figure 4-46 Response graph for S/N ratio (Capacitance) | 130 |
| Figure 4-47 Response graph for S/N ratio (ESR) | 130 |
| Figure 5-1 Process flowchart for cylindrical EDLC | 136 |
| Figure 5-2 Process flowchart for coin EDLC | 138 |
| Figure 6-1 Charge-discharge curve for CY-2 at 200 mA | 155 |
| Figure 6-2 Initial capacitance of the CY-2..... | 156 |
| Figure 6-3 EIS for CY-2 | 156 |
| Figure 6-4 Charge-discharge for CY-2 after 50 cycles..... | 157 |
| Figure 6-5 Capacitance of CY-2 after 50 cycles | 158 |
| Figure 6-6 Charge-discharge curve for CY-2 after 100 cycles | 159 |
| Figure 6-7 Capacitance measurement of CY-2..... | 159 |
| Figure 6-8 Charge-discharge curve for CY-2 after 300 cycles | 160 |
| Figure 6-9 Capacitance measurement for CY-2 after 300 cycles | 161 |
| Figure 6-10 Initial charge-discharge test for CY-3 | 162 |
| Figure 6-11 Initial capacitance measurement for CY-3..... | 162 |
| Figure 6-12 Initial CV curve for CY-3 | 163 |
| Figure 6-13 Charge-discharge curve for CY-3 after 100 cycles | 164 |
| Figure 6-14 Capacitance measurement for CY-3..... | 164 |
| Figure 6-15 Charge-discharge curve for CY-3 after 350 cycles | 165 |
| Figure 6-16 Capacitance measurement for CY-3..... | 166 |

| | |
|---|-----|
| Figure 6-17 Charge-discharge curve for CY-3 after 1000 cycles | 167 |
| Figure 6-18 Capacitance measurement for CY-3..... | 167 |
| Figure 6-19 Initial charge-discharge curve for CY-4..... | 168 |
| Figure 6-20 CV curve for CY-4 | 169 |
| Figure 6-21 Initial charge-discharge curve for CY-5..... | 170 |
| Figure 6-22 Initial capacitance measurement for CY-5..... | 170 |
| Figure 6-23 Charge-discharge for CY-5 after 100 cycles | 171 |
| Figure 6-24 EIS curve for CY-5 after 100 cycles | 172 |
| Figure 6-25 CV for CY-5 after 100 cycles..... | 172 |
| Figure 6-26 Initial charge-discharge curve for CY-6..... | 173 |
| Figure 6-27 Initial CV for CY-6 | 174 |
| Figure 6-28 Initial charge-discharge curve for CY-7..... | 174 |
| Figure 6-29 Initial charge-discharge curve for CY-9..... | 175 |
| Figure 6-30 Capacitance measurement for CY-9..... | 176 |
| Figure 6-31 Initial CV for CY-9 | 177 |
| Figure 6-32 Charge-discharge for CY-9 after 100 cycles..... | 178 |
| Figure 6-33 Capacitance measurement for CY-9..... | 178 |
| Figure 6-34 Charge-discharge for CY-9 after 500 cycles..... | 179 |
| Figure 6-35 Capacitance measurement for CY-9..... | 180 |
| Figure 6-36 Charge-discharge curve for CY-11 after 100 cycles | 181 |
| Figure 6-37 Capacitance measurement | 182 |
| Figure 6-38 Charge-discharge curve for CY-11 after 500 cycles | 183 |

| | |
|--|-----|
| Figure 6-39 Capacitance measurement of CY-11 | 183 |
| Figure 7-1 Charge-discharge curve for prototype B-2 after 10 cycles..... | 186 |
| Figure 7-2 Capacitance for prototype B-2 | 187 |
| Figure 7-3 CV curve for B-2 after 10 cycles..... | 188 |
| Figure 7-4 Charge-discharge curve for B-2 after 100 cycles..... | 189 |
| Figure 7-5 Capacitance for B-2..... | 190 |
| Figure 7-6 CV curve for B-2 after 100 cycles..... | 191 |
| Figure 7-7 Charge-discharge curve for prototype B-3 after 10 cycles..... | 192 |
| Figure 7-8 CV curve for the B-3 prototype after 10 cycles | 193 |
| Figure 7-9 Charge–discharge curve for B-3 after 100 cycles | 193 |
| Figure 7-10 Capacitance of B-3 after 100 cycles..... | 194 |
| Figure 7-11 CV curve for B-3 after 100 cycles..... | 195 |
| Figure 7-12 Charge-discharge for prototype B-4 after 10 cycles | 196 |
| Figure 7-13 Capacitance for prototype B-4 | 197 |
| Figure 7-14 CV curve for B-4 after 10 cycles..... | 198 |
| Figure 7-15 Charge-discharge curve for B-4 after 100 cycles..... | 198 |
| Figure 7-16 Capacitance for B-4..... | 199 |
| Figure 7-17 CV for B-4 after 100 cycles | 200 |
| Figure 7-18 Charge-discharge for prototype B-5 after 10 cycles | 200 |
| Figure 7-19 Capacitance for B-5..... | 201 |
| Figure 7-20 CV for prototype B-5 after 10 cycles | 202 |
| Figure 7-21 Charge-discharge for B-5 after 100 cycles..... | 202 |

| | |
|--|-----|
| Figure 7-22 Capacitance for B-5..... | 203 |
| Figure 7-23 CV curve for B-5 after 100 cycles..... | 204 |
| Figure 7-24 Charge-discharge for Prototype B-6 after 10 cycles | 205 |
| Figure 7-25 Capacitance for B-6..... | 205 |
| Figure 7-26 CV for B-6 after 10 cycles | 206 |
| Figure 7-27 Charge-discharge for B-6 after 100 cycles..... | 207 |
| Figure 7-28 Capacitance of B-6 | 208 |
| Figure 7-29 CV curve for B-6 after 100 cycles..... | 208 |
| Figure 7-30 Charge-discharge for B-7 after 10 cycles..... | 209 |
| Figure 7-31 Capacitance of B-7 | 210 |
| Figure 7-32 CV curve for B-7 after 10 cycles..... | 211 |
| Figure 7-33 Charge-discharge for B-7 after 100 cycles..... | 211 |
| Figure 7-34 Capacitance of B-7 | 212 |
| Figure 7-35 CV curve for B-7 after 100 cycles..... | 213 |
| Figure 7-36 Charge-discharge for B-8 after 10 cycles..... | 214 |
| Figure 7-37 Capacitance of B-8 | 214 |
| Figure 7-38 CV for B-8 after 10 cycles | 215 |
| Figure 7-39 Charge-discharge for B-8 after 100 cycles..... | 216 |
| Figure 7-40 Capacitance of B-8 | 216 |
| Figure 7-41 CV curve for B-8 after 100 cycles..... | 217 |
| Figure 7-42 Charge-discharge for B-9 after 10 cycles..... | 218 |
| Figure 7-43 Capacitance for B-9..... | 218 |

| | |
|---|-----|
| Figure 7-44 CV curve for B-9 after 10 cycles..... | 219 |
| Figure 7-45 Charge-discharge for B-9 after 100 cycles..... | 220 |
| Figure 7-46 Capacitance of B-9 | 221 |
| Figure 7-47 CV curve for B-9 after 100 cycles..... | 222 |
| Figure 7-48 Charge-discharge for B-10 after 10 cycles..... | 222 |
| Figure 7-49 Capacitance for B-10 after 10 cycles | 223 |
| Figure 7-50 CV curve for B-10 after 10 cycles..... | 224 |
| Figure 7-51 Charge-discharge for B-10 after 100 cycles..... | 224 |
| Figure 7-52 Capacitance of B-10 after 100 cycles..... | 225 |
| Figure 7-53 CV curve for B-10 after 100 cycles..... | 226 |
| Figure 7-54 Charge-discharge for B-11 after 10 cycles..... | 227 |
| Figure 7-55 Capacitance of B-11 | 227 |
| Figure 7-56 Charge-discharge for B-11 after 100 cycles..... | 228 |
| Figure 7-57 Capacitance of B-11 | 229 |
| Figure 7-58 CV curve for B-11 after 100 cycles..... | 230 |
| Figure 7-59 Charge-discharge for B-12 after 10 cycles..... | 231 |
| Figure 7-60 Capacitance of B-12 | 231 |
| Figure 7-61 Charge-discharge for B-12 after 100 cycles..... | 232 |
| Figure 7-62 Capacitance of B-12 | 233 |
| Figure 7-63 CV curve for B-12 after 100 cycles..... | 234 |
| Figure 7-64 Charge-discharge for B-13 after 10 cycles..... | 235 |
| Figure 7-65 Capacitance of B-13 | 235 |

| | |
|---|-----|
| Figure 7-66 Charge-discharge for B-13 after 100 cycles..... | 236 |
| Figure 7-67 Capacitance of B-13 | 237 |
| Figure 7-68 CV curve for B-13 after 100 cycles..... | 238 |
| Figure 7-69 Charge-discharge for B-14 after 10 cycles..... | 239 |
| Figure 7-70 Capacitance for B-14..... | 239 |
| Figure 7-71 CV curve for B-14 after 10 cycles..... | 240 |
| Figure 7-72 Charge-discharge for B-14 after 100 cycles..... | 241 |
| Figure 7-73 Capacitance for B-14..... | 241 |
| Figure 7-74 CV curve for B-14 after 100 cycles..... | 242 |
| Figure 7-75 Charge-discharge for B-15 after 10 cycles..... | 243 |
| Figure 7-76 Capacitance of B-15 | 243 |
| Figure 7-77 Charge-discharge after 100 cycles | 244 |
| Figure 7-78 Capacitance of B-15 | 245 |
| Figure 7-79 CV curve for B-15 after 100 cycles..... | 246 |
| Figure 7-80 Charge-discharge for B-16 after 10 cycles..... | 247 |
| Figure 7-81 Capacitance of B-16 | 247 |
| Figure 7-82 Charge-discharge for B-16 after 100 cycles..... | 248 |
| Figure 7-83 Capacitance of B-16 | 249 |
| Figure 7-84 CV curve for B-16 after 100 cycles..... | 250 |
| Figure 7-85 Charge-discharge for B-17 after 10 cycles..... | 251 |
| Figure 7-86 Capacitance of B-17 | 251 |
| Figure 7-87 Charge-discharge for B-17 after 100 cycles..... | 252 |

| | |
|---|-----|
| Figure 7-88 Capacitance of B-17 | 253 |
| Figure 7-89 CV curve for B-17 after 100 cycles..... | 254 |
| Figure 7-90 Charge-discharge for B-18 after 10 cycles..... | 254 |
| Figure 7-91 Capacitance of B-18 | 255 |
| Figure 7-92 Charge-discharge for B-18 after 100 cycles..... | 256 |
| Figure 7-93 Capacitance of B-18 | 256 |
| Figure 7-94 CV curve for B-18 after 100 cycles..... | 257 |

List of Tables

| | |
|---|-----|
| Table 2-1 Comparison between battery and supercapacitor | 10 |
| Table 2-2 An orthogonal array of L8 | 29 |
| Table 3-1 Starting values of the parameters..... | 36 |
| Table 3-2 Materials used for fabrication of model Cap-1 | 38 |
| Table 3-3 LAJU PAC specification | 40 |
| Table 4-1 Different supercapacitor prototypes fabricated | 77 |
| Table 4-2 Materials used for the fabrication | 78 |
| Table 4-3 The measured parameters of the Cap-1 | 79 |
| Table 4-4 Materials used for the fabrication | 81 |
| Table 4-5 The parameters list of the Cap-2..... | 82 |
| Table 4-6 Capacitances of Cap-3 obtain at different scan rates..... | 84 |
| Table 4-7 Materials used for fabrication | 85 |
| Table 4-8 Cap-3 specifications..... | 86 |
| Table 4-9 Compositional percentages of AC & PVDF..... | 88 |
| Table 4-10 Capacitance and ESR measurements..... | 89 |
| Table 4-11 Cap-4.1 parameters | 90 |
| Table 4-12 Cap-4.2 parameters. | 93 |
| Table 4-13 Cap-4.3 parameters | 95 |
| Table 4-14 Cap-5 prototypes parameter's..... | 98 |
| Table 4-15 Materials used for the cylindrical prototypes | 102 |
| Table 4-16 Capacity measurements for CY-1 to CY-11..... | 103 |

| | |
|---|-----|
| Table 4-17 ESR measurements for CY-1 to CY-11 | 103 |
| Table 4-18 Comparison between CY-1 to CY-11..... | 115 |
| Table 4-19 Capacitances and ESR of the coin prototypes B-1 to B-18..... | 123 |
| Table 4-20 Control factors and levels of the experiment..... | 126 |
| Table 4-21 Experimental layout..... | 127 |
| Table 4-22 Response table for S/N ratio (Capacitance)..... | 129 |
| Table 4-23 Response table for S/N ratio (ESR)..... | 129 |

ACRONYMS

AC – Activated Carbon

ANOVA - Analysis of Variance

CB - Carbon Black

CNT – Carbon Nano Tubes

CV - Cyclic Voltammetry

DOE - Design of Experiment

EDLC - Electrical Double layer Capacitor

ESR – Equivalent Series Resistance

GA - Genetic Algorithms

KCl - Potassium Chloride

Na₂SO₄ - Sodium Sulphate

OA – Orthogonal Arrays

PTFE – Polytetrafluoroethylene

PVDF - polyvinylidene Difluoride

S/N - Signal-to-Noise Ratio

SEM - Scanning Electron Microscope

1. Introduction

1.1 Introduction

This project deals with establishing a manufacturing process for EDLC on a pilot plant basis. There is no current literature on establishing pilot plants for this device, however [1, 5, 6, 8-12] have described various methods of making supercapacitor based on trial and error method, without the use of any optimization for the manufacturing process. Many researchers have reported laboratory scale processes [1, 11, 13-17] but there is currently no literature on pilot plant manufacturing of EDLC capacitors.

Supercapacitors or electrochemical double-layer capacitors (EDLCs), as a kind of energy storage devices, have high energy density, great power density and long life cycle [18]. EDLCs are power sources that store energy within the electrochemical double layer formed at the solid (active material) and the solution (electrolyte) interface [19]. Supercapacitors have the highest available capacitance values per unit volume and the greatest energy density of all capacitors. Its capacitance values are up to 10,000 times that of electrolytic capacitors [18]. Supercapacitors bridge the gap between capacitors and rechargeable batteries. In terms of specific energy, as well as in terms of specific power, this gap covers several orders of magnitude. However, batteries still have about ten times the capacity of supercapacitors [20]. On the other hand, the supercapacitors have more than ten times the specific power, which makes it one of the best options in energy storage devices.

This thesis proposes the use of Design of Experiment (DOE) approach, to determine the most significant factors of the fabrication process. DOE allows multiple parameters to be evaluated with a limited number of experiments. With the use of the

Taguchi methodology, in this thesis, the number of required experiments was reduced from $(3^3) = 27$ experiments to only 9 experiments while at the same time producing a more robust product.

The Taguchi technique is an experimental design method using "off-line quality control" because it is a method of ensuring good performance in the design stage of products or processes. The Taguchi technique was developed by Genichi Taguchi to improve the quality of manufactured goods, but it can also be applied to other fields such as biotechnology [21]. With DOE using the Taguchi approach, one can economically achieve product/process design optimization in the manufacturing industry. The objective of using the Taguchi technique is to analyse the outcome of the experiment and then use it as a reference for future experiments. Furthermore, several parameters are set, and samples are made within a limited range, which is altered for each iteration, instead of following the conventional approach of making lots of samples to test each parameter. Once the parameter that affects most the fabrication process of supercapacitor have been determined, the levels at which these parameters should be varied must be evaluated. This method was applied to some of the fabricating process factors of the different supercapacitor packaging.

1.2 Problem Statement

Energy storage is one of the most important achievements in the engineering fields, and it is done by using devices or physical media to store energy for later use, such as kinetic energy (momentum) or potential energy (chemical, electrical, temperature).

In the case of electrical energy storage, battery is the main and the most widely used storage device, Secondary batteries store a considerable amount of energy, but it takes a long time to charge. Capacitors charge much faster, but they cannot store large amount of energy. There was a need for a storage device that can fill the gap between the batteries and the capacitor; supercapacitors charge quickly and will hold a large amount of energy for a long time.

The objective of this research is to build and setup a supercapacitor pilot plant for manufacturing of EDLC for a volume of up to 10unit/hour for cylindrical supercapacitor and coin supercapacitor packages.

One of the foremost issues in establishing the supercapacitor pilot plant is designing a process which is able to fulfil the stated quality and throughput requirements of specific capacitance and equivalent series resistance (ESR). That is done by designing the manufacturing process-flow, which details the steps of making the supercapacitor for different packaging (cylindrical and coin).

Another research issue is to identify and optimize the significant factors of the fabrication process by adopting Taguchi DOE methodology. The Taguchi method is preferred here because of its ability to minimize the number of experiments needed and provide enough optimization information, which will provide a considerable cost and time saving.

1.3 Research Objectives

The issues as stated previously are related to the following research objectives:

1. To design and build the pilot plant for supercapacitor.
2. To design a fabrication process flow for the coin packaging supercapacitor.
3. To design a fabrication process flow for the cylindrical packaging supercapacitor.
4. To use Design of Experiment to find the most significant process factors.
5. To optimize the fabricating process using Taguchi method.
6. To test the prototypes according to the international standards (BS EN 62391-1:2006, BS EN 62391-2-1: 2006, BS EN 62391-2-1: 2006 and DOD-C-29501/3 NOT 1).

1.4 Research Scope

The project proposes a design, setting up of supercapacitor pilot plant, and using DOE to try and find the most significant manufacturing processes for optimization; those ultimate goals should be achievable within the allocated time and resources.

The project was divided into sections as follows:

- Aims and Objectives
- Literature Review
- Design the manufacturing process flow.

- Design of Experiment using the Taguchi method.
- Build the first prototypes.
- Data analysis.
- Optimize the manufacturing process.
- Fabricate the final product (cylindrical and coin supercapacitor).
- Test the final supercapacitor to the international standards.

1.5 Contribution of the Thesis

This thesis proposes systematic method to optimize the supercapacitor fabrication process using the DOE by adapting the Taguchi technique, unlike the trial and error method reported in the literature and used in the industry now a days. By utilizing the DOE the number of experiments is reduced to minimum, which in turns saves time, resources and expenses.

This project sets the basics lines for integrating the genetic algorithms with Taguchi technique, for future research in improving the optimization process for EDLC fabrication.

Hence, this project proposes a way supercapacitor fabrication is optimized in the scientific research and manufacturing fields.

1.6 Thesis Outline

This section briefly outlines the contents of every chapter:

- **Chapter one:** *Introduction* - The first chapter gives an introduction to the readers on what the project is basically about, its objectives, planning and also includes brief descriptions of every chapter in this thesis.
- **Chapter two:** *Literature Review* - This chapter discusses some of the previous studies, which serve as essential references to this project.
- **Chapter three:** *Methodology* - This chapter briefly shows how the experimental and non-experimental procedures were carried out in order to obtain the valuable data that will be analyzed and discussed in the chapter four.
- **Chapter four:** *Results* - This part consists of all the data obtained following the methodology in the previous chapter. Those data are interpreted in terms of tables, graphs and necessary discussions.
- **Chapter five:** *Conclusion* - The final chapter summarizes the project as a whole before drawing conclusions on whether the objectives have been met or not. Several possible future work improvements are listed.

2. Literature Review

2.1 Introduction

Batteries and electrochemical capacitors (ECs) are among the leading efficient electrical energy storage (EES) technologies today. Both devices are based on electrochemistry; in the case of the batteries, the energy is stored in chemical compounds capable of generating the charge, while ECs store energy physically. ECs have higher energy density than conventional dielectric capacitors and higher power density than batteries. Other advantages of ECs include fast charging rate and long life cycle (up to 500,000 cycles) [22].

Electrochemical capacitor is also known as supercapacitor, ultracapacitor or electrical double layer capacitor. The first patent on supercapacitor was filed in 1957 by Becker of General Electric Corporation [23] for the capacitor based on porous carbon material with high surface area. The first attempt to market the supercapacitor was made in 1969, by SOHIO, using high surface area carbon materials with tetraalkylammonium salt electrolyte [24]. In the 90's, supercapacitors received much attention in the context of hybrid electric vehicles. Commercial productions of electrochemical supercapacitors in the current markets are based on the high surface area porous carbon materials as well as based on noble metal dioxide systems. For example, Matsushita Electric Industrial (Panasonic, Japan) developed Gold capacitors and Pinnacle Research (USA) especially made high performance supercapacitors for military applications [18]. Table 2-1 shows a comparison of the properties and performance between battery and supercapacitor [25].

Table 2-1 Comparison between battery and supercapacitor

| Function | Supercapacitor (general) | Lithium-ion (general) |
|----------------------------------|-------------------------------------|----------------------------------|
| Charge time | 1–10 seconds | 10–60 minutes |
| Cycle life | 1 million or 30,000h | 500 and higher |
| Cell voltage | 2.3 to 2.75V | 3.6 to 3.7V |
| Specific energy (Wh/kg) | 5 (typical) | 100–200 |
| Specific power (W/kg) | Up to 10,000 | 1,000 to 3,000 |
| Cost per Wh | \$20 (typical) | \$0.50-\$1.00 (large system) |
| Service life (in vehicle) | 10 to 15 years | 5 to 10 years |
| Charge temperature | –40 to 65°C | 0 to 45°C |
| Discharge temperature | –40 to 65°C | –20 to 60°C |

There has been great interest in developing and refining more efficient energy storage devices. One such device, the supercapacitor, has matured significantly over the last decade and emerged with the potential to facilitate major advances in energy storage.

Rather than operating as a stand-alone energy storage device, supercapacitors work well as low-maintenance memory backup to bridge short power interruptions.

Supercapacitors have also made critical inroads into electric powertrains. The virtue of ultra-rapid charging and delivery of high current on demand makes the supercapacitor an ideal candidate as a peak-load enhancer for hybrid vehicles, as well as fuel cell applications [25]

Supercapacitor initial charge can be achieved very fast, and the topping charge will take extra time in the range of 10 seconds. Provision must be made to limit the initial current inrush when charging an empty supercapacitor. The supercapacitor cannot go into overcharge and does not require full-charge detection; the current simply stops flowing when the capacitor is full [25].

The supercapacitor has a virtually unlimited number of cycles. Unlike the electrochemical battery, which has a defined number of life cycles, there is little wear and tear by cycling a supercapacitor. Nor does age affect the device, as it would for a battery. Under normal conditions, the capacity of a supercapacitor fades from the original 100% to 80 % in 10 years. Applying higher voltages than specified shortens the life of supercapacitor. The supercapacitor is able to function well at hot and cold temperatures [25].

Batteries are typically low power devices compared to capacitors, which have power densities as high as 106 W/kg, but low energy densities. From this point of view, supercapacitors combine the properties of high power density and higher energy density, and also have long life cycles due to the absence of chemical reactions. A comprehensive review of the historical background, properties, and principles of capacitors has been given by Conway [18].

Recently the supercapacitor has emerged with the potential to enable major advances in the energy storage devices. The supercapacitors energy density is greater than those of conventional capacitors while the power density is greater than those of batteries. All these unique features make the supercapacitors to become an attractive power solution for an increasing number of energy storage applications [26].

The Ragone plot below compares the performance of a range of electrochemical devices. It shows that supercapacitors can deliver very high power but the storage capacity is very limited. On the other hand fuel cells can store large amounts of energy but have a relatively low power output. Figure 2-1 shows the Ragone plot of energy storage devices. The plot shows that, the supercapacitor (Ultracapacitor) fill in the gap between batteries and conventional capacitors [27].

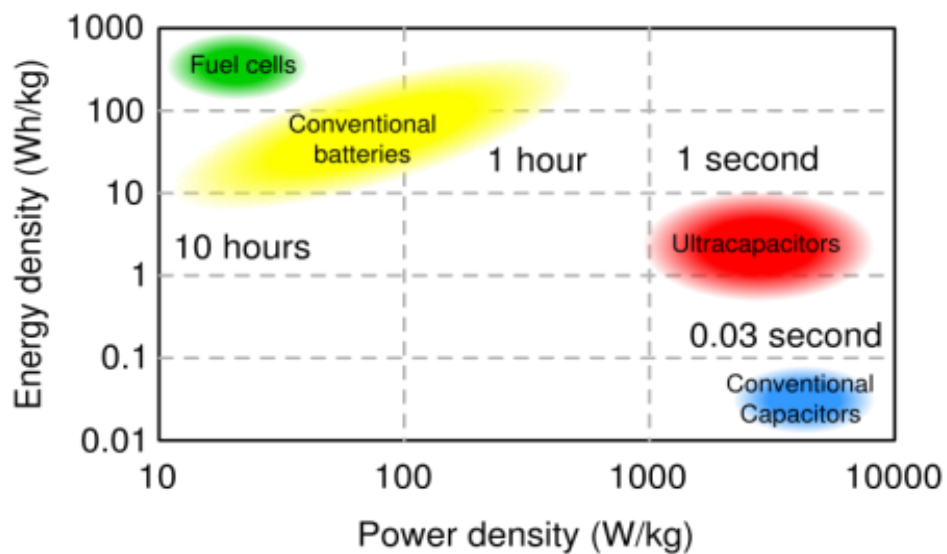


Figure 2-1 Ragone plot of energy storage devices [27]

2.2 Supercapacitor Classes

Based upon current R&D trends, supercapacitors can be divided into three general classes: electrochemical double-layer capacitors, pseudocapacitors, and hybrid capacitors. Figure 2-2 shows the different classes of supercapacitors. Each class is characterized by its unique mechanism for storing charges.

These are, respectively, non-Faradaic, Faradaic, and a combination of the two. Faradaic processes, such as oxidation-reduction reactions, involve the transfer of charge between electrode and electrolyte. A non-Faradaic mechanism, by contrast, does not involve any chemical redox process. Rather, charges are distributed on surfaces by physical processes that do not involve the making or breaking of chemical bonds.

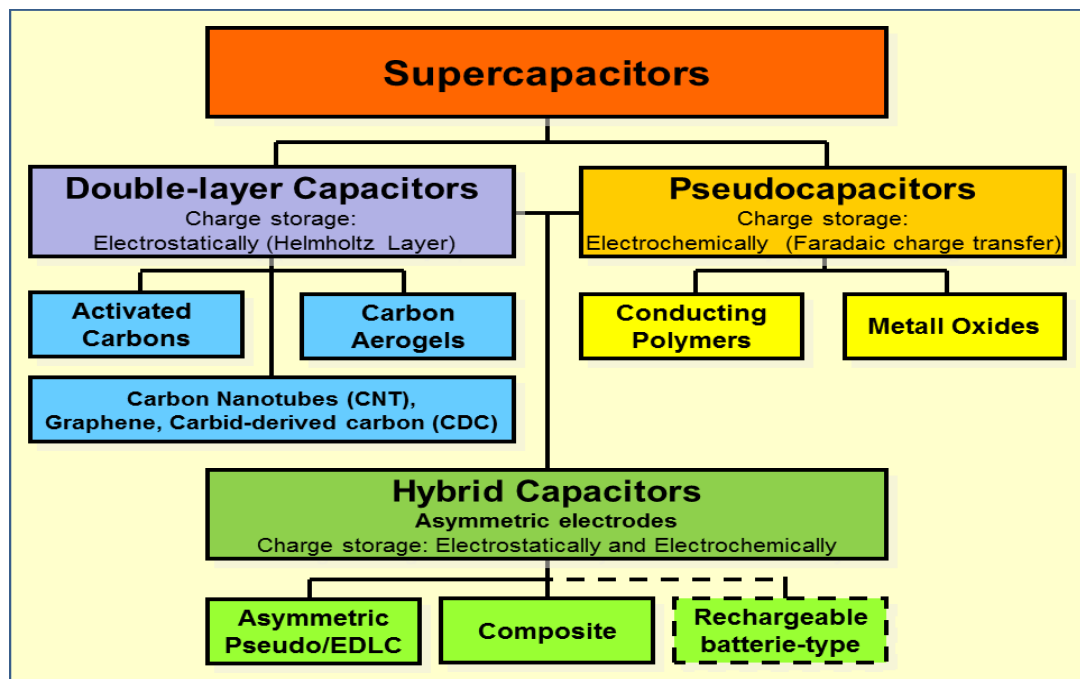


Figure 2-2 Supercapacitor classes [26]

2.2.1 Electrical Double Layer Capacitors (EDLC)

Electrical double layer results from strong interactions between the ions/molecules in the solution and the electrode surface. At the metal-solution interface, there is a thin layer of charge on the metal surface, which results from an excess or deficiency of electrons. On the other hand, in the vicinity of the electrode surface, there is an opposite charge in solution due to an excess of either cations or anions. Thus the electrical double layer is made up of the whole array of charged species and oriented dipoles existing at the metal-solution interface [28].

Figure 2-3 provides a schematic diagram of a typical EDLC.

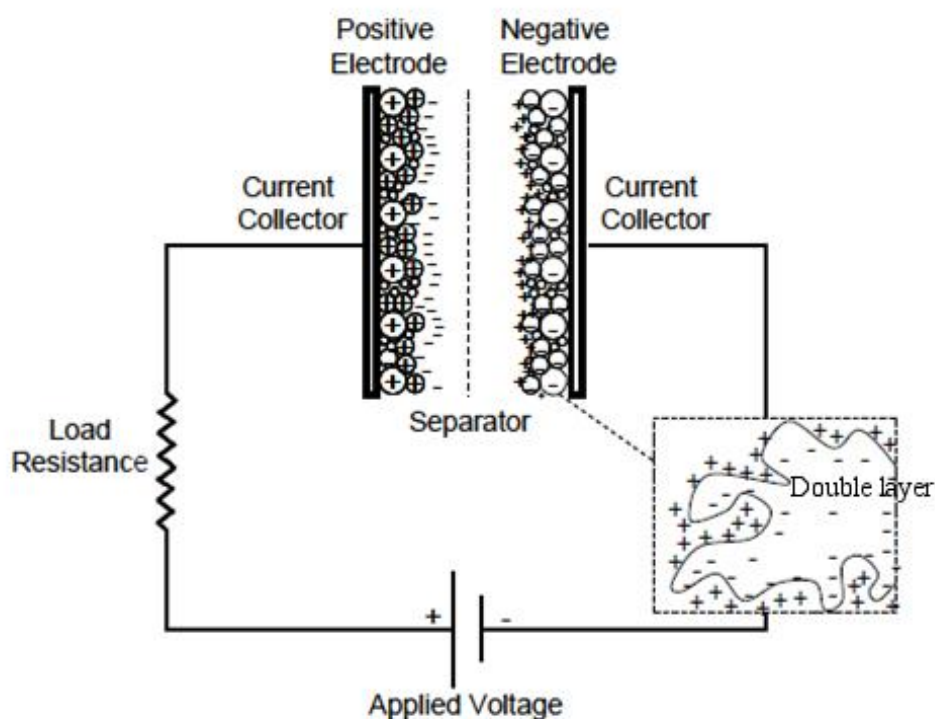


Figure 2-3 EDLC construction [28]

Carbon-base material with high surface area like, activated carbon, carbon aerogels and carbon nano tubes (CNT) are used to fabricate the double layer supercapacitors.

2.2.1.1 Activated Carbon

Activated carbon is the most commonly used electrode material in EDLCs, because it is less expensive and possesses a higher surface area than other carbon-based materials. Activated carbons utilize a complex porous structure composed of differently sized micropores (< 2 nm), mesopores (2-50 nm), and macropores (>50 nm) to achieve their high surface areas. Even though the capacitance is directly proportional to surface area, research evidence suggests that, for activated carbons, not all of the high surface area contributes to the capacitance of the supercapacitor [29-31]. This is believed to be caused by electrolyte ions that are too big to diffuse into the smaller micropores in the activated carbon, thus preventing utilizing some of the surface area for charge storage [32, 33]. Research also suggests an empirical relationship between the distribution of pore sizes, the energy density, and the power density of the device. Larger pore sizes correlate with higher power densities and smaller pore sizes correlate with higher energy densities. As a result, the pore size distribution of activated carbon electrodes is a major area of research in EDLC design [29-33]. Many researchers have focused on determining the optimal pore size for different electrolytes (ion size) and improving the control of the pore size distribution during fabrication of the electrode material.

Carbon materials generally have high surface area, 1000 ~ 2000 m²/g. High surface area and porosities can be achieved by carbonization, physical or chemical activation

[34-36]. Generally activated carbon is in powder form, so some processing is necessary to transform the powder into solid compact electrodes. These methods include permanent pressure [32] and adding binders such as polytetrafluoroethylene (PTFE), [37, 38] poly vinylidene fluoride hexafluoropropylene (PVDF), [39] methylcellulose, and aqueous dispersions of polystyrene, styrene/butadiene copolymer and ethylene/acrylic acid copolymer [40]. Theoretically, the specific capacitance of carbon materials should increase with surface area. However, several activated carbon materials with different parameters (surface area, pore size, pore size distribution and pore volume) were studied and those parameters were correlated with the electrochemical capacitance. However, it was found that the hypothesis is not necessarily true in practical cases [31, 37]. It was reported by authors of [30] that the porous texture of the carbon determines the ionic conductivity, which is related to the mobility of ions inside the pores. The rate of electrochemical accessibility is determined by the mobility of ions inside the pores, which is different from that in bulk electrolytes. Therefore, a resistor network was suggested to be considered in the equivalent circuit model instead of one resistor due to the uneven resistance throughout the whole materials.

A new activated carbon with high specific capacitance and low cost was prepared using cotton stalk as a raw material. The prepared activated carbon achieved a specific surface area of $1,481 \text{ cm}^2/\text{g}$ and specific capacitance of 114 F/g [15].

2.2.1.2 Carbon Aerogels

Carbon aerogels have been used as an electrode material for EDLCs. Carbon aerogels are formed from a continuous network of conductive carbon nano-particles with interspersed mesopores. Due to the continuous structure and their ability to bond chemically to the current collector, carbon aerogels do not require the application of an additional adhesive binding agent like in the case of activated carbon. As a binderless electrode, carbon aerogels have been shown to have a lower ESR than activated carbons [29, 41, 42]. Their low ESR yields higher power, and this is the primary area in supercapacitor research involving carbon aerogels. In order to improve the capacitance of carbon materials, functional groups are introduced into the carbon materials because the functional groups are related to the pseudocapacitance, which is a very effective method of increasing the capacitance [43, 44].

Carbon aerogels derived from organic sol-gel process were prepared by means of ambient drying technique. The Brunauer Emmett Teller (BET) surface areas of obtained carbon aerogels were in the range 600–1000 m²/g. Electrochemical performances of the carbon aerogels electrodes were studied by cyclic voltammetry, galvanostatic charge/discharge measurements and electrochemical impedance measurement. The measurements showed that the electrodes can achieve a specific capacitance of 183.6 F/g [45].

Activated carbon aerogel with high specific surface area has been prepared via CO₂ and potassium hydroxide (KOH) activation processes. The prepared aerogel, which possesses pore volume of 2.73 cm³/g and specific surface area of 2119 m²/g, exhibits

high specific capacitances of 250 F/g and 198 F/g at the current densities of 0.5 A/g and 20 A/g respectively in 6 M KOH aqueous solution [46].

2.2.1.3 Carbon Nano Tubes (CNT)

Recently there is an increasing interest in the use of carbon nano tubes CNT as an EDLC electrode material [29, 47-49]. Electrodes made from CNT are grown as an entangled mat of carbon nano tubes, with an open and accessible network of mesopores. Unlike other carbon-based electrodes, the mesopores in CNT electrodes are interconnected, allowing a continuous charge distribution that uses almost all of the available surface area. Thus, the surface area is utilized more efficiently to achieve capacitances comparable to those in activated carbon-based supercapacitors, even though CNT electrodes have a modest surface area compared to activated carbon electrodes [29, 50].

Because the electrolyte ions can more easily diffuse into the mesoporous network, CNT electrodes also have a lower ESR than activated carbon [50, 51]. In addition, several fabrication techniques have been developed to reduce the ESR even further. Especially, carbon nano tubes can be grown directly onto the current collectors, subjected to heat-treatment, or cast into colloidal suspension thin films [23, 51, 52]. The efficiency of the entangled mat structure allows energy densities to be comparable to other activated carbon-based materials and the reduced ESR allows higher power densities to be achieved. Figure 2-4 shows SEM image of CNT structure.

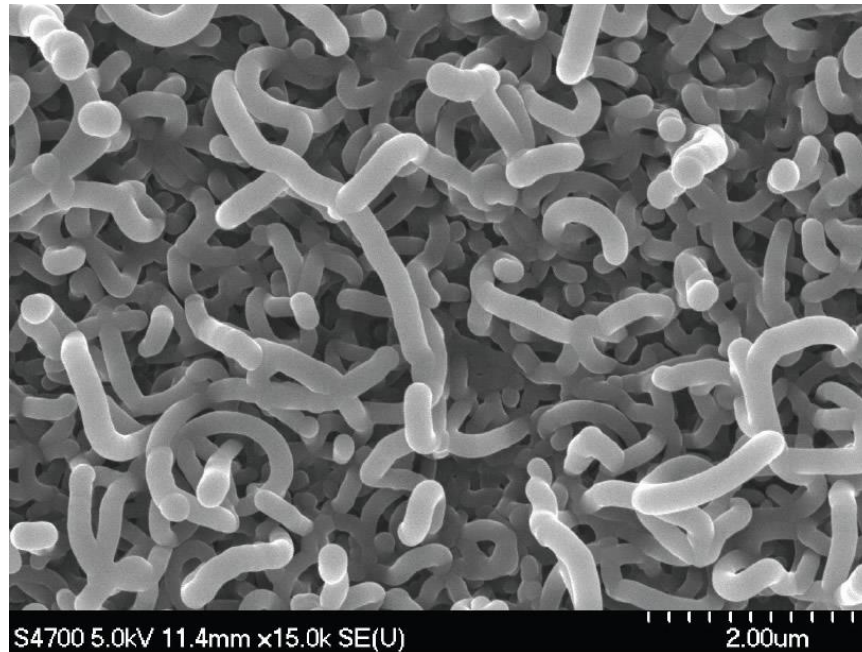


Figure 2-4 SEM image of entangled mat of carbon nano tubes [53].

A stand-up structure of CNTs were directly grown on the (CF) carbon fiber paper by microwave plasma-enhanced chemical vapor deposition [54]. Electrochemical measurements demonstrate that the capacitance of the electrode is around 176 F/g at a charging/discharging current density of $0.5\text{mA}/\text{cm}^2$. The stand-up structure of CNT/CF has a high capacitance, attributable to its large surface area, high electrical conductivity and direct growth with low energy-loss [54].

2.2.2 Pseudocapacitors

In the case of EDLCs, the charge is stored electrostatically, while pseudocapacitors store charge faradaically through the transfer of charge between electrode and electrolyte. This is accomplished through electrosorption, reduction-oxidation reactions, and intercalation processes [18, 55, 56]. These Faradaic processes may allow pseudocapacitors to achieve greater capacitances and energy densities than

EDLCs [57-59]. The two materials that are used for electrodes in pseudocapacitors are metal oxides and conducting polymers. Since the pseudocapacitance is faradaic in origin, and quite different from the classical electrostatic capacitance observed in the double layer, the charge will transfer across the double layer, similar to discharging and charging in a battery.

2.2.2.1 Metal Oxide Supercapacitor

Because of their relatively higher conductivity, metal oxides have been explored as a possible electrode material for pseudocapacitors [12, 20, 59-61]. The majority of relevant research focuses on ruthenium oxide. This is because other metal oxides have yet to obtain comparable capacitances. The capacitance of ruthenium oxide is achieved through the insertion and removal, or intercalation, of protons into its amorphous structure. In its hydrous form, the capacitance exceeds that of carbon-based and conducting polymer materials [60, 61]. Furthermore, the ESR of hydrous ruthenium oxide is lower than that of other electrode materials. As a result of low ESR, ruthenium oxide pseudocapacitors may be able to achieve higher energy and power densities than EDLCs or conducting polymer pseudocapacitors. However, despite this potential, the success of ruthenium oxide has been limited by its high cost. Thus, a major area of research is the development of new fabrication methods and novel composite materials, with the aims to reduce the production cost of ruthenium oxide [12, 20, 59].

Copper oxide (CuO) nanoparticles have been synthesized through a sonochemical assisted precipitation followed by thermal treatment[4]. Symmetric supercapacitors

have been assembled in real two-electrode configurations and their electrochemical performances have been investigated using various electrochemical methods including cyclic voltammetry, electrochemical impedance spectroscopy, and chronopotentiometric charge/discharge cycles. It showed specific capacitance of 245 F/g at current density of 0.1 A/g. Conducting charge/discharge measurements for 1000 cycles and in different current densities, it has been found that the composite material is a promising candidate for supercapacitor application, in terms of cycle ability and rate capability [4].

2.2.2.2 Conducting Polymers

Conducting polymers is considered to have relatively high capacitance and conductivity, while with a low ESR and fabrication cost if compared to carbon-based electrode materials [31]. In particular, the n/p-type polymer configuration, with one negatively charged (n-doped) and one positively charged (p-doped) it found to have the greatest energy and power densities. However, a lack of efficient, n-doped conducting polymer materials has prevented these pseudocapacitors from reaching their potential [30, 58]. Additionally, it is believed the mechanical stress on conducting polymers during reduction-oxidation reactions limits the stability of these pseudocapacitors through many charge-discharge cycles [20, 30, 60]. This reduced life cycle stability has limited the development of conducting polymer pseudocapacitors.

G-PEDOT nanocomposite was synthesized using a chemical oxidative polymerization technique. The electrochemical charge/discharge characteristics of

G-PEDOT nanocomposites were investigated in different electrolytic media, and the specific discharge capacitance was estimated to be 374 F/g. This has revealed that the G-PEDOT nanocomposite could be a transformable and viable electrode material for supercapacitor applications [62].

In another study a hybrid asymmetric supercapacitor is constructed by employing two different nanostructured conducting polymers of polypyrrole (PPy) and self-doped polyaniline (SDPA). The maximal working potential window of 1.3V is associated with more than 97 F/g of total electrode materials. The cell maintains approximately 70% of its initial capacitance after 1000 cycles with ESR below $1.6\Omega/\text{cm}^2$. Moreover, the proposed supercapacitor exhibits high capacitance retention of 89% at a higher current density $40\text{mA}/\text{cm}^2$, indicating good electrochemical stability and primary charge/discharge rate capability [63].

2.2.3 Hybrid Capacitors

The hybrid supercapacitors attempt to exploit the advantages and mitigate the disadvantages of EDLCs and pseudocapacitors to get better performance characteristics. Using both Faradaic and non-Faradaic processes to store charge, hybrid capacitors have achieved energy and power densities greater than EDLCs without sacrificing the in cycling stability and affordability. Research has focused on three different types of hybrid capacitors, distinguished by their electrode configuration: composite, asymmetric, and battery-type.

2.2.3.1 Composites Supercapacitor

Composite electrodes used carbon-based materials with either conducting polymer or metal oxide materials and incorporate both physical and chemical charge storage mechanisms together in a single electrode. The carbon-based materials facilitate a capacitive double-layer of charge and also provide a high-surface-area backbone that increases the contact between the deposited pseudocapacitive materials and electrolyte. The pseudocapacitive materials are able to further increase the capacitance of the composite electrode through faradaic reactions [64, 65].

Composite electrodes constructed from CNT and polypyrrole, a conducting polymer, have been particularly successful. Several experiments have demonstrated that this electrode is able to achieve higher capacitances than either a pure CNT or pure polypyrrole polymer-based electrode [64-66]. This is attributed to the accessibility of the entangled mat structure, which allows a uniform coating of polypyrrole and a three-dimensional distribution of charge. Moreover, the structural integrity of the entangled mat has been shown to limit the mechanical stress caused by the insertion and removal of ions in the deposited polypyrrole. Therefore, unlike conducting polymers, these composites have been able to achieve a cycling stability comparable to that of EDLCs [64, 65].

Polypyrrole (PPy)/carbon aerogel (CA) composite materials were prepared by chemical oxidation polymerization, used as active electrode material for supercapacitor. The results based on cyclic voltammograms show that the composite material has a high specific capacitance of 433F/g, the specific capacitance was stabilized after 500 cycles [67].

2.2.3.2 Asymmetric Supercapacitor

Asymmetric hybrids combine Faradaic and non-Faradaic processes by coupling an EDLC electrode with a pseudocapacitor electrode. In particular, the coupling of an activated carbon negative electrode with a conducting polymer positive electrode has received a great deal of attention [30, 68, 69]. While conducting polymer electrodes generally have higher capacitances and lower resistances than activated carbon electrodes, they also have lower maximum operating voltages and less cycling stability. Asymmetric hybrid capacitors that couple these two electrodes mitigate the extent of this trade off to achieve higher energy and power densities if compared to EDLCs. Also, they have better cycling stability than the conventional pseudocapacitors [30, 68, 69].

A composite material consisting of graphene oxide exfoliated with microwave radiation, and manganosite MnO is synthesized for supercapacitor electrodes [70]. Asymmetric supercapacitor was constructed with the composite containing 90% MnO–10% mw rGO (w/w). CV and EIS were used to characterize the supercapacitor, from the resulting analysis. The device exhibited a specific capacitance of 51.5 F/g and excellent capacity retention of 82% after 15,000 cycles [70].

2.2.3.3 Battery-Type

Battery-type hybrids supercapacitors couple two electrodes, a supercapacitor electrode with a battery electrode. This configuration reflects the demand for higher energy supercapacitors and higher power batteries, combining the energy characteristics of batteries with the power, life cycle, and recharging times of

supercapacitors. Research has focused primarily on using nickel hydroxide, lead dioxide, and LTO ($\text{Li}_4\text{Ti}_5\text{O}_{12}$) as one electrode and activated carbon as the other [71-74]. Although there is less experimental data on battery type hybrids than on other types of supercapacitors, the data that is available suggests that these hybrids may be able to bridge the gap between supercapacitors and batteries. Despite the promising results, the general consensus is that more research will be necessary to determine the full potential of battery-type hybrids [72, 73].

2.3 Taguchi Method

A part from the materials, the process of fabricating the supercapacitor from the material previously mentioned is conducted here. In particular, an investigation is conducted on how to optimally optimize the process using activated carbon.

Design of experiments (DoE) methods were integrated by Dr. Genichi Taguchi into the product and process development making, one of his key ideas to be the concept of robust design. This involves designing products and processes with suitable parameters and settings [75].

For the optimization of the production process the DoE and ANOVA methodologies were used. DOE provides methods of experimental design for performing analysing test series in a systematic and efficient way. The application has been proven to be very helpful when investigating a process that involves many parameters. As a scientific approach to experimentation, DOE incorporates statistical principles to ensure an objective investigation and finally drawing conclusions that are convincing from the experimental study [76].

Essentially, a DOE project has three phases: i) Design ii) Experiment and iii) Analysis.

Using DOE one can determine the optimal levels of processes or design parameters. But finding these optimal levels is not always easy task. Industrial experiments do not always go as planned because a non-systematic approach is often taken by the experimenters. Thus, the following is a step by step plan that helps to conduct the experiment, analyse results and implement solutions [77]:

- *Recognition and Formulation*: Recognizing the problem is an important step, not understanding the problem makes it more difficult to solve.
- *Quality Characteristics*: The selection of quality characteristics to measure the experimental output. These outputs can be variable or attribute in nature.
- *Selecting Parameters*: It is the most important step of the experimental design procedure. If the wrong factors are selected or the important factors of the experiment are ignored, then the results may be inaccurate.
- *Classifying Factors*: After selecting the design and process parameters, the next step is to classify them into control, noise and signal factors:
 1. Control factors are those factors that can be controlled by the experimenter.
 2. Noise factors are those factors that cannot be controlled, and they are difficult or are too expensive to control in the production environment.

3. Signal factors are those that affect the target performance of the characteristic, but generally have no influence on variability in the performance characteristic of the product or process.

- *Determining levels:* A level is the value that a factor holds in an experiment. The number of levels depends on the nature of the design and process parameter and whether or not the chosen parameter is qualitative or quantitative.

The levels need to be in an operational range of the product or process. Taguchi recommends the use of three levels if nonlinearity is expected in the main effect of control factor that affect quality characteristic.

- *Interactions:* Interaction between two design and process parameters exists when the effect of one parameter on the quality characteristic is different at different levels of the other parameter. The designer should determine which interaction should be studied.

- *Orthogonal Array (OA):* OAs are a set of tables of numbers created by Taguchi that allow experimenters to study the effect of a large number of control and noise factors on the quality characteristic in a minimum number of trials. Taguchi proposed the use of OAs for planning the optimization experiments.

- *Conducting Phase:* Conducting the experiment and recording the results. To ensure the validity of the experiment, the following points should be considered prior to conducting the experiment:

- **Location:** an appropriate location that is unaffected by external sources of noise.

- **Resource availability:** Making sure the necessary equipment, operation and materials are available before starting.
 - **Cost-benefit analysis:** Verifying the experiment is necessary and justify that the benefits to be gained from the experiment will exceed the cost of the experiment.
 - **Data sheets:** Use uncoded data sheets for running the experiment and coded data sheets for analysing the data.
 - **Randomize the trials:** Randomization is critical to ensure that bias is evaded during data gathering.
 - **Replicate the experiment:** Replication is a process of running the experimental trials more than once.
- *Analysis Phase:* After conducting the experiment, the results are analysed and interpreted. If the experiment was planned and designed properly and conducted in accordance with the data sheet, then statistical analysis will provide sound and valid conclusions.
- *Implementation:* To validate the conclusions from the experiment, a confirmatory experiment should be performed.

The design phase is decisive as it is where the level of information attainable is determined by the analysis of the experiment results [75]

For a particular combination of levels of the control factors, if the variation in the response is small, the combination is termed robust. Subsequently, orthogonal arrays are used to construct a fractional factorial design with treatment combinations as combinations of levels of both control and noise factors. Furthermore, the orthogonal

arrays employ statistical methods of average and analysis of variance (ANOVA) to analyse results based on the deviation from the target. This will then allow the selection of the design conditions that is most consistent and yield reduced variation [75]. OA are a special set of Latin squares, constructed by Taguchi to lay out the product design experiments. By using this table, an orthogonal array of standard procedure can be used for a number of experimental situations. Common 2-level factors OA as shown in Table 2-2 [78].

Table 2-2 An orthogonal array of L8

| Trial number | Factors | | | | | | |
|--------------|---------|---|---|---|---|---|---|
| | A | B | C | D | E | F | G |
| 1 | 0 | 0 | 0 | 0 | 0 | 0 | 0 |
| 2 | 0 | 0 | 0 | 1 | 1 | 1 | 1 |
| 3 | 0 | 1 | 1 | 0 | 0 | 1 | 1 |
| 4 | 0 | 1 | 1 | 1 | 1 | 0 | 0 |
| 5 | 1 | 0 | 1 | 0 | 1 | 0 | 1 |
| 6 | 1 | 0 | 1 | 1 | 0 | 1 | 0 |
| 7 | 1 | 1 | 0 | 0 | 1 | 1 | 0 |
| 8 | 1 | 1 | 0 | 1 | 0 | 0 | 1 |

The array is designated by the symbol L8, involving seven 2-level factors, zeros and ones. The array has a size of 8 rows and 7 columns. The number (zeros/ones) in the row indicate the factor levels (be it a fluid viscosity, chemical compositions, voltage levels, etc.) and each row represents a trial condition. The vertical columns represent the experimental factors to be studied. Each of the assigned columns contain four levels of zeros (0), and four levels of ones (1), these conditions, can combine in four possible ways, such as (0,0), (0,1), (1,0), (1,1), with 27 possible combinations of levels. The columns are said to be orthogonal or balanced, since the combination of

the levels occurred at the same number of times, when two or more columns, of an array are formed. Thus, all seven columns of an L array are orthogonal to each other.

The OA facilitates the experimental design process by assigning factors to the appropriate columns. In this case, referring to Table 2-2, there are at most seven 2-level factors, these are arbitrarily assigned factors A, B, C, D, E, F, and G to columns 1, 2, 3, 4, 5, 6, 7 and 8 respectively, for an L8 array. From Table 2-2, eight trials of experiments are needed, with the level of each factor for each trial-run as indicated on the array. The experimental descriptions are reflected through the condition level. For example, 0 may indicate that the factor is not applied, and 1 represents the factor that is fully applied. The factors may be variation in chemical concentration, material purity, and mechanical pressure and so on. The experimenter may use different designators for the columns, but the eight trial-runs will cover all combinations, independent of column definition. In this way, the OA assures consistency of the design carried out by different experimenters. The OA also ensures that factors influencing the end product's quality are properly investigated and controlled during the initial design stage [78].

2.4 Pilot Plant in this research

Generally, pilot plants are used to reduce the risks associated with building full process plants. The pilot plants are important in two ways [79]:

1. They are substantially less expensive to build than full-scale plants. The investor does not put as much capital at risk on a project that may be inefficient or unfeasible. Further, design changes can be made more cheaply at the pilot scale

and obstacles in the process can be worked out before the large plant is constructed.

2. They provide valuable data for design of the full-scale plant, such as scientific data about reactions, material properties, and corrosiveness. Designers use data from the pilot plant to refine the design of the production scale facility.

If a process is well defined and the engineering parameters are known, pilot plants are not used. Pilot plant is relative term in the sense that pilot plants are typically smaller than full scale production plants, they built in a range of sizes. Some pilot plants are built in laboratories using the available laboratory equipment. Others are constructed of fabricated metal on dedicated concrete slabs and cost millions of dollars.

After data is collected from operation of the supercapacitor pilot plant, a larger production scale facility may be built. The engineers will continue to operate the supercapacitor pilot plant in order to test ideas for new products or different operating conditions. Alternatively, they may be operated as another production facility. Figure 2-5 shows the glove box in our pilot plant. The glove box provides a clean and moisture free (0.001 ppm) environment for the assembly and the sealing processes of the EDLC fabrication. More details on the pilot plant will be provided in sections 3.5.6.



Figure 2-5 Glove box

3. Methodology

3.1 Introduction

This chapter describes the methodology that was followed to establish and optimize the manufacture of supercapacitor prototypes appropriate for various packages.

The packages that were produced are of the coin and cylinder types. These were chosen in order to ensure that the common optimized process parameters found in the step stated in Chapter Two could be used with minor alteration for both the packages. In other words the basic process was tested for the two different packages. According to the literature [11, 80] the significant parameters and individual process limits were identified, and were used to fabricate the first prototypes. Process limits are based on the capability of the equipment and the target capacitance and ESR. Equipment capabilities were determined either experimentally or through manufacturer specifications. The fabricating process was optimized using Taguchi technique and optimized output is confirmed through various measurements and testing. The prototypes described in this chapter are carbon nanotubes (CNT) supercapacitors and activated carbon (AC) supercapacitors, both materials were used with different prototypes packaging. The optimization method and the testing methods are described in this chapter.

Figure 3-1 below illustrates the methodology steps that were followed during this research, to achieve the deliverables:

1. Methodology to optimize the manufacturing process using the Taguchi Technique.
2. Optimized process for coin type supercapacitor.
3. Optimized process for cylindrical supercapacitor.

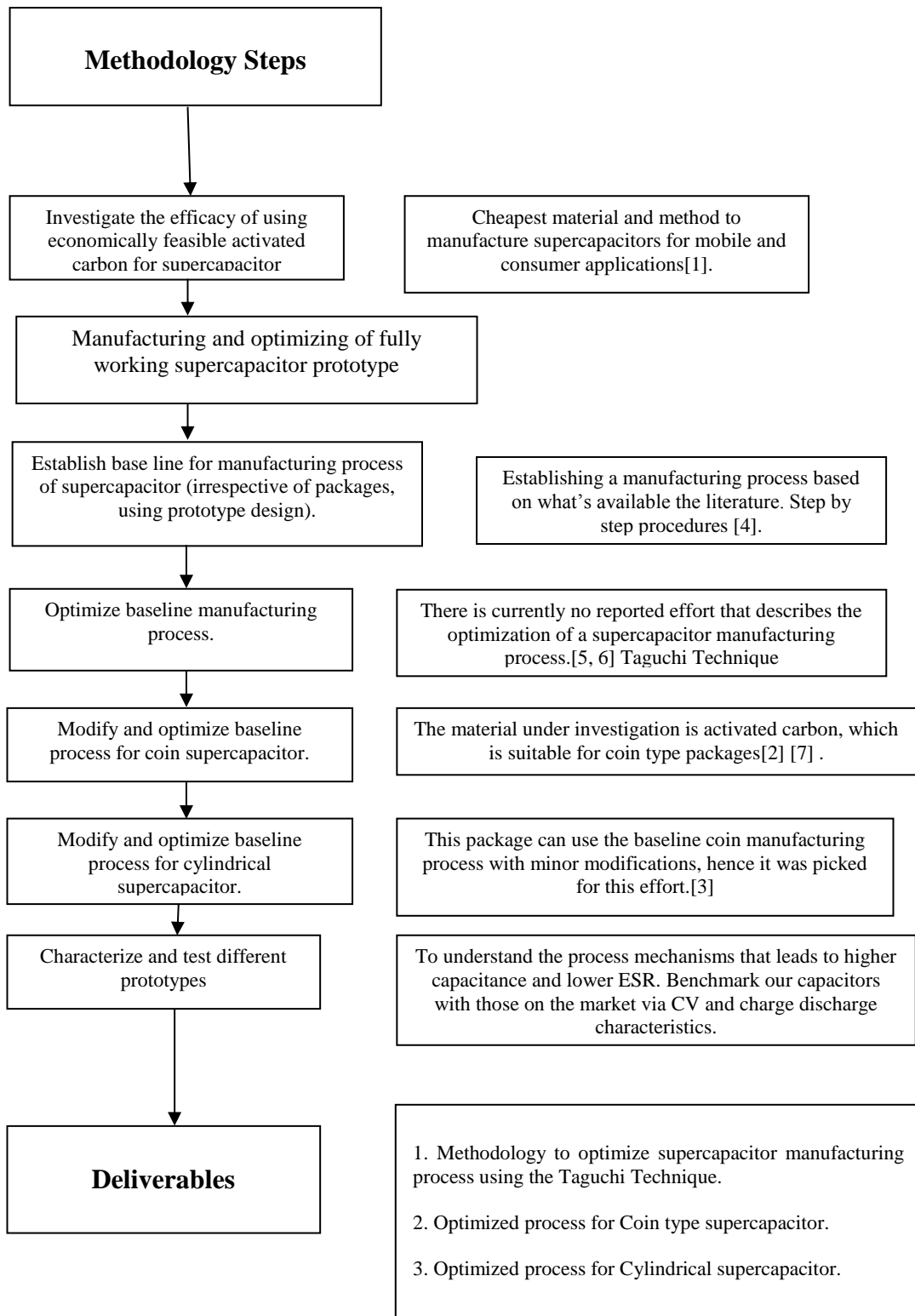


Figure 3-1 Methodology steps

3.2 Fabrication of the first supercapacitor prototypes

The first supercapacitor prototypes were fabricated following the state of the art mentioned in the literature [11, 14, 17, 80-83] and patents [1, 5, 6, 16, 84, 85]. Table 3-1 shows the starting parameters obtained from literature and they were used to fabricate the first prototypes. The percentages (AC, CNT, CB and binder) shown below were obtained from the ranges discussed by the corresponding references and were used as a starting point for the fabrication process. The following confirmation experiments were carried out to verify the baseline process parameters.

Table 3-1 Starting values of the parameters

| Parameter | Percentage/Reference |
|----------------------|---|
| CNT % | 80% [80], 85% [81]. |
| AC % | 90% [14], 75% [11], 75-90% [86], 88-92% [10], 85-90% [9], 80% [13]. |
| Binder % | 10% [80], 10% [14], 5% [11], 5.5-12% [10], 5-8% [9], 10% [13]. |
| Carbon Black CB % | 10% [80], 15% [81], 20% [11], 0.1 [86], 2-10% [85], 9% [13]. |

3.2.1 Supercapacitor using Carbon Nano Tubes

Carbon Nanotubes (CNT) were first reported and characterized by Iijima [87] and Endo [88]. It consists of high ratio cylinders of carbon atoms and it can be classified

as: **a)** Single walled (SWCNT), **b)** Multi-walled (MWCNT). Due to its high surface area it has been used extensively in supercapacitor research.

3.2.1.1 Supercapacitor with CNT Model Cap-1

A prototype supercapacitor cell was fabricated using multi-walled carbon nanotubes (MWNTs) as an active material, which theoretically have higher surface area than the single-walled nanotubes (SWNTs), PVDF as binder, aqueous KCl (1M) as electrolyte. Titanium foil used as current collector, two flat plastic sheets used as the casing for the cell, epoxy resin was used to seal the two plastic casing together. The cell was tested using the Autolab potentiostat, a cyclic voltammetry CV test was run to observe the cell behavior. An almost ideal CV graph is obtained and the capacitance of cell was measured to 0.0617 F. Figure 3-2 shows the picture of the fabricated cell.



Figure 3-2 CNT supercapacitor prototype model Cap-1

Table 3-2 shows the materials used for the fabrication process:

Table 3-2 Materials used for fabrication of model Cap-1

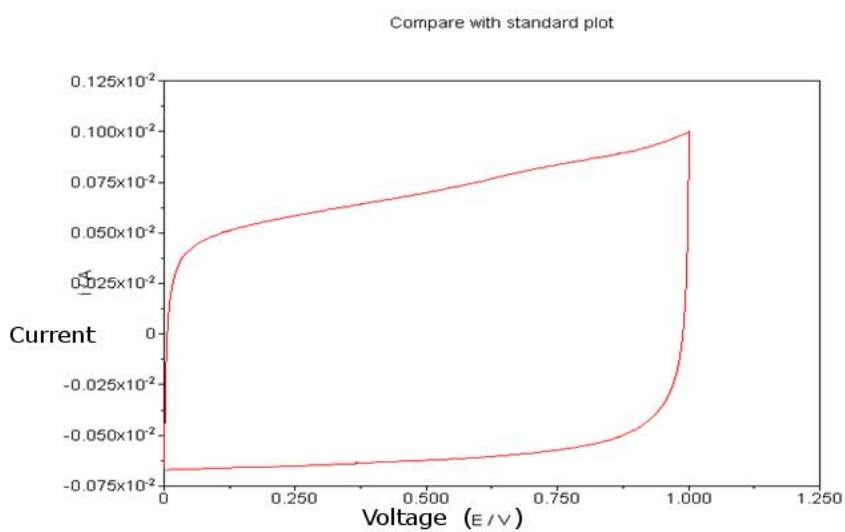
| Material | Description |
|-------------------|-----------------------|
| Activate material | CNT (0.5 g) |
| Binder | PVdF (50 mg) |
| Electrolyte | KCl (1M) |
| Titanium foil | 4cm x 4cm x 0.00127cm |
| Plastic sheets | 7cm x 7cm x 0.3cm |
| Separator | Filter paper 5x5cm |

The preparation started with mixing the CNT with the polymer PVDF binder, which will bind the CNT powder together and will help adhere the CNT to the current collector. Isopropanol was used as a mixing agent and solvent to form slurry. The slurry was then coated on the current collectors and dried in the vacuum oven for 1 hour at 80°C to remove the isopropanol. Then the two electrodes were sandwiched together separated by the filter paper, which acted as electronic isolator but ion permeable medium. The next step was to inject the electrolyte KCL to the assembled cell, and seal it from the elements. Autolab potentiostat was used to run the cyclic voltammetry test and charge-discharge test which were then used to measure capacitance and ESR.

The CV curve of the device shows capacitor behaviour, which is in ideal case, resembles a square shape.

Figure 3-3 shows the CV curve of Cap-1 prototype.

Figure 4: Test of cyclic voltammetry on dummy cell (WE(a))



C:\Autolab\Data\#1-CNT\#1-CNT-10mv.ocw
07/07/2008 11:22:33 AM

Figure 3-3 Cyclic voltammetry for the supercapacitor cell (Cap-1 at 10mV/s)

3.2.1.2 Supercapacitor with CNT Model Cap-2

The second supercapacitor was made using the same process for the first cell, except the coated layer of CNT on the current collector was made twice thicker, by coating with more layers of the CNT. The capacitance for this cell was measured to be 0.21 F. Figure 3-4 shows the fabricated cell.



Figure 3-4 CNT supercapacitor cell Cap-2

3.2.2 Supercapacitor prototypes using Activated Carbon

The next prototypes were fabricated using Activated Carbon (AC) as it is cheaper and more widely available in the market. A new configuration has been used for fabricating these prototypes, as the flat configuration that have been adapted for CNT electrodes fabrication is found not suitable, since they are not robust, hard to seal, size is too big and not economical.

The activated carbon (LAJU PAC) was used for the first prototype, which was purchased from (Laju group - Malaysia) and it had the specifications shown in Table 3-3.

Table 3-3 LAJU PAC specification

| Vendor/ spec | Surface Area m ² /g | Ash % | Moisture % | Capacitance with PC F/g | Capacitance with KOH F/g | PH | Particle size |
|-----------------|--------------------------------------|----------|---------------|-------------------------------|--------------------------------|------------|------------------|
| Laju / AC | <1000 | < 3% | < 15% | 40 | 40 | 11 - 13 | <45um |

3.2.2.1 Supercapacitor with AC Model Cap-3

This supercapacitor was fabricated using a 0.9 g coconut shell-based activated carbon (90%) mixed with 0.1 g of poly vinylidene fluoride (PVDF) polymer powder (10%). Then, isopropanol was added to the mixture as a solvent and mixing agent. The mixing was done using an ultrasonic bath for 30 minutes. After that, the slurry was dried for 30 minutes at 80⁰C in oven until all the isopropanol is evaporated. The powder was then used to make the supercapacitor electrodes.

The supercapacitor casing and current collector are made from a stainless steel material. The cell is a button-shaped capacitor. The weight of the active material used to fabricate the electrode is measured at 1mg on each current collector. The activated carbon was pressed using a die at 3 tones for 2 minutes to shape it and to stick it to the current collector. The two electrodes are electrically separated using a filter paper and the cell was filled with few drops of electrolyte KCL (1 M). The cell then was sealed using epoxy to prevent the electrolyte from evaporation. Figure 3-5 shows a picture of the fabricated supercapacitor with 15mm diameter.



Figure 3-5 Supercapacitor cell Cap-3

3.2.2.2 Supercapacitor with AC model Cap-4

In this part, three supercapacitors were fabricated using coconut shell-based activated carbon with different PVDF binder concentrations using 1 M potassium chloride (KCl) as electrolyte. The objective is to find the optimum value of binder that gives the highest specific capacitance. Figure 3-6 shows the three fabricated cells.



Figure 3-6 Supercapacitors picture: Cap-4.1, Cap-4.2 and Cap-4.3

The cells were fabricated via following steps:

- 1) 0.9 g of coconut-shell-based activated carbon (AC) is weighed using an electronic balance.
- 2) 0.1 g of PVDF powder is weighed and then mixed with the AC powder.
- 3) The first and second steps were repeated for the other two cells.
- 4) Isopropanol was added to the three samples as mixing and solvent agent.
- 5) Then the samples were sonicated using ultrasonic for one hour.
- 6) The samples were heated (water bath 80⁰C) for 2 hours to remove the solvent.

Electrode Fabrication procedures:

- 1) Stainless steel mesh was used as the current collectors for the supercapacitors cells. It was cut with the following dimensions, as shown in Figure 3-7 below.

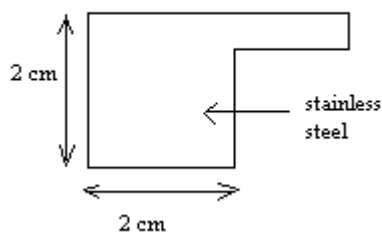


Figure 3-7 Electrode dimensions

- 2) The stainless steel electrodes are washed with isopropanol to ensure that the surface is clean from any oils or grease. Then, each electrode is weighed and their mass is recorded.
- 3) A thin layer of the coconut AC with 10% PVDF is coated onto the electrodes, then the electrodes were dried in vacuum oven for 2 hours, and then weighted again, to know the amount of AC on each electrode.
- 4) A filter paper is used to separate each pair of electrodes and it was laminated using a laminating plastic and laminating machine.
- 5) The laminated supercapacitors cells then filled with electrolyte 1 M KCl.
- 6) Steps 4, 5 and 6 were repeated for 15% and 20% PVDF binder.

3.2.2.3 Supercapacitor with AC Model Cap-5

Two supercapacitor cells was fabricated using coconut shell-based activated carbon aqueous, KCl (1 M) as electrolyte, stainless steel mesh as current collector.

The fabrication of this cell was done the following steps:

A. Preparing the activated carbon:

1) Coconut shell-based activated carbon (AC) is weighed and added to PVDF and isopropanol was added to the mix as mixing agent.

Below are the prepared samples:

a) Capacitor Cap-5.1: Coconut AC with 10% PVDF

b) Capacitor Cap-5.2: Coconut AC with 15% PVDF

2) Samples were then placed in the ultrasonic bath for mixing, and then heated to remove the isopropanol. When the sample was fully dry it was mixed in powder form.

3) A die was then used to press the powder to disk shape AC. Pressure used was 3 tones, using hydraulic press.

A two pressed AC disks were then attached to stainless steel mesh current collector, and separated by the filter paper as electrical isolating material, and the electrodes were placed in the casing.

4) Electrolyte (KCL) added to the assembled cell, and the cell then sealed using epoxy resin. Figure 3-8 shows the assembled supercapacitor cell.



Figure 3-8 Capacitor Cap-5

5) The supercapacitor cells were tested using the Autolab.

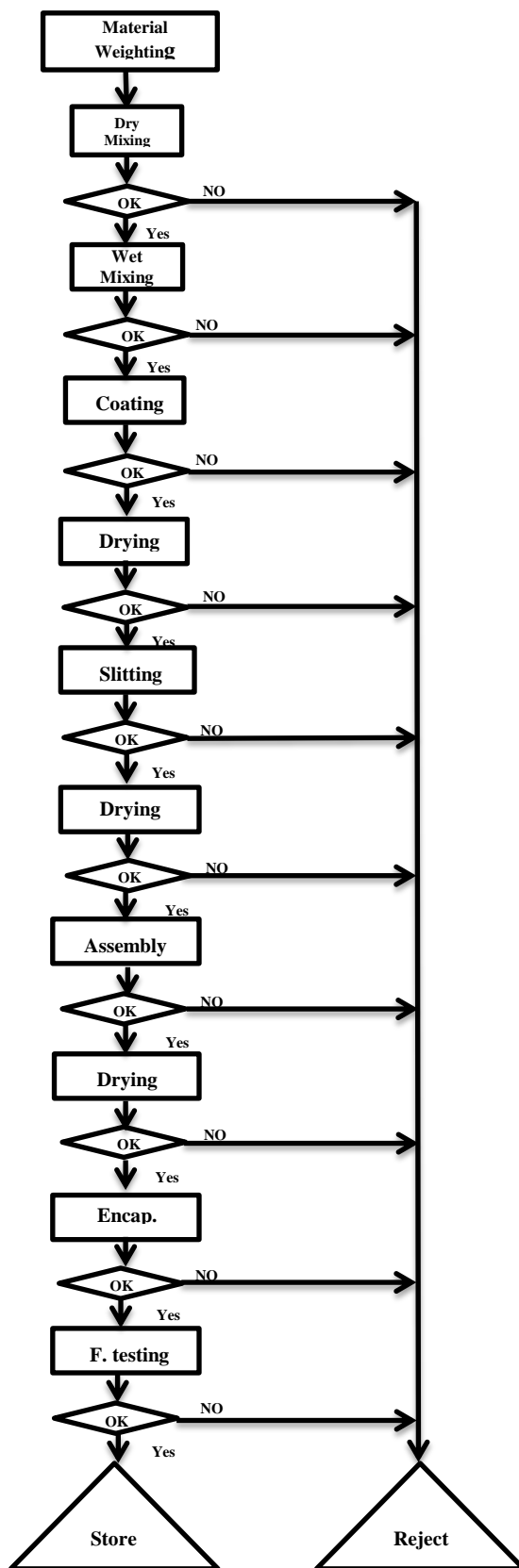
The Cap-5.2 supercapacitor cell shows very good resemblance of an ideal supercapacitor, at scan rate of 5 mV/s.

3.3 Fabrication Processes of Optimized Prototype using activated carbon

The former packages (Cap-1 to Cap-5) showed some weaknesses, either at the fabrication process or sealing process, the size and durability was an issue too. New packaging methods were needed. Cylindrical and coin shape packaging were proposed; the new packaging offer a better sealing and smaller size, as they have been used in the industry for typical capacitors and batteries.

3.3.1 Cylindrical Supercapacitor Fabrication Process

The fabrication process was performed according to the process flowchart for the cylindrical supercapacitor, shown in Figure 3-9. Some of the critical processes are the AC percentage, binder percentage and mixing time.



| | |
|---|---|
| Weighting: Activated carbon, Carbon black and PVdF | AC: 85%, CB: 10%, PVdF: 5% |
| Ultrasonic mixing | 30 minutes |
| Mechanical mixing | 2-3 hours |
| Coating the slurry on the Aluminium current collector | 100-150um |
| Dry the current collector on vacuum oven | 120 ⁰ C for 1 hour |
| Cut the current collector to the desired dimensions | |
| Dry the current collectors under vacuum | 120 ⁰ C for 1 hour |
| Winding the current collector with the separator | Using the winding machine |
| Dry the electrodes to remove the moisture | 120 ⁰ C for 2 hours |
| Add the electrolyte and seal | Done inside the glove box |
| Test the final prototype | Autolab, Gamry and temperature cycle oven |

Figure 3-9 Process flow chart for cylindrical supercapacitor fabrication

(1) Mixing:

The mixing process involves weighing the raw materials by using an analytical balance and then mixing the ingredients using a mechanical overhead stirrer. The mixing process was performed in two stages which are dry and wet mixing. The dry mixing involves the mixing of the powdered activated carbon and powdered carbon black. The wet mixing is done by adding solvents to the powders to form a slurry, the slurry of the activate materials is made by mixing activated carbon (85%), binder (PVDF, 5%), carbon black (10%) and solvents, using the Overhead Stirrer Model (MSP-1) shown in Figure 3-10.



Figure 3-10 Overhead Stirrer Model (MSP-1)

The mixing process has to be done with the right mixing speed and mixing time, to achieve the right viscosity. The right viscosity will insure the best coating results of the slurry on the electrodes.

(2) Coating:

Aluminum foil is coated with the active material slurry to form the electrodes for the supercapacitor, doctor blade was used to coat the slurry on the aluminum foil. The coating thickness was 100-150 μm , the coating machine is shown in Figure 3-11.



Figure 3-11 The coating process

The doctor blade used in the coating process is shown in Figure 3-12. The blade of the wet film applicator has two built-in metric micrometre heads for adjusting the knife blade so that clearances of the blade can be accurately set from 0-8 mm in 10 micron increments.

The applicator consists of:

- A special anodized aluminium frame to guide the knife blade. The frame has two end sections which serve as hand grips for the operator when drawing down wet films.
- A stainless steel knife blade with a precision ground edge. The slides in slots at the end sections which allows vertical adjustments of the blade.

- Two springs attached to the knife-blade and top plate. These exert an upward pressure on the blade and maintain it in contact against the two micrometre spindles to retain gap settings of the blade.
- Two precision made micrometre heads that can easily be set to give film thickness from 0-8 mm in increments of 10 microns. The accuracy of the micrometre heads is ± 2 microns.

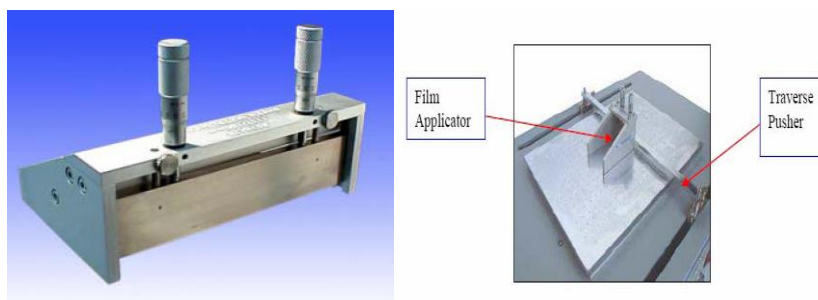


Figure 3-12 The dr. blade used for the coating process

(3) Drying:

The coated foil was dried in vacuum oven model (OV-11) to remove all the solvents used in the mixing process, which will degrade the electrodes if it wasn't removed completely. Figure 3-13 shows the vacuum oven used for the drying process. The drying process was conducted at 120°C for one hour, to remove the solvents.



Figure 3-13 The drying vacuum oven

After drying the electrodes, the electrodes were roll pressed to make sure the active material adhere well to the aluminum foil. The roll press machine is shown in Figure 3-14.



Figure 3-14 The roll pressing machine

(4) Slitting:

The aluminum foil coated with the active material is cut to the desired dimensions to form the electrodes. The slitting process is shown in Figure 3-15.

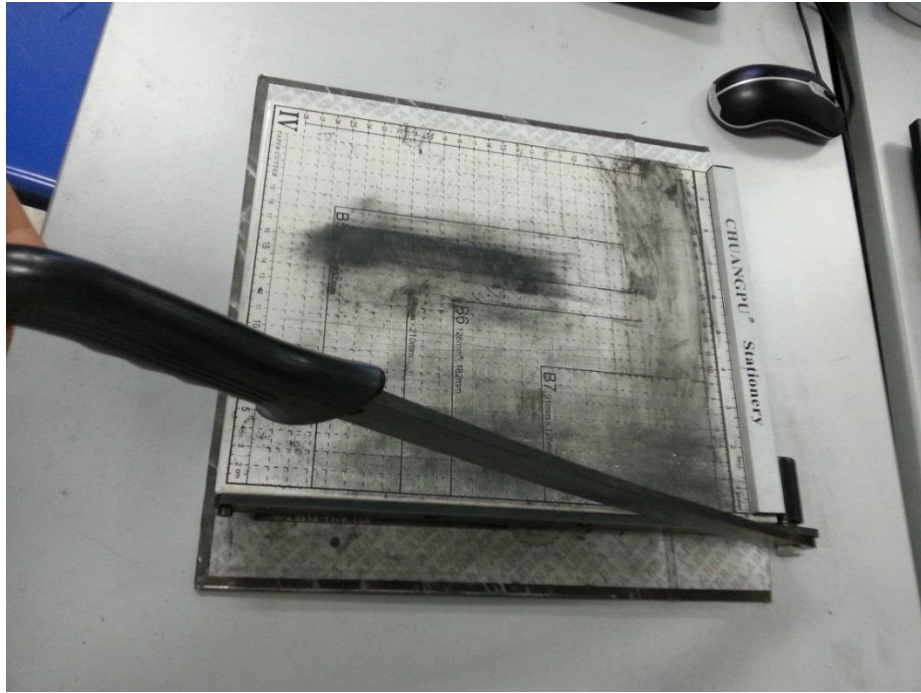


Figure 3-15 The slitting process

(5) Stitching:

Leads are attached to the current collectors using ultrasonic bonding to form contacts with the cathode and anode foil layers. Ultrasonic welding machine was used to attach the leads to the current collectors. The welder used is shown in Figure 3-16.



Figure 3-16 The ultrasonic welding machine

(6) Winding:

Separator paper layers are coiled between the electrodes layers, separating the conductive layers, as shown in Figure 3-17. Then the cell is wetted with an electrolyte under vacuum, before the assembly process. The winding machine used was custom made for the fabricating supercapacitor prototype with required dimensions.



Figure 3-17 The winding process

(7) Assembly:

After wetting, the cell was inserted into the case, a rubber seal is put on the leads and the cell is sealed. This process has to be done in glove box under controlled environment; moisture level has to be around 0.001 ppm in the case of organic electrolyte. Figure 3-18 shows the assembly process of the cell.

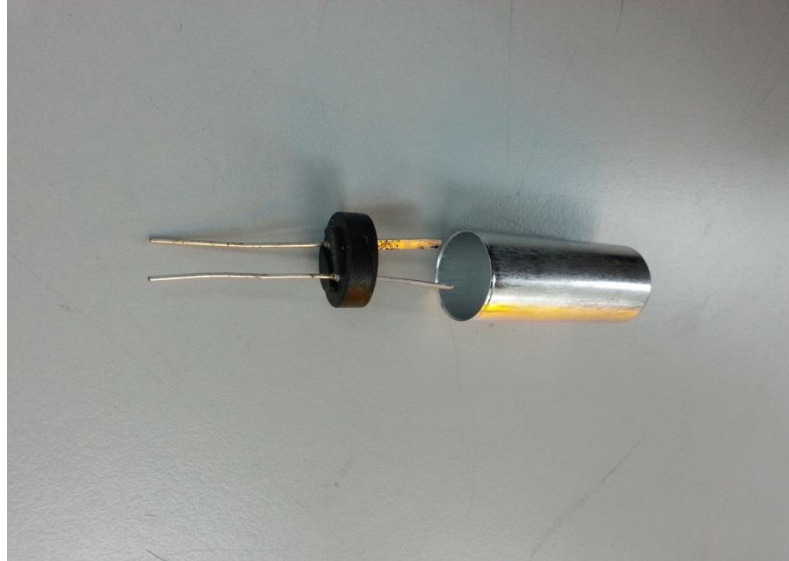


Figure 3-18 The assembly process of the cell

The glove box (KK011AS) used in the assembly process shown in Figure 3-19. The glove box provides the isolation from the environment (moisture and contaminant) as it can affect the durability of the capacitor.



Figure 3-19 The glove box

The final cylindrical supercapacitor prototype with the Sahz company trade mark (EnerStora) is shown in Figure 3-20.



Figure 3-20 The final product of supercapacitor

3.3.2 Coin Supercapacitor Fabrication Process

The fabrication process was performed according to the process flowchart for the coin supercapacitor manufacture as shown in Figure 3-21. Some of the critical processes are the AC percentage, binder percentage and mixing time are evaluated accordingly.

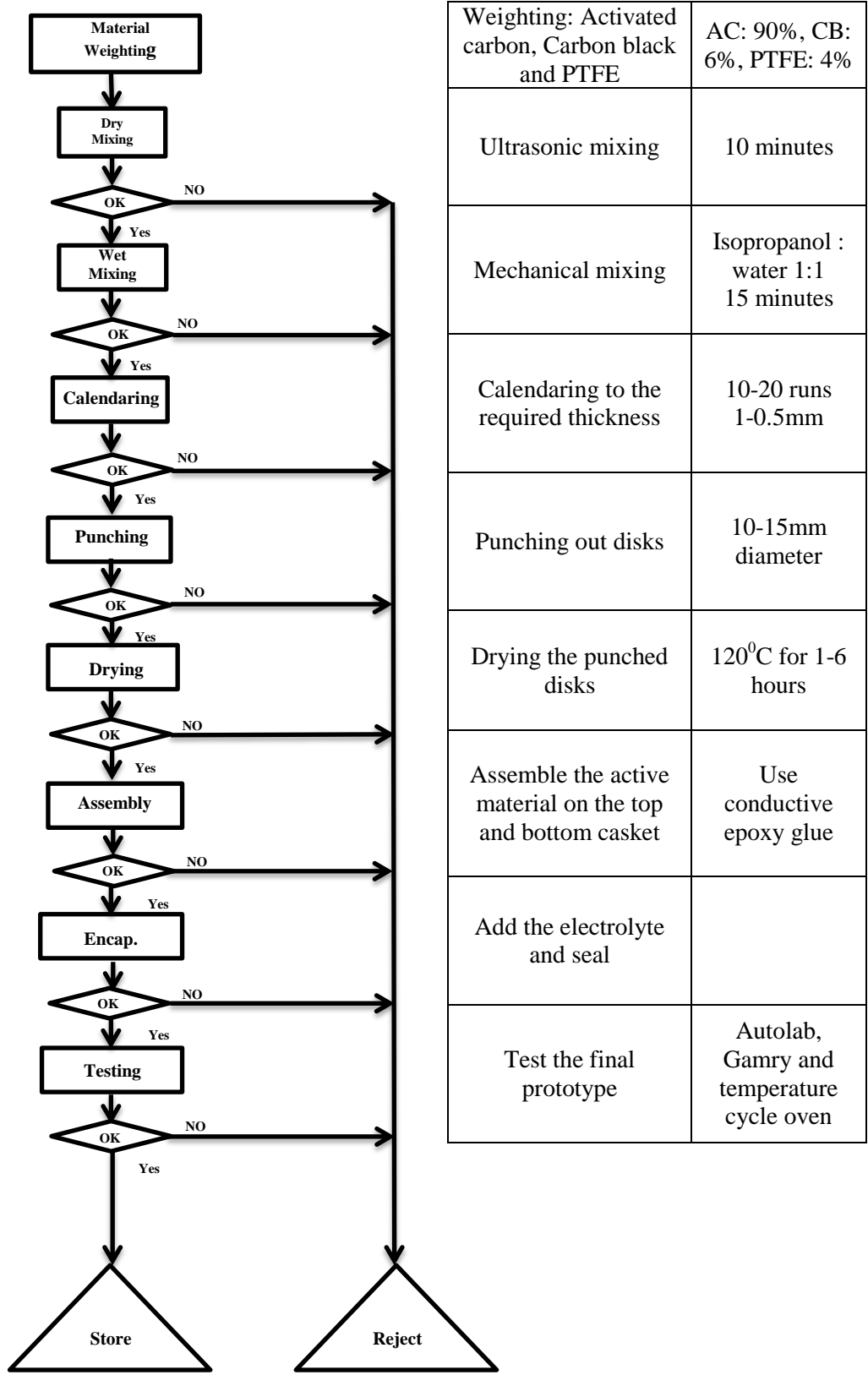


Figure 3-21 Process flowchart for the coin supercapacitor manufacturing

(1) Mixing:

The mixing process involves weighing the raw materials using an analytical balance and mixing the raw materials using a mechanical overhead stirrer. The mixing process is divided into two stages: a) dry mixing b) wet mixing. The dry mixing was done by mixing of the activated carbon powder and carbon black powder for a certain amount and time. This is followed by adding solvent to the mixed powders. The solvent consists of isopropanol and deionized water with ratio of 1:1. Lastly, the binder polytetrafluoroethylene (PTFE) is added to the paste, the mixing process is continued until the paste becomes a dough. Figure 3-22 shows the mixing machine and the final active material dough.



Figure 3-22 a) mixing the powders b) the dough

(2) Dough Calendering:

Activated material dough is rolled to form a sheet of desired thickness, this was done by using the calendering machine as shown in Figure 3-23. The machine has a heating element to heat the dough during the rolling process, the dough was rolled down in steps until the desired thickness is reached.

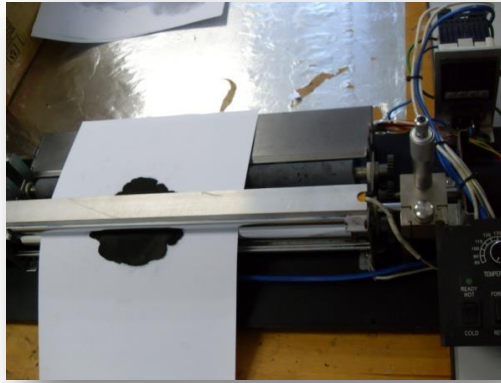


Figure 3-23 Calendering machine during calendering process

The active material after the calendering process is in sheet form, with a thickness of 0.7 mm. Figure 3-24 shows the dough sheet.



Figure 3-24 Dough sheet

(3) Punching:

Disks with specific diameter were punched out of the active material sheet, and then dried in vacuum oven to remove the solvents at 80⁰C. The punched disks are shown in Figure 3-25.

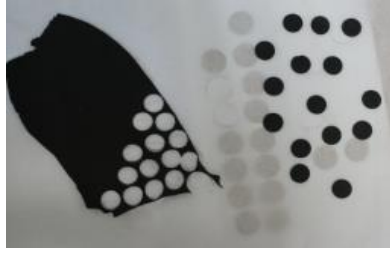


Figure 3-25 Punching process

The carbon sheet was punched using a 16 mm diameter circular shaped puncher. The carbon electrodes were then heated in the vacuum oven under pre-determined temperature and time to dry the punched disks.

(4) Adhesion:

A conductive adhesive (carbon black and PVDF) is used to glue the punched electrodes to the metal case and cap of the capacitor. This was done to improve the contact between the electrode and the current collector, which will result in lower ESR. Figure 3-26 shows the case and the cap with the active material disks attached.

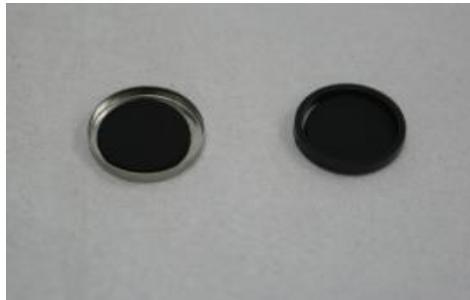


Figure 3-26 Active material disks glued to the case and the cap

(5) Electrolyte Filling:

Liquid electrolyte was added to the case and cap. The removal (heating under vacuum) of the solvents (isopropanol and deionized water) will make it easier for

the electrolyte ions to penetrate through the activated carbon pores which will lead to achieve more capacitance. The presence of solvents is expected to give unnecessary high resistance ESR and cause electrodes deterioration.

(6) Assembly and Sealing:

The final process in manufacturing the supercapacitor is the assembly and then sealing. The case and cap are assembled with a separator paper between them to electrically isolate but allowing ion transfer between the electrodes. Figure 3-27 shows the cases, caps and separators ready for the assembly process.



Figure 3-27 The cases, caps and separators

Then, the set was sealed using the crimper and the hydraulic press at 1 ton of pressure, the crimper and the press are shown in Figure 3-28.



(a)

(b)

Figure 3-28 a) the crimper b) the hydraulic press

(7) Testing:

All of the coin cells were subjected to electrical testing, that included the CV, charge-discharge and ESR testing. The Autolab AUT83475 and the Gamry 600 were used to perform the testing. Both testing equipments are shown in Figure 3-29.

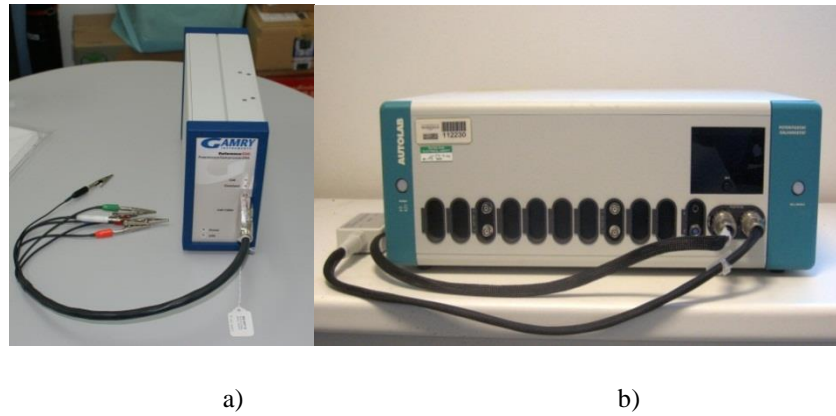


Figure 3-29 Testing equipment a) Gamry b) Autolab

The final disk shaped supercapacitor is shown in Figure 3-30, the casing model used for this supercapacitor is CR2016.



Figure 3-30 Final coin supercapacitor

The specifications of the CR2016 casing model are:

- Case (SS304)
- Cap (SS304) & Gasket (PP)
- Plate (SS304, 1.0t)
- Spring (SS304)

Figure 3-31 shows the CR2016 casing used for packaging the supercapacitor.



Figure 3-31 CR2016 casing

The dimensions of the CR2016 are shown in **Figure 3-32**.

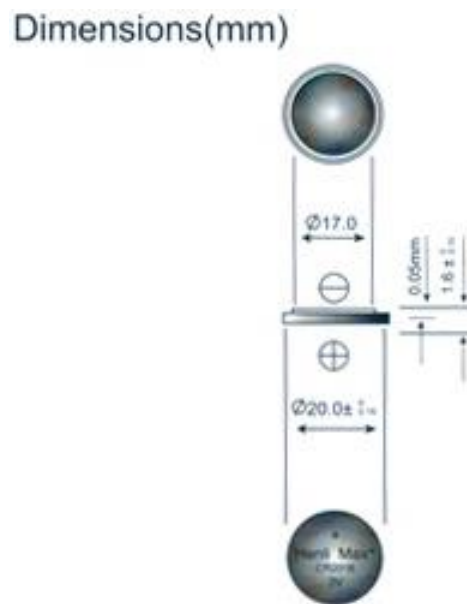


Figure 3-32 CR2016 dimensions

3.4 Electrolyte

Two different electrolytes were used in this research a) aqueous electrolyte and organic electrolyte. The aqueous electrolytes used were the KCl and Na₂SO₄, since they are in solid state, certain amounts of KCL was diluted in deionized water to achieve the desired concentration. This was done following the formula:

$$\text{Mass (g)} = \text{Concentration Volume (L)} * \text{Molecular Weight (g/mol)} \quad \text{Eq 3.1}$$

The organic electrolyte used was 1 M TEABF₄ in PC in acetonitrile solution. The specifications of the electrolyte are shown in Figure 3-33.

| Date : 28TH. SEP. 2009' | | Product : PuriEL(Battery Electrolyte) 1M TEABF ₄ in PC | |
|--------------------------------|-------------------|---|--------------|
| Quantity : 1kg | | Maker : TECHNOSEMICHEM CO.,LTD. | |
| Lot No. : TS9-1459 | | Shipment Date : 30TH. SEP. 2009' | |
| Item | Unit | Specification | Test Results |
| PC | wt% | 81.7 ± 1.0 | 81.7 |
| TEABF ₄ | wt% | 18.3 ± 0.5 | 18.3 |
| Moisture | ppm | - | 18.8 |
| HF | ppm | < 50 | Pass |
| Color | APHA | < 50 | Pass |
| Density (20°C) | g/ml ³ | - | 1.196 |
| Na | ppm | < 5 | Pass |
| K | ppm | < 5 | Pass |
| Ca | ppm | < 5 | Pass |
| Pb | ppm | < 5 | Pass |
| Fe | ppm | < 5 | Pass |
| Cl | ppm | < 5 | Pass |
| SO ₄ | ppm | < 10 | Pass |

Figure 3-33 Organic electrolyte specifications

3.5 Testing Processes

3.5.1 Cyclic Voltammetry

Cyclic voltammetry (CV) provides a measure of a supercapacitor's charge-response with regard to a changing voltage, and is therefore a means of evaluating capacitance. The procedure for obtaining a voltammogram is simple and required to apply series of changing voltages with a constant sweep rate (dV/dt) and record the charging current. The capacitance C can then be calculated using:

$$C = \frac{I}{s} \quad \text{Eq 3.2}$$

where I is the current and s is the sweep rate in V/s [89]. Often the voltammetry will be graphed as capacitance vs. voltage instead of current vs. voltage. An ideal capacitor with no resistance would display a rectangular shape, but most real EDLC voltammograms take the shape of a parallelogram with irregular peaks as shown in Figure 3-34.

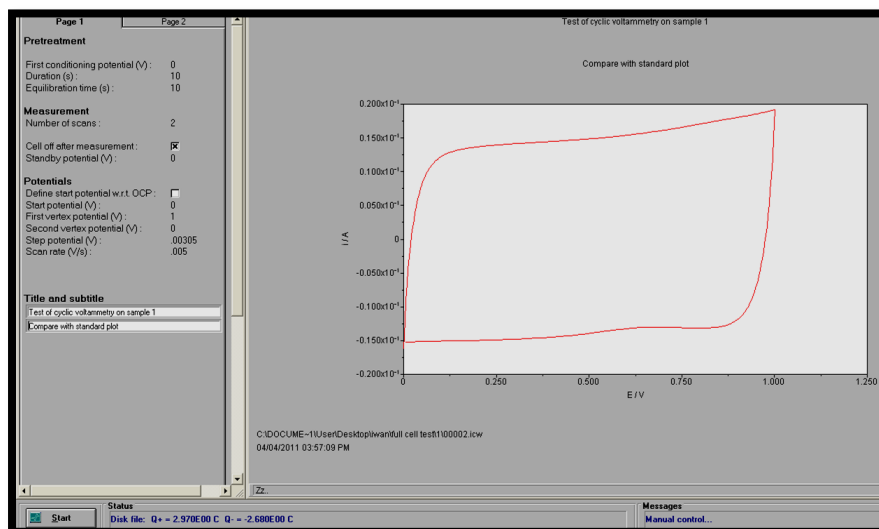


Figure 3-34 Voltammogram

Faster sweep rates correspond to charging and discharging at higher power levels. Multiple plots obtained at increasing sweep rates are therefore often displayed on the same graph to demonstrate the impact of power levels on the charging characteristics. From such plots it is evident that capacitance decreases at higher frequencies.

Voltammetry can also provide an indication of the degree of reversibility of an electrode reaction. A voltammogram that depicts a mirror-image represents a reversible reaction, but an irreversible process will have two separate charge and discharge profiles, the ends of which do not meet. Reversibility is an important factor in the search for new materials [56].

3.5.2 Constant-current charging

A method of evaluating a supercapacitor's energy and power densities is to perform constant-current charging. Charging or discharging the cell at constant current results in a voltage response. The current integral, $\int i dt$, is therefore a measure of charge delivery, and power is then determined by the product $I \times V$, and energy by $\frac{1}{2} Q \times V$ [80]. If the EDLC is assumed to be a capacitance in series with an ESR, the ESR can be determined by the ratio of voltage change to current change. This procedure is only accurate at low currents, however, and there is a significant departure from predicted behaviour at higher currents [90].

The galvanostatic charge-discharge test is used to measure the capacitance and the ESR of the supercapacitor. The charge-discharge graph of potential vs time is shown in Figure 3-35. The peak is enlarged to observe the current-resistance (IR) drop due to low electronic conductivity of the electrolyte used [90].

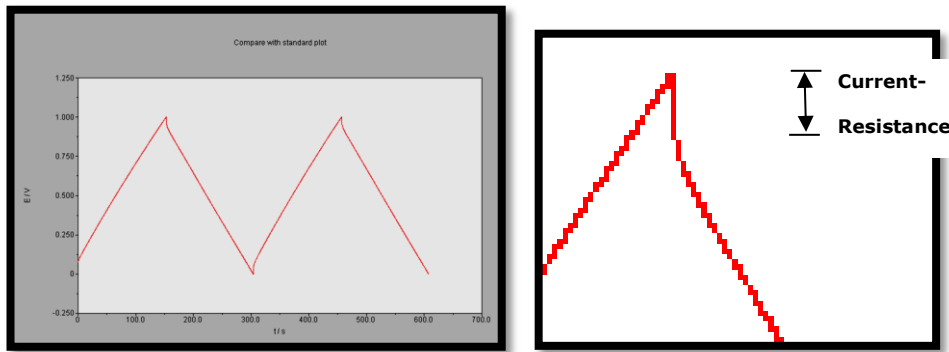


Figure 3-35 Charge-discharge graph

The equivalent series resistance, ESR value can be determined by using the following:

$$ESR (\Omega) = \frac{IR \text{ drop } (V)}{\text{current } (I)} \quad \text{Eq 3.3}$$

3.5.3 Impedance spectroscopy

Impedance spectroscopy is a powerful method of evaluating a component's performance in the frequency domain. Special equipment is required to apply a small AC voltage and measure the changes in magnitude and phase over a range of frequencies. The impedance can then be plotted on a Nyquist diagram as shown in Figure 3-36.

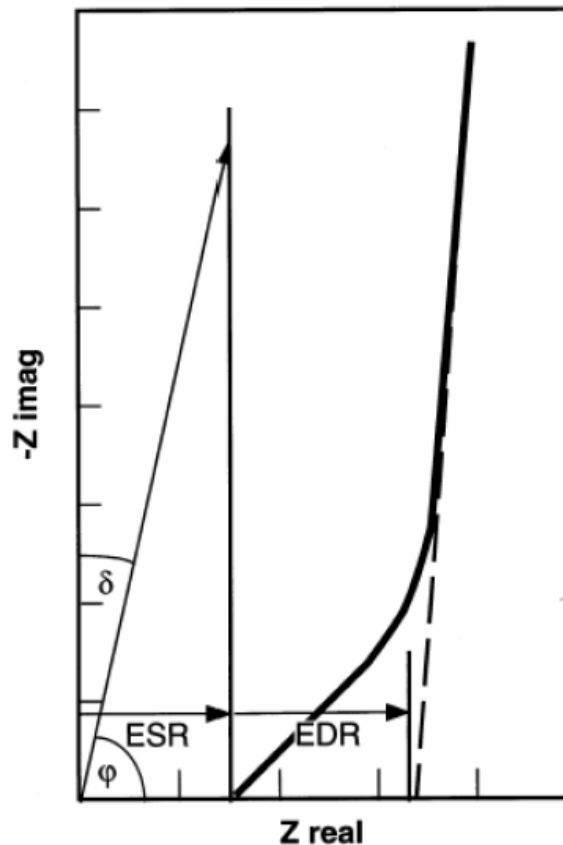


Figure 3-36 Nyquist diagram [20]

An ideal capacitor is represented by a vertical straight line shifted on the real axis by its ESR. At low frequencies a supercapacitor approaches a near vertical straight line shifted on the real axis by the ESR.

3.5.4 Constant-power cycling

Cyclic voltammetry, constant-current charging and impedance measurements are generally better suited to low-power measurements. During high-power operation they do not provide useful data for modelling, mainly due to the fact that most of the parameters to be determined are voltage-dependent, but changes in voltage are used to determine them. Constant-power cycling, however, can provide useful time

constant information at particular power levels which can be used to evaluate different components [91]. The procedure for power cycling involves charging the EDLC at a fixed power level until a chosen voltage is reached, at which point the current is reversed and discharging takes place.

3.5.5 Taguchi Technique

The Taguchi technique is an experimental design method using "off-line quality control" because it is a method of ensuring good performance in the design stage of products or processes. In our case we have used this approach to optimize the supercapacitor. The Taguchi technique was developed by Genichi Taguchi to improve the quality of manufactured goods, but it can also be applied to biotechnology [21]. Design of Experiments (DOE) using the Taguchi approach, one can economically achieve product/process design optimization in the manufacturing industry. The objective of using the Taguchi technique is to analyze the outcome of the experiment and then use it as a reference for future experiments. Furthermore, several parameters are set, and samples are made within a limited range, which is altered for each iteration, instead of following the conventional approach of making lots of samples to test each parameter. Once the parameter affecting a process have been determined, the levels at which these parameters should be varied must be evaluated.

This research addresses the implementation of Taguchi's technique in the optimization of supercapacitor manufacturing process. Design of experiments (DOE) can be used to determine the optimal levels for processes or design parameters. However, finding these optimal levels is not always an easy task. Industrial

experiments do not always go as planned because a nonsystematic approach is often taken by the experimenters. Thus, the following is a step-by-step plan for conducting the experiment, analyzing the results and implementing the solutions [92]:

- I- Recognition and Formulation: Recognizing the problem is an important step, not understanding the problem makes it more difficult to solve.
- II- Quality Characteristics: The selection of quality characteristics to measure the experiment's output. These outputs can be variable or attribute in nature.
- III- Selecting Parameters: It is the most important step of the experimental design procedure. If the wrong factors are selected or important factors are ignored, then the results may be inaccurate.
- IV- Classifying Factors: After selecting the design and process parameters, the next step is to classify them into control, noise and signal factors:
 - a) Control factors are those factors that can be controlled by the experimenter.
 - b) Noise factors are those factors that cannot be controlled, and they are difficult or are too expensive to control in the production environment.
 - c) Signal factors are those that affect the target performance of the characteristic, but generally have no influence on variability in the performance characteristic of the product or process.
- V- Determining levels: A level is the value that a factor holds in an experiment. The number of levels depends on the nature of the design and process parameter and whether or not the chosen parameter is qualitative or quantitative.

The levels need to be in an operational range of the product or process. Taguchi recommends the use of three levels if nonlinearity is expected in the main effect of control factor on the quality characteristic.

VI- Interactions: Interaction between two design and process parameters exists when the effect of one parameter on the quality characteristic is different at different levels of the other parameter. The interaction that should be studied needs to be determined. Orthogonal Array: (OA) are a set of tables of numbers created by Taguchi that allow experimenters to study the effect of a large number of control and noise factors on the quality characteristic in a minimum number of trials. Taguchi proposed the use of OAs for planning the optimization experiments. Conducting Phase: Conducting the experiment and recording the results. To ensure the validity of the experiment, the following points should be considered prior to conducting the experiment:

- **Location:** an appropriate location that is unaffected by external sources of noise.
- **Resource availability:** Making sure the necessary equipment, operation and materials are available before starting.
- **Cost-benefit analysis:** Verifying the experiment is necessary and justify that the benefits to be gained from the experiment will exceed the cost of the experiment.
- **Data sheets:** Use uncoded data sheets for running the experiment and coded data sheets for analyzing the data.
- **Randomize the trials:** Randomization is critical to ensure that bias is evaded during data gathering.
- **Replicate the experiment:** Replication is a process of running the experimental trials more than once.

VII- Analysis Phase: After conducting the experiment, analyze and interpret the results. If the experiment was planned and designed properly and conducted in accordance with the data sheet, then statistical analysis will provide sound and valid conclusions.

VIII- Implementation: To validate the conclusions from the experiment, a confirmatory experiment should be performed.

In this study, the capacitance (F) and the ESR of the supercapacitor are the desirable quality characteristics. There are other characteristics that can be measured, but the above quality characteristics are considered the most important criterion in this experiment.

The experimental procedure was carried out in a controlled environment in which the experimental conditions remained constant. This ensures that there is no effect on the results from external factors and that the only conditions varied during the experiment are the three control factors, which are binder percentage (PVDF), mixing duration and carbon black (CB) percentage. In particular, room temperature remained constant at 22 °C and remained stable during all of the experiments. The same quantities and types of materials were used for all cells. The fabrication process and testing equipment also remained the same.

Taguchi advocates the use of orthogonal array (OA) designs to assign the factors chosen for the experiment [93]. Orthogonal arrays allow one to compute the main effects via a minimum number of experimental trials [94]. OA are simple and useful tools for planning industrial experiments. Using an orthogonal array, an experimental plan can easily be constructed by assigning factors to columns of the orthogonal

array and then matching the different column symbols with the different factor levels [95]. Because there are 3 factors with 3 levels each, an L_9 orthogonal array was chosen. This means that 9 experimental trials with different combinations of the factors should be conducted to study the main effects. In general, the Taguchi design is preferred because it reduces the number of experiments significantly [96].

3.5.6 The Pilot Plant

The supercapacitor pilot plant will aid in designing the high volume manufacturing plant by enabling the optimization of the process using optimization techniques and determining the Bill of Material (B.O.M.) and Cost of goods sold (COGS) in order to set an appropriate price point for different products.

The pilot plant will also allow testing of the prototypes to the industry standards, and IEEE standards for our discrete products including the supercapacitor bank.

The pilot plant was designed based on the fabrication process steps of the supercapacitor, and the fabrications line in the pilot plant was divided to the following fabrication process stages:

- 1- The weighing stage: this area is dedicated to handling of the raw materials (AC, CB and Binders), where the analytical balance used to weigh the required amounts of raw material.
- 2- The mixing stage: at this area of the fabrication line, the raw materials are mixed together with the solvents, the mixing process is done using overhead mixing machine mentioned earlier.

- 3- Coating and dry stage: this part of the fabrication line is dedicated to the coating of the active material on the current collector using a dr. blade, and drying the electrodes inside the vacuum oven.
- 4- Slitting and stitching stage: at this stage the electrodes are cut to the required dimensions and the terminals are stitched to the electrodes. The winding process of the electrodes and the separator is done at this stage, before the assembly and the sealing process.
- 5- Assembly and sealing stage: at this stage the electrodes are assembled with the casing and the electrolyte is added before the sealing process. This is done inside the glove box in the case of organic electrolyte.

Figure 3-37 shows the fabrication setup for the pilot plant, illustrating the different stages of the fabrication process.

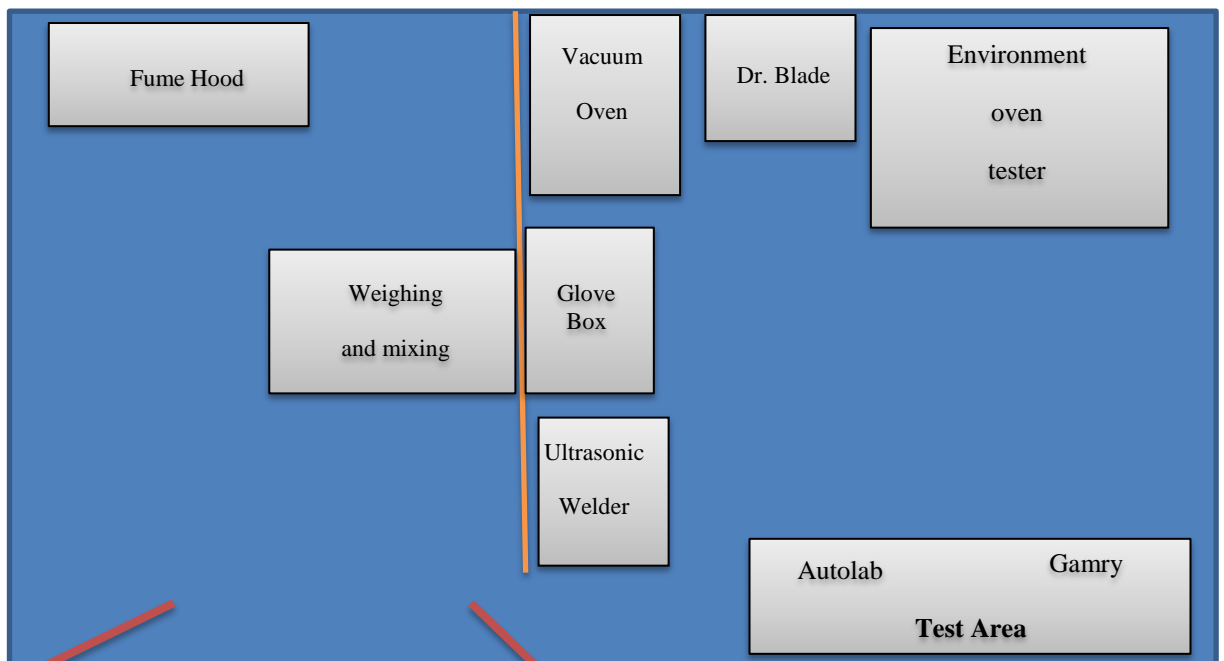


Figure 3-37 Pilot plant fabrication line setup

Figure 3-38 and Figure 3-39 show the pilot plant rooms and the different stations in each room.

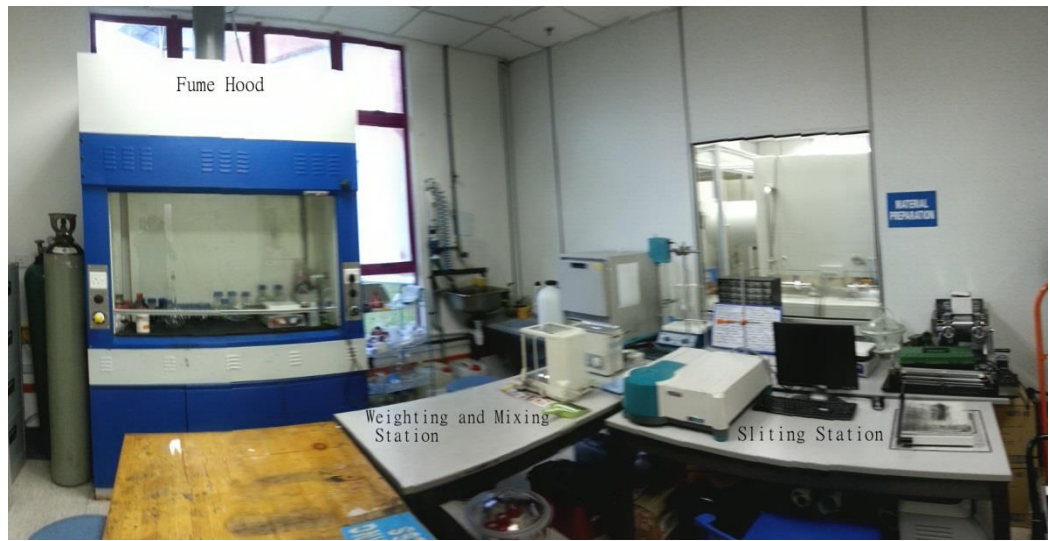


Figure 3-38 Pilot plant room 1



Figure 3-39 Pilot plant room 2

4. Results

4.1 Introduction

In this chapter, the experimental results of all the fabricated supercapacitor prototypes are presented, with listing of all the main parameters of each cell, such as, materials used, date of fabrication, CV testing, charge-discharge testing, capacitance measurements, Electrical Impedance Spectroscopy (EIS) and Equivalent Series Resistance (ESR).

In the first trial to fabricate a supercapacitor carbon nano tubes (CNT) were used as an active material. In the second trial, a few prototypes were fabricated using AC (activated carbon). The coconut AC was bought locally.

Table 4-1 shows the different supercapacitor prototypes that were fabricated and tested in the pilot plant. It shows a comparison between capacitance, ESR, packaging, active material and advantages and disadvantages of each prototype

Table 4-1 Different supercapacitor prototypes fabricated

| Prototype | Capacitance (F) | ESR (Ω) | Packaging type | Active material | Remarks |
|----------------|--------------------|---------------------|-------------------|--------------------|--|
| Cap-1 | 0.0617 | 17.9 | Flat | CNT | Bulky – CNT expensive |
| Cap-2 | 0.21 | 15 | Flat | CNT | Bulky – CNT expensive |
| Cap-3 | 0.354 | 14.5 | Disk | AC (coconut) | Packing not practical |
| Cap-4.3 | 1.275 | 22 | Flat | AC (coconut) | Packaging not practical |
| Cap-5.1 | 0.28 | 14.3 | Disk | AC (coconut) | Packaging not practical |
| B-7 | 3.33 | 3.36 | Coin | MSP-20 | Practical packaging, high capacitance, low ESR |
| CY-3 | 27.02 | 1.44 | Cylindrical | AC (coconut) | Practical packaging, very high capacitance, very low ESR |

4.2 EDLC prototypes using Carbon Nano Tubes

In the first attempt to fabricate a supercapacitor in the pilot plant, two simple prototypes were made using CNT as an active material, titanium sheet as current collectors and plastic sheets as packaging material.

4.3 EDLC prototype with flat panel geometry from CNT (Cap-1)

A supercapacitor cell was fabricated using CNT as active material, PVDF as a binder, aqueous KCl (1M) as electrolyte, titanium foil as a current collector, two flat plastic sheets as the casing for the cell and epoxy resin to seal the cell. Table 4-2 shows the materials used for fabricating Cap-1.

Table 4-2 Materials used for the fabrication

| Material | Description |
|-------------------|--------------------------|
| Activate material | CNT (0.5 g) |
| Binder | PVDF (50 mg) |
| Electrolyte | KCl (1M) |
| Titanium foil | 4cm x 4cm x 0.00127cm |
| Plastic sheets | 7cm x 7cm x 0.3cm |
| Separator | Filter paper (5cm x 5cm) |

The cell was tested using the Autolab potentiostat, a cyclic voltammetry CV test was run to observe the cell behavior. An almost ideal CV Graph was obtained and the capacitance of the cell was 0.0617 F. Figure 4-1 shows a picture of the fabricated cell. Manufacturing date was 3rd of March 2008.



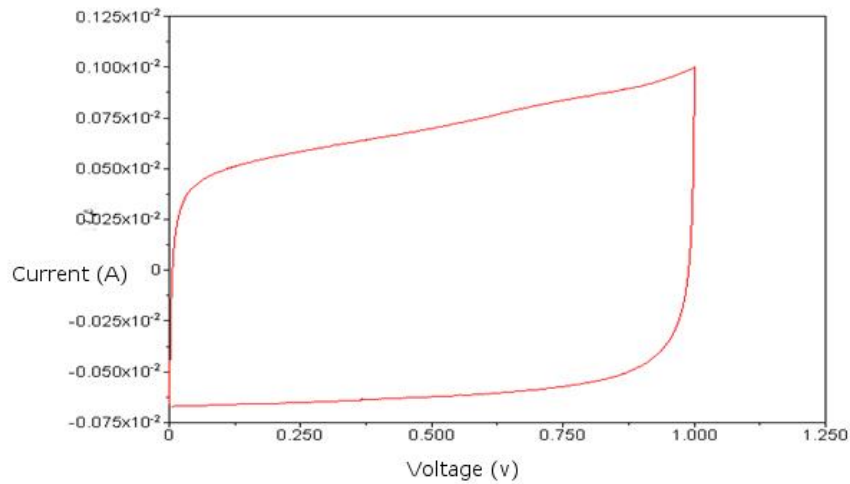
Figure 4-1 CNT supercapacitor Cap-1

Table 4-3 shows the measured parameters of this cell. The specific capacitance is 40 F/g and the ESR is 17.9 Ω . As this was the first fabricated cell, the capacitance was acceptable but the ESR was in the high range. Improvements to lower the ESR and increase the capacitance in the following prototypes are needed.

Table 4-3 The measured parameters of the Cap-1

| Capacitor | Capacitance (F) | Specific capacitance (F/g) | ESR (Ω) |
|-----------|--------------------|-------------------------------|---------------------|
| Cap-1 | 0.0617 | 40 | 17.9 |

Figure 4-2 shows the CV measurements for this supercapacitor cell. The measurement was done at a scan rate of 10mV/s and voltage window of 1 volt and the CV curve confirms capacitor behaviour, which is ideally a square shape curve.



C:\Autolab\Data\#1-CNT\#1-CNT-10mv.ocw
07/07/2008 11:22:33 AM

Figure 4-2 Cyclic voltammety curve for Cap-1 (at scan rate of 10mV/s)

4.3.1 EDLC prototype with flat panel geometry from CNT (Cap-2)

The second prototype supercapacitor was fabricated using the same process used for the first prototype, except the coated layer of CNT on the current collector was made thicker, by coating a thicker layer of the CNT slurry. The capacitance for this cell is 0.21 F, which is improved by a factor of 3.4 compared to the first prototype. On the other hand the ESR was still high. Fabricating date is 10th of March 2008. Table 4-4 shows the materials used for the fabrication process:

Table 4-4 Materials used for the fabrication

| Material | Description |
|-------------------|-----------------------|
| Activate material | CNT (0.5 g) |
| Binder | PVDF (50 mg) |
| Electrolyte | KCl (1M) |
| Titanium foil | 4cm x 4cm x 0.00127cm |
| Plastic sheets | 7cm x 7cm x 0.3cm |
| Separator | Filter paper |

The voltage rating for this cell is 1 V, the capacitance is 0.21 F and the specific capacitance is 42 F/g. Figure 4-3 shows the fabricated cell.



Figure 4-3 Supercapacitor cell Cap-2

Table 4-5 lists the parameters for the supercapacitor cell Cap-2, including the capacitance and the specific capacitance.

Table 4-5 The parameters list of the Cap-2

| Capacitor No. | Capacitance (F) | Specific capacitance (F/g) |
|---------------|--------------------|-------------------------------|
| Cap-2 | 0.21 | 42 |

Figure 4-4 shows the CV for the cell at a scan rate of 10 mV/s and voltage window of 1 V. The CV curve shows a typical supercapacitor behavior.

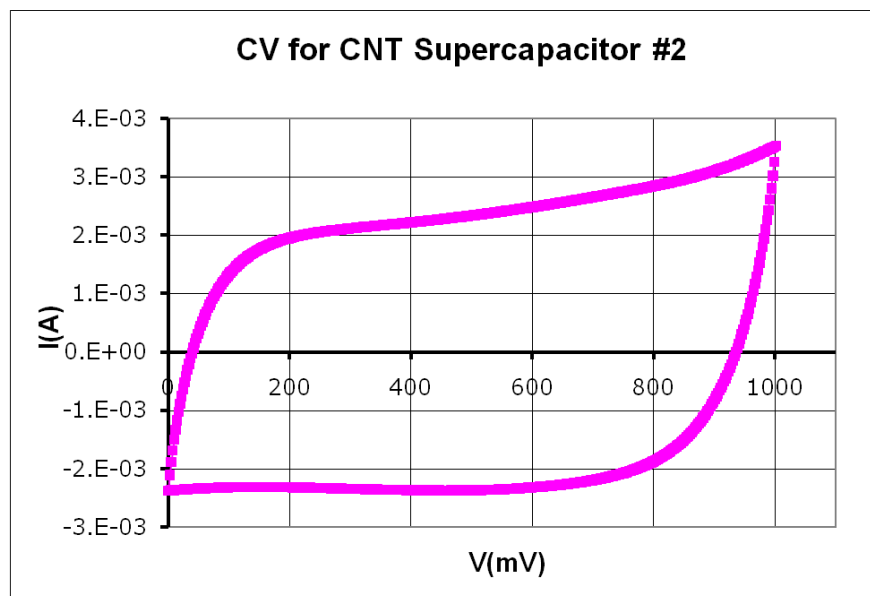


Figure 4-4 Cyclic voltammetry for Cap-2 supercapacitor at 10 mV/s

4.4 Supercapacitor prototypes using Coconut shell-based Activated Carbon

4.4.1 Disk-shape prototype using AC (Cap-3)

Figure 4-5 shows a picture of the fabricated supercapacitor. Fabrication date is 27th of March 2008.

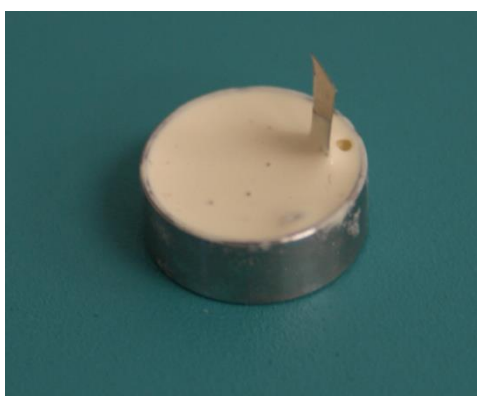


Figure 4-5 Picture of the supercapacitor cell Cap-3

Degassing was used to remove the air in the pressed powder, which was done by placing the electrodes in the vacuum oven. Before degassing, the capacitance was measured and found to be 0.24 F and the ESR is 14.5 Ω . After degassing the capacitance was increased to 0.354 F at 5 mV/s scan rate, and the weight of each electrode was 1 mg. The increase in capacitance attributed to removing the air in the electrodes, which allowed more electrolyte penetration. Table 4-6 lists the different capacitances obtained at different scan rates. The lower the scan rates the higher the capacitance.

Table 4-6 Capacitances of Cap-3 obtain at different scan rates

| Capacitance (F) | Scan Rate (mV/s) |
|--------------------|---------------------|
| 0.207 | 50 |
| 0.268 | 20 |
| 0.3196 | 10 |
| 0.354 | 5 |

The specific capacitance was calculated using the following steps:

The area of the supercapacitor:

$$A = \eta R^2 = 1.13 \text{ cm}^2 \quad \text{Eq 4.1}$$

$$\text{Specific capacitance} = \frac{0.354}{1 \times 10^{-2}} * 2 = 70.8 \text{ F/g} \quad \text{Eq 4.2}$$

The specific capacitance is 70.8 F/g for the first disk-shape prototype design. The cell had some design problems, like the electrode active material did not have enough mechanical strength to hold together. This caused the supercapacitor to lose a lot of potential capacitance after few days. Furthermore, the sealing (silicon epoxy) was not proper, and the electrolyte leaked out and the cell dried out during the testing process.

Table 4-7 below shows the materials used to fabricate this prototype:

Table 4-7 Materials used for fabrication

| Material | Description |
|---------------------------------|---|
| Activate material | Coconut shell-based Activated Carbon 90% |
| Binder | 10% PVDF |
| Electrolyte | KCl (1M) |
| Dimensions | 1.13 cm (Diameter) |
| Separator | Filter paper |
| Current Collector Configuration | Circular |
| Current Collector Material | stainless steel mesh |
| Voltage Rating | 1 V |
| Capacitance | 0.354 F at 5 mV/s |
| Specific Capacitance | 70.8 F/g |

Table 4-8 lists the parameters for the supercapacitor cell Cap-3, including the capacitance, the specific capacitance and the ESR.

Table 4-8 Cap-3 specifications

| Capacitor No. | Capacitance (F) | Specific capacitance (F/g) | ESR (Ω) |
|---------------|-----------------|----------------------------|------------------|
| Cap-3 | 0.354 | 70.8 | 14.5 |

Figure 4-6 shows the CV measurements for the Cap-3. Clearly it shows the capacitor typical behavior, and the cell was tested at scan rate 10 mV/s and a range of 0 V to 1 V window.

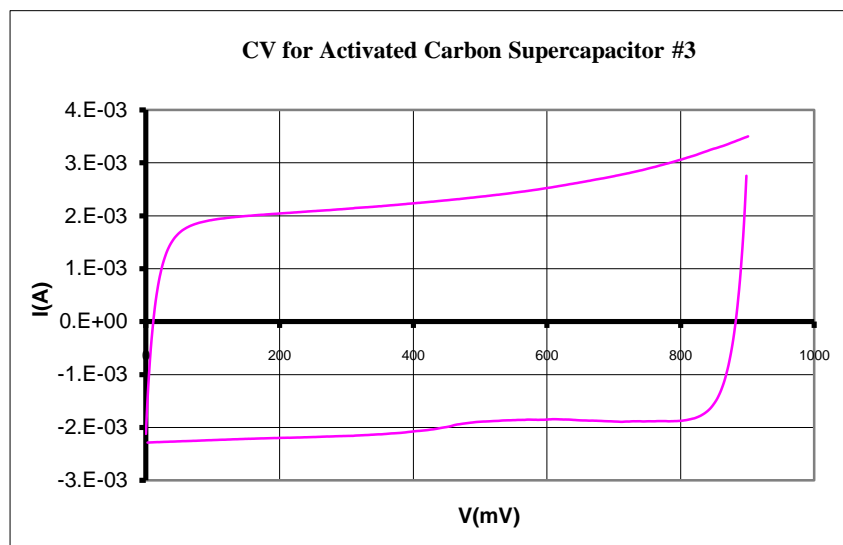


Figure 4-6 Cyclic voltammetry for Cap-3 supercapacitor (scan rate 10 mV/s)

The electrochemical impedance spectroscopy (EIS) testing was done for this cell at range of frequency 0.01 Hz – 10 KHz. The capacitance behavior can be seen in Figure 4-7, where, the semicircle and the straight line represent a capacitor behavior.

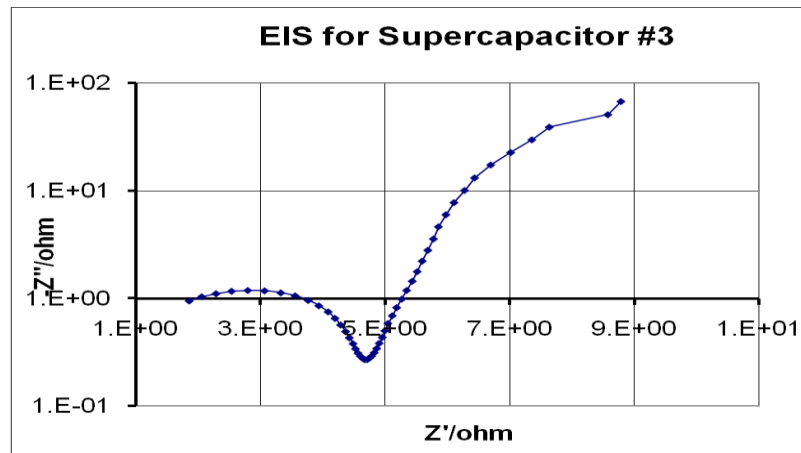


Figure 4-7 EIS testing for Cap-3 supercapacitor

Figure 4-8 shows the charge–discharge curve for the Cap-3. This curve was used to measure the capacitance and ESR for the cell, using the drop in at the beginning of the discharge cycle the ESR was calculated.

Knowing the charging current I and the voltage drop V the ESR can be calculated using the following equation, where the drop is equal to:

$$V = I * R \tag{Eq 4.3}$$

In this case ESR was 14.5 Ω , which is rather high for supercapacitor, and that can be attributed to the problem of the AC particle to particle contact and the electrical contact between the current collector and the active material [97].

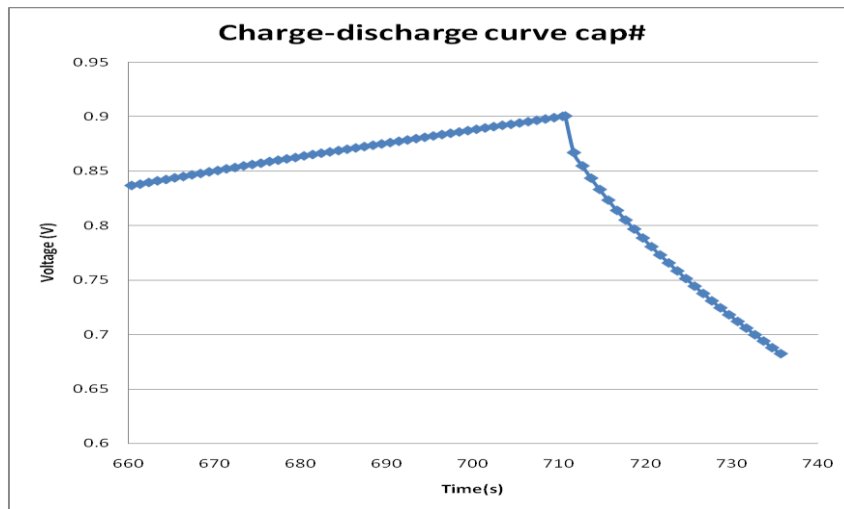


Figure 4-8 Charge-discharge curve for Cap-3

4.4.2 Flat -shape supercapacitor prototype (Cap-4)

In this part, three supercapacitor cells were fabricated using coconut shell-based activated carbon with different PVDF binder concentrations and 1 M potassium chloride (KCL) as electrolyte. The objective of this part is to find the optimum value of binder that will provide the highest specific capacitance. Table 4-9 lists the three cells parameters and the percentages of each material used to fabricate each cell. Fabrication date is 30th of June 2008.

Table 4-9 Compositional percentages of AC & PVDF.

| Prototype | AC weigh (g) | PVDF powder weigh (g) | PVDF Concentration (%) |
|-----------|--------------|-----------------------|------------------------|
| Cap-4.1 | 0.9 | 0.1 | 10 |
| Cap-4.2 | 0.85 | 0.15 | 15 |
| Cap-4.3 | 0.8 | 0.2 | 20 |

Table 4-10 shows the fabricated cells specific capacitance and the ESR. It can be seen that, the more binder used the higher the ESR, which could be attributed to the fact that the binder is considered as electrical isolating material. The capacitance measured at scan rate 5mV/s and the ESR measured at 20 mA charging current.

Table 4-10 Capacitance and ESR measurements

| PVDF % | Equivalent Series Resistances (ESR, Ω) | Specific Capacitance (F/g) |
|---------------|---|-----------------------------------|
| 10 | 10.1 | 40 |
| 15 | 11 | 19.9 |
| 20 | 22 | 44 |

The largest specific capacitance, 44 F/g is obtained using a sample of coconut-shell-based activated carbon with 20% PVDF concentration. The amount of sample fabricated on each electrode should be constant and same for each supercapacitor for a better comparison purpose.

Specific capacitance for the 10% PVDF prototype

$$\left(\frac{1.04 F}{52 mg}\right) * 2 = 40 F/g \quad \text{Eq 4.4}$$

For 15% PVDF,

$$\left(\frac{0.975 F}{98 mg}\right) * 2 = 19.9 F/g \quad \text{Eq 4.5}$$

For 20% PVDF,

$$\left(\frac{1.275 F}{58 mg}\right) * 2 = 44 F/g \quad \text{Eq 4.6}$$

Following are the parameters and the measurements done on the three prototypes. The parameters are the capacitance, the specific capacitance and ESR, the testing done are the CV, EIS and the charge-discharge.

- Prototype of Cap-4.1

Table 4-11 shows the measured parameters of this cell. Figure 4-9, Figure 4-10 and Figure 4-11 show the CV, EIS and the charge discharge curve respectively.

Table 4-11 Cap-4.1 parameters

| Prototype | Capacitance (F) | Specific capacitance (F/g) | ESR (Ω) |
|-----------|--------------------|-------------------------------|---------------------|
| 4.1 | 0.975 | 19.9 | 11 |

The CV test was done to observe the behavior of the cell, for a window of 1 V and 5 mV/s scan rate. The CV curve shape is close to a perfect ideal supercapacitor behavior, which should look like a square.

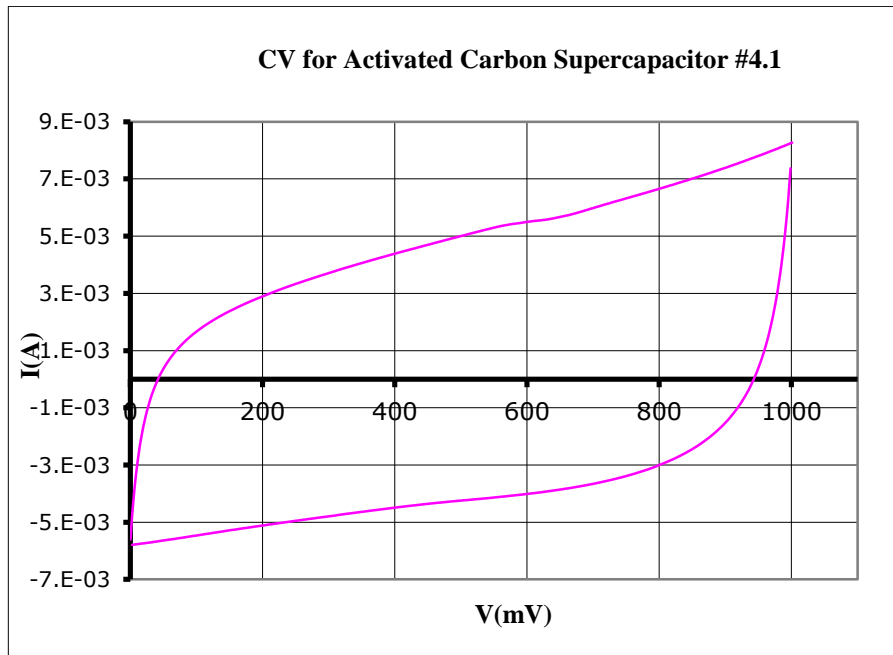


Figure 4-9 Cyclic voltammetry for Cap-4.1 supercapacitor (5mV/s)

The EIS plot shows the characteristics of supercapacitor, which displays a curve in the high-frequency and a linear curve in the low-frequency region. The curve in the high-frequency region is related to the reaction kinetics at the electrode and electrolyte interfaces. The linear curve at the low-frequency region can be attributed to the diffusion controlled process in the electrolyte. The internal resistance of the cell can be obtained from the high-frequency interception of real axis.

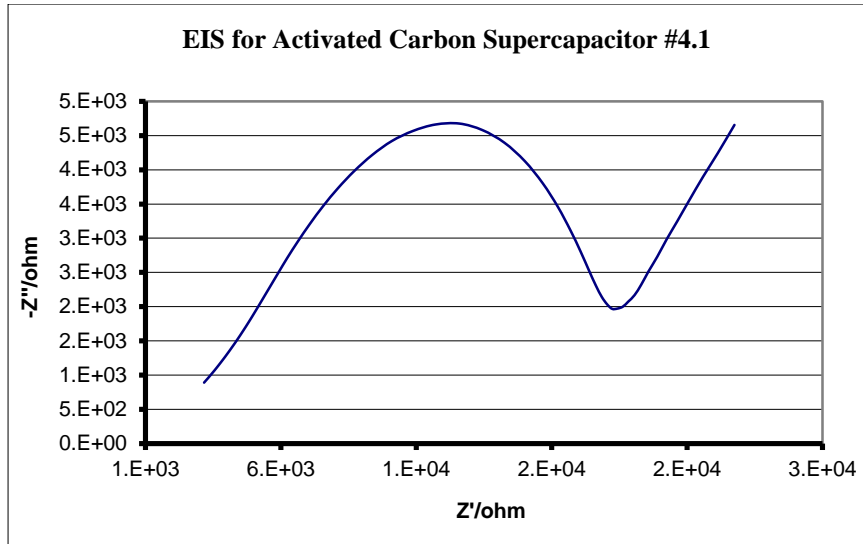


Figure 4-10 EIS measurements for Cap-4.1

Charge–discharge measurements were conducted to determine the capacitance and the ESR of the cell at different number of life cycles.

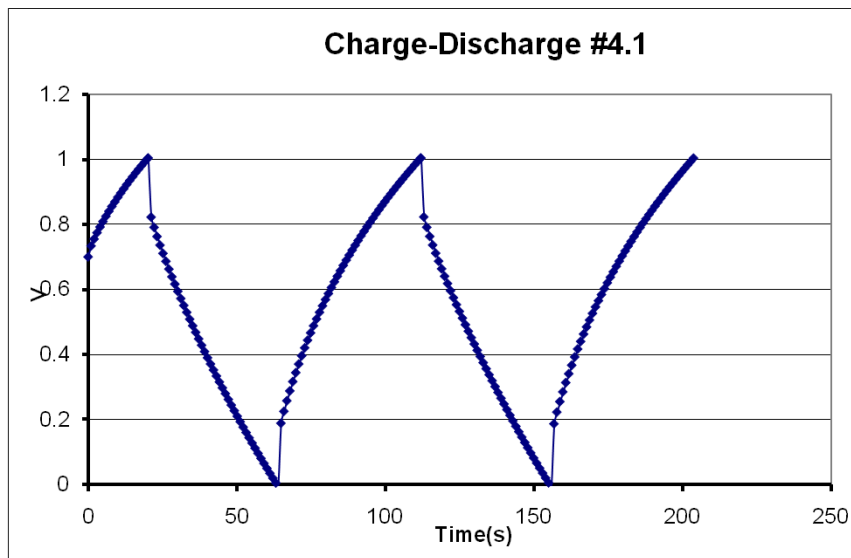


Figure 4-11 Charge-discharge measurements for Cap-4.1

- **Prototype of Cap-4.2**

Table 4-12 shows the measured parameters of this cell. Figure 4-12, Figure 4-13 and Figure 4-14 show the CV, EIS and the charge discharge curve respectively.

Table 4-12 Cap-4.2 parameters.

| Prototype | Capacitance (F) | Specific capacitance (F/g) | ESR (Ω) |
|-----------|--------------------|-------------------------------|---------------------|
| 4.2 | 1.04 | 40 | 10 |

The CV test was done to observe the behavior of the cell, for a voltage window of 1 V and 10 mV/s scan rate. The CV curve shape is a close resemblance to a perfect ideal supercapacitor behavior. The capacity of this cell is higher than the (Cap-4.1), the improvement can be noticed in the CV curve, which resembles the square shape of ideal supercapacitor.

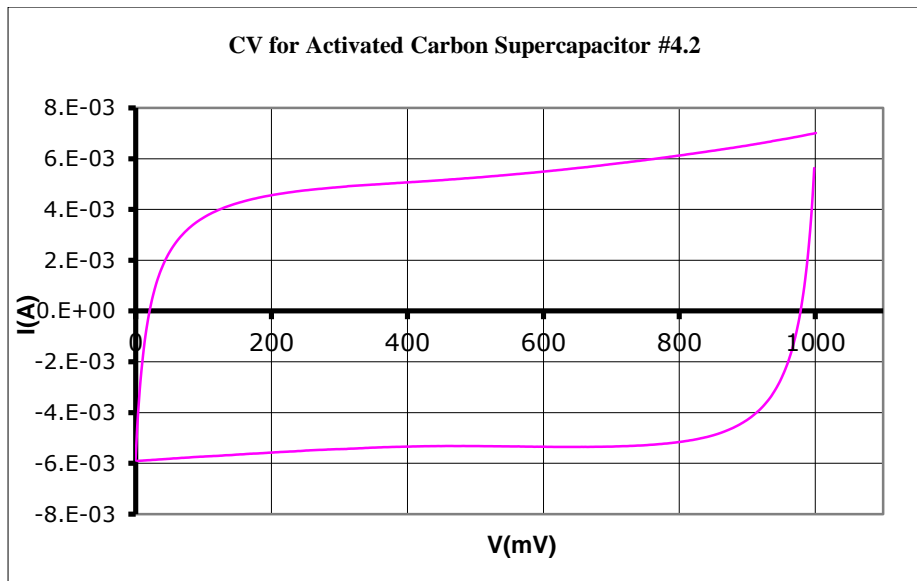


Figure 4-12 Cyclic voltammetry for Cap-4.2 at 10mV/s

The EIS plot shows the characteristics of supercapacitor, the ESR for this cell is almost the same value as for Cap-4.1.

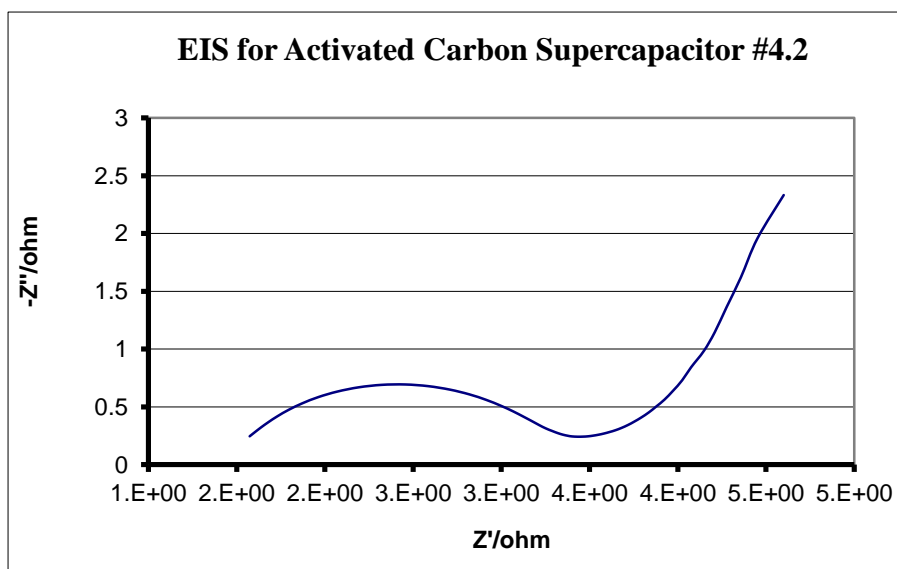


Figure 4-13 EIS measurements for Cap-4.2

Charge–discharge measurements were conducted to determine the capacitance and the ESR of the cell at different number of life cycles.

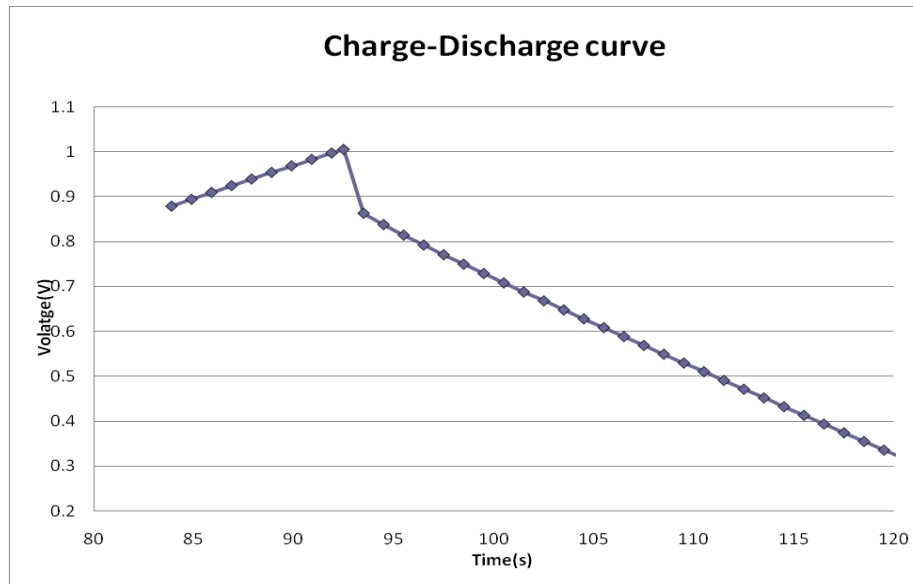


Figure 4-14 Charge-discharge measurements for Cap-4.2

- **Prototype of Cap-4.3**

Table 4-13 shows the measured parameters of this cell Figure 4-15 and Figure 4-16 show the CV and EIS curves respectively. Fabrication date is 30th of June 2008.

Table 4-13 Cap-4.3 parameters

| Prototype | Capacitance (F) | Specific capacitance (F/g) | ESR (Ω) |
|-----------|--------------------|-------------------------------|---------------------|
| 4.3 | 1.275 | 44 | 22 |

The CV test was done to observe the behavior of the cell, for a window of 1 V and 10 mV/s scan rate. The CV curve shape is a close resemblance to an ideal supercapacitor behavior. The capacity had improved compared to Cap-4.2.

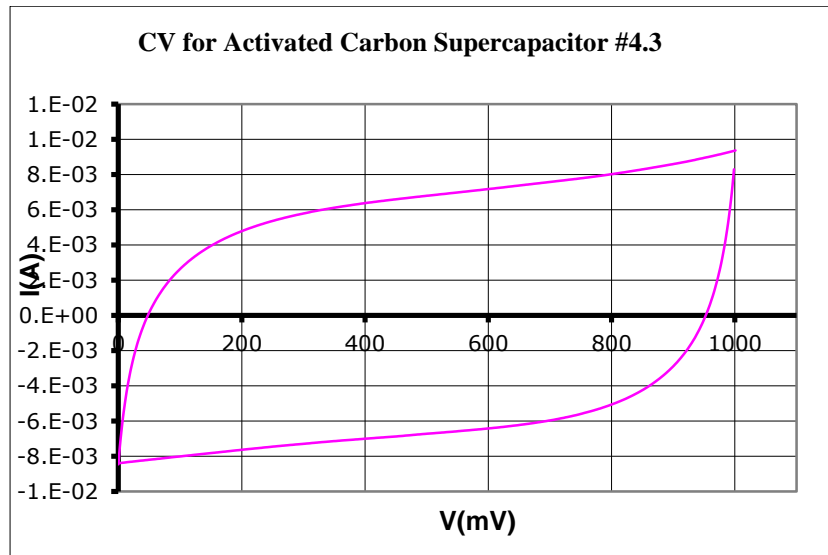


Figure 4-15 Cyclic voltammetry for Cap-4.3 at 10 mV/s

The EIS plot shows the characteristics of supercapacitor, the ESR for this cell is higher compared to Cap-4.2. That could be due to the thicker layer of the active material.

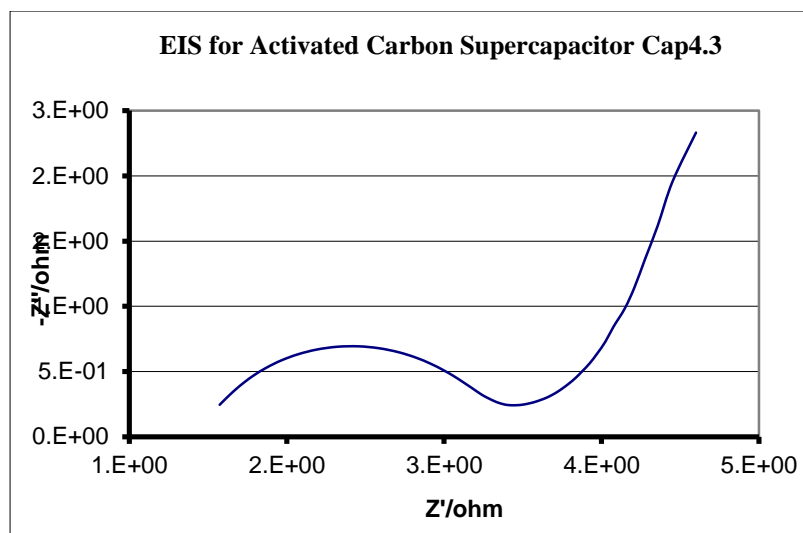


Figure 4-16 EIS measurements for Cap-4.3

4.4.3 Disk-shape supercapacitor Prototype Cap-5

Two supercapacitor cells were fabricated using coconut shell-based activated carbon, aqueous KCl (1M) as electrolyte, stainless steel mesh as current collector. Figure 4-17 shows the assembled supercapacitor cell.

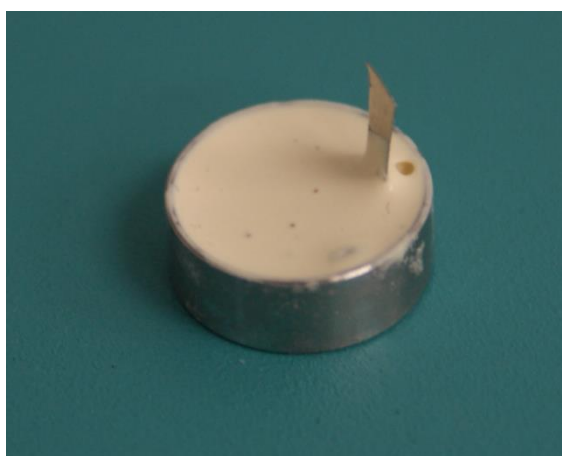


Figure 4-17 Supercapacitor Cap-5

Table 4-14 shows the results of testing under potential window of 1 V & scan rate of 5 mV/s. Fabrication date 2nd of July 2008.

Table 4-14 Cap-5 prototypes parameter's

| prototype | Capacitance (F) | Specific capacitance (F/g) | ESR (Ω) |
|-----------|-----------------|----------------------------|------------------|
| 5.1 | 0.28 | 56 | 14.3 |
| 5.2 | 0.118 | 40 | 17.9 |

Figure 4-18, shows the CV measurements for the Cap-5.1 cell. The CV curve resembles the ideal supercapacitor behavior. The capacitance for this prototype is 0.28 F.

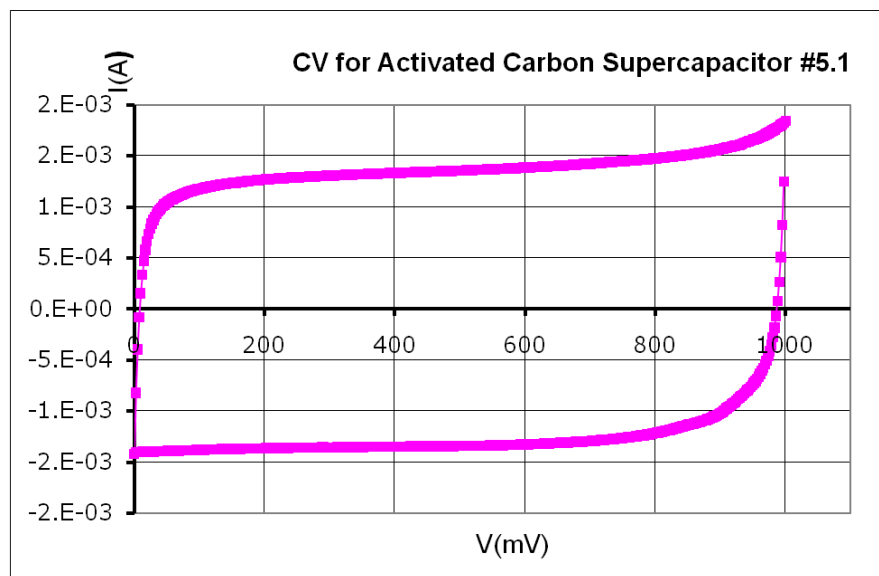


Figure 4-18 Cyclic voltammetry for the Cap-5.1

Figure 4-19 shows the EIS curve for the Cap-5.1 supercapacitor cell, which shows the supercapacitor behavior.

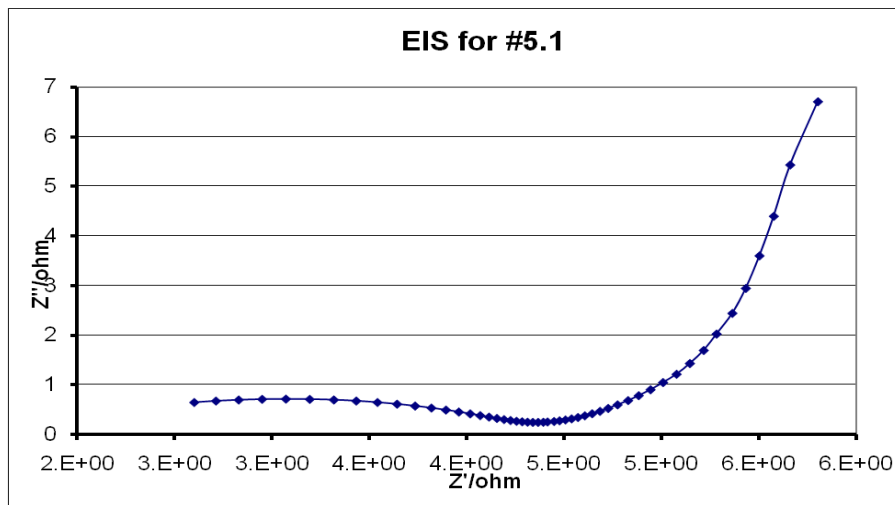


Figure 4-19 EIS measurements for Cap-5.1 supercapacitor

Figure 4-20, shows the charge-discharge curve for the Cap-5.1 supercapacitor cell, which used to measure the ESR and the capacitance for this cell. The ESR for this prototype is 14.3 Ω .

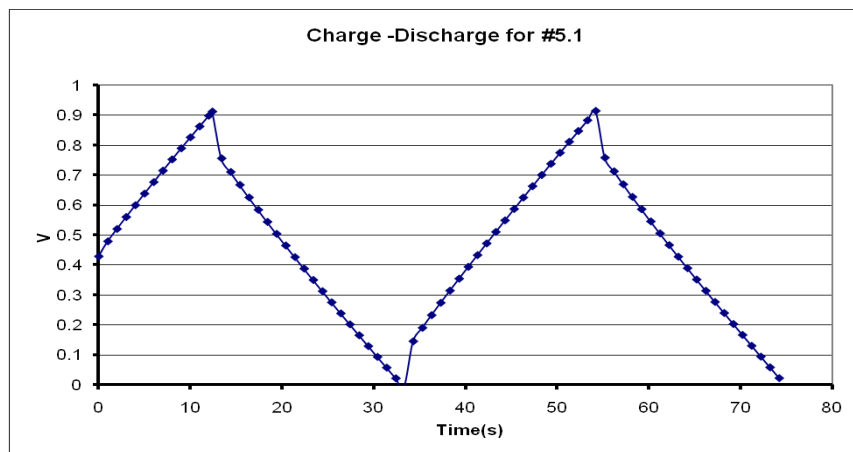


Figure 4-20 Charge-discharge measurements for Cap-5.1

Figure 4-21 shows the CV measurements for the Cap-5.2 supercapacitor cell. It shows very good resemblance of the ideal supercapacitor behavior, scan rate was 5 mV/s.

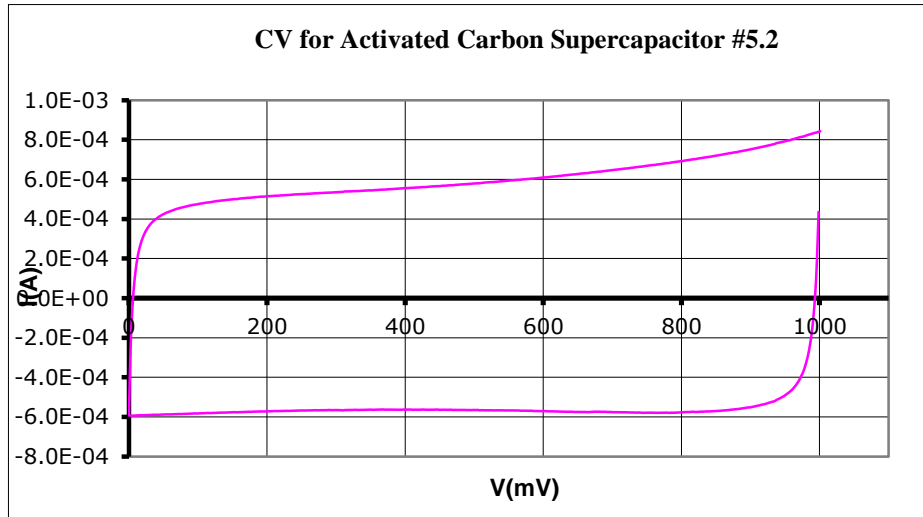


Figure 4-21 Cyclic voltammetry for Cap-5.2

Figure 4-22 shows the EIS curve for the Cap-5.2 supercapacitor cell. From this curve the capacitance were measured to confirm the charge-discharge curve capacitance measurement.

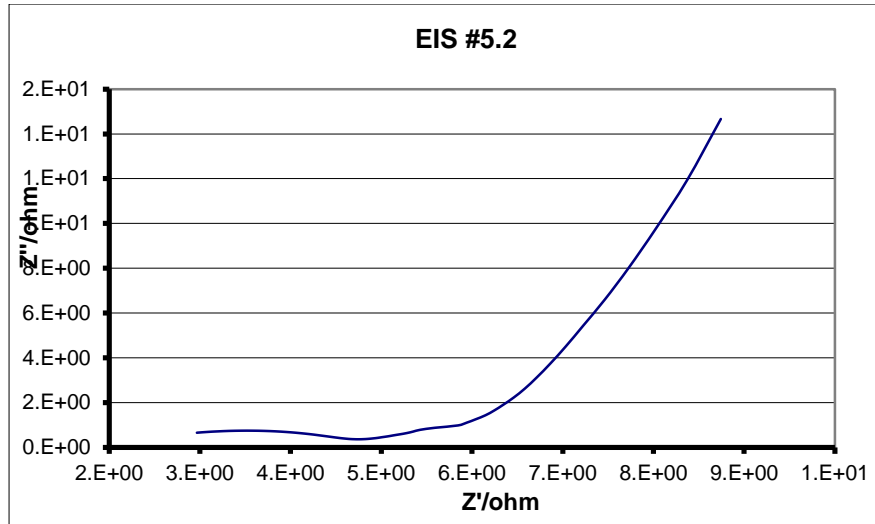


Figure 4-22 EIS measurements for Cap-5.2

Figure 4-23 shows the charge-discharge curve for the Cap-5.2 supercapacitor cell, which used to measure the ESR and the capacitance for this cell.

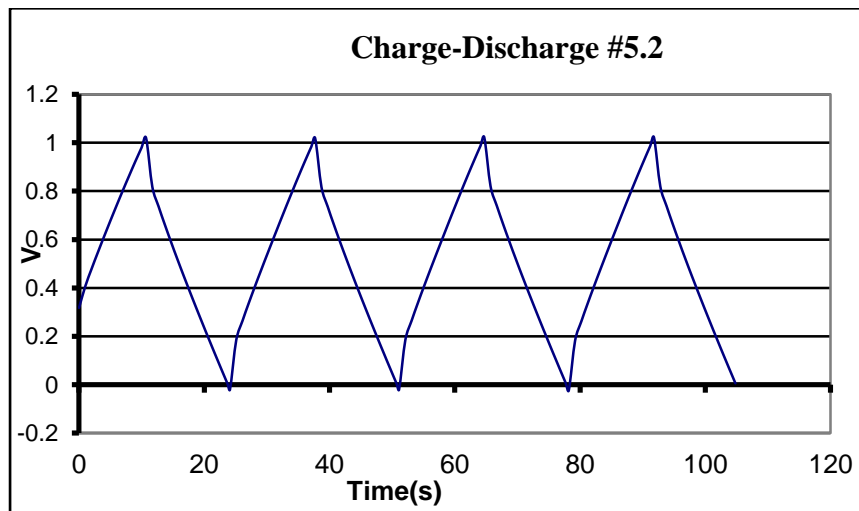


Figure 4-23 Charge-discharge measurements for Cap-5.2

4.5 Cylindrical Supercapacitor Prototypes

Few cylindrical supercapacitor prototypes were fabricated using different AC (coconut, MSP-20) and different conductive agent (carbon black, KETJEN black), the fabricated prototypes were labeled CY-1 to CY-18.

Table 4-15 lists the materials and the amounts used for fabrication. The percentages of the materials used were as follows (AC 80%, CB 10%, PVDF 10%).

Table 4-15 Materials used for the cylindrical prototypes

| prototype | Activated Carbon | | Conductive agent | | Binder | |
|----------------------|------------------|------------|------------------|------------|--------|------------|
| | Type | Amount (g) | Type | Amount (g) | Type | Amount (g) |
| CY-1 | Coconut (AC) | 4 | Carbon Black | 0.5 | PVDF | 10 |
| CY-2 | Coconut (AC) | 4 | Carbon Black | 0.5 | PVDF | 10 |
| CY-3 | Coconut (AC) | 4 | Carbon Black | 0.5 | PVDF | 10 |
| CY-4 | MSP-20 | 4 | KETJEN BLACK | 0.5 | PVDF | 10 |
| CY-5 | MSP-20 | 4 | KETJEN BLACK | 0.5 | PVDF | 10 |
| CY-6 to CY-11 | MSP-20 | 4 | KETJEN BLACK | 0.5 | PVDF | 10 |

Table 4-16 shows the capacitance for the fabricated prototypes (CY-1 to CY-11).

Table 4-16 Capacity measurements for CY-1 to CY-11

| Prototype | Capacitance (F) | | | | | | | | | |
|-----------|-----------------|-----|-------|-----|-------|-------|-------|-------|-------|--|
| | No. of cycles | | | | | | | | | |
| | 1 | 5 | 10 | 50 | 100 | 300 | 350 | 1000 | 2550 | |
| CY-1 | 15.87 | - | 18.18 | - | 18.18 | 16.67 | 16.12 | 13.79 | 14.18 | |
| CY-2 | 7.19 | - | - | 8.1 | 10.91 | 12 | - | 15 | - | |
| CY-3 | 29.41 | - | 30 | - | 30.67 | - | 28.57 | 27.02 | - | |
| CY-4 | Not working | | | | | | | | | |
| CY-5 | - | 6.1 | - | - | - | - | - | - | - | |
| CY-6 | Not working | | | | | | | | | |
| CY-7 | Not working | | | | | | | | | |
| CY-8 | Not working | | | | | | | | | |
| CY-9 | 12.9 | - | 10 | - | 8.75 | - | 9.1 | 9 | - | |
| CY-10 | Not working | | | | | | | | | |
| CY-11 | 5.22 | - | 5.2 | - | - | - | 5.27 | 5.3 | - | |

Table 4-17 shows the ESR for the fabricated prototypes (CY-1 to CY-11).

Table 4-17 ESR measurements for CY-1 to CY-11

| Prototype | ESR (Ω) | | | | | | | | | | |
|-----------|------------------|------|------|------|-------|--------|------|-----|------|------|--|
| | No. of cycles | | | | | | | | | | |
| | 1 | 5 | 10 | 50 | 100 | 300 | 350 | 500 | 1000 | 2550 | |
| CY-1 | 3.14 | | 3.22 | - | 0.66 | 0.5445 | 0.92 | | 1.31 | 0.54 | |
| CY-2 | 3.65 | | - | 3.29 | 2.93 | 2.72 | - | | 2 | - | |
| CY-3 | 3.35 | | - | - | 0.964 | - | 1.46 | | 1.44 | - | |
| CY-4 | Not working | | | | | | | | | | |
| CY-5 | - | 14.6 | - | - | - | - | - | | - | - | |
| CY-6 | Not working | | | | | | | | | | |
| CY-7 | Not working | | | | | | | | | | |

| | | | | | | | | | | |
|-------|-------------|--|--|--|------|--|--|------|-----|--|
| CY-8 | Not working | | | | | | | | | |
| CY-9 | 1.81 | | | | 1.05 | | | 1.92 | 2 | |
| CY-10 | Not working | | | | | | | | | |
| CY-11 | | | | | 1.54 | | | 1.5 | 1.5 | |

4.5.1 Cylindrical Prototype CY-1

Charge–discharge measurements were conducted to determine the capacitance and the ESR of each cell at different number of life cycles. Figure 4-24 shows the first cycles of charge–discharge curve. CV test was run to observe the behavior of the cells.

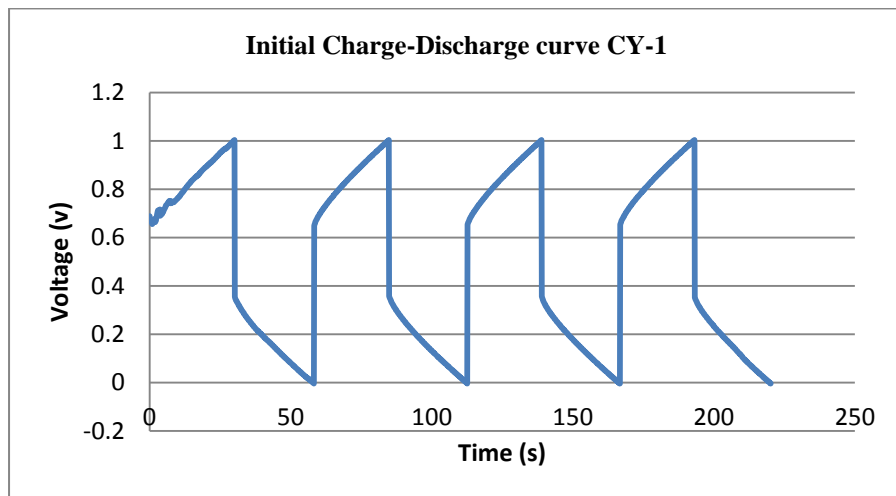


Figure 4-24 Charge-discharge curve CY-1

Using the slope of the charge-discharge curve the capacitance was measured using:

$$C = i/\text{slope}$$

Eq 4.7

The voltage drop on the charge-discharge curve is used to measure the ESR, using:

$$\text{Voltage drop} = IR \quad \text{Eq 4.8}$$

Knowing the charging current and the voltage drop the ESR can be calculated using

$$R(\text{ESR}) = \text{voltage drop}/I \quad \text{Eq 4.9}$$

Figure 4.27 shows a portion of charging curve and its measured slope, the capacity was calculated and found to be 15.87 F.

$$C = i/\text{slope} = 0.2/0.0126 = 15.87 \text{ F}$$

$$\text{ESR} = 3.14 \Omega$$

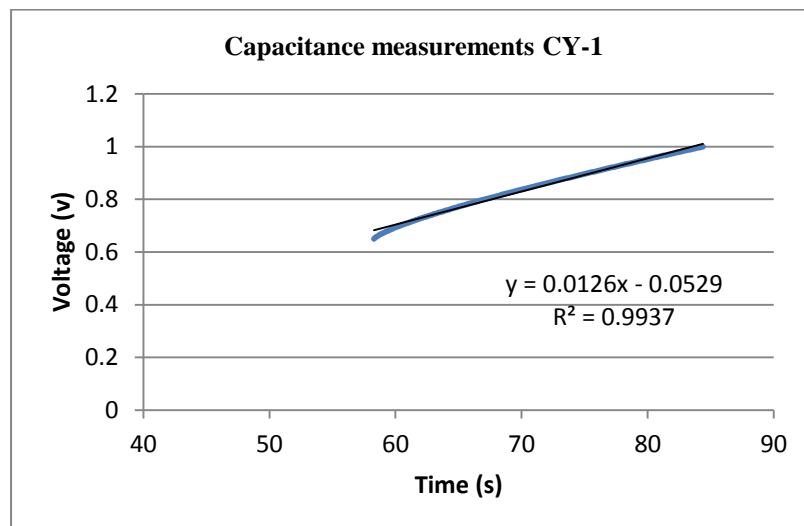


Figure 4-25 Initial capacitance measurements of CY-1 at 0.2 mA

The CV test was also done to determine the behavior of the cell, for a window of 2 V and 20 mV/s scan rate. The shape is not a perfect resemblance for a supercapacitor behavior, which should look like a square, but because it is the first life cycle of the supercapacitor the shape is imperfect. Figure 4-26 shows the CV curve.

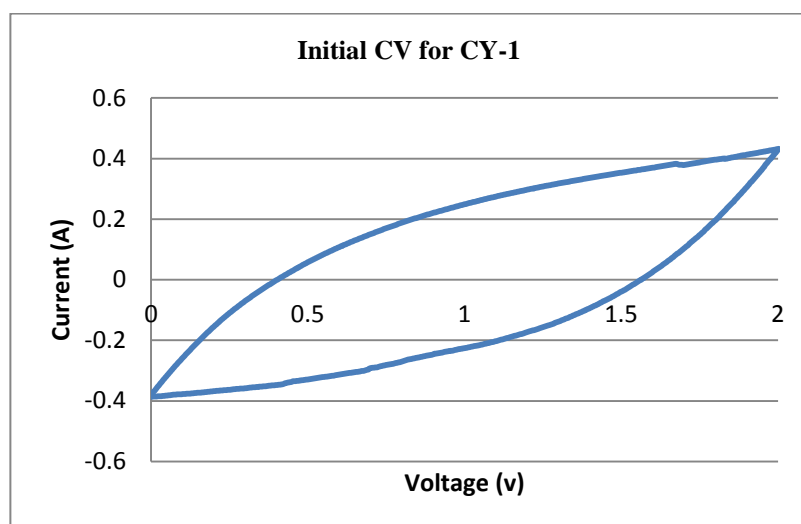


Figure 4-26 Initial CV for CY-1 at 20mv/s

Figure 4.29 shows the EIS Nyquist plot for the supercapacitor prototype CY-1, the EIS plot shows the characteristics of supercapacitor, which displays a semicircle in the high-frequency and a linear curve in the low-frequency region. The semicircle in the high-frequency region is related to the reaction kinetics at the electrode and electrolyte interfaces. The linear curve at the low-frequency region can be attributed to the diffusion controlled process in the electrolyte. The internal resistance of the cell can be obtained from the high-frequency interception of real axis.

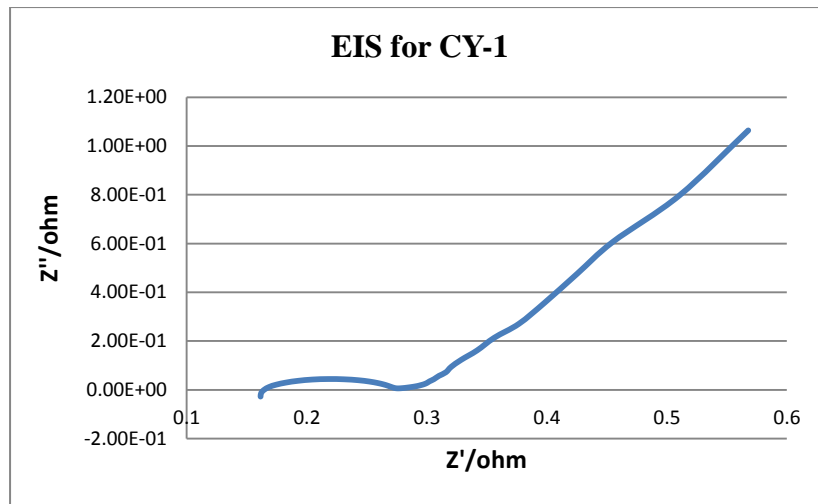


Figure 4-27 EIS for supercapacitor prototype CY-1

After cycling the supercapacitor for 10 cycles the capacitance was measured again; the new capacitance is 18.18 F. The improved capacity can be attributed to more penetration of the electrolyte inside the activated carbon, which leads to utilization of more activated carbon surface area. Figure 4-28 shows the charge-discharge curve after 10 cycles.

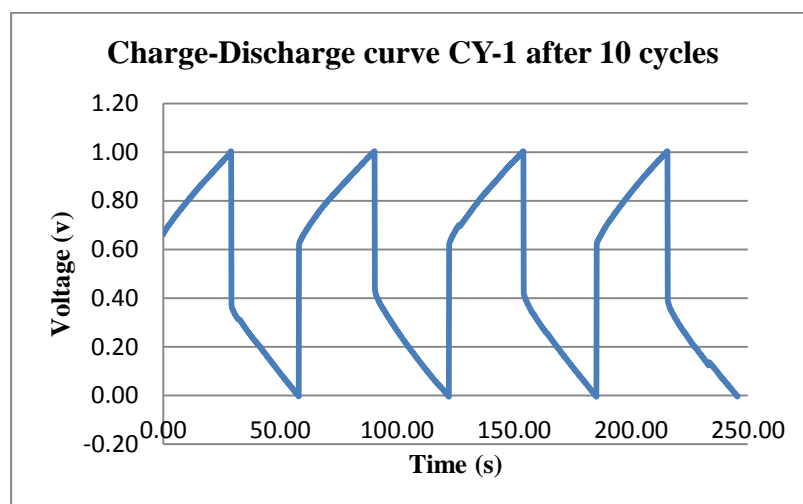


Figure 4-28 Charge-discharge curve at 0.2mA after 10 cycles

The slope of the charge curve was used to measure the capacitance of the prototype, using Eq 4.7. Figure 4-29 shows the charging curve slope for the cell CY-1.

$$C = i/\text{slope} = 0.2/0.011 = 18.18 \text{ F}$$

$$R(ESR) = \text{voltage drop} / I = (1 - 0.356) / 0.2 = 3.22 \Omega$$

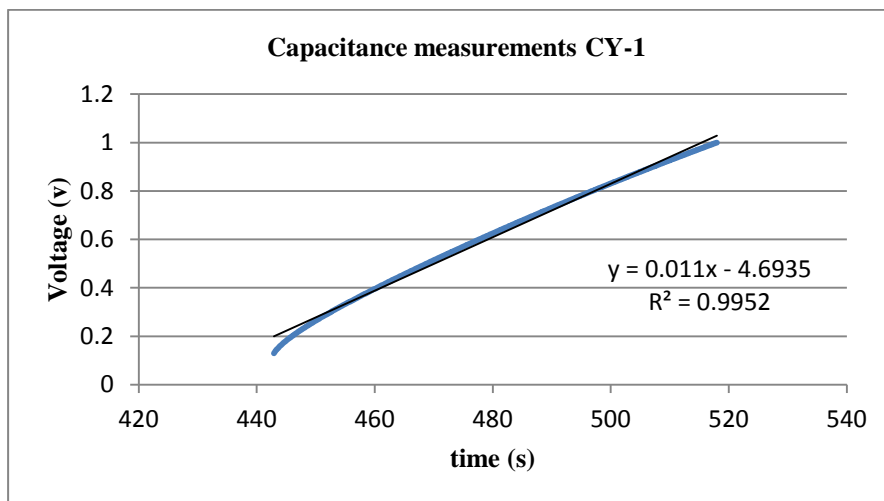


Figure 4-29 Capacitance measurements of CY-1 at 0.2 mA after 10 cycles

After 100 cycles the supercapacitor still maintain the same capacity of 18.18 F

$$C = i/\text{slope} = 0.2/0.011 = 18.18 \text{ F}$$

$$ESR = 3.22 \Omega$$

After 350 life cycles the capacity of the supercapacitor starts to stabilize and behave more like a supercapacitor. Figure 4-30 shows the charge-discharge curve where it can be seen that the supercapacitor has a good charging behavior.

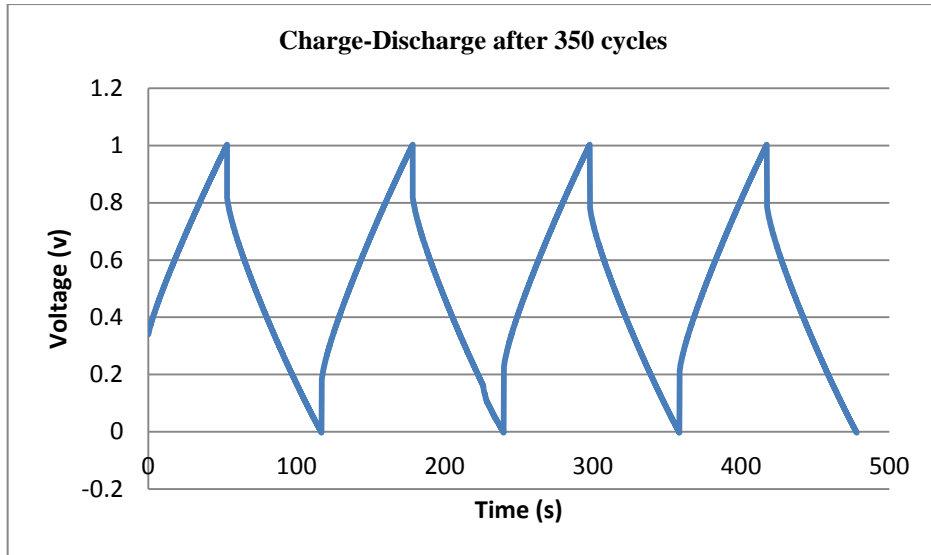


Figure 4-30 Charge-discharge after 350 cycles

Figure 4-31 shows the charging curve that was used to calculate the capacitance of the cell.

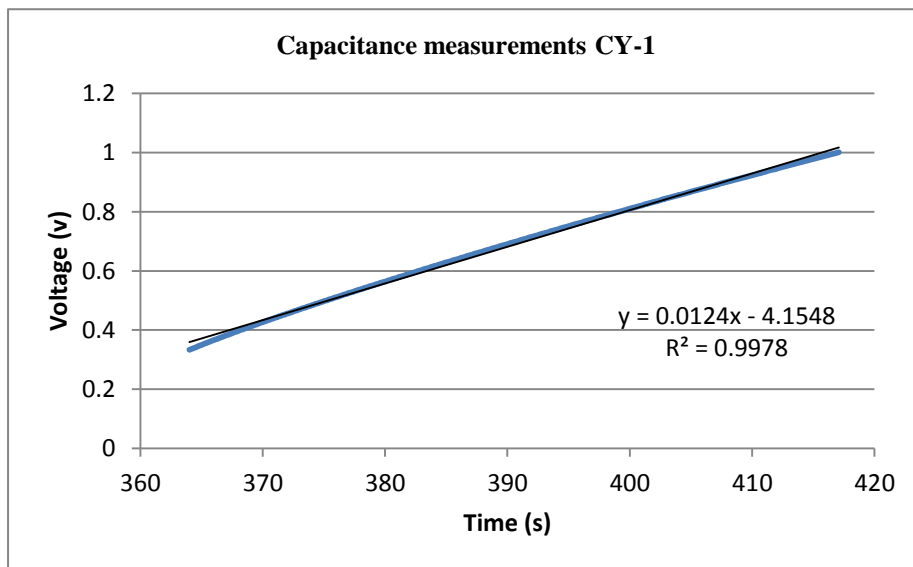


Figure 4-31 Capacitance measurements CY-1 after 350 cycles

$$C = i/\text{slope} = 0.2/0.0124 = 16.12 \text{ F}$$

$$\text{ESR} = 0.92 \Omega$$

The CV curve of the cell is shown in Figure 4-32 and it resembles a supercapacitor behavior, it is close to perfect square shape.

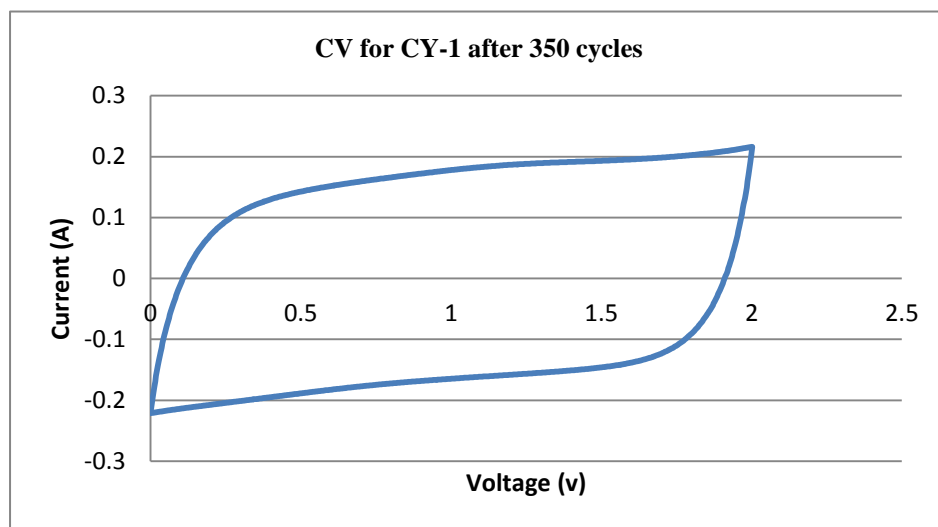


Figure 4-32 CV for CY-1 after 350 cycles

After cycling the prototype for 1000 cycles, the capacity was measured again. The new value for the capacitance is 13.79 F. Figure 4-33 shows the charge-discharge curve and Figure 4-34 shows the curve used to calculate the capacity of the supercapacitor.

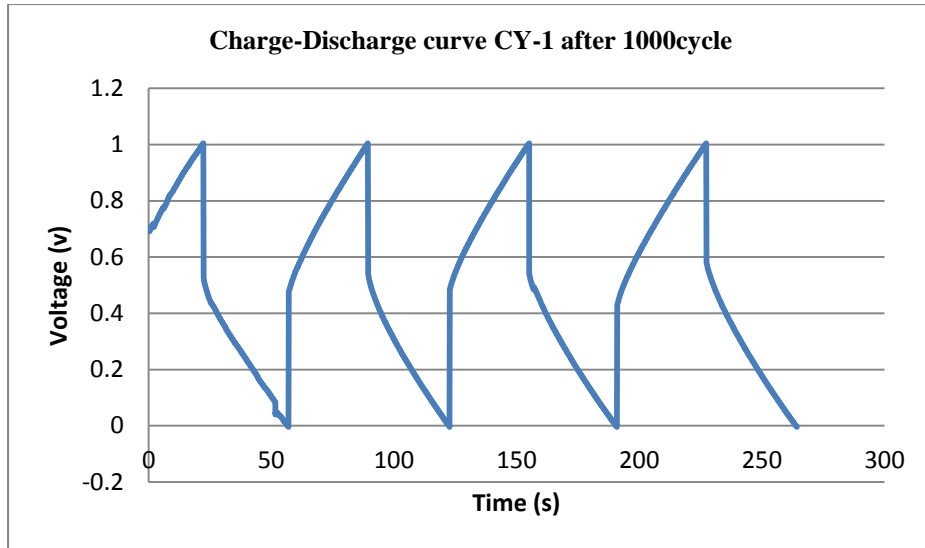


Figure 4-33 Charge-discharge curve CY-1 after 1000 cycles

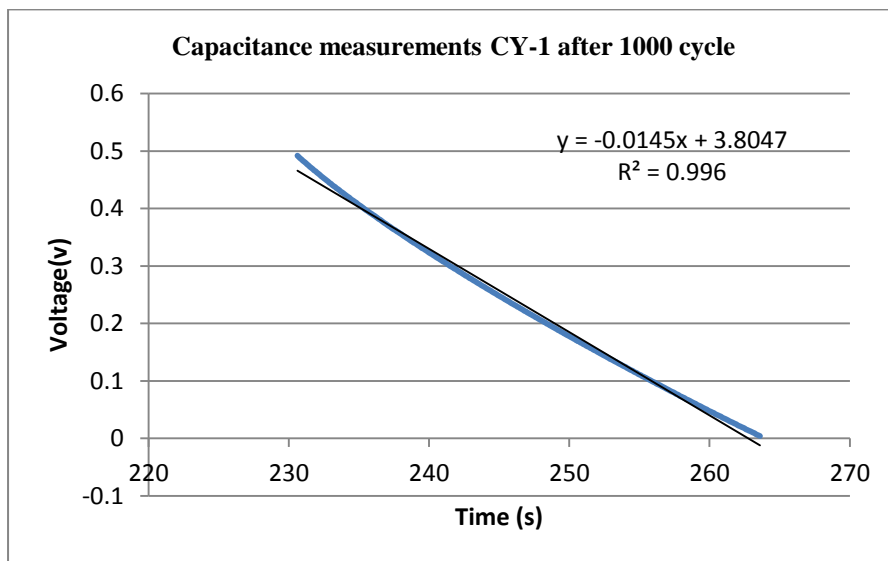


Figure 4-34 Capacitance measurements CY-1 after 1000 cycles

$$C = i/\text{slope} = 0.2/0.0145 = 13.79 \text{ F}$$

$$\text{ESR} = 2.31 \text{ } \Omega$$

The CV curve of the cell is shown in Figure 4-35. The curve is close to a perfect square and hence the cell's behaviour resembles that of a supercapacitor.

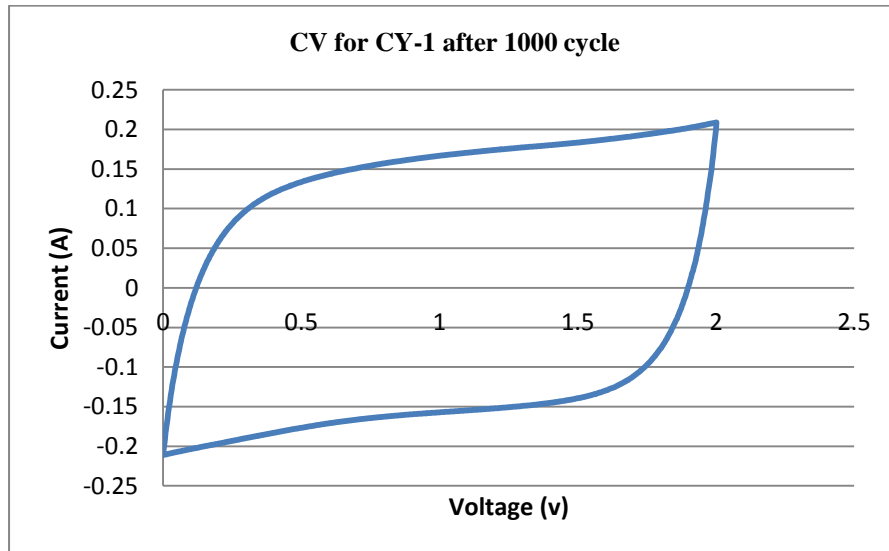


Figure 4-35 CV for CY-1 after 1000 cycle

The prototype was cycled for 2550 cycles and retested. Figure 4-36 shows the charge-discharge curve after 2550 cycles and a good charging and discharging patterns can be seen.

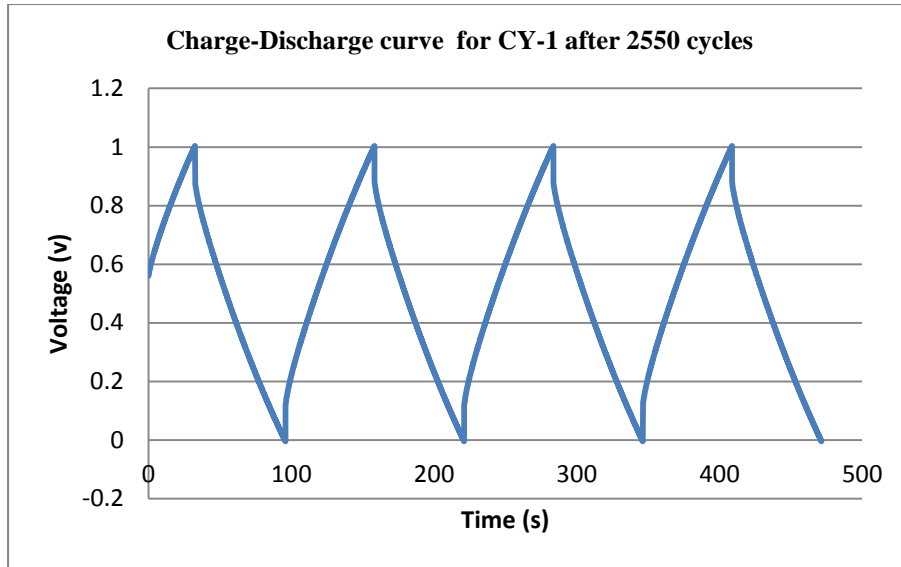


Figure 4-36 Charge-discharge curve CY-1 after 2550 cycles

Figure 4-37 shows the slope curve used to calculate the capacitance of the prototype cell. The calculated capacitance is 14.18 F.

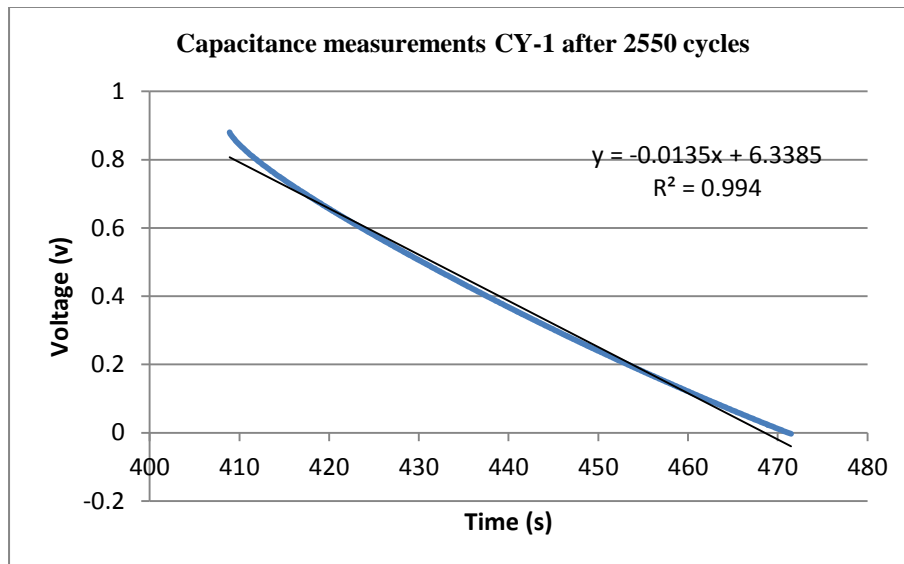


Figure 4-37 Capacitance measurements CY-1 after 2550 cycles

$$C = i/\text{slope} = 0.2/0.0135 = 14.81 \text{ F}$$

$$\text{ESR} = 0.54 \Omega$$

Figure 4-38 shows a near perfect CV curve, after 2550 cycles, the scan rate used was 10 mV/s.

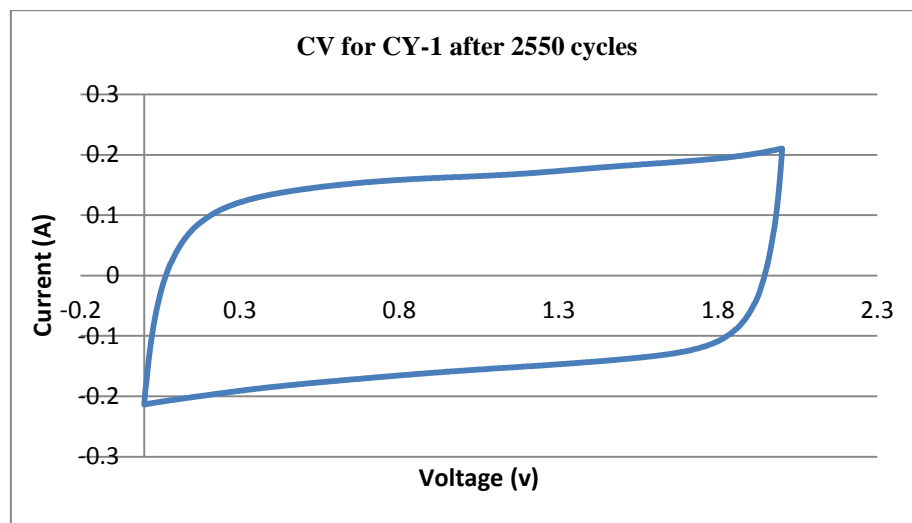


Figure 4-38 CV curve for CY-1 after 2550 cycles

4.5.2 Cylindrical prototypes CY-2 to CY-11

For the detailed measurements (CV, EIS and charge-discharge) of the prototypes CY-2 to CY-11, refer to the Appendix A.

4.6 Comparison between CY-1 to CY-11

Table 4-18 shows the different prototypes fabricated. It can be seen, CY-3 has the highest capacitance (27.02 F) compared to the rest of the prototypes, and its ESR is

low (1.44 Ω), which is considered one of the aims of supercapacitor fabrication process.

Table 4-18 Comparison between CY-1 to CY-11

| Prototype | Capacitance (F) | ESR (Ω) | CV curve | Remarks |
|-----------|-----------------|------------------|---|----------------------------------|
| CY-1 | 13.79 | 1.31 |  | Medium capacitance low ESR |
| CY-2 | 15 | 2 |  | Medium capacitance Medium ESR |
| CY-3 | 27.02 | 1.44 |  | High capacitance Low ESR |
| CY-4 | No data | No data |  | No data |
| CY-5 | No data | No data |  | No data |
| CY-6 | No data | No data |  | No data |
| CY-7 | No data | No data |  | No data |
| CY-8 | No data | No data | No data | No data |
| CY-9 | 9 | 2 |  | Low capacitance Medium ESR |

| | | | | |
|-------|---------|---------|---|-------------------------------|
| CY-10 | No data | No data | No data | No data |
| CY-11 | 5.3 | 1.5 |  | Low capacitance Medium ESR |

CY-1 had medium capacitance (13.79 F) with low ESR (1.3 Ω), the rest of the prototypes have either low capacitance or the prototypes failed, which can be due to poor contact between the current collector and the terminal or failed sealing.

The CV curve can give a good indication about the health condition of the supercapacitor, as seen for CY-4 to CY-7, where the CV curve is very narrow.

4.7 Coin Supercapacitor prototypes

The coin supercapacitor prototypes were fabricated using the CR2016 lithium battery packaging and aqueous electrolyte was used for all the coin supercapacitor prototypes. Figure 4-39 shows a picture of the coin supercapacitor prototype.



Figure 4-39 Coin supercapacitor prototype

Charge–discharge measurements were conducted to determine the capacitance and ESR of each cell at different number of life cycles. CV tests were run to observe the behavior of the cells.

4.7.1 Coin prototype B-1

The first coin prototype B-1 was tested using the charge- discharge method with 50 mA constant current. The first test was done at 10 cycles. Figure 4-40 shows the charge-discharge curve for B-1.

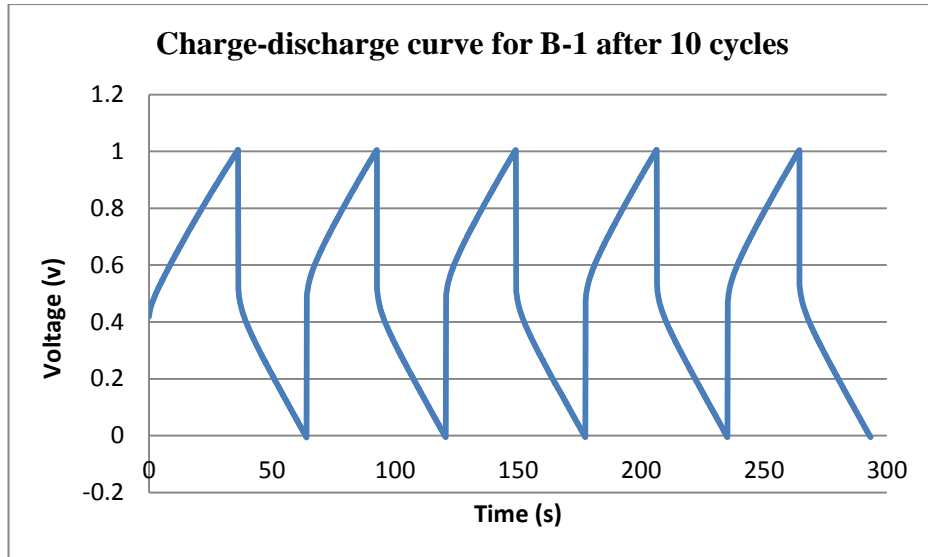


Figure 4-40 Charge-discharge for prototype B-1 after 10 cycles

Portion of the charge-discharge curve is used to calculate the capacitance of the B-1 prototype. Figure 4-41 shows the curve used to measure the slope which is then used to calculate the capacitance.

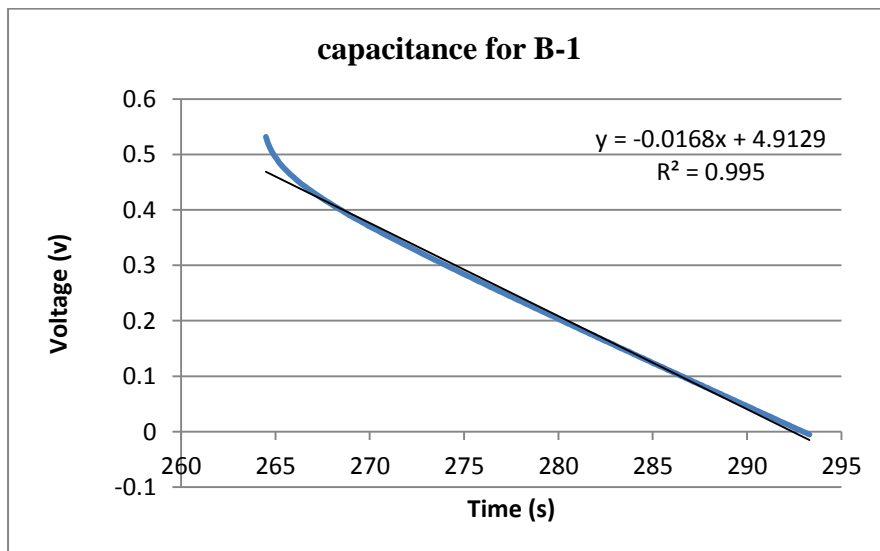


Figure 4-41 Capacitance for prototype B-1

$$C = \frac{0.05}{0.0168} = 2.97 \text{ F}$$

$$ESR = \frac{1 - 0.516}{0.05} = 9.68 \ \Omega$$

The B1 prototype was tested using CV method to observe its behavior. Figure 4-42 shows the CV curve which closely resembles the ideal supercapacitor square shape curve.

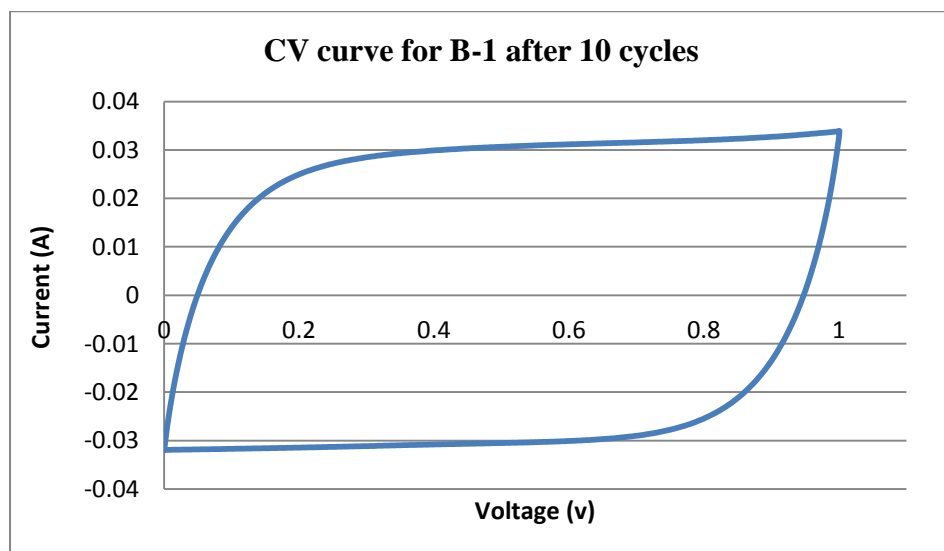


Figure 4-42 CV curve for prototype B-1 after 10 cycles

The B-1 coin prototype was cycled for 100 cycles and tested again to observe the changes to the capacitance and the ESR values. Figure 4-43 shows the charge-discharge curve after 100 cycles.

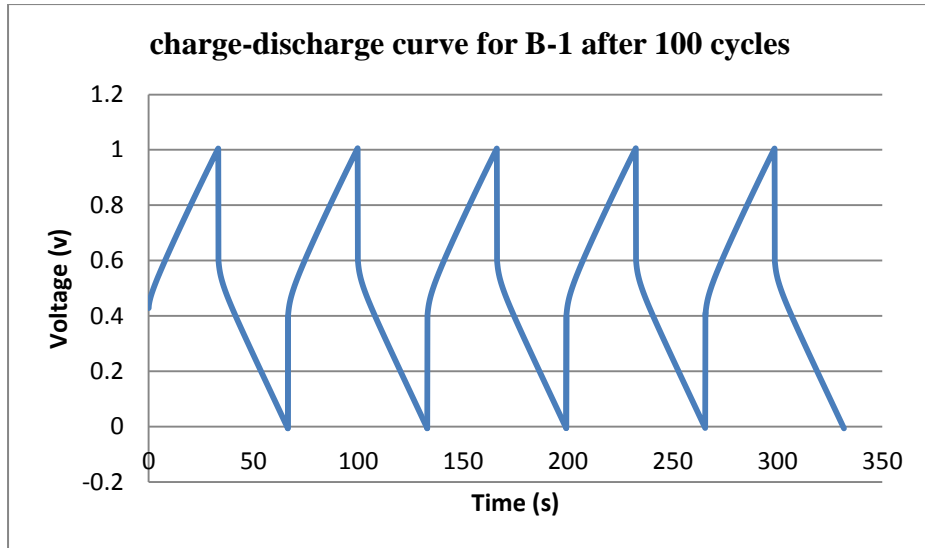


Figure 4-43 Charge-discharge curve for B-1 after 100 cycles

The new value for the capacitance was increased to 3.125 F from 2.97 F, on the other hand the ESR was decreased to 7.96 Ohms from 9.68 Ohms, and this could be due to poor contact between the active material and the current collector. Figure 4-44 shows the curve used to measure the capacitance of the B-1 prototype.

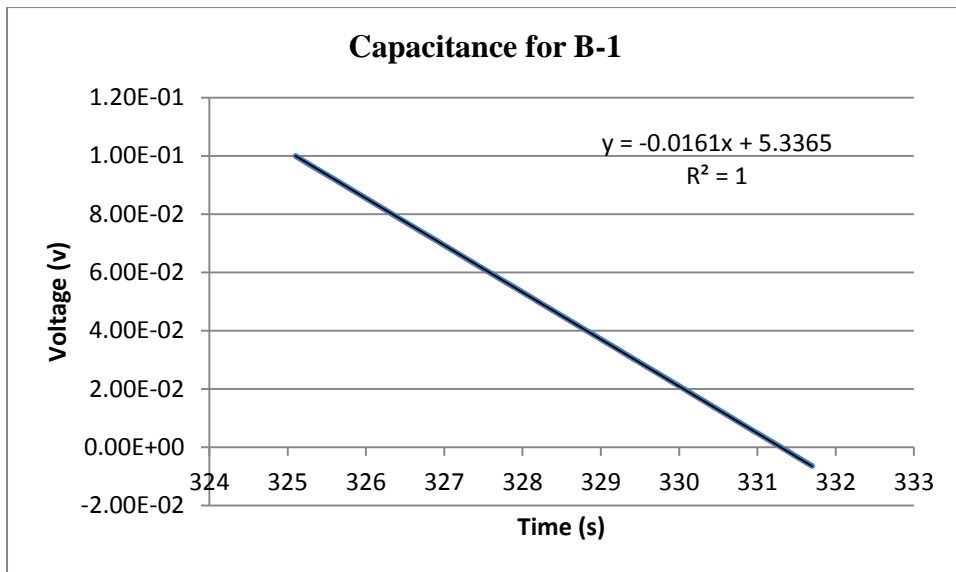


Figure 4-44 Capacitance for B-1

$$C = \frac{0.05}{0.016} = 3.125 \text{ F}$$

$$ESR = \frac{1 - 0.602}{0.05} = 7.96 \Omega$$

The CV curve after 100 cycles reassembles the ideal supercapacitor curve. Figure 4-45 shows the CV curve after 100 cycles.

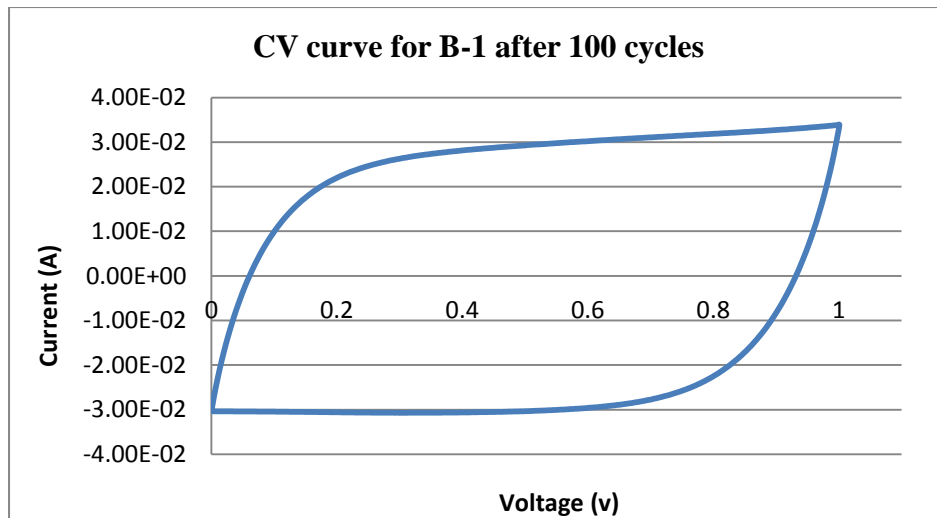


Figure 4-45 CV curve for B-1 after 100 cycles

4.7.2 Coin prototypes B-2 to B-18

For the detailed measurements (CV, EIS and charge-discharge) of the prototypes B-2 to B-18, refer to Appendix B.

4.8 Comparison between different coin prototypes

Table 4-19 shows the list of capacitances and ESR for the coin prototypes B-1 to B-18 at 10 and 100 cycles. The highest capacitance obtained was 3.333 F for the B-7 prototype after cycling the prototype for 100 cycles, and the lowest capacitance obtained was 1.034 F for the B-9 prototype after 100 cycles. The lowest ESR is 3.36 Ω for the B-7 prototype. By comparing the highest capacitance the lowest ESR in Table 4-19, it was concluded that, B-7 prototype is the best supercapacitor coin prototype.

Table 4-19 Capacitances and ESR of the coin prototypes B-1 to B-18

| Prototype | Capacitance (F) | ESR (Ω) | CV curve | Remarks |
|------------------|------------------------|----------------------------------|--|--------------------------------|
| B-1 | 3.125 | 7.96 |  | High capacitance Medium ESR |
| B-2 | 2.778 | 12.92 |  | Medium capacitance High ESR |
| B-3 | 1.199 | 17.96 |  | Low capacitance High ESR |
| B-4 | 1.219 | 16.38 |  | Low capacitance High ESR |
| B-5 | 2.478 | 12.78 |  | Medium capacitance High ESR |
| B-6 | 1.538 | 28.13 |  | Low capacitance High ESR |
| B-7 | 3.333 | 3.36 |  | High capacitance Low ESR |

| | | | | |
|-------------|-------|-------|--|----------------------------------|
| B-8 | 1.162 | 29.1 |  | Low capacitance High ESR |
| B-9 | 1.034 | 28.77 |  | Low capacitance High ESR |
| B-10 | 3.158 | 5.6 |  | High capacitance Medium ESR |
| B-11 | 2.777 | 5.08 |  | Medium capacitance Medium ESR |
| B-12 | 2.941 | 6.72 |  | Medium capacitance Medium ESR |
| B-13 | 2.487 | 11.46 |  | Medium capacitance High ESR |
| B-14 | 2.76 | 12.2 |  | Medium capacitance High ESR |
| B-15 | 2.824 | 6 |  | Medium capacitance medium ESR |

| | | | | |
|-------------|-------|-------|--|--------------------------------|
| B-16 | 2.659 | 10.28 |  | Medium capacitance High ESR |
| B-17 | 2.617 | 10.68 |  | Medium capacitance High ESR |
| B-18 | 2.673 | 12.84 |  | Medium capacitance High ESR |

4.9 Optimizing Supercapacitor using Taguchi Technique

In this part by use of the Taguchi methodology to optimize the coin supercapacitor the number of experiments has been reduced for three factors at three levels from $(3^3) = 27$ experiments to only 9 set of experiments. In terms of materials, the core materials that have been used in the fabrication are: activated carbon (AC) as the active material, carbon black (CB) as the conducting agent and PVDF polymer as the binder material. A total of nine experiments were conducted, where the percentage composition of PVDF and CB were varied for different mixing times in order to find the most significant process parameter affecting the capacitance and the ESR. 1 M lithium perchlorate (LiClO_4) in acetonitrile was used as the electrolyte. Coin shape supercapacitors with a diameter of 13 mm have been fabricated. The cell

capacitances were found to range from 24.91 – 51.23 mF. The capacitive properties of the fabricated cells were evaluated by cyclic voltammetry (CV), EIS and charge-discharge measurements using an Autolab potentiostat (PGSTAT302N).

The chosen control factors and levels which are selected are shown in Table 4-20.

Table 4-20 Control factors and levels of the experiment

| Factor | Labelled | Level 1 | Level 2 | Level 3 |
|----------------------------|-----------------|----------------|----------------|----------------|
| PVDF % | A | 2 | 3 | 5 |
| Mixing time (Hours) | B | 1 | 2 | 3 |
| Carbon Black % | C | 5 | 10 | 15 |

The experimental procedures were carried out in a controlled environment, where the experiment conditions remained constant. This ensures that there is no effect on the results from external factors and the only conditions during the experiment which varied in their values are the three control factors. In particular, room temperature remained constant at 22°C and the environment humidity is kept stable during all experiments. Same quantities and type of materials were used for all cells. Also the fabricating process and the testing equipments remained the same.

Table 4-21 shows the 9 trials and the measured capacitance and ESR for each cell.

Table 4-21 Experimental layout

| Exp. | Quality Characteristics | | | Capacitance (mF) | ESR (Ω) |
|------|-------------------------|------------------------|------|---------------------|---------------------|
| | A | B | C | | |
| | PVDF % | Mixing time (Hours) | CB % | | |
| 1 | 1 | 1 | 1 | 33.57 | 336 |
| 2 | 1 | 2 | 2 | 35.32 | 530 |
| 3 | 1 | 3 | 3 | 38.36 | 516 |
| 4 | 2 | 1 | 2 | 41.91 | 524 |
| 5 | 2 | 2 | 3 | 24.91 | 685 |
| 6 | 2 | 3 | 1 | 51.23 | 329 |
| 7 | 3 | 1 | 3 | 43.86 | 146 |
| 8 | 3 | 2 | 1 | 44.76 | 337 |
| 9 | 3 | 3 | 2 | 50.75 | 286 |

The traditional method of calculating the average effects of factors to determine the desirable factor levels is to look at the simple average of the results. Although calculating the average is simpler, it does not capture the variability of data within the group. A better way to compare the population behavior is to use the mean-squared deviation (MSD) of the results. For convenience of linearity and to accommodate wide-ranging of data, a log transformation of MSD (S/N) is recommended for analysis of experimental results, Signal-to-noise ratio (S/N), is the ratio of the power of the signals to the power of the noise. A high S/N ratio will mean that there is high sensitivity with the least error of measurement. In Taguchi analysis using S/N ratios, a higher value is always desirable regardless of the quality characteristic [98]. In this case, as the objective was to maximize the capacitance of

the supercapacitor, it is therefore to select the S/N ratio related to larger-the-better quality characteristics Eq 4.10, as for the ESR the objective is to minimize it, so the S/N ratio selected is the smaller-the-better Eq 4.11.

$$\left(\frac{S}{N}\right) \text{ ratio} = -10 \log_{10} \left(\left(\frac{1}{y_1^2} + \frac{1}{y_2^2} + \dots + \frac{1}{y_n^2} \right) / n \right) \quad \text{Eq 4.10}$$

$$\left(\frac{S}{N}\right) \text{ ratio} = -10 \log_{10} \left((y_1^2 + y_2^2 + \dots + y_n^2) / n \right) \quad \text{Eq 4.11}$$

where,

n= number of values at each trial condition

y_i= each observed value.

The S/N ratio is treated as a response (output) of the experiment, which is a measure of variation when uncontrolled noise factors are present in the system [92].

To maximize the signal-to-noise ratio, (which in effect means, to reduce the quality loss caused by variability about the nominal value), two things need to be done:

- 1- Select values for the control factors which minimize variability. In this way we minimize the effect of the noise factors, that is, we aim to make it ‘robust’.
- 2- Select values for the control factors which change the mean value of the quality characteristic to correspond to the nominal value.

The analysis will therefore be in two parts:

- Find which control factors have the greatest effect on variability. Select values for these control factors accordingly.

- Find which control factor has the greatest effect on the mean, other than those already set to minimize the variability. Select a value for this control factor to bring the predicted value of the quality characteristic as near as possible to the nominal value.

Table 4-22 and Table 4-23 show the average S/N ratio values for capacitance and ESR respectively.

Table 4-22 Response table for S/N ratio (Capacitance)

| | A | B | C |
|----------------|--------------|--------------|--------------|
| Level 1 | 3.102 | 3.181 | 3.229 |
| Level 2 | 3.068 | 3.012 | 3.231 |
| Level 3 | 3.328 | 3.316 | 3.028 |

Table 4-23 Response table for S/N ratio (ESR)

| | A | B | C |
|----------------|---------------|---------------|---------------|
| Level 1 | -5.342 | -5.134 | -5.047 |
| Level 2 | -5.453 | -5.459 | -5.327 |
| Level 3 | -4.858 | -5.182 | -5.401 |

Figure 4-46 and Figure 4-47 illustrate the main effects plot of the control factors for the experiment (using the values from Table 4-22 and Table 4-23 respectively).

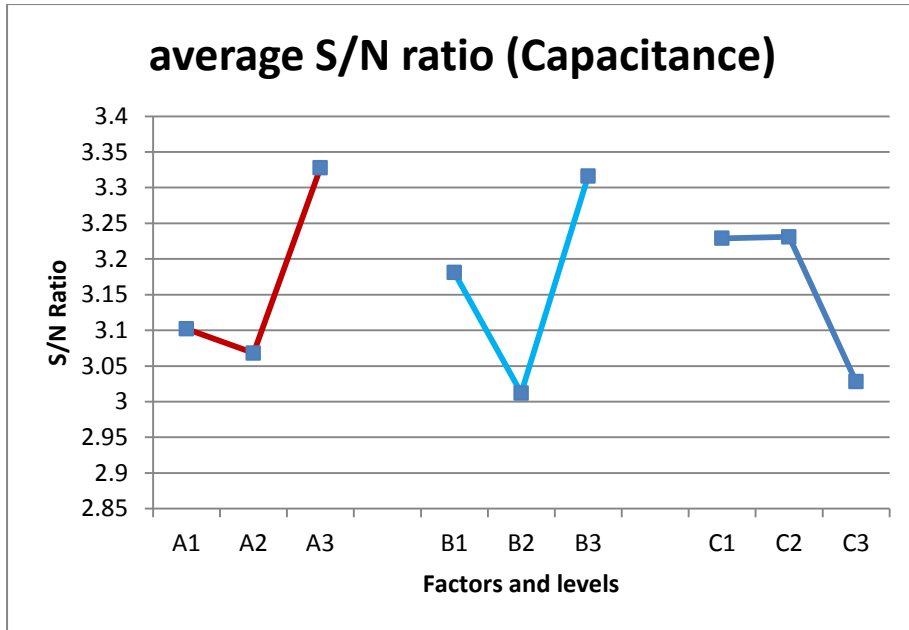


Figure 4-46 Response graph for S/N ratio (Capacitance)

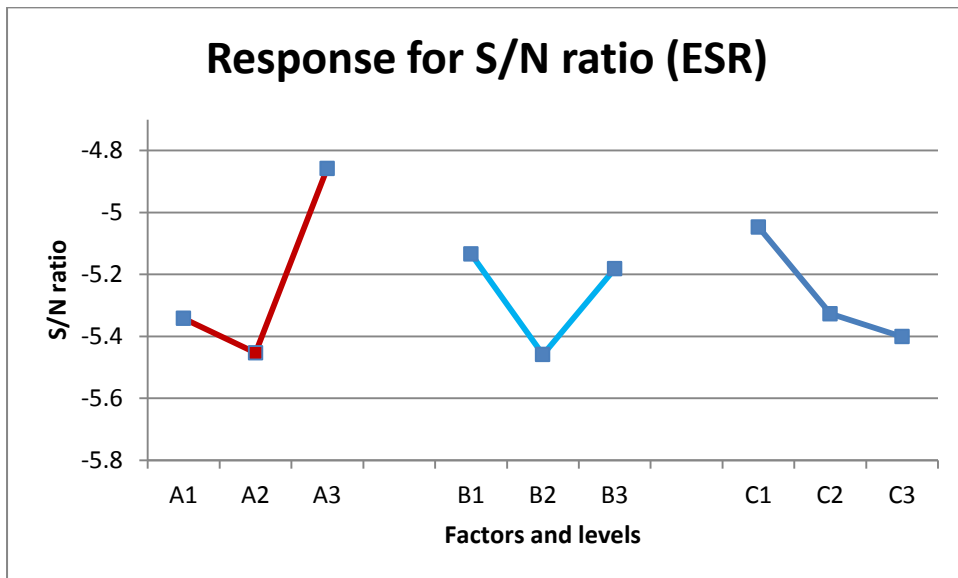


Figure 4-47 Response graph for S/N ratio (ESR)

Table 4-22 and Figure 4-46 show that the most significant factors for capacitance is control factor A (PVDF %), followed by factor B (mixing time). Factor C is less significant.

Since, the objective of this work is to optimize the capacitance, we need to maximize the S/N ratio in order to minimize variability. Thus, both factors A and B need to be set to level 3.

Similarly, Table 4-23 and Figure 4-47 show that the most significant factors for ESR are factor A (PVDF %), followed by factor C (Carbon Black %). The effect of factor B (mixing time) is of less significance, the optimum levels are A3 and C1.

The experiment enabled the behavior of the system to be understood by the engineering team in a short period of time and resulted in significantly improved performance (with the opportunity to design further experiments for possible greater improvements).

The results indicated that binder percentage and mixing time have greater effect on the capacitance, whereas for the ESR, binder and carbon black percentages were found to be more significant. In order to study the effect of variables in a minimum number of trials, the Taguchi approach for experimental design was adopted [8]. The project illustrated the techniques that can be used in order to gain the best outcome at minimum cost. It was clearly demonstrated that the Taguchi methodology of DOE is applicable and adaptable in supercapacitor optimization purposes.

At the end of the experiment, a final confirmation experiment was performed, and the supercapacitor cell was manufactured using the optimised factors: PVDF

percentage (5%), mixing time (3H) and carbon black percentage (5%). The capacitance of the cell is 54.70 mF.

4.10 Optimization of process factors using Taguchi technique and Genetic Algorithm

In collaboration with Genetic Algorithm (GA) research group (Nottingham Malaysia campus), a proposed approach that deals with the optimization of various responses problems in Taguchi method using Genetic Algorithm (GA) as a measure of quality assurance of the products and the processes. A brief description of the work done will be given here. For the full text paper please refer to Appendix C. Taguchi method is always applied in single-response problems and with the aid of the employment of past experiences and engineering judgments, at times is used to tackle the optimization of various responses problems. This hybrid approach maintains the robustness of the products and processes even in the requirement of measuring multiple responses of the products and processes. In this work, an extensive methodology in application of the proposed approach on process fabrication supercapacitor is presented. This approach utilizes the information acquired from the signal-to-noise ratio (SNR) and GA method aims in maximizing the weighted SNR (WSNR). Experimental result shows that this proposed approach has the potential and power to solve multiple response problems. A comparison of the result between the proposed approach and the result from Overall Evaluation

Criteria (OEC) is concluded based on the improvement in dB of the SNR and the standard deviation. Finally, the variance analysis plays an important role in identifying the most statistically significant factors in the process. The main contribution of this approach is to effectively and efficiently tackle the multiple response problems such as fabrication process of supercapacitor where the capacitance and equivalent series resistance (ESR) are equally important. Additionally, the proposed approach achieves the desired robustness for environmental condition and component variation.

5. Conclusion

5.1 Conclusion

This thesis was set out to design and implement a production line for supercapacitors and then to explore the concept of using statistical techniques to optimize the fabrication process of supercapacitor. The research objectives are reviewed and the results are analysed in order to re-establish the links between the results here and the significance of those results to the research topic.

The first research objective of the thesis was to design and build the pilot plant for fabrication of supercapacitor. The pilot plant was designed and built from scratch, to handle two lines of fabrication packages, coin and cylindrical packaging. It is equipped with the necessary equipments for the fabrication process; all the equipments used are presented in chapter 3. This pilot plant design was implemented in the department and was used to subsequently make all the prototypes. This satisfies the first research objective of the thesis.

The second research objective of this thesis was to design a fabrication process flowchart for the cylindrical packaging supercapacitor. A detailed step by step manufacturing process flowchart was designed and implemented for the cylindrical packaging supercapacitor. The process flowchart identifies the type, and the amount of materials used, starting from the raw materials and ending with the tested final prototype. It also illustrates each of the steps (mixing, drying, and coating) parameters (time, temperature, coating thickness). Figure 5-1 illustrates the process flowchart for the cylindrical packaging. With this cylindrical supercapacitors could be made and the infrastructure to improve the process was also implemented. This concludes the second objective is achieved.

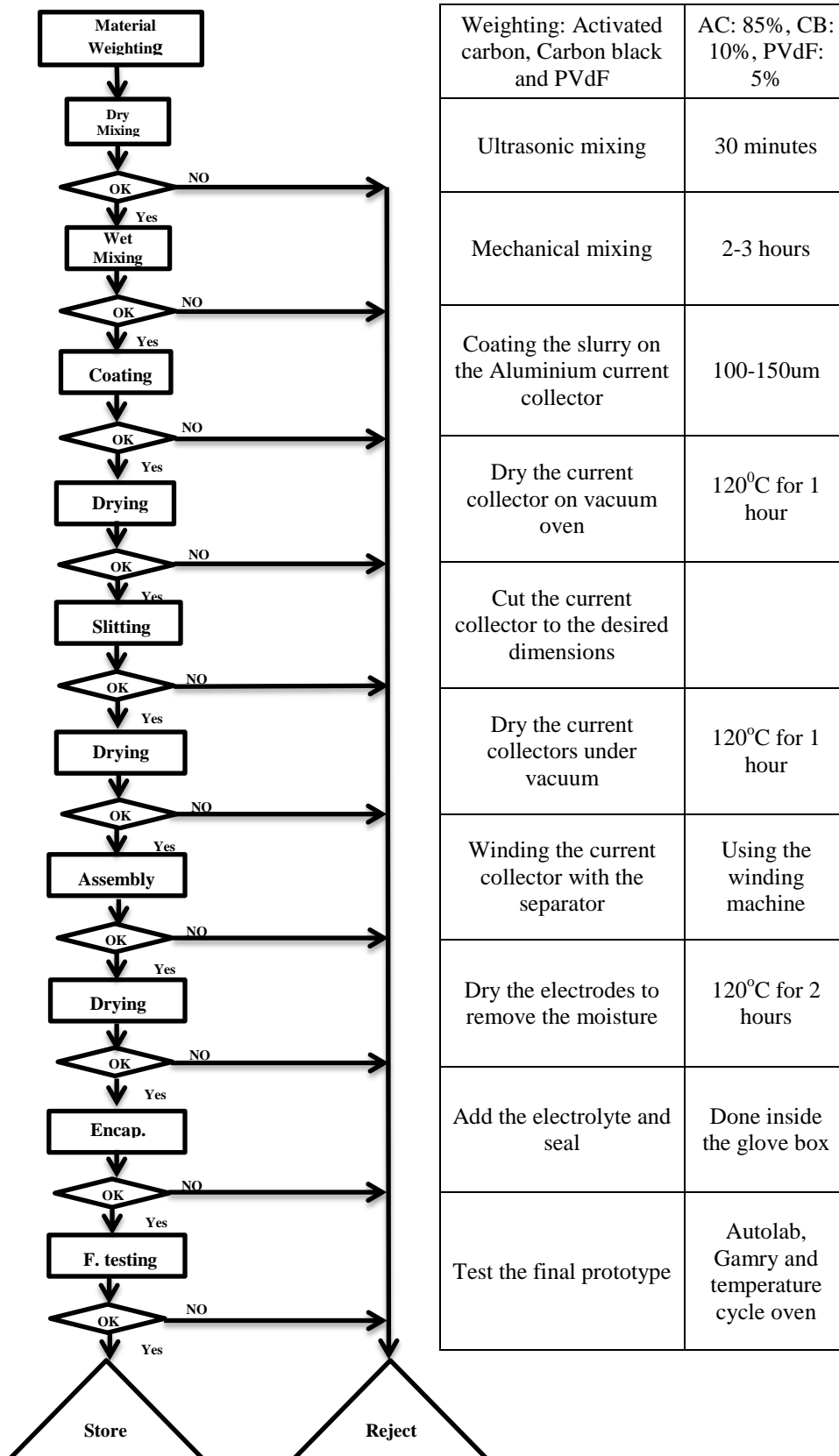


Figure 5-1 Process flowchart for cylindrical EDLC

The third research objective of this thesis was to design a fabrication process flowchart for the coin packaging supercapacitor. As in the second objective a detailed step by step manufacturing process flowchart was designed and implemented for the coin packaging supercapacitor. This process flowchart identifies the type, and the amount of materials used, starting from the raw materials (AC, binders and CB) and ending with the final tested prototype. It also illustrates each of the steps (dry mixing, vacuum drying, punching) and parameters (materials percentages, calendaring thickness, vacuum drying time). Figure 5-2 shows the process flowchart for the coin EDLC. Hence the third objective is achieved.

The fourth objective was to use Taguchi method to identify the most significant process factors of the supercapacitor manufacturing process. The project illustrated that the technique can be applied to achieve the best outcome at minimum cost (less time and materials needed) in supercapacitor fabrication. The analysis of the results obtained using Taguchi method showed that this method is one of most reliable, effective, and beneficial. A most economical way to optimize an experimental design and the appropriate conditions to obtain an extremely high-quality product can be found using this methodology. This method can also be applied to optimize other important design characteristics and attribute quality characteristics, which will also yield interesting results. With regards to the EDLC, the results indicated that binder percentage, mixing time and conducting agent percentage are some of the significant factors that can be optimised properly. The output of the experiment indicated that the binder percentage and the mixing time are the most crucial factors that optimize capacitance (maximize) and ESR (minimize) of the supercapacitor prototypes.

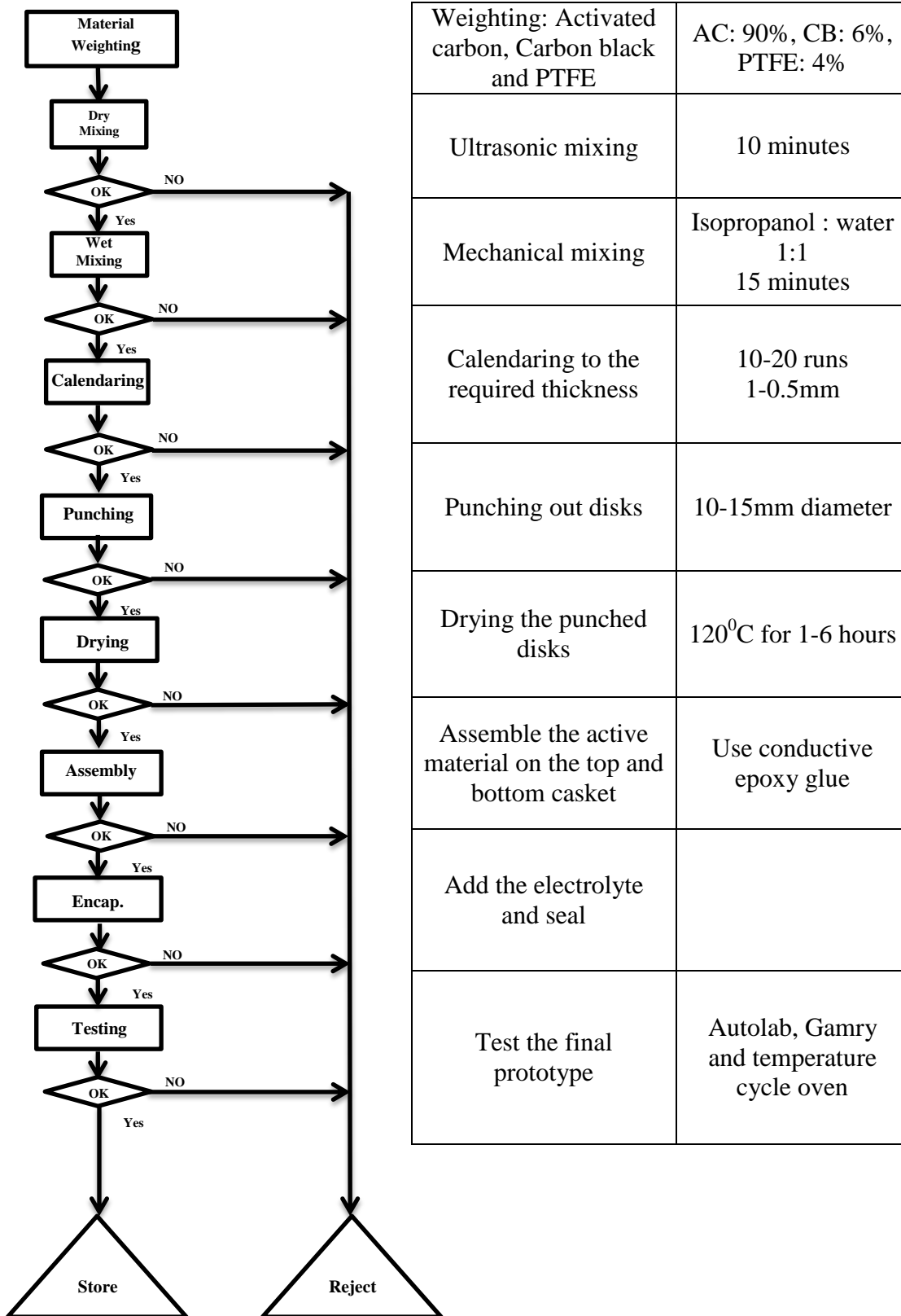


Figure 5-2 Process flowchart for coin EDLC

The fifth objective was to optimize the fabricating process using Taguchi method. After identifying the most significant process factors, the levels of those factors were varied and retested, to find the best level of each factor (percentages, temperature, time) that will increase the capacitance and decrease the ESR.

The experiments showed that, the most significant factor for capacitance is control factor A (PVDF %). The effect of factor B (Mixing time) is crucial as well, but factor C seems to be of a less significance. The optimum levels for factor A is 5% and for factor B is 3 hours. The most significant factors for ESR are factor A (PVDF %), followed by factor C (Carbon Black %). The effect of factor B (mixing time) is of less significance, the optimum levels are A3 (5%) and C1 (5%).

Using those new factors values, a confirmation experiment was conducted to confirm the new factors levels are the optimum values for capacitance and ESR. At the end of the experiment, a final confirmation experiment was performed, and EDLC cell was manufactured using the optimised factors: PVDF percentage (5%), mixing time (3H) and carbon black percentage (5%). The capacitance of the cell is 54.70 mF.

The final objective of the thesis is to test the supercapacitor prototypes to the international standards (ISO) and to compare it with the supercapacitors available on the market. The currently available supercapacitors were tested and their performance (capacitance and ESR) were compared to the fabricated prototypes. The results indicated that, the electrochemical performance of the prototypes are in good resemblance to the supercapacitors available on the market, a cyclic voltammetry (CV) and charge-discharge analysis were conducted to compare the behaviour of

each prototype. A selected prototype samples were sent to companies in mobile applications in Korea and the Netherlands for benchmark testing to confirm that the prototypes meet the ISO standards.

5.2 Future work

There could be more studies to be conducted on the optimisation of other various processes factors, such as the percentages of raw materials (binder, AC, CB), mixing process (time, temperature, mixing speed), coating process (thickness, coating speed, slurry viscosity) and drying process (temperature, time, vacuum). This will consequently improve the overall fabrication process resulting in time and resources savings. This effort can also be used to increase product robustness in terms of improving the standard variation of the eventual capacitance of the packaged product.

A separate effort on improving or increasing the breakdown voltage of the electrolyte and also studies on increasing pseudo-capacitance through the addition of “dopants” in an optimized way can assist in increasing the overall capacitance by many times.

Finally, an effective approach that deals with the integration of Taguchi method with a Genetic Algorithm (GA) is another area that is feasible for future analysis. This approach allows us to better optimize the process of increasing both product robustness and pseudo-capacitance at the same time without compromising one for the other.

The main contribution of this approach is to effectively and efficiently handle multi response problem involved in the fabrication of supercapacitors, in order to enhance the capacitance and ESR of the EDLC. The integration was used to optimize a weighted signal-to-noise ratio (WSNR) which is essential in identifying the most robust process factors. Consequently, the GA is used to enhance the WSNR value and thus maximize the strength of the signal over noise. Experimental result shows that the proposed approach has the potential and ability to solve multi response problem for this domain.

6. References

1. Curran, P.M., Carbon electrode for use in aqueous electrochemical devices and method of preparation, 2007, Google Patents.
2. Ajina, A. and D. Isa, Symmetrical Supercapacitor Using Coconut Shell-Based Activated Carbon. *Sigma*. 99: p. S42647.
3. Yee, C.Y., et al., Optimization of Process Factors in Super capacitor Fabrication Using the Genetic Algorithm to Optimize Taguchi Signal-to-Noise Ratios. *idea*, 2012. 1(2).
4. Pendashteh, A., M.F. Mousavi, and M.S. Rahmanifar, Fabrication of anchored copper oxide nanoparticles on graphene oxide nanosheets via an electrostatic coprecipitation and its application as supercapacitor. *Electrochimica Acta*, 2013. 88(0): p. 347-357.
5. Endo, M., et al., Method of manufacturing polarizable electrode for electric double-layer capacitor, 1994, Google Patents.
6. Katai, K., et al., Method of making electrochemical capacitor electrode, electrochemical capacitor electrode, electrochemical capacitor, and method of making the same, 2006, Google Patents.
7. Ajina, A. and D. Isa. Capacitance and equivalent series resistance (ESR) optimization using the Taguchi technique for EDLC's. in *Electronic Devices, Systems and Applications (ICEDSA)*, 2010 Intl Conf on. 2010. IEEE.

8. Rhyder, R.F., Manufacturing process design and optimization 1997: M. Dekker.
9. Zhong, L., X. Xi, and B. Zou, ELECTROCHEMICAL DOUBLE LAYER CAPACITOR, 2008, Google Patents.
10. Katai, K., et al., Method of making electrochemical capacitor electrode, electrochemical capacitor electrode, electrochemical capacitor, and method of making the same, 2006, Google Patents.
11. Subramanian, V., et al., Supercapacitors from activated carbon derived from banana fibers. The Journal of Physical Chemistry C, 2007. 111(20): p. 7527-7531.
12. Burke, A., Ultracapacitors: why, how, and where is the technology. Journal of power sources, 2000. 91(1): p. 37-50.
13. Curran, P.M., Carbon electrode for use in aqueous electrochemical devices and method of preparation, 2007, Google Patents.
14. Wang, Y., et al., Supercapacitor devices based on graphene materials. The Journal of Physical Chemistry C, 2009. 113(30): p. 13103-13107.
15. Chen, M., et al., Preparation of activated carbon from cotton stalk and its application in supercapacitor. Journal of Solid State Electrochemistry, 2012: p. 1-8.
16. Kazaryan, S.A., et al., Electrode for use with double electric layer electrochemical capacitors having high specific parameters, 2011, Google Patents.

17. Stoller, M.D., et al., Graphene-based ultracapacitors. *Nano letters*, 2008. 8(10): p. 3498-3502.
18. Conway, B.E., *Electrochemical Supercapacitors, Scientific Fundamental and Technological Applications*, 1999, Plenum Publishers.
19. Nishino, A., Capacitors: operating principles, current market and technical trends. *Journal of power sources*, 1996. 60(2): p. 137-147.
20. Kötz, R. and M. Carlen, Principles and applications of electrochemical capacitors. *Electrochimica Acta*, 2000. 45(15): p. 2483-2498.
21. Rao, R.S., et al., The Taguchi methodology as a statistical tool for biotechnological applications: A critical appraisal. *Biotechnology journal*, 2008. 3(4): p. 510-523.
22. Zuleta, M., P. Björnbom, and A. Lundblad, Effects of Pore Surface Oxidation on Electrochemical and Mass-Transport Properties of Nanoporous Carbon. *Journal of The Electrochemical Society*, 2005. 152(2): p. A270-A276.
23. Becker, H.E., *LOW VOLTAGE ELECTROLYTIC CAPACITOR*, 1957: U.S.
24. Boos., D.I., *ELECTROLYTIC CAPACITOR HAVING CARBON PASTE ELECTRODES*, 1970: U.S.
25. ; Available from: <http://batteryuniversity.com>.
26. Halper, M.S. and J.C. Ellenbogen, *Supercapacitors: A brief overview*. Report No. MP 05W0000272, The MITRE Corporation, McLean, Virginia, 2006.

27. John M. Miller, J.-N.-J.M., plc and Richard Smith and I. Maxwell Technologies, ULTRACAPACITOR ASSISTED ELECTRIC DRIVES FOR TRANSPORTATION. MAXWELL TECHNOLOGIES WHITE PAPER, 2009.
28. Allen, J.B. and R.F. Larry, Electrochemical methods: fundamentals and applications. Department of Chemistry and Biochemistry University of Texas at Austin, John Wiley & Sons, Inc, 2001.
29. Qu, D. and H. Shi, Studies of activated carbons used in double-layer capacitors. Journal of power sources, 1998. 74(1): p. 99-107.
30. Frackowiak, E. and F. Beguin, Carbon materials for the electrochemical storage of energy in capacitors. Carbon, 2001. 39(6): p. 937-950.
31. Arbizzani, C., M. Mastragostino, and F. Soavi, New trends in electrochemical supercapacitors. Journal of power sources, 2001. 100(1): p. 164-170.
32. Shi, H., Activated carbons and double layer capacitance. Electrochimica Acta, 1996. 41(10): p. 1633-1639.
33. Gamby, J., et al., Studies and characterisations of various activated carbons used for carbon/carbon supercapacitors. Journal of power sources, 2001. 101(1): p. 109-116.
34. Torregrosa, R. and J.M. Martín-Martínez, Activation of lignocellulosic materials: a comparison between chemical, physical and combined activation in terms of porous texture. Fuel, 1991. 70(10): p. 1173-1180.

35. Rodriguez-Reinoso, F. and M. Molina-Sabio, Activated carbons from lignocellulosic materials by chemical and/or physical activation: an overview. *Carbon*, 1992. 30(7): p. 1111-1118.
36. Laine, J. and S. Yunes, Effect of the preparation method on the pore size distribution of activated carbon from coconut shell. *Carbon*, 1992. 30(4): p. 601-604.
37. Laforgue, A., et al., Polythiophene-based supercapacitors. *Journal of power sources*, 1999. 80(1): p. 142-148.
38. Frank Rose, M., et al., Limiting factors for carbon-based chemical double-layer capacitors. *Journal of power sources*, 1994. 47(3): p. 303-312.
39. Osaka, T., et al., An electrochemical double layer capacitor using an activated carbon electrode with gel electrolyte binder. *Journal of The Electrochemical Society*, 1999. 146(5): p. 1724-1729.
40. Beck, F. and M. Dolata, Fluorine-free binders for carbon black based electrochemical supercapacitors. *Journal of applied electrochemistry*, 2001. 31(5): p. 517-521.
41. Wang, J., et al., Morphological effects on the electrical and electrochemical properties of carbon aerogels. *Journal of The Electrochemical Society*, 2001. 148(6): p. D75-D77.
42. Arico, A.S., et al., Nanostructured materials for advanced energy conversion and storage devices. *Nature materials*, 2005. 4(5): p. 366-377.

43. Zanto, E., J. Ritter, and B. Popov. Sol-gel derived carbon aerogels and xerogels for use as the anode in the lithium ion battery. in Proceedings-Electrochemical Society. 1999. Electrochemical Society.
44. Lin, C. and J. Ritter, Effect of synthesis pH on the structure of carbon xerogels. Carbon, 1997. 35(9): p. 1271-1278.
45. Li, J., et al., Structure and electrochemical properties of carbon aerogels synthesized at ambient temperatures as supercapacitors. Journal of Non-Crystalline Solids, 2008. 354(1): p. 19-24.
46. Liu, D., et al., Preparation of activated carbon aerogels with hierarchically porous structures for electrical double layer capacitors. Electrochimica Acta, 2013. 89(0): p. 571-576.
47. Du, C., J. Yeh, and N. Pan, High power density supercapacitors using locally aligned carbon nanotube electrodes. Nanotechnology, 2005. 16(4): p. 350.
48. Niu, C., et al., High power electrochemical capacitors based on carbon nanotube electrodes. Applied Physics Letters, 1997. 70(11): p. 1480-1482.
49. Picó, F., et al., Single-walled carbon nanotubes as electrodes in supercapacitors. Journal of The Electrochemical Society, 2004. 151(6): p. A831-A837.
50. Frackowiak, E., et al., Supercapacitor electrodes from multiwalled carbon nanotubes. Applied Physics Letters, 2000. 77(15): p. 2421-2423.

51. An, K.H., et al., Electrochemical properties of high-power supercapacitors using single-walled carbon nanotube electrodes. *Advanced functional materials*, 2001. 11(5): p. 387-392.
52. Yoon, B.J., et al., Electrical properties of electrical double layer capacitors with integrated carbon nanotube electrodes. *Chemical Physics Letters*, 2004. 388(1): p. 170-174.
53. University's, M.T. 2006; Available from: <http://www.phy.mtu.edu/newsletter/research/FatNanotubeArt2006.html>.
54. Hsu, H.-C., et al., Stand-up structure of graphene-like carbon nanowalls on CNT directly grown on polyacrylonitrile-based carbon fiber paper as supercapacitor. *Diamond and Related Materials*, 2012. 25(0): p. 176-179.
55. Conway, B., V. Birss, and J. Wojtowicz, The role and utilization of pseudocapacitance for energy storage by supercapacitors. *Journal of power sources*, 1997. 66(1): p. 1-14.
56. Conway, B.E., Transition from “supercapacitor” to “battery” behavior in electrochemical energy storage. *Journal of The Electrochemical Society*, 1991. 138(6): p. 1539-1548.
57. Ryu, K.S., et al., Symmetric redox supercapacitor with conducting polyaniline electrodes. *Journal of power sources*, 2002. 103(2): p. 305-309.
58. Mastragostino, M., C. Arbizzani, and F. Soavi, Polymer-based supercapacitors. *Journal of power sources*, 2001. 97: p. 812-815.

59. Kim, I.H. and K.B. Kim, Ruthenium oxide thin film electrodes for supercapacitors. *Electrochemical and Solid-State Letters*, 2001. 4(5): p. A62-A64.
60. Zheng, J., P. Cygan, and T. Jow, Hydrous ruthenium oxide as an electrode material for electrochemical capacitors. *Journal of The Electrochemical Society*, 1995. 142(8): p. 2699-2703.
61. Zheng, J. and T. Jow, A new charge storage mechanism for electrochemical capacitors. *Journal of The Electrochemical Society*, 1995. 142(1): p. L6-L8.
62. Alvi, F., et al., Graphene–polyethylenedioxythiophene conducting polymer nanocomposite based supercapacitor. *Electrochimica Acta*, 2011. 56(25): p. 9406-9412.
63. Ghenaatian, H.R., M.F. Mousavi, and M.S. Rahmanifar, High performance hybrid supercapacitor based on two nanostructured conducting polymers: Self-doped polyaniline and polypyrrole nanofibers. *Electrochimica Acta*, 2012. 78(0): p. 212-222.
64. Jurewicz, K., et al., Supercapacitors from nanotubes/polypyrrole composites. *Chemical Physics Letters*, 2001. 347(1): p. 36-40.
65. Frackowiak, E., et al., Supercapacitors based on conducting polymers/nanotubes composites. *Journal of power sources*, 2006. 153(2): p. 413-418.
66. Frackowiak, E., et al., Nanotubular materials for supercapacitors. *Journal of power sources*, 2001. 97: p. 822-825.

67. An, H., et al., Polypyrrole/carbon aerogel composite materials for supercapacitor. *Journal of power sources*, 2010. 195(19): p. 6964-6969.
68. Mastragostino, M., C. Arbizzani, and F. Soavi, Conducting polymers as electrode materials in supercapacitors. *Solid State Ionics*, 2002. 148(3): p. 493-498.
69. Laforgue, A., et al., Activated carbon/conducting polymer hybrid supercapacitors. *Journal of The Electrochemical Society*, 2003. 150(5): p. A645-A651.
70. Antiohos, D., et al., Manganosite–microwave exfoliated graphene oxide composites for asymmetric supercapacitor device applications. *Electrochimica Acta*, (0).
71. Pell, W.G. and B.E. Conway, Peculiarities and requirements of asymmetric capacitor devices based on combination of capacitor and battery-type electrodes. *Journal of power sources*, 2004. 136(2): p. 334-345.
72. Du Pasquier, A., et al., A comparative study of Li-ion battery, supercapacitor and nonaqueous asymmetric hybrid devices for automotive applications. *Journal of power sources*, 2003. 115(1): p. 171-178.
73. Wang, X. and J. Zheng, The optimal energy density of electrochemical capacitors using two different electrodes. *Journal of The Electrochemical Society*, 2004. 151(10): p. A1683-A1689.
74. Li, H., L. Cheng, and Y. Xia, A Hybrid Electrochemical Supercapacitor Based on a 5 V Li-Ion Battery Cathode and Active Carbon. *Electrochemical and Solid-State Letters*, 2005. 8(9): p. A433-A436.

75. Roy, R.K., Design of experiments using the Taguchi approach: 16 steps to product and process improvement 2001: Wiley-Interscience.
76. Soravia, S. and A. Orth, Design of Experiments. Ullmann's Encyclopedia of Industrial Chemistry, 2007.
77. Antony, J. and F.J. Antony, Teaching the Taguchi method to industrial engineers. Work Study, 2001. 50(4): p. 141-149.
78. Information, C.U.U. Orthogonal Arrays 2005; Available from: <http://kernow.curtin.edu.au/www/Taguchi/SET7.HTM>.
79. wikipedia. Pilot plant. 2008; Available from: http://en.wikipedia.org/wiki/Pilot_plant.
80. Ng, K.C., M. Cloke, and G.Z. Chen, Nano-sized Mn₂O₃ prepared by a novel solvolysis route as an electrochemical capacitor electrode material. The Journal, 2008.
81. Zhang, S., et al., Nanocomposites of manganese oxides and carbon nanotubes for aqueous supercapacitor stacks. Electrochimica Acta, 2010. 55(25): p. 7447-7453.
82. Seung-Shik Shin, N.-S.C., Baek-Hyun Lee, Shi-Joon Sung, Jung-Ki Park, Electrochemical Characteristics of an Electric Double Layer Capacitor Using an Activated Carbon Powder Dept. of Chemical & Biomolecular Engineering, KAIST

83. Zuckerbrod, D., Performance of Carbon-PTFE Electrodes and PTFE Separators in Electrochemical Double Layer Capacitors (EDLCs) David Zuckerbrod, Robert Sassa, Marianne Szabo, Meagan Mizenko.
84. Kosuda, A. and S. Maruyama, Electrochemical capacitor, 2007, Google Patents.
85. Zhong, L., X. Xi, and B. Zou, ELECTROCHEMICAL DOUBLE LAYER CAPACITOR, 2008, Google Patents.
86. Kosuda, A. and S. Maruyama, Electrochemical capacitor, 2007, Google Patents.
87. Iijima, S., Helical microtubules of graphitic carbon. *nature*, 1991. 354(6348): p. 56-58.
88. Oberlin, A., M. Endo, and T. Koyama, Filamentous growth of carbon through benzene decomposition. *Journal of Crystal Growth*, 1976. 32(3): p. 335-349.
89. Conway, B. and W. Pell, Power limitations of supercapacitor operation associated with resistance and capacitance distribution in porous electrode devices. *Journal of power sources*, 2002. 105(2): p. 169-81.
90. Mahon, P.J., et al., Measurement and modelling of the high-power performance of carbon-based supercapacitors. *Journal of power sources*, 2000. 91(1): p. 68-76.
91. Du, X., et al., Studies on the performances of silica aerogel electrodes for the application of supercapacitor. *Ionics*, 2009. 15(5): p. 561-565.
92. Antony, J., G. Knowles, and T. Taner, 10 steps to optimal production. *Quality*, 2001. 40(9): p. 45-49.

93. Taguchi, G., Introduction to quality engineering: designing quality into products and processes 1986.
94. Ross, P.J., Taguchi techniques for quality engineering: loss function, orthogonal experiments, parameter and tolerance design. 1988.
95. Tsui, K.L., Strategies for planning experiments using orthogonal arrays and confounding tables. Quality and Reliability Engineering International, 1988. 4(2): p. 113-122.
96. Box, G., S. Bisgaard, and C. Fung, An explanation and critique of Taguchi's contributions to quality engineering. Quality and Reliability Engineering International, 1988. 4(2): p. 123-131.
97. Raymundo-Pinero, E., et al., Performance of manganese oxide/CNTs composites as electrode materials for electrochemical capacitors. Journal of The Electrochemical Society, 2005. 152(1): p. A229-A235.
98. Roy, R., Design of experiments using the Taguchi method, 16 steps to product and process improvement, 2001, John Wiley & Sons, Inc., New York.

7. Appendix A

7.1 Cylindrical supercapacitor CY-2

The second prototype cylindrical supercapacitor CY-2 was fabricated and tested, the same way as the first prototype CY-1. Figure 7-1 shows the initial charge-discharge measurements using Autolab, the constant charging-discharging current was 200 mA.

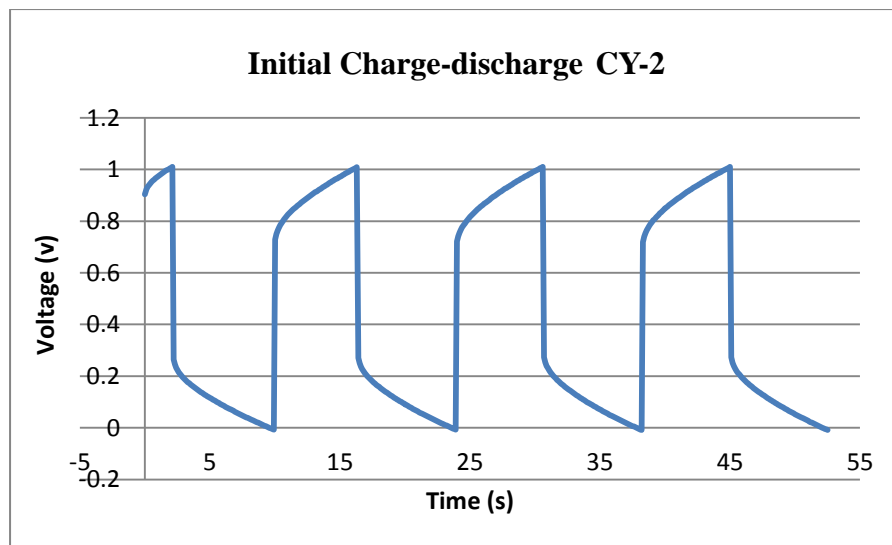


Figure 7-1 Charge-discharge curve for CY-2 at 200 mA

The capacitance of this prototype is calculated using the slope of the charge-discharge curve which is shown in Figure 7-2. The initial capacitance of this prototype is 7.19 F, which is lower than the capacitance of prototype CY-1, this could be due the supercapacitor not cycled yet to make sure the electrolyte wet the entire electrodes surface and reach inside the porous of the activated carbon.

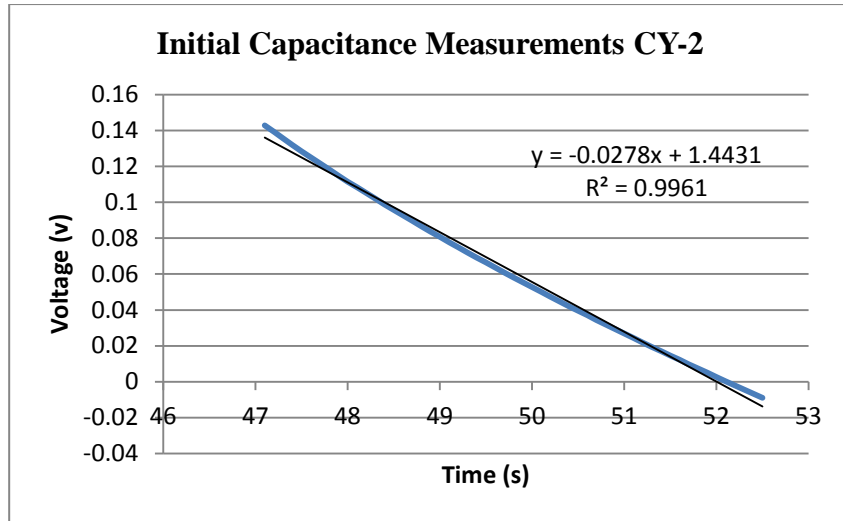


Figure 7-2 Initial capacitance of the CY-2

$$C = i/\text{slope} = 0.2/0.0278 = 7.19 \text{ F}$$

$$\text{ESR} = 3.65 \Omega$$

Figure 7-3 confirms the prototype have a supercapacitor EIS characteristics, with the semicircle at high frequencies and the straight line at lower frequencies range.

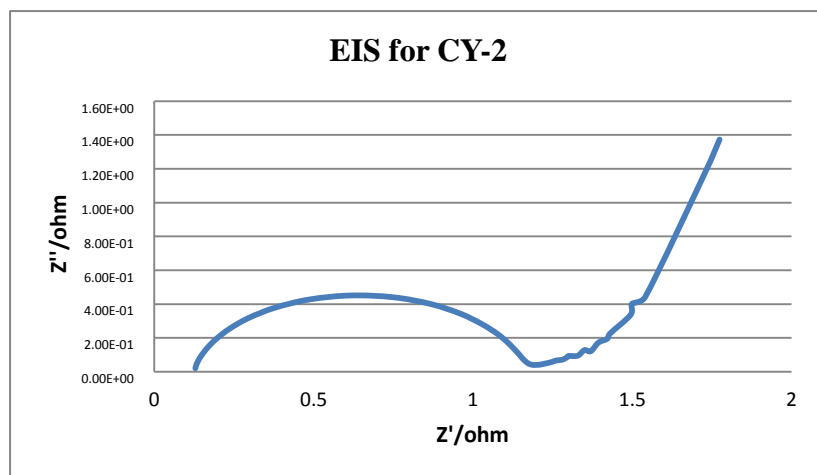


Figure 7-3 EIS for CY-2

After cycling the prototype for 50 cycles, the capacitance was measured again using the charge-discharge curve. Figure 7-4 shows the charge-discharge curve for the CY-2 after 50 cycles.

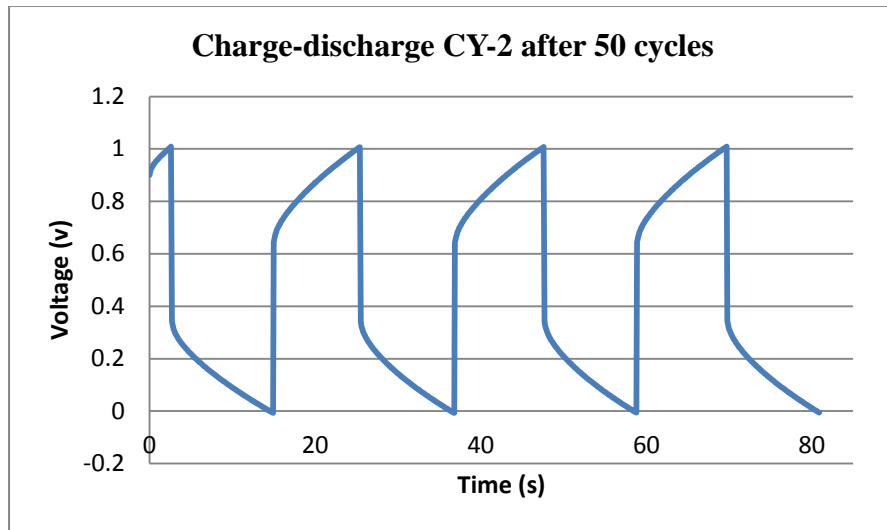


Figure 7-4 Charge-discharge for CY-2 after 50 cycles

Figure 7-5 shows the part of the charge-discharge curve that used to calculate the capacitance of the CY2 prototype after 50 cycles. After, cycling the CY2 prototype its capacitance increased by almost 1 F to 8.1 F, this could be due to the penetration of the electrolyte deep inside the AC, which results in more surface area being utilized.

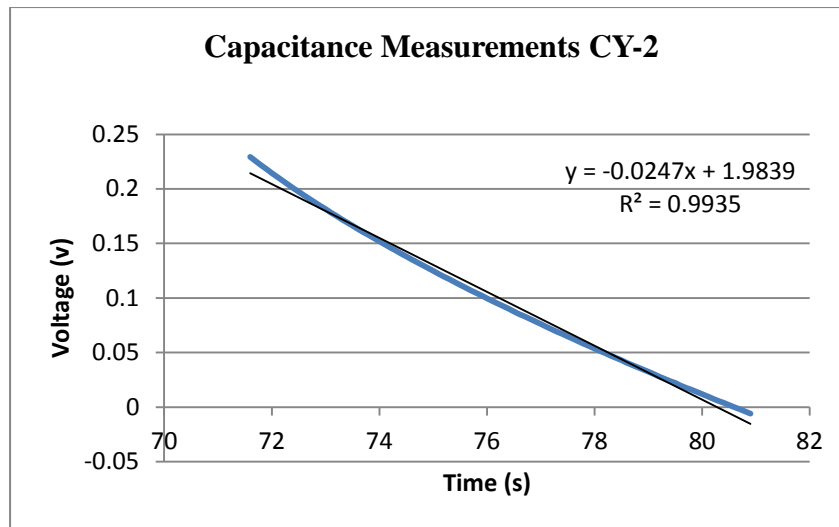


Figure 7-5 Capacitance of CY-2 after 50 cycles

$$C = i/\text{slope} = 0.2/0.0247 = 8.1 \text{ F}$$

$$\text{ESR} = 3.29 \Omega$$

The prototype was cycled for 100 cycles and the capacitance was measured using the slope of the charge-discharge curve. Figure 7-6 shows the charge-discharge curve for CY-2 after 100 cycles.

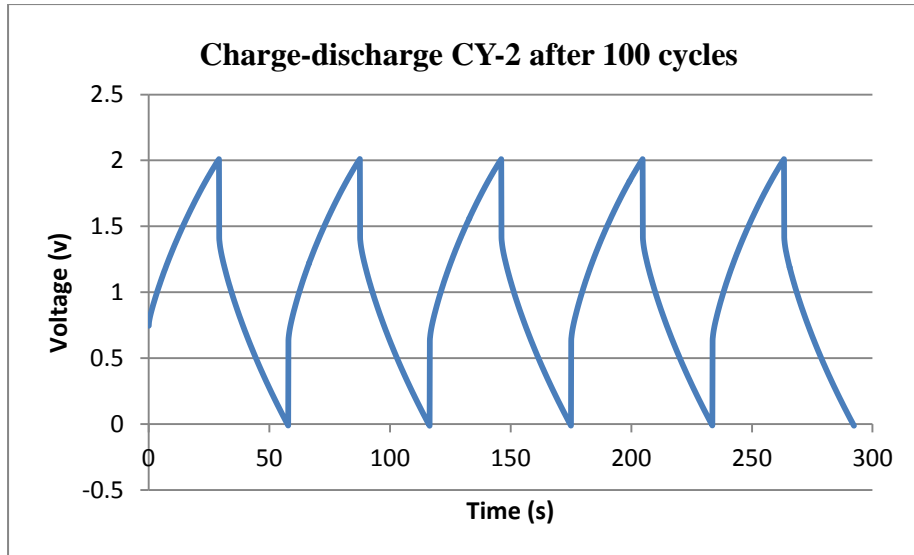


Figure 7-6 Charge-discharge curve for CY-2 after 100 cycles

Figure 7-7 shows the curve used to calculate the capacitance of the CY-2 prototype, the capacitance measured is 10.91 F, increased from 8.1 F.

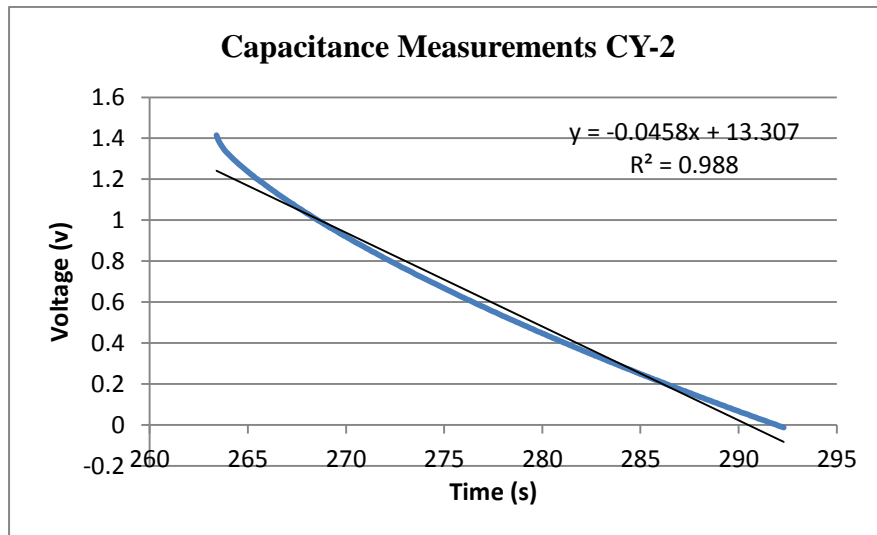


Figure 7-7 Capacitance measurement of CY-2

$$C = i/\text{slope} = 0.5/0.0258 = 10.91 \text{ F}$$

$$\text{ESR} = 2.93 \Omega$$

The prototype was further cycled for 300 cycles and then its capacitance was measured, Figure 7-8 shows the charge-discharge curve after 300 cycles.

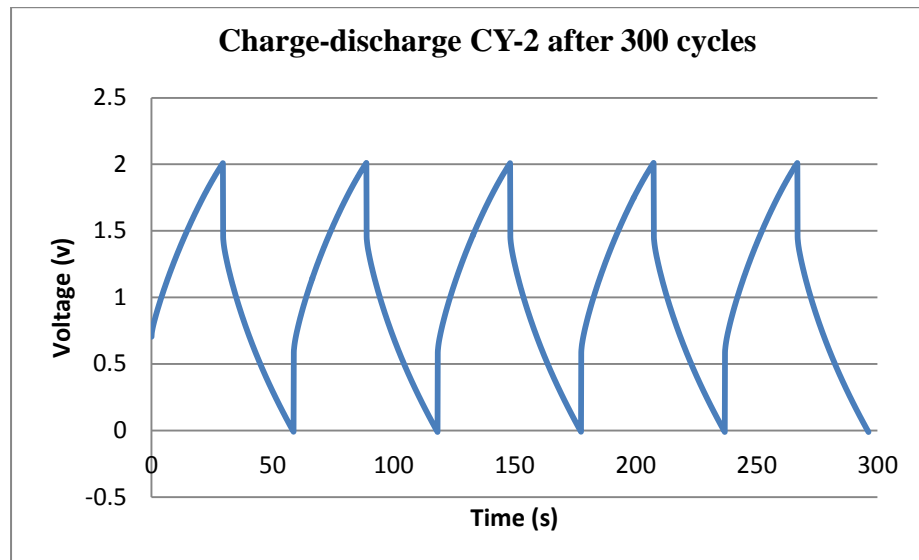


Figure 7-8 Charge-discharge curve for CY-2 after 300 cycles

Figure 7-9 shows the curve used to calculate the capacitance of the CY-2 prototype after 300 cycles, the capacitance measured is 12 F.

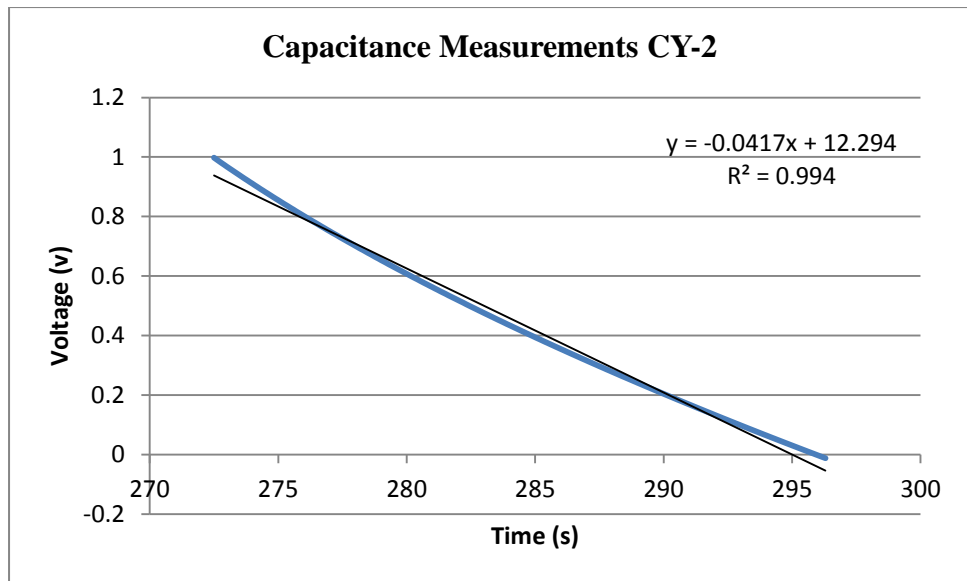


Figure 7-9 Capacitance measurement for CY-2 after 300 cycles

$$C = i/\text{slope} = 0.5/0.0417 = 12 \text{ F}$$

$$\text{ESR} = 2.72 \Omega$$

7.2 Cylindrical prototype CY-3

The third prototype cylindrical supercapacitor CY-3 was fabricated and tested the same way as the first two prototypes. Figure 7-10 shows the initial charge-discharge measurements using Autolab, the constant charging-discharging current was 200 mA.

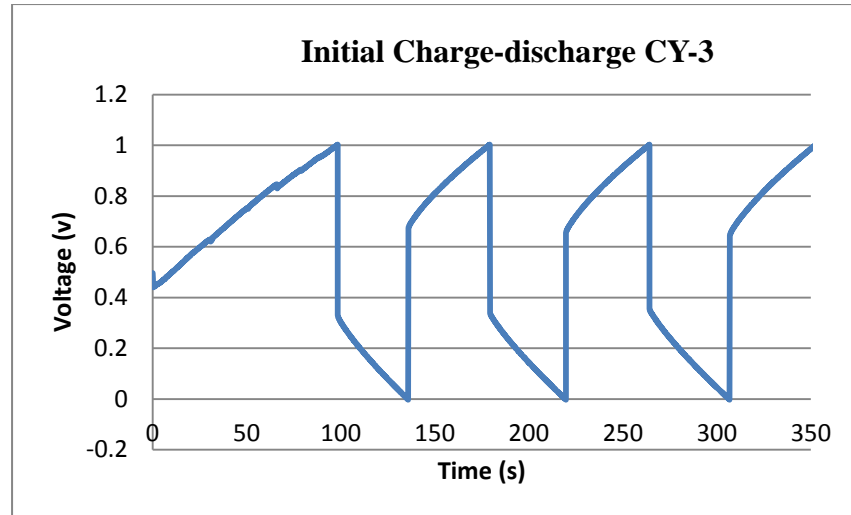


Figure 7-10 Initial charge-discharge test for CY-3

Figure 7-11 shows the curve used to calculate the initial capacitance of the CY-3 prototype, the capacitance measured is 29.41 F.

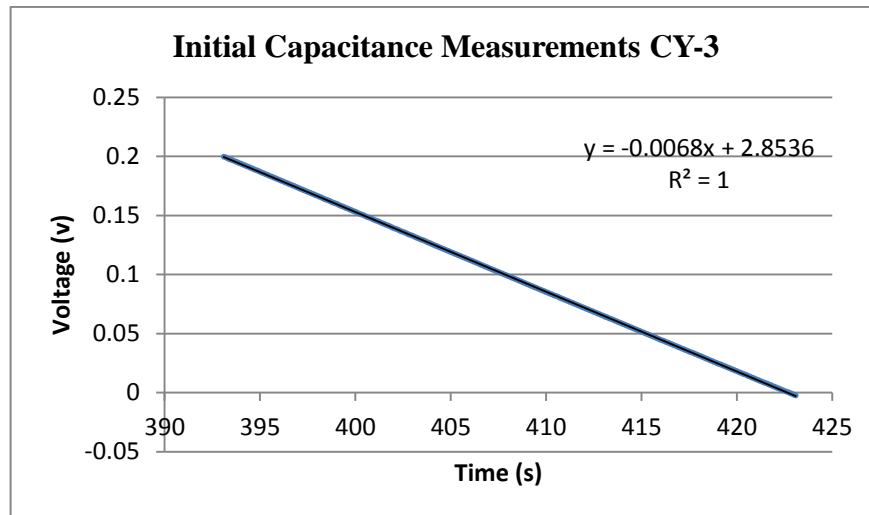


Figure 7-11 Initial capacitance measurement for CY-3

$$C = i/\text{slope} = 0.2/0.0068 = 29.41 \text{ F}$$

$$\text{ESR} = 3.35 \Omega$$

The CV test was also done to observe the behavior of the cell, for a voltage window of 2 V and scan rate of 20 mV/s, the curve shape resembles a supercapacitor which ideally should look like a square, but because it is the first life cycle of the supercapacitor the shape is imperfect. Figure 7-12 shows the CV curve.

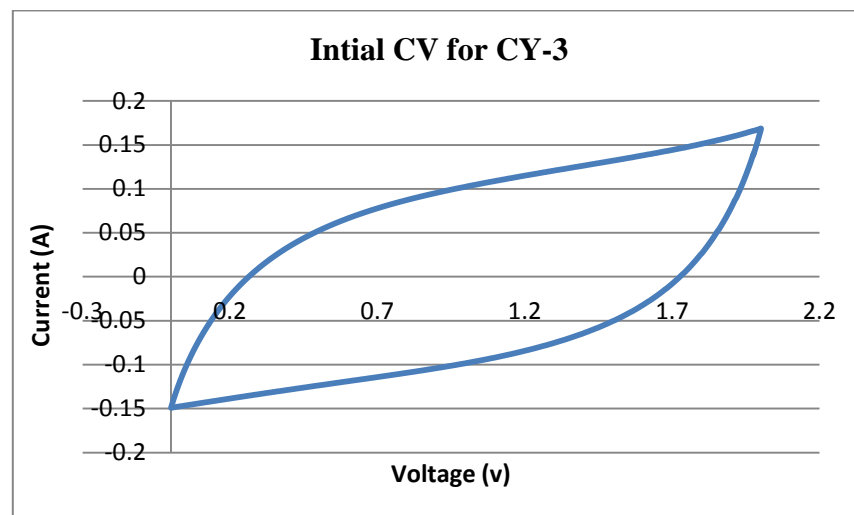


Figure 7-12 Initial CV curve for CY-3

The CY-3 prototype was cycled for 100 cycles and then the capacitance and ESR were measured using the charge-discharge curve. Figure 7-13 shows the charge-discharge curve after 100 cycles.

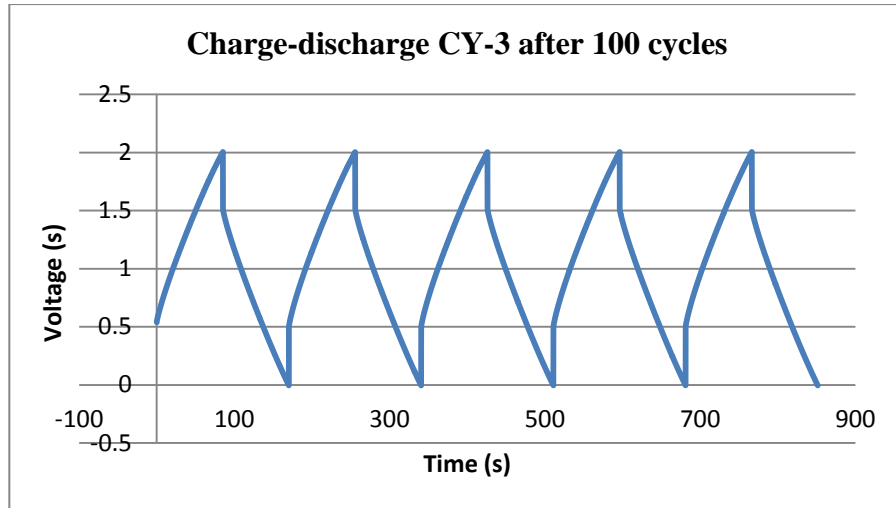


Figure 7-13 Charge-discharge curve for CY-3 after 100 cycles

Figure 7-14 shows the curve used to calculate the initial capacitance of the CY-3 prototype after 100 cycles, the capacitance measured increased to 30.67 F from 29.41 F.

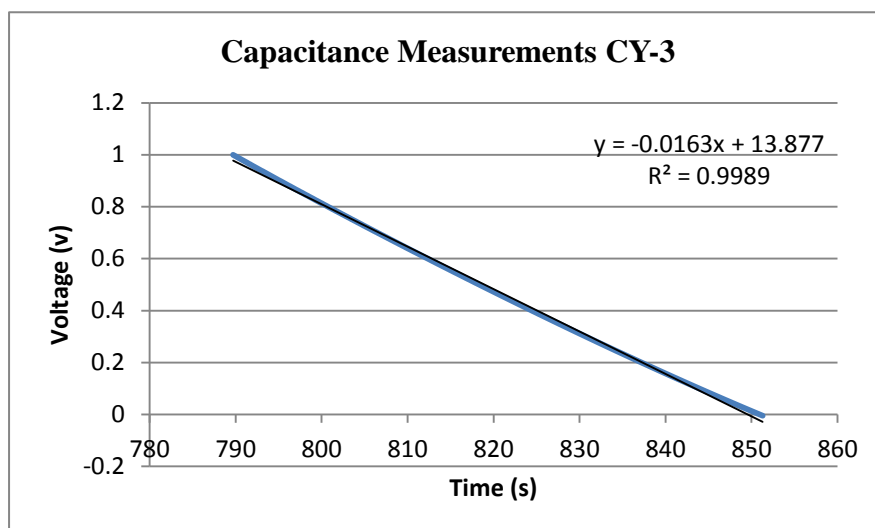


Figure 7-14 Capacitance measurement for CY-3

$$C = i/\text{slope} = 0.5/0.0163 = 30.67 \text{ F}$$

$$\text{ESR} = 0.964 \Omega$$

The CY-3 prototype was cycled for 350 cycles, and the capacitance was measured. Figure 7-15 shows the charge-discharge curve after 350 cycles.

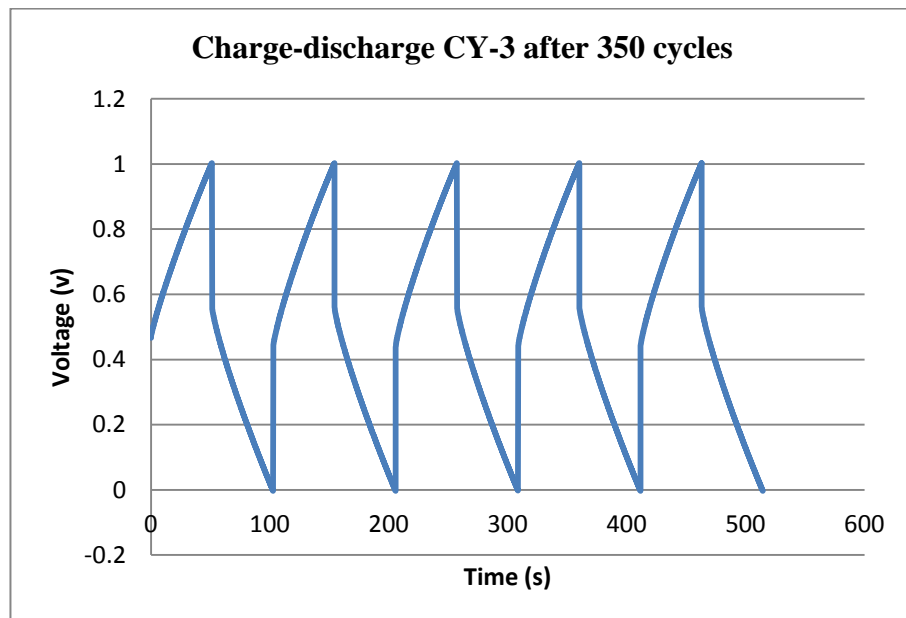


Figure 7-15 Charge-discharge curve for CY-3 after 350 cycles

Figure 7-16 shows the curve used to calculate the capacitance of the CY-3 prototype after 350 cycles, the capacitance measured decreased to 28.57 F from 30.76 F.

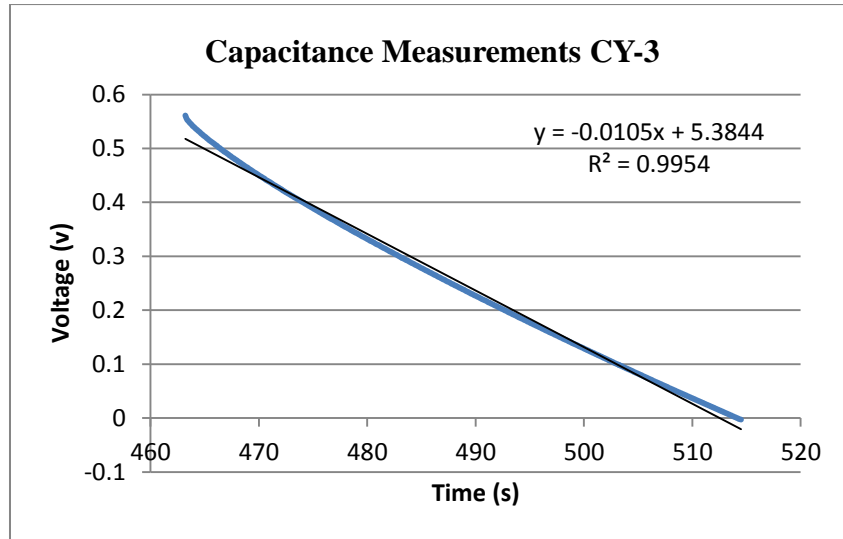


Figure 7-16 Capacitance measurement for CY-3

$$C = i/\text{slope} = 0.3/0.0105 = 28.57 \text{ F}$$

$$\text{ESR} = 1.46 \Omega$$

The CY-3 prototype was cycled for 1000 Cycles, and the capacitance was measured. Figure 7-17 shows the charge-discharge curve after 1000 cycles.

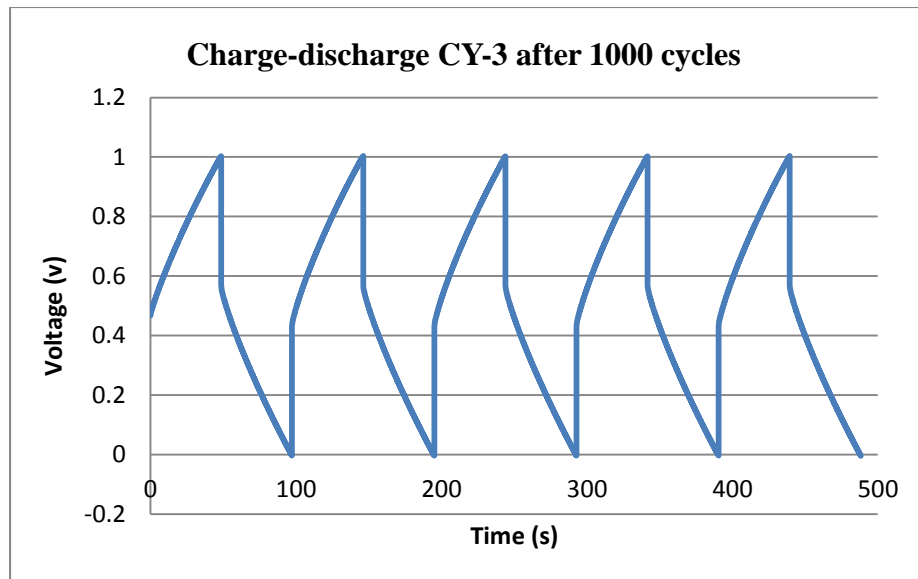


Figure 7-17 Charge-discharge curve for CY-3 after 1000 cycles

Figure 7-18 shows the curve used to calculate the capacitance of the CY-3 prototype after 1000 cycles, the capacitance measured decreased to 27.02 F from 28.57 F.

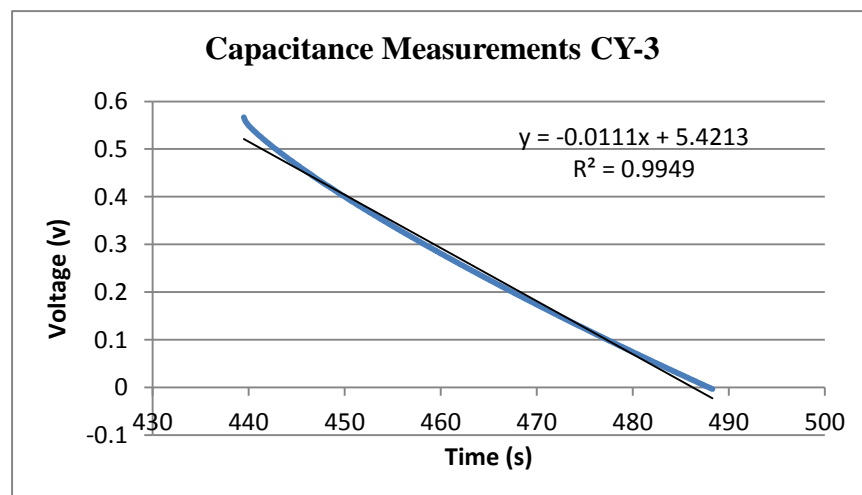


Figure 7-18 Capacitance measurement for CY-3

$$C = i/\text{slope} = 0.3/0.0111 = 27.02 \text{ F}$$

$$\text{ESR} = 1.44 \Omega$$

7.3 Cylindrical prototype CY-4

This prototype had a defect during the manufacturing process, could be a short between the electrodes or a bad contact between the electrodes and current collectors. Preventive steps will be taken in the following prototypes fabrication to avoid such failures, charge-discharge test was run on the prototype and the result curve shown in Figure 7-19, it doesn't show proper charge-discharge characteristics.

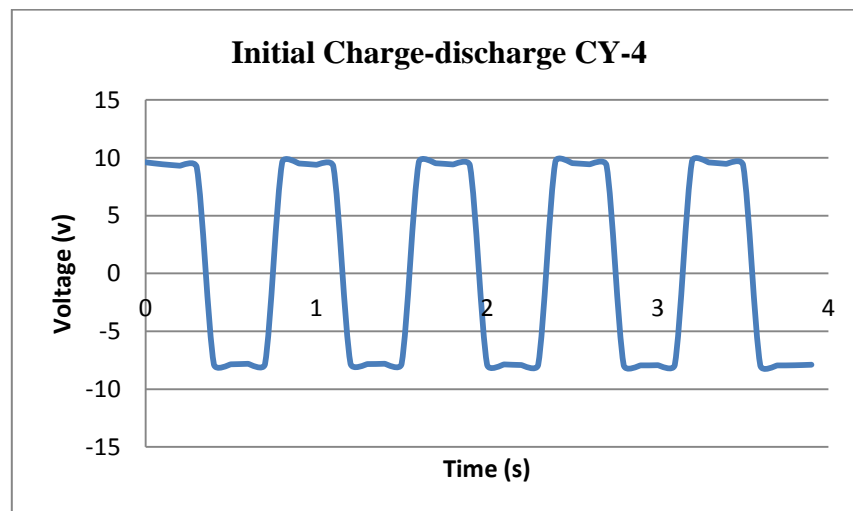


Figure 7-19 Initial charge-discharge curve for CY-4

The CV test was also run to observe the behavior of the cell and to confirm it doesn't show the capacitor characteristics, Figure 7-20 Shows the CV curve, which shows a very narrow curve.

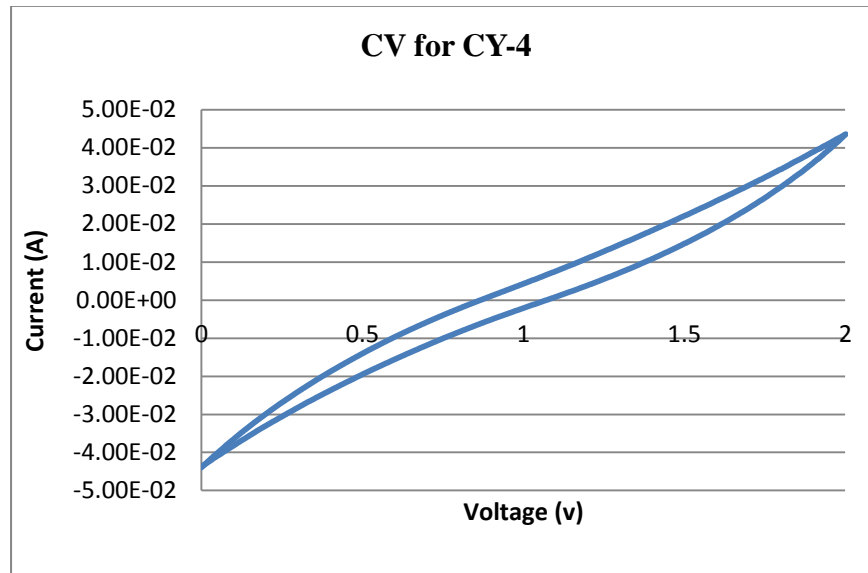


Figure 7-20 CV curve for CY-4

7.4 Cylindrical prototype CY-5

This prototype was tested using charge-discharge method, the initial test result is shown in Figure 7-21, and the CY-5 was tested using a 50 mA constant current.

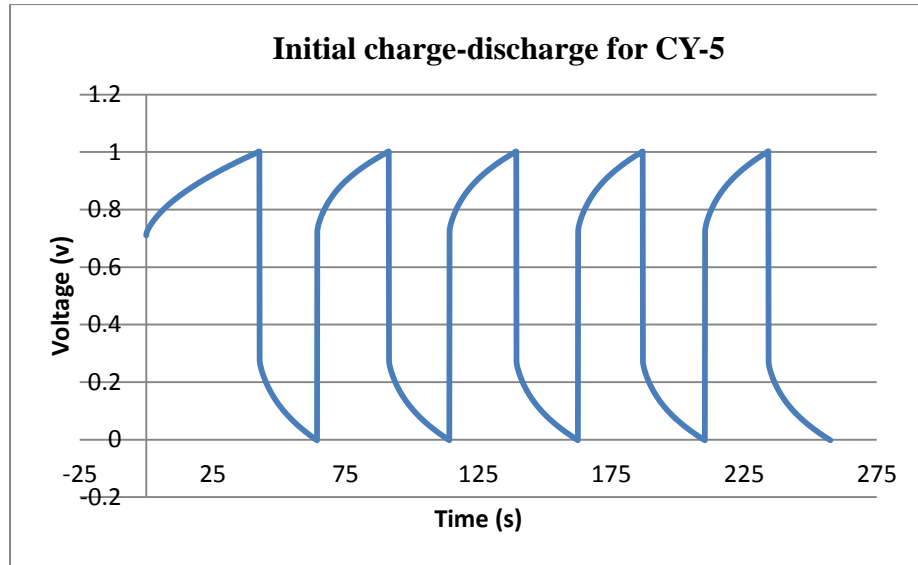


Figure 7-21 Initial charge-discharge curve for CY-5

The charge-discharge curve was used to measure the capacitance of the CY-5 prototype, as shown in Figure 7-22. The measured capacitance was 6.1 F.

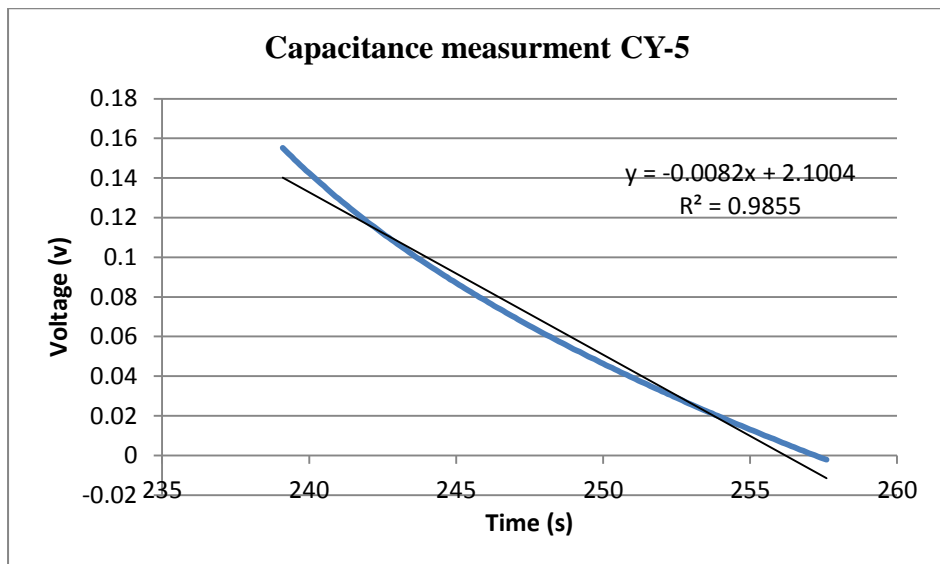


Figure 7-22 Initial capacitance measurement for CY-5

$$C = i/\text{slope} = 0.05/0.0082 = 6.1 \text{ F}$$

$$\text{ESR} = 14.5 \Omega$$

After the CY-5 was cycled for 100 cycles, it was tested again the test shows the prototype has failed. This could be due a dried electrolyte or short circuit between the electrodes. Figure 7-23 shows the charge-discharge curve.

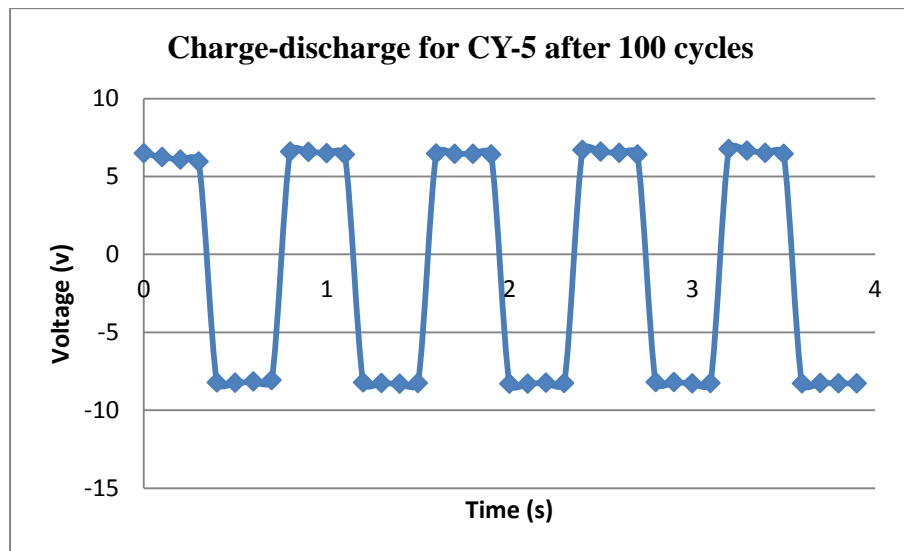


Figure 7-23 Charge-discharge for CY-5 after 100 cycles

EIS test was conducted to confirm the prototype had failed during testing process, Figure 7-24 shows the EIS curve which don't show a proper supercapacitor behavior.

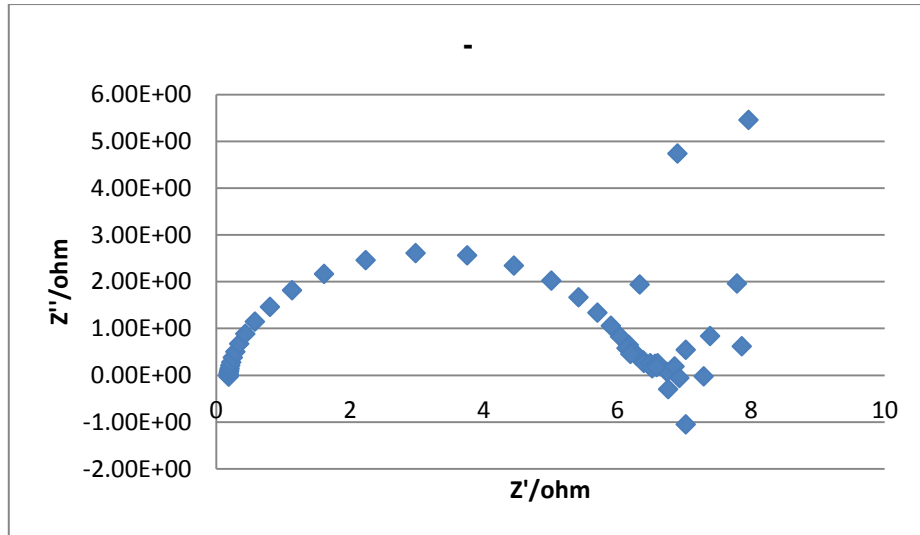


Figure 7-24 EIS curve for CY-5 after 100 cycles

CV test was conducted to confirm the prototype had failed, Figure 7-25 shows the CV curve which shows a very narrow curve.

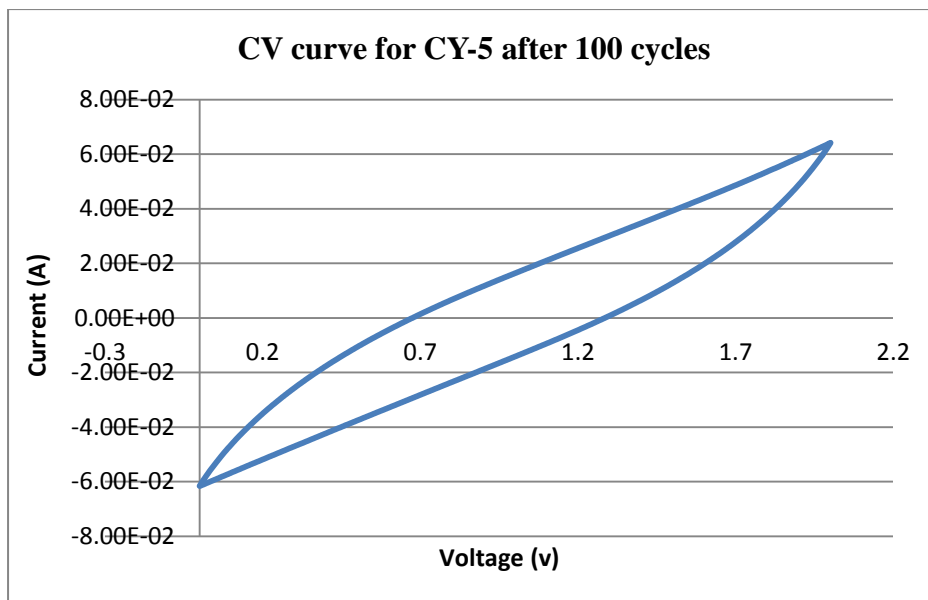


Figure 7-25 CV for CY-5 after 100 cycles

7.5 Cylindrical prototype CY-6

The charge-discharge test of the YC-6 prototype is showing a capacitor behavior but with very small capacitance, the curve shows a rapid charging and discharging hinting the capacity of this prototype is very small compared to the previous prototypes. Figure 7-26 shows the charge-discharge curve.

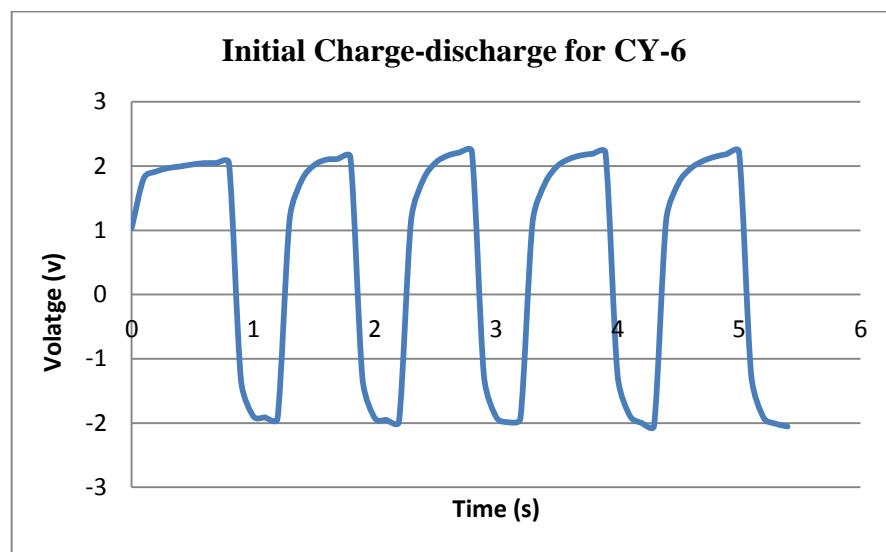


Figure 7-26 Initial charge-discharge curve for CY-6

The narrow curve of the CV test confirms the CY-6 doesn't have high capacity. Figure 7-27 shows the CV curve. This prototype was abandoned and no further testing was done.

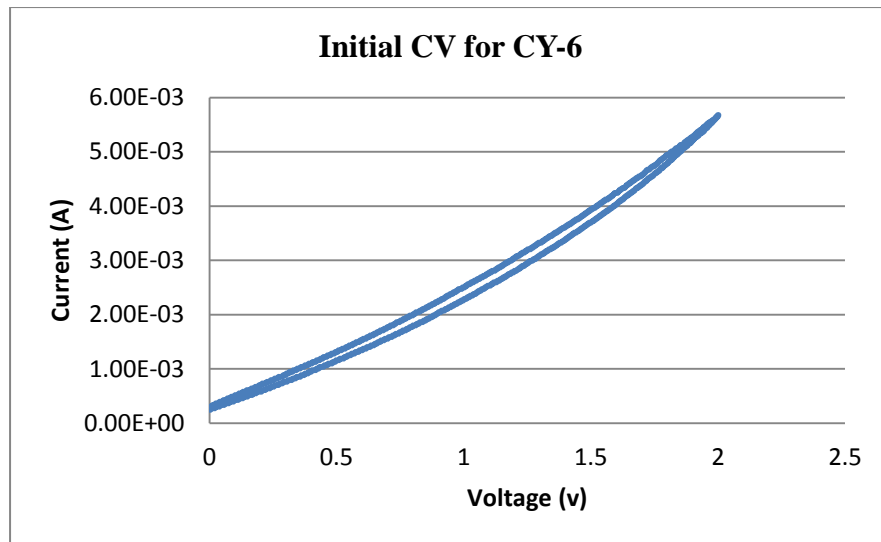


Figure 7-27 Initial CV for CY-6

7.6 Cylindrical prototype CY-7

Figure 7-28 shows the initial charge-discharge curve, the curve show abnormal capacitor behavior. This could be due to fault during the manufacturing process.

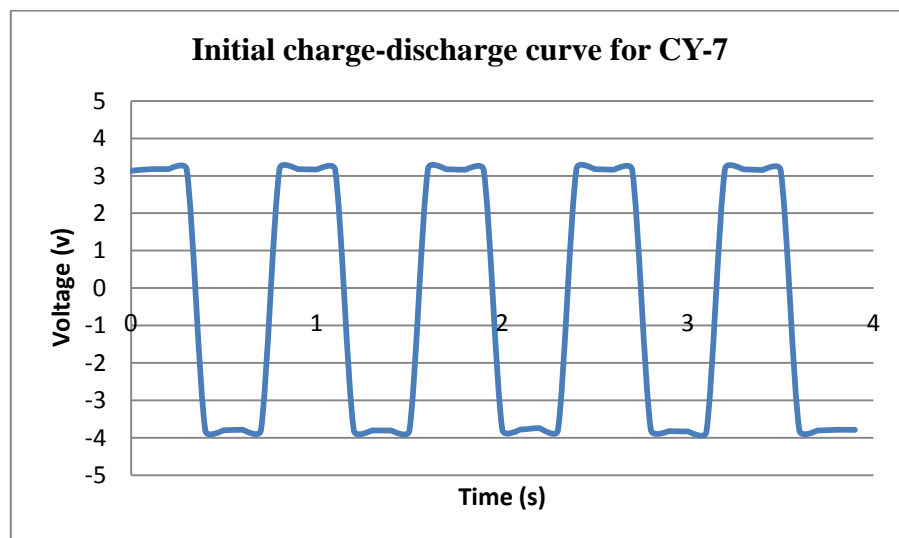


Figure 7-28 Initial charge-discharge curve for CY-7

7.7 Cylindrical prototype CY-8

The CY-8 prototype had faulty sealing cap, so it was excluded from the testing process.

7.8 Cylindrical prototype CY-9

The CY-9 prototype was tested to find its capacitance and ESR, charge-discharge curve test was conducted with 200 mA constant current. Figure 7-29 shows the initial charge-discharge curve.

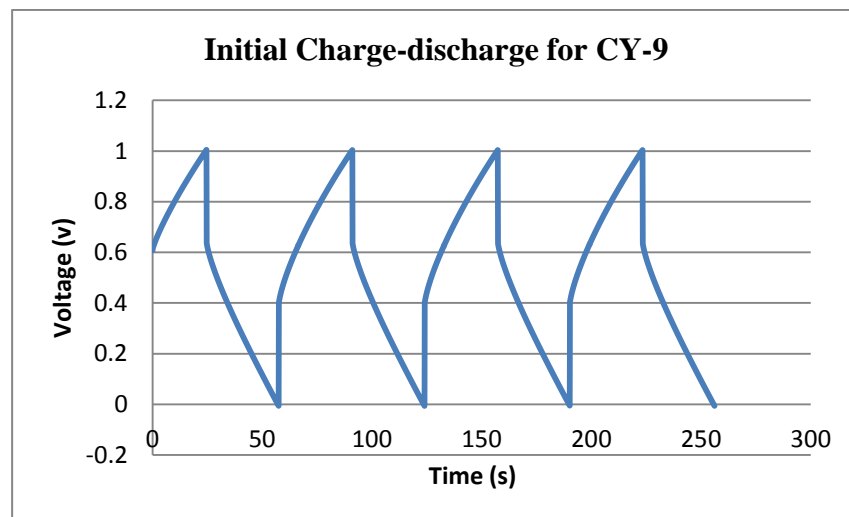


Figure 7-29 Initial charge-discharge curve for CY-9

Figure 7-30 Show the curve used to calculate the capacitance for the CY-9 prototype, the initial capacitance is 12.9 F.

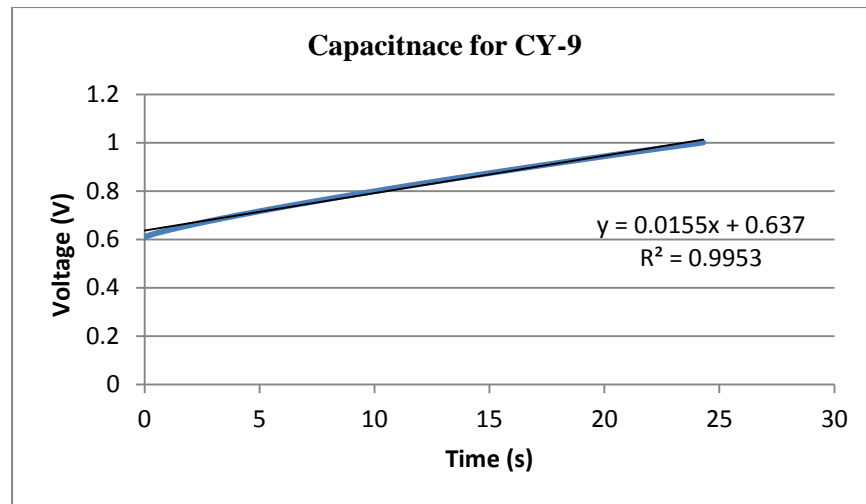


Figure 7-30 Capacitance measurement for CY-9

$$C = i/\text{slope} = 0.2/0.0155 = 12.9 \text{ F}$$

$$\text{ESR} = 1.81 \Omega$$

The CV test was conducted to observe the behavior of the CY9 prototype, Figure 7-31 shows the CV curve, which resembles the ideal supercapacitor behavior.

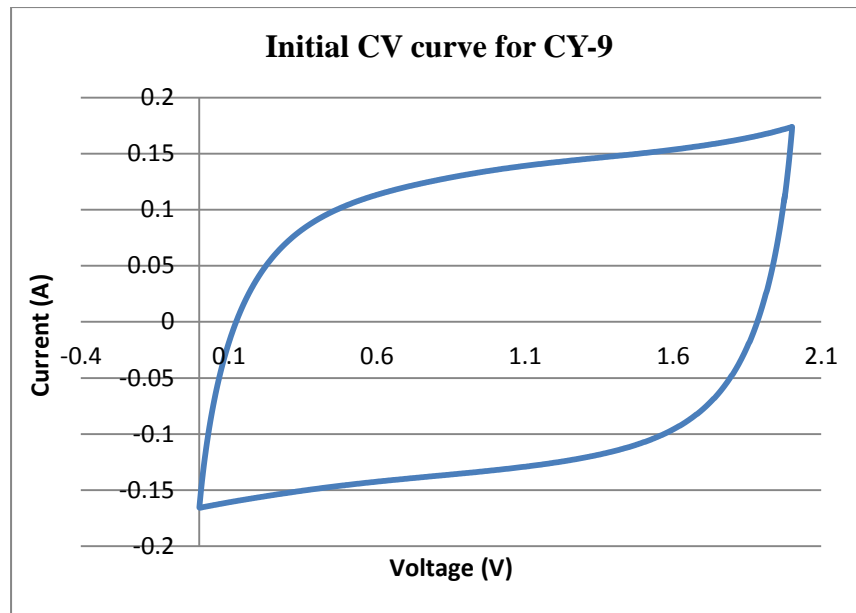


Figure 7-31 Initial CV for CY-9

After cycling the prototype for 100 cycles its capacitance was measured again, Figure 7-32 shows the charge-discharge curve, which was used to calculate the capacitance and ESR.

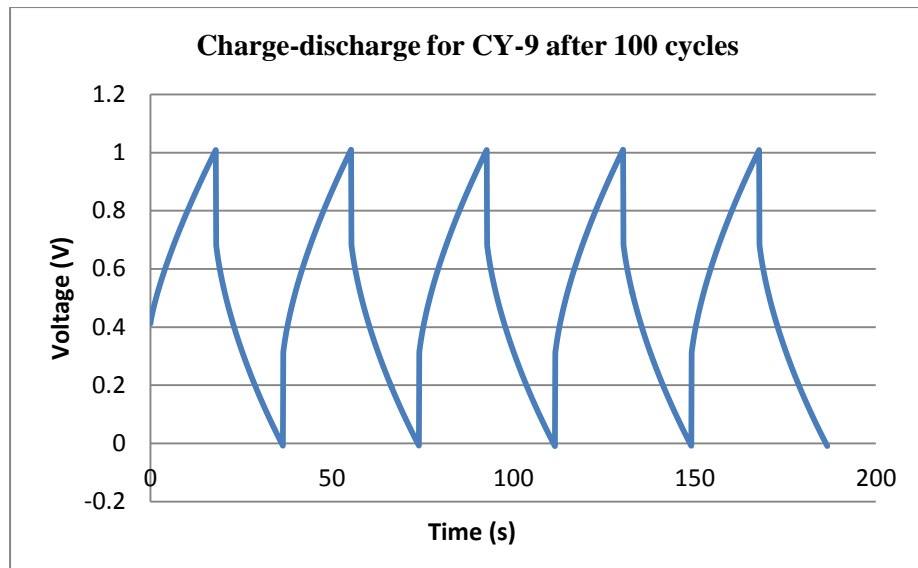


Figure 7-32 Charge-discharge for CY-9 after 100 cycles

Figure 7-33 shows the curve used to calculate the capacitance for the CY-9 prototype, the calculated capacitance was decreased from 12.9 F to 8.75 F.

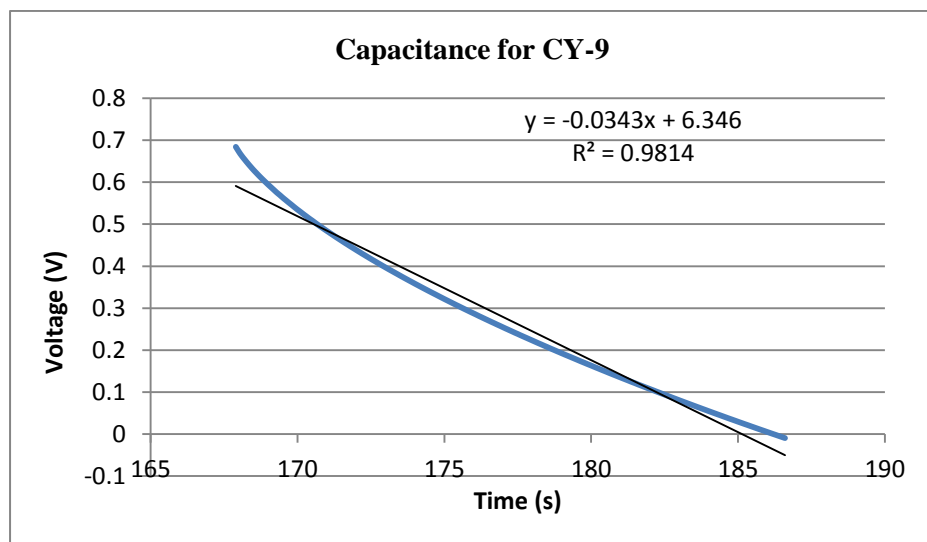


Figure 7-33 Capacitance measurement for CY-9

$$C = i/\text{slope} = 0.3/0.0343 = 8.75 \text{ F}$$

$$\text{ESR} = 1.05 \Omega$$

The prototype was cycled further for 500 cycles and retested, Figure 7-34 shows the charge-discharge curve after 500 cycles.

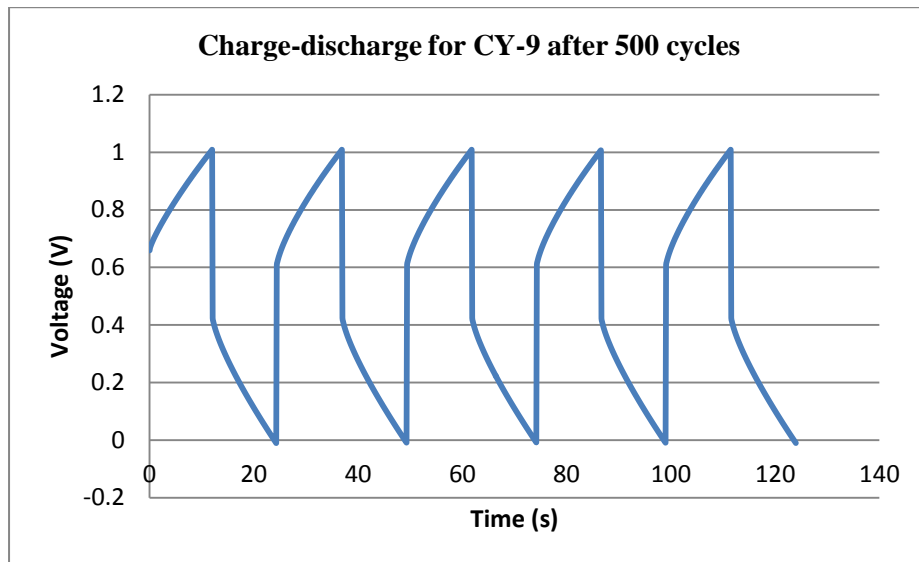


Figure 7-34 Charge-discharge for CY-9 after 500 cycles

Figure 7-35 shows the curve used to calculate the capacitance after 500 cycles. The capacitance had increased from 8.75 F to 9.1 F.

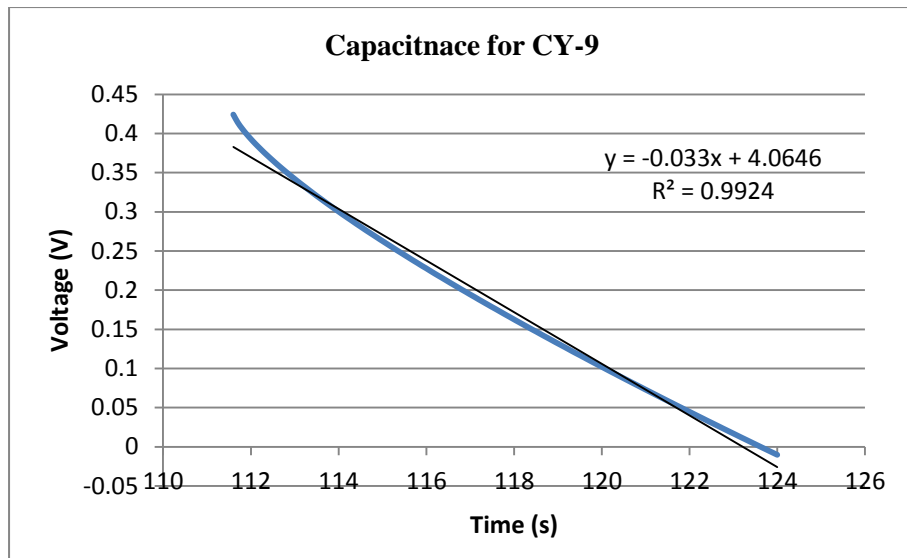


Figure 7-35 Capacitance measurement for CY-9

$$C = i/\text{slope} = 0.3/0.033 = 9.1 \text{ F}$$

$$\text{ESR} = 1.92 \Omega$$

7.9 Cylindrical prototype CY-10

This prototype had a failure during the manufacturing process, so it was excluded from the testing process.

7.10 Cylindrical prototype CY-11

The CY-11 prototype was tested to find its capacitance, charge-discharge curve test was conducted with 300 mA constant current. Figure 7-36 shows the charge-discharge curve.

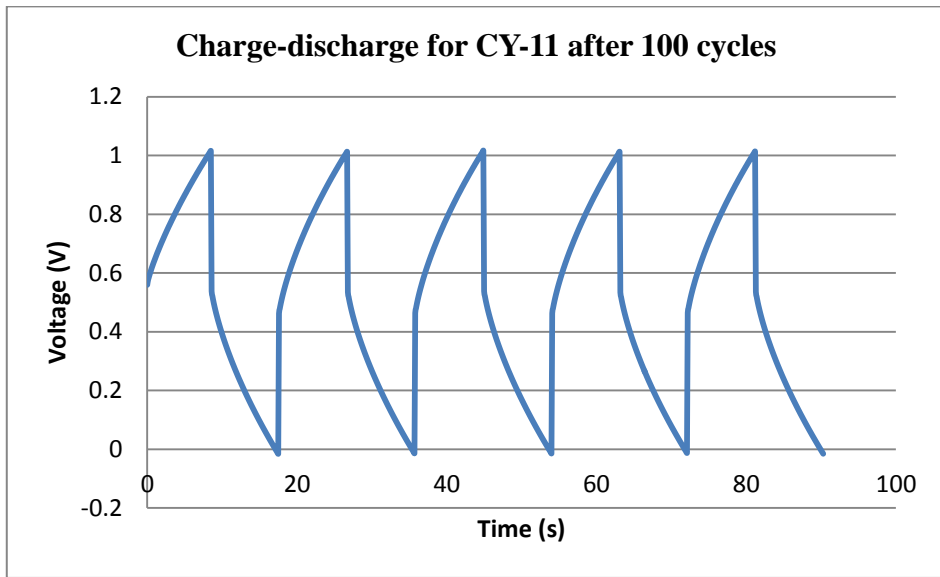


Figure 7-36 Charge-discharge curve for CY-11 after 100 cycles

Figure 7-37 shows the curve used to calculate the capacitance after 100 cycles.

The capacitance is 5.22 F.

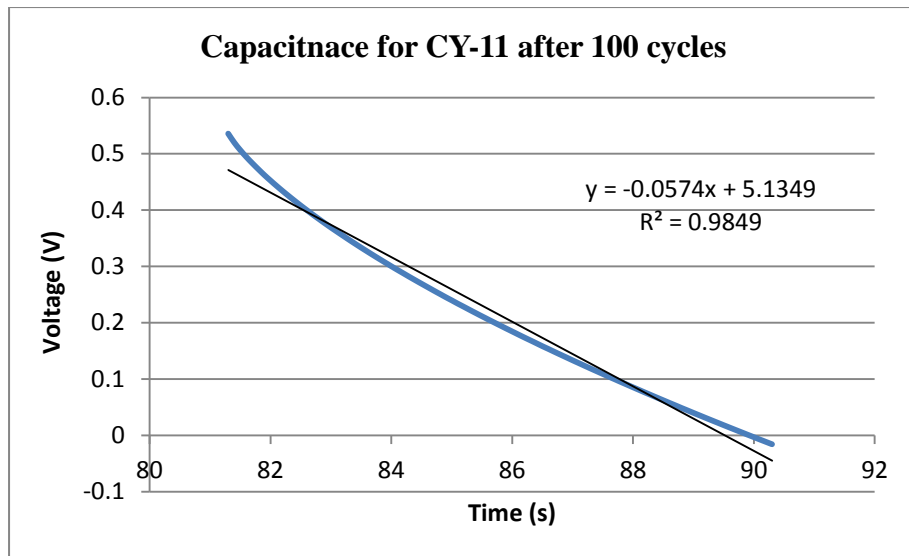


Figure 7-37 Capacitance measurement

$$C = i/\text{slope} = 0.3/0.0574 = 5.22 \text{ F}$$

$$\text{ESR} = 1.54 \Omega$$

The prototype was cycled further for 500 cycles and retested, Figure 7-38 shows the charge-discharge curve after 500 cycles.

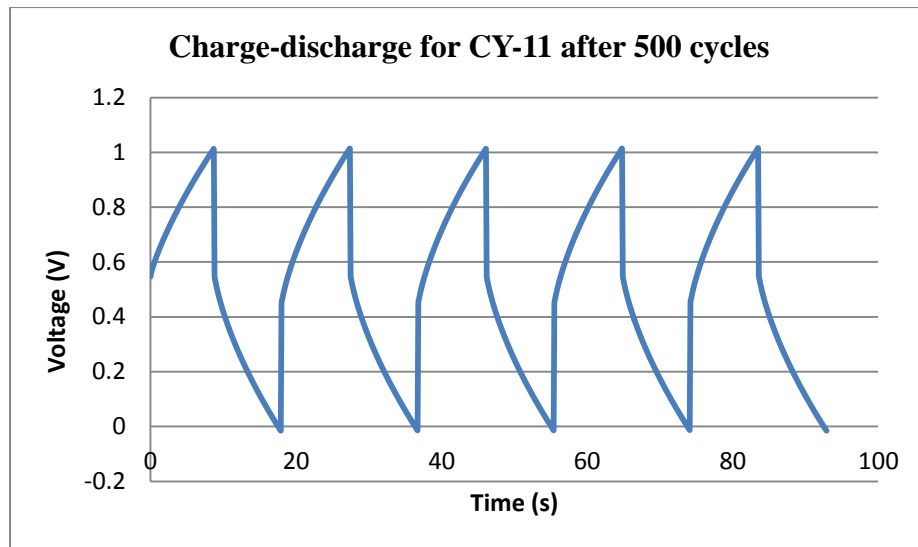


Figure 7-38 Charge-discharge curve for CY-11 after 500 cycles

Figure 7-39 shows the curve used to calculate the capacitance after 500 cycles.

The capacitance is 5.27 F.

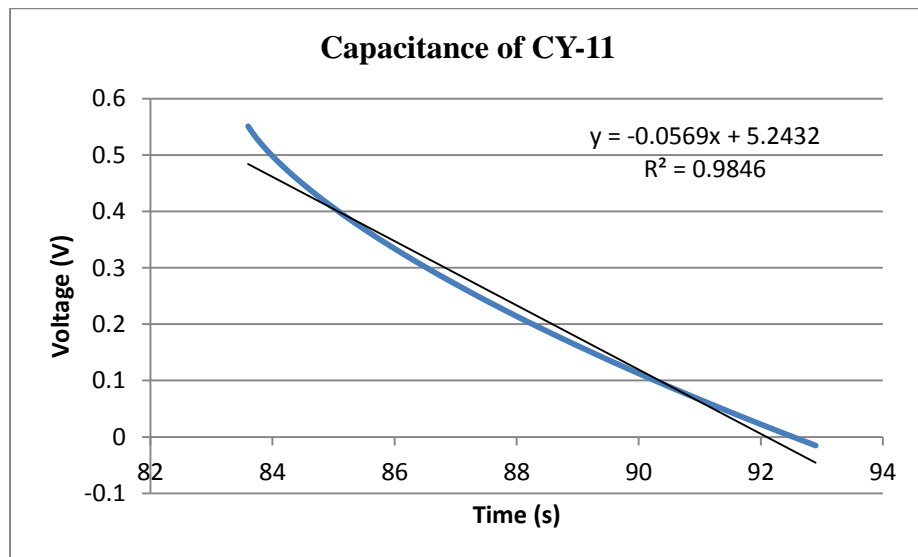


Figure 7-39 Capacitance measurement of CY-11

$$C = i/\text{slope} = 0.3/0.0569 = 5.27 \text{ F}$$

$$\text{ESR} = 1.5 \Omega$$

8. Appendix B

8.1 Coin prototype B-2

The second supercapacitor coin prototype B-2 was tested using the charge-discharge test with 50 mA constant current. The first test was done at 10 cycles.

Figure 8-1 shows the charge-discharge curve for B-2.

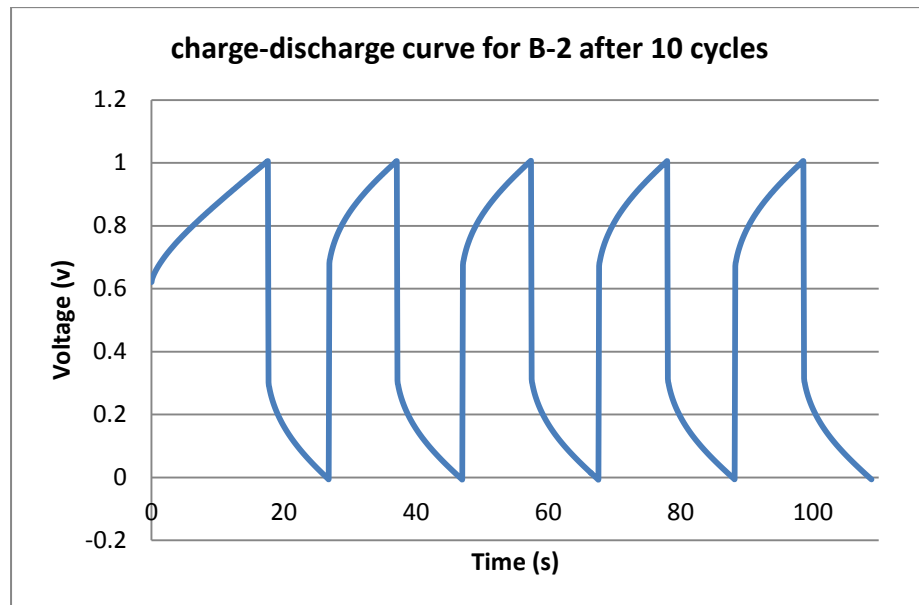


Figure 8-1 Charge-discharge curve for prototype B-2 after 10 cycles

Portion of the charge-discharge curve is used to calculate the capacitance of the B-2 prototype, Figure 8-2 shows the curve used to measure the slope which then used to calculate the capacitance.

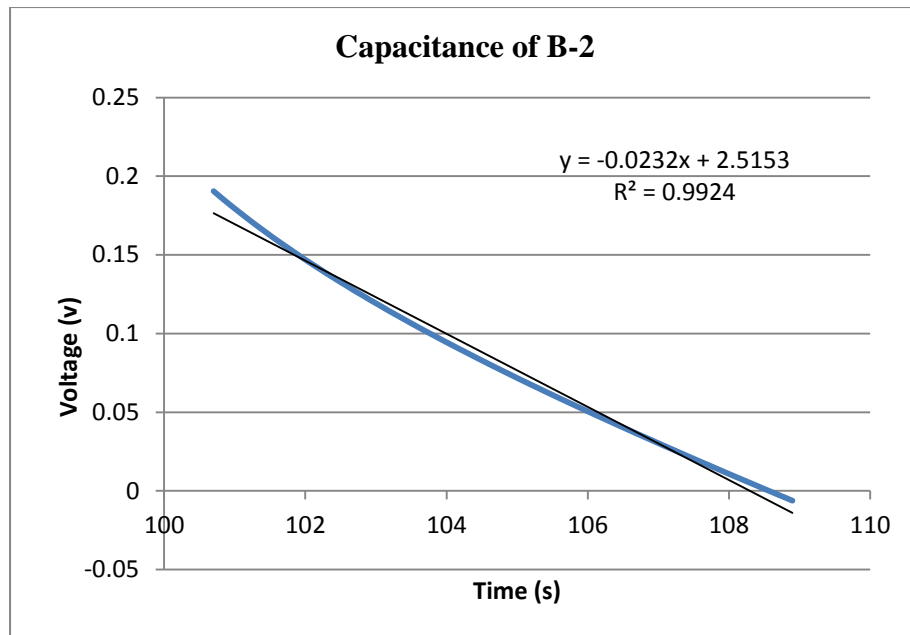


Figure 8-2 Capacitance for prototype B-2

$$C = \frac{0.05}{0.0232} = 2.155 \text{ F}$$

$$ESR = \frac{1 - 0.308}{0.05} = 13.84 \Omega$$

The B-2 prototype was tested using CV to observe its behavior, Figure 8-3 shows the CV curve which resembles the ideal supercapacitor square shape curve.

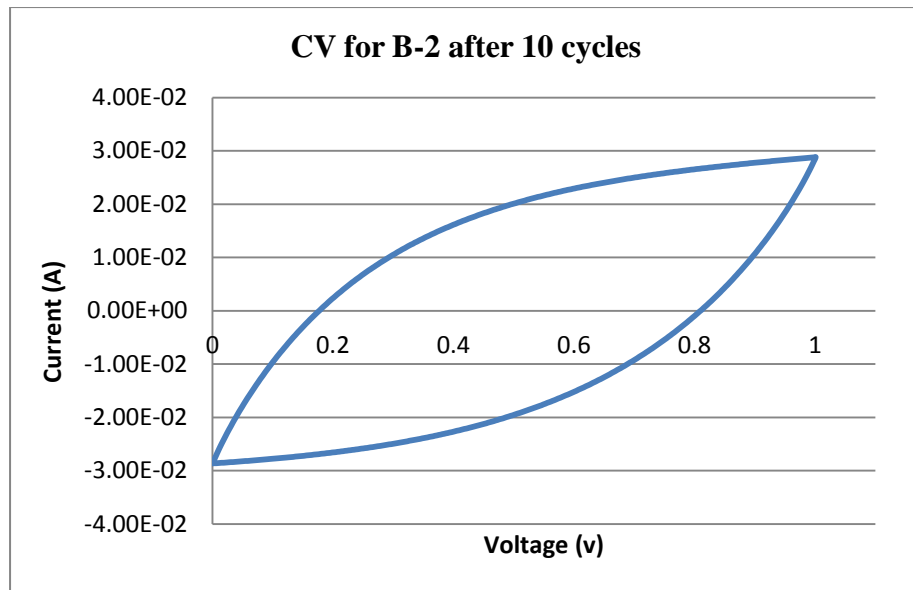


Figure 8-3 CV curve for B-2 after 10 cycles

The B-2 supercapacitor coin prototype was cycled for 100 cycles and tested again to observe the changes to the capacitance and the ESR values. Figure 8-4 shows the charge-discharge curve after 100 cycles.

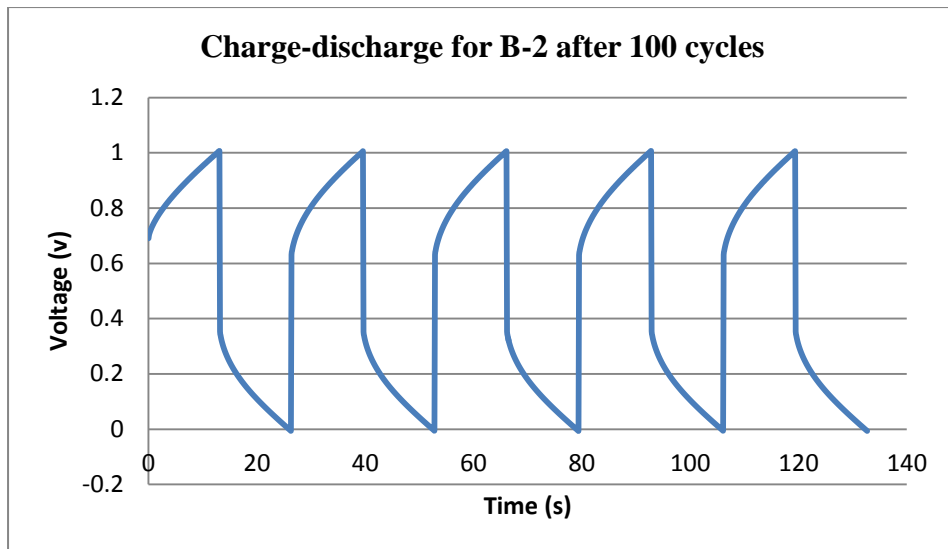


Figure 8-4 Charge-discharge curve for B-2 after 100 cycles

The new value for the capacitance was increased to 2.778 F from 2.155 F, and the ESR was decreased to 12.92 Ohms from 13.84 Ohms, this could be due to the electrolyte penetrating deeper into the active material. Figure 8-5 shows the curve used to measure the capacitance of the B-2 prototype.

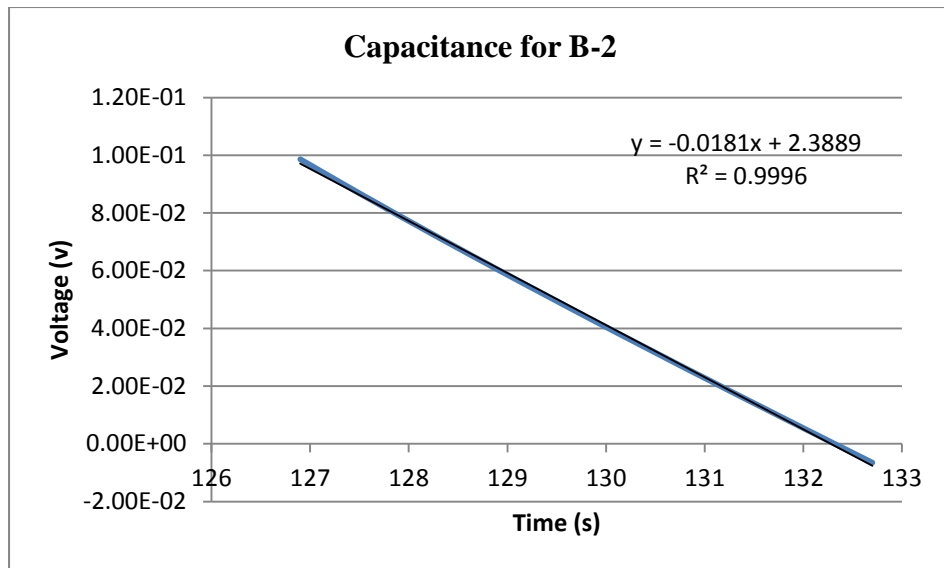


Figure 8-5 Capacitance for B-2

$$C = \frac{0.05}{0.018} = 2.778 \text{ F}$$

$$ESR = \frac{1 - 0.354}{0.05} = 12.92 \Omega$$

The CV curve after 100 cycles reassembles the ideal supercapacitor curve. Figure 8-6 shows the CV curve after 100 cycles.

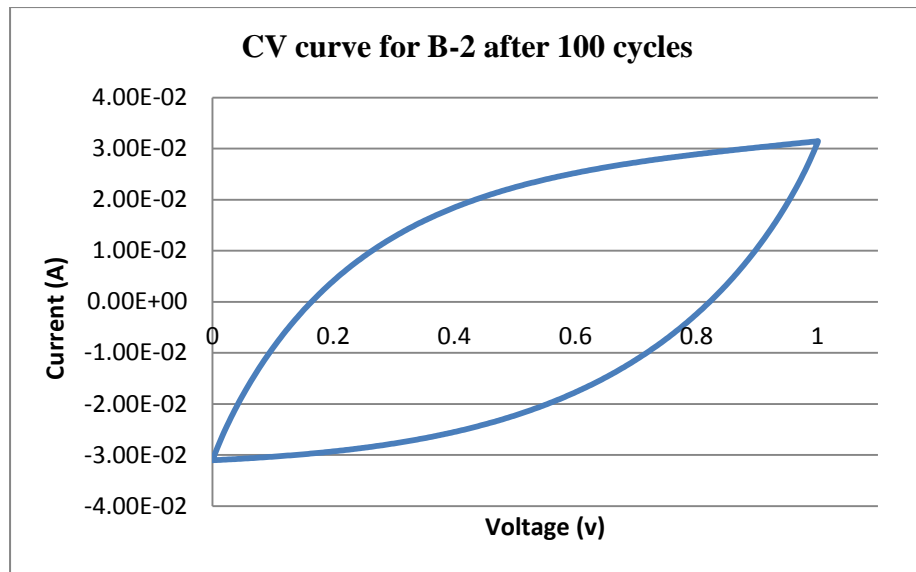


Figure 8-6 CV curve for B-2 after 100 cycles

8.2 Coin prototype B-3

In the case of B-3 prototype the initial charge-discharge test didn't show the expected shape, we got squared shape curve as shown in Figure 8-7, which could be due to the prototype having a high ESR or the capacitance is small. The prototype was tested with 50 mA constant current.

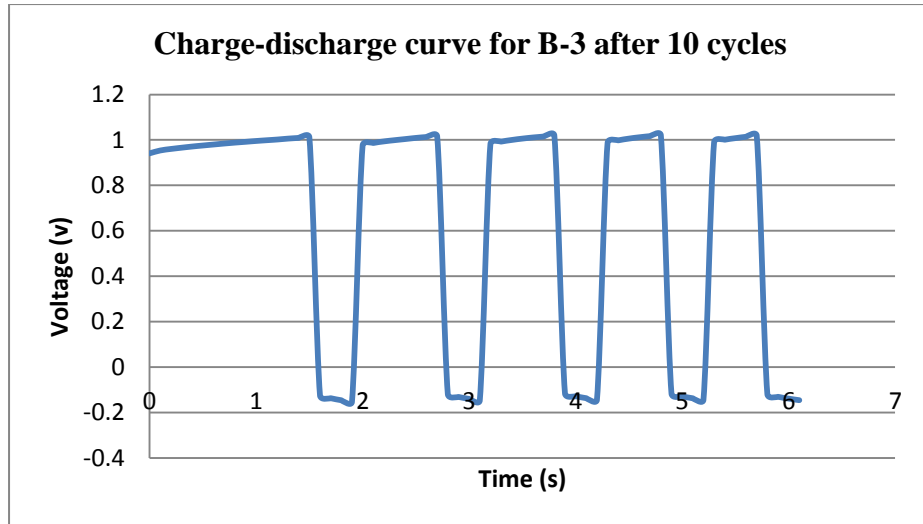


Figure 8-7 Charge-discharge curve for prototype B-3 after 10 cycles

The prototype was tested using CV, the curve show a narrow area, which indicates a small capacitance, Figure 8-8 shows the current is small compared to the earlier prototypes that can be due to high ESR.

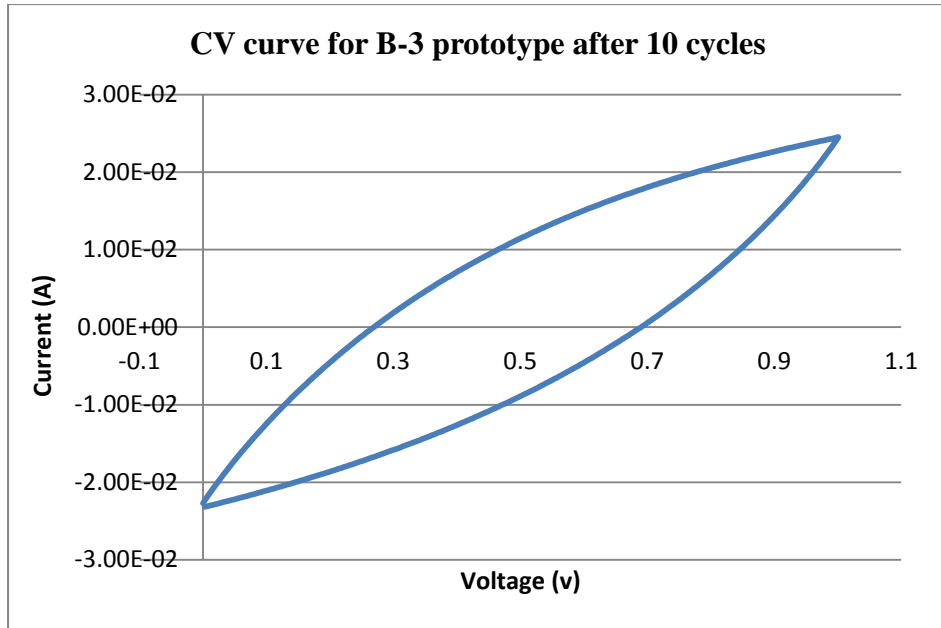


Figure 8-8 CV curve for the B-3 prototype after 10 cycles

The prototype was cycled for another 100 cycles and tested again. The charge-discharge curve in Figure 8-9 shows some improvements, but the ERS value still high.

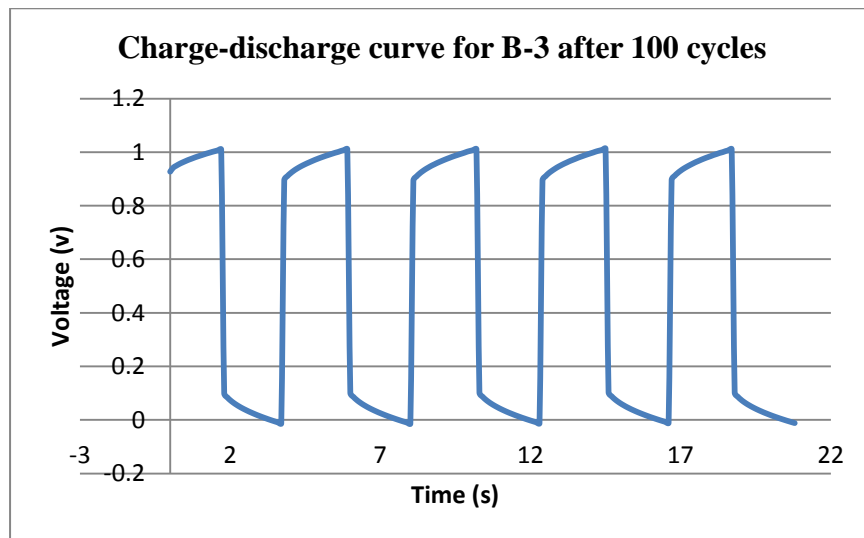


Figure 8-9 Charge-discharge curve for B-3 after 100 cycles

Portion of the charge-discharge curve is used to calculate the capacitance of the B-3 prototype, Figure 8-10 shows the curve used to measure the slope which then used to calculate the capacitance.

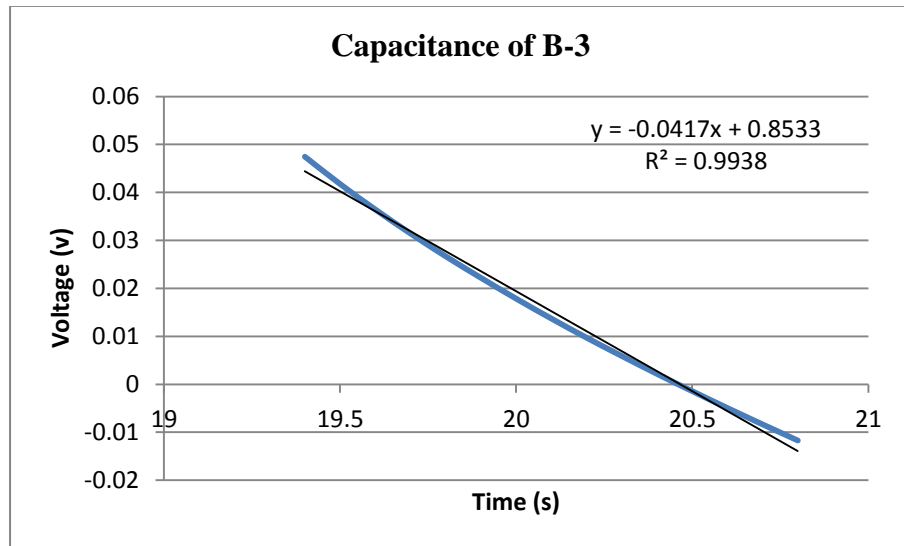


Figure 8-10 Capacitance of B-3 after 100 cycles

$$C = \frac{0.05}{0.0417} = 1.199 \text{ F}$$

$$ESR = \frac{1 - 0.102}{0.05} = 17.96 \Omega$$

The capacitance for this prototype is smaller than the previous prototypes, and the ESR is higher, this could be due to the bad contact at the electrodes, between the active material and the current collector.

The CV curve after 100 cycles shows a bit of improvement compared to the first CV test, Figure 8-11 shows the CV curve after 100 cycles.

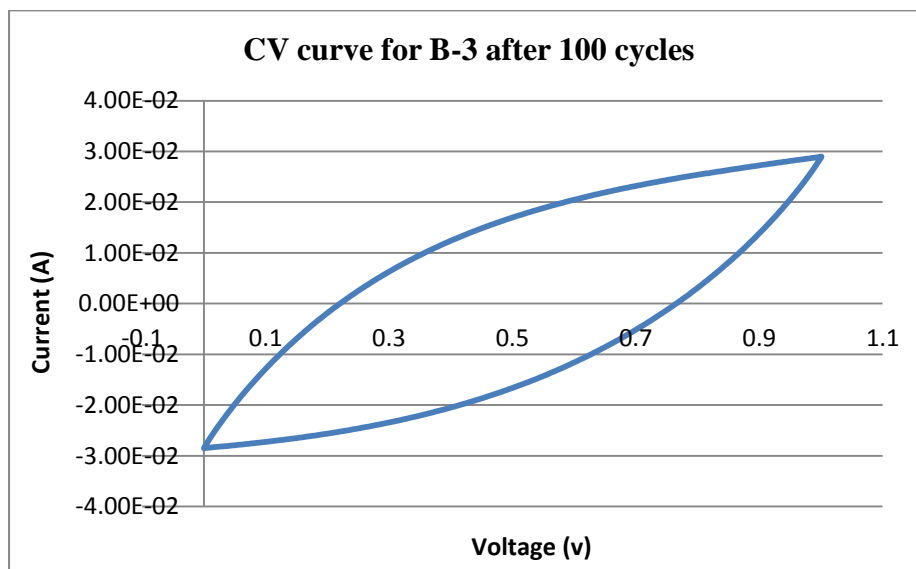


Figure 8-11 CV curve for B-3 after 100 cycles

8.3 Coin prototype B-4

The fourth coin prototype B-4 was tested using the charge-discharge with 50 mA constant current. The first test was done at 10 cycles. Figure 8-12 shows the charge-discharge curve for B-4.

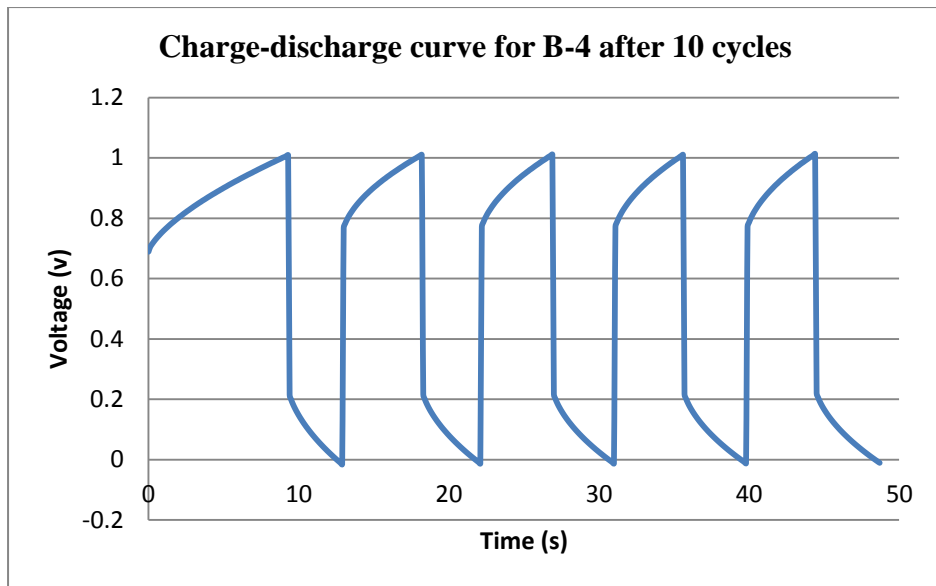


Figure 8-12 Charge-discharge for prototype B-4 after 10 cycles

Portion of the charge-discharge curve was used to calculate the capacitance of the B-4 prototype, Figure 8-13 shows the curve used to measure the slope which was used to calculate the capacitance.

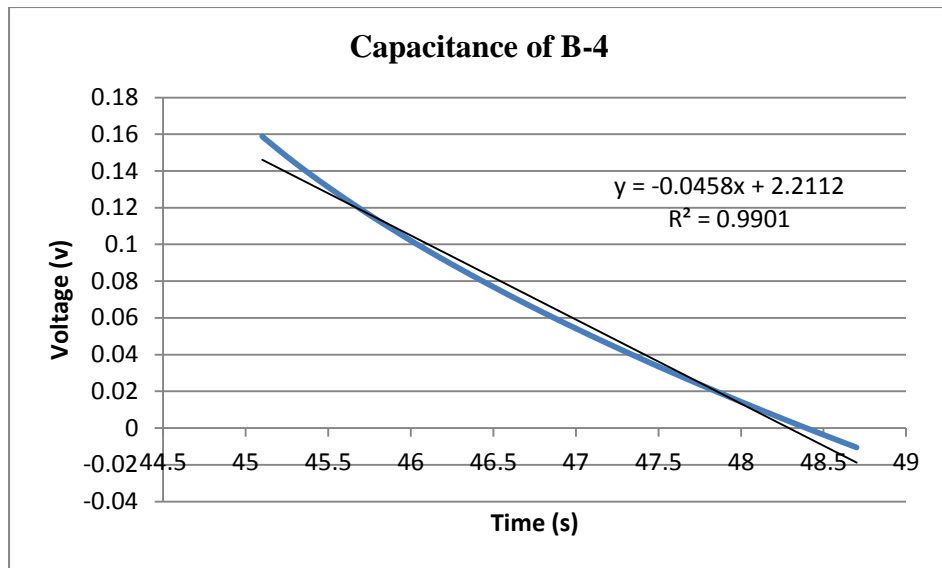


Figure 8-13 Capacitance for prototype B-4

$$C = \frac{0.05}{0.0458} = 1.091 F$$

$$ESR = \frac{1 - 0.217}{0.05} = 15.66 \Omega$$

The B-4 prototype was tested using CV to observe its behavior, Figure 8-14 shows the CV curve.

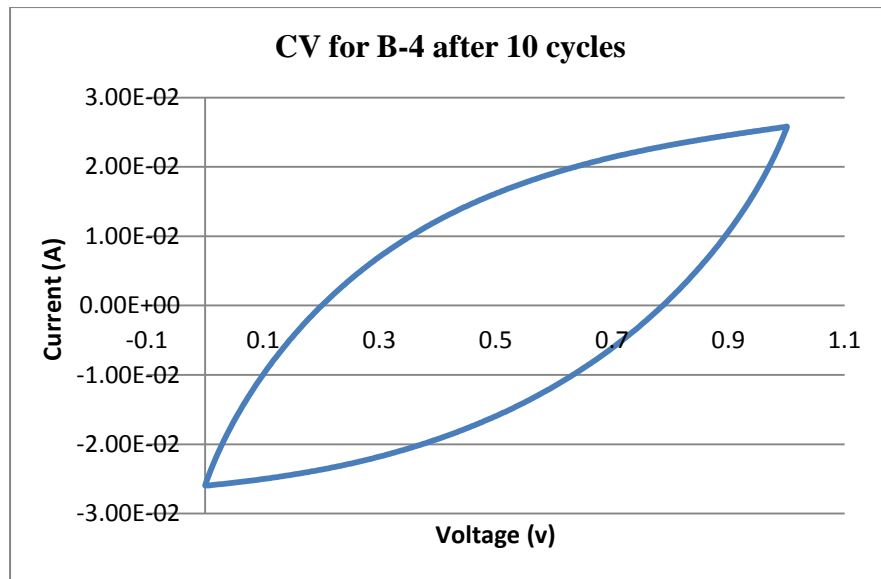


Figure 8-14 CV curve for B-4 after 10 cycles

The B-4 coin prototype was cycled for 100 cycles and tested again to observe the changes to the capacitance and the ESR values. Figure 8-15 shows the charge-discharge curve after 100 cycles.

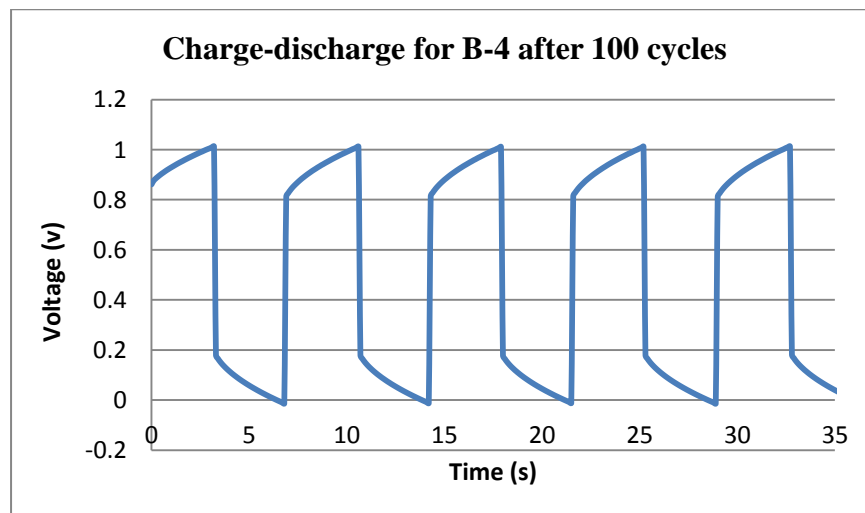


Figure 8-15 Charge-discharge curve for B-4 after 100 cycles

The new value for the capacitance was increased to 1.219 F from 1.091 F, similarly the ESR was increased to 16.38 Ohms from 15.66 Ohms. Figure 8-16 shows the curve used to measure the capacitance of the B-4 prototype.

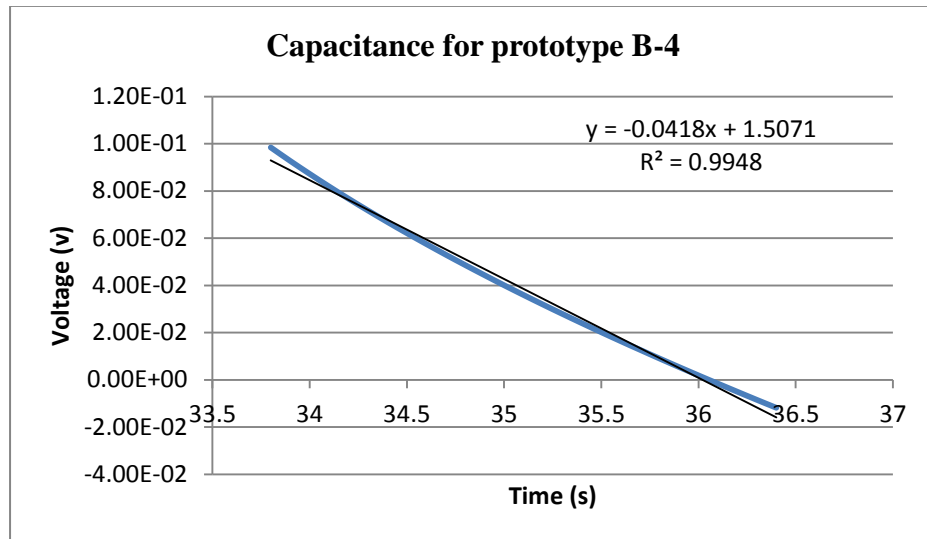


Figure 8-16 Capacitance for B-4

$$C = \frac{0.05}{0.041} = 1.219 \text{ F}$$

$$ESR = \frac{1 - 0.181}{0.05} = 16.38 \Omega$$

The CV curve after 100 cycles reassembles the ideal supercapacitor curve. Figure 8-17 shows the CV curve after 100 cycles.

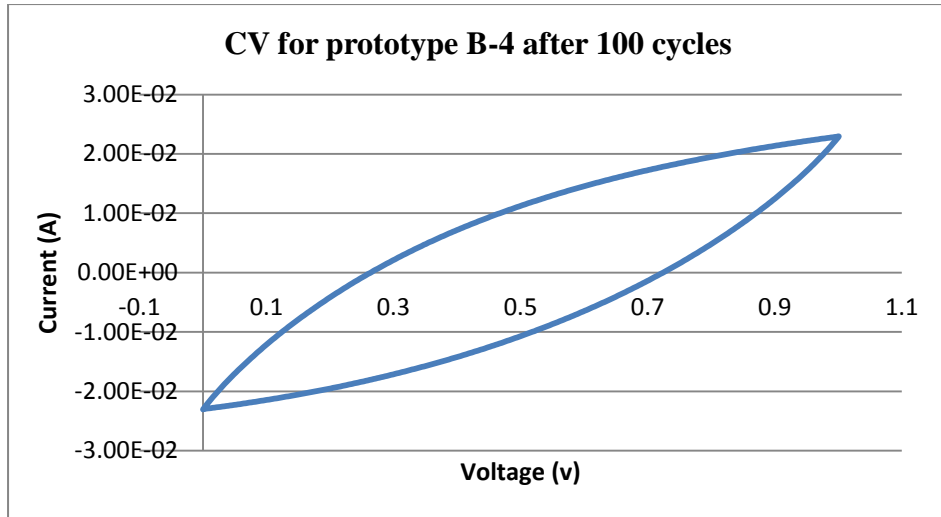


Figure 8-17 CV for B-4 after 100 cycles

8.4 Coin prototype B-5

The coin prototype B-5 was tested using the charge- discharge test with 50 mA constant current. The first test was done at 10 cycles. Figure 8-18 shows the charge-discharge curve for B-5.

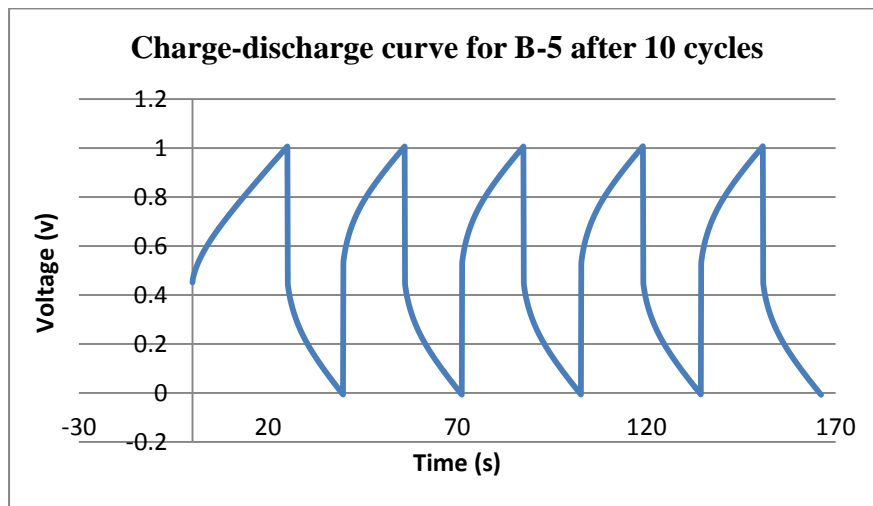


Figure 8-18 Charge-discharge for prototype B-5 after 10 cycles

Portion of the charge-discharge curve was used to calculate the capacitance of the B-5 prototype, Figure 8-19 shows the curve used to measure the slope which was used to calculate the capacitance.

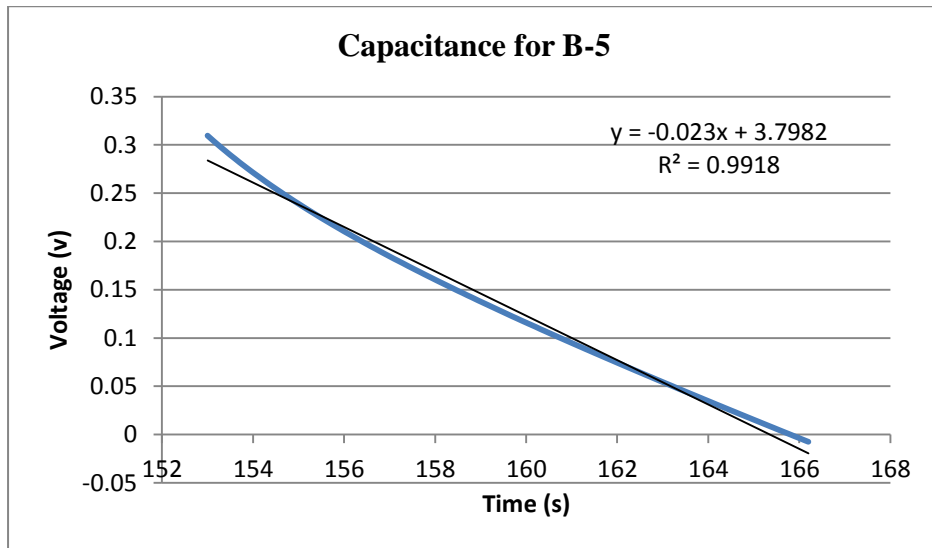


Figure 8-19 Capacitance for B-5

$$C = \frac{0.05}{0.023} = 2.173 \text{ F}$$

$$ESR = \frac{1 - 0.449}{0.05} = 11.02 \Omega$$

The B-5 prototype was tested using CV to observe its behavior, Figure 8-20 shows the CV curve which closely resembles the ideal supercapacitor square shape.

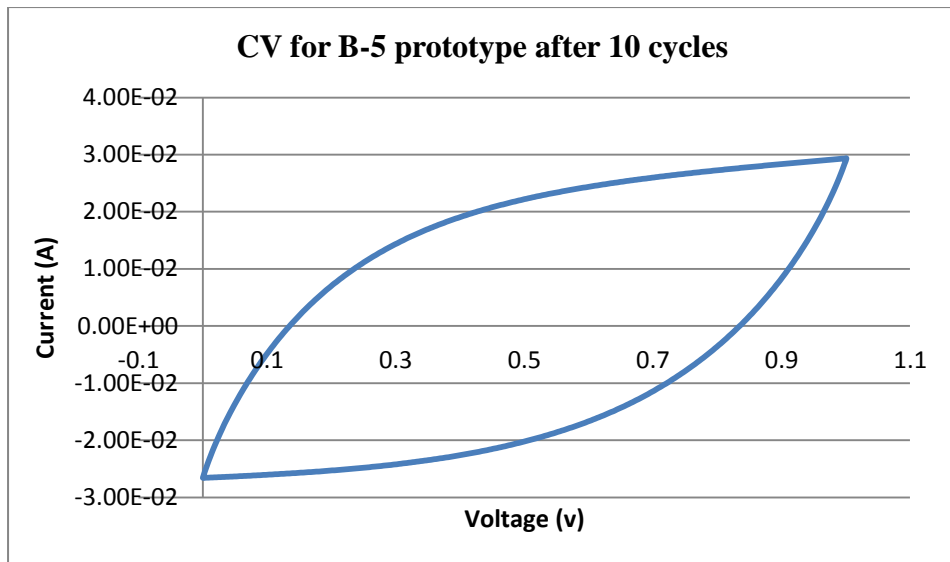


Figure 8-20 CV for prototype B-5 after 10 cycles

The B-5 coin prototype was cycled for 100 cycles and tested again to observe the changes to the capacitance and the ESR values. Figure 8-21 shows the charge-discharge curve after 100 cycles.

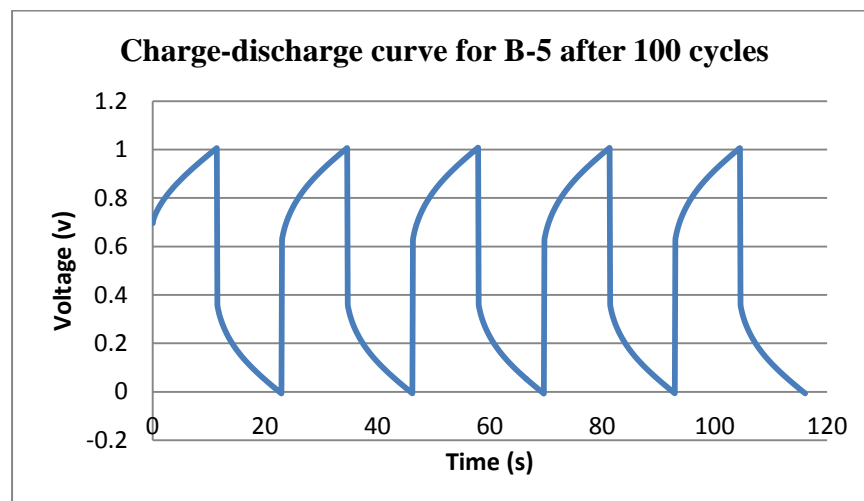


Figure 8-21 Charge-discharge for B-5 after 100 cycles

The new value for the capacitance was increased to 2.487 F from 2.173 F, similarly the ESR was increased to 12.78 Ohms from 11.02 Ohms. Figure 8-22 shows the curve used to measure the capacitance of the B-5 prototype.

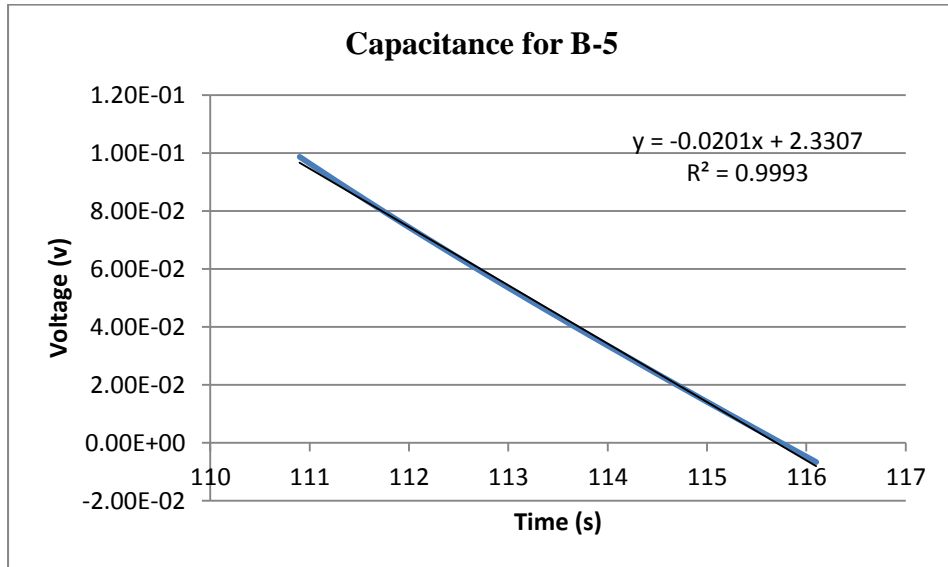


Figure 8-22 Capacitance for B-5

$$C = \frac{0.05}{0.0201} = 2.487 \text{ F}$$

$$ESR = \frac{1 - 0.361}{0.05} = 12.78 \Omega$$

The CV curve after 100 cycles reassembles the ideal supercapacitor curve. Figure 8-23 shows the CV curve after 100 cycles.

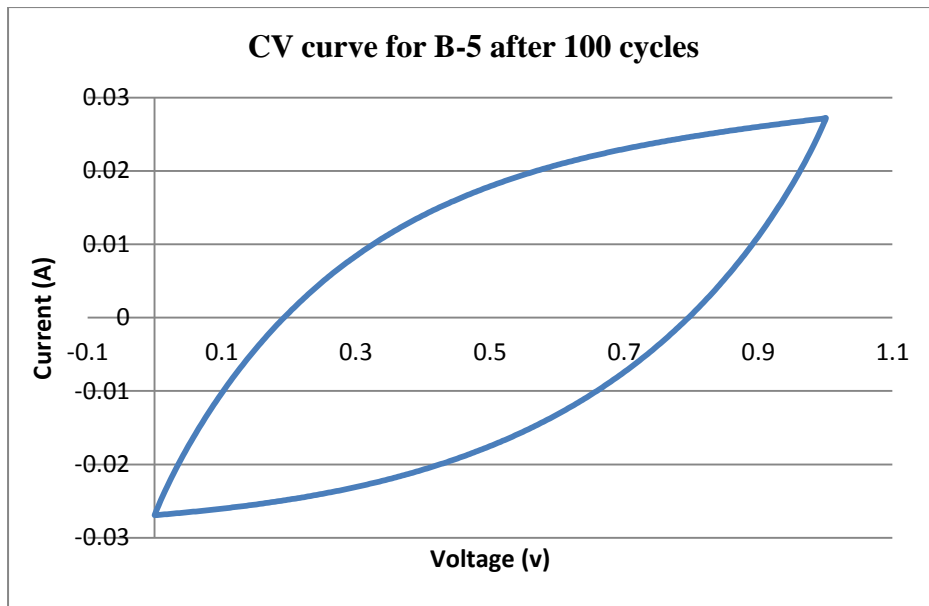


Figure 8-23 CV curve for B-5 after 100 cycles

8.5 Coin Prototype B-6

The coin prototype B-6 was tested using the charge- discharge with 30 mA constant current. The first test was done at 10 cycles. Figure 8-24 shows the charge-discharge curve for B-6.

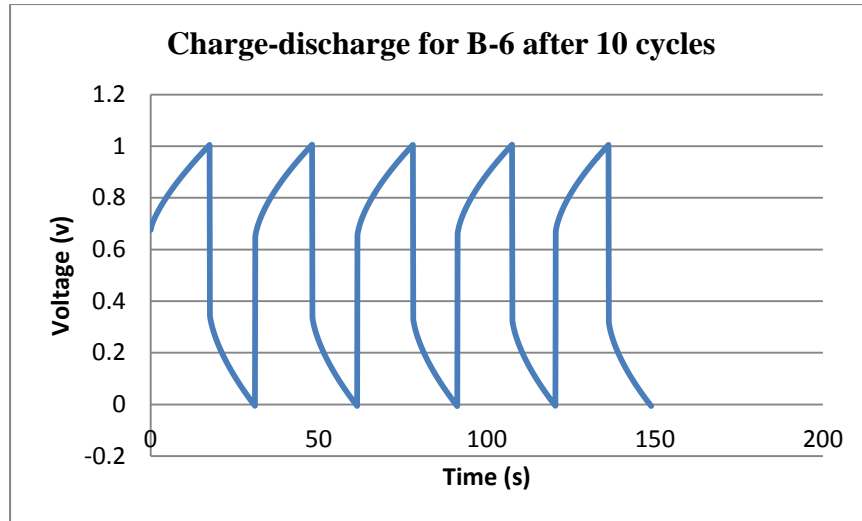


Figure 8-24 Charge-discharge for Prototype B-6 after 10 cycles

Portion of the charge-discharge curve was used to calculate the capacitance of the B-6 prototype, Figure 8-25 shows the curve used to measure the slope which was used to calculate the capacitance.

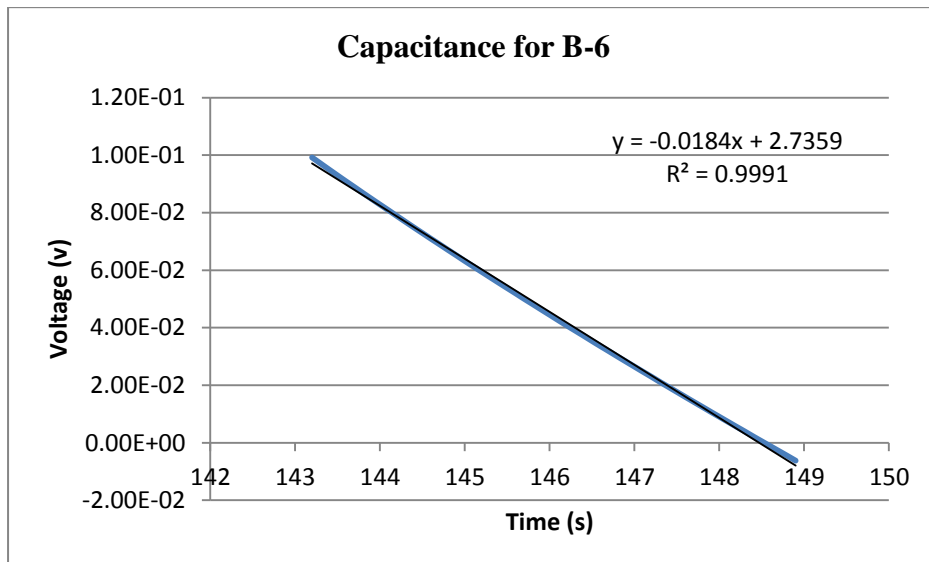


Figure 8-25 Capacitance for B-6

$$C = \frac{0.03}{0.0184} = 1.63 \text{ F}$$

$$ESR = \frac{1 - 0.3325}{0.03} = 22.25 \Omega$$

The B-6 prototype was tested using CV test to observe its behavior, Figure 8-26 shows the CV curve.

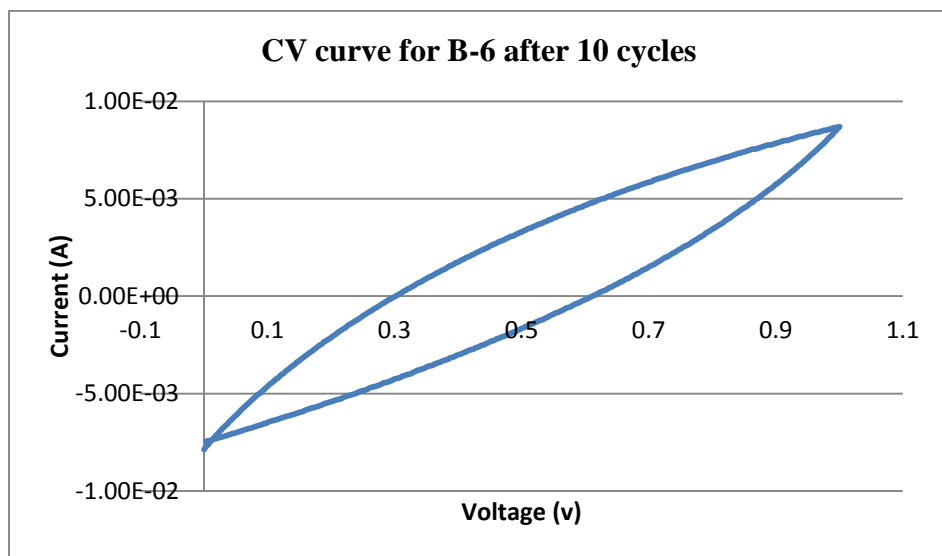


Figure 8-26 CV for B-6 after 10 cycles

The B-6 coin prototype was cycled for 100 cycles and tested again to observe the changes to the capacitance and the ESR values. Figure 8-27 shows the charge-discharge curve after 100 cycles.

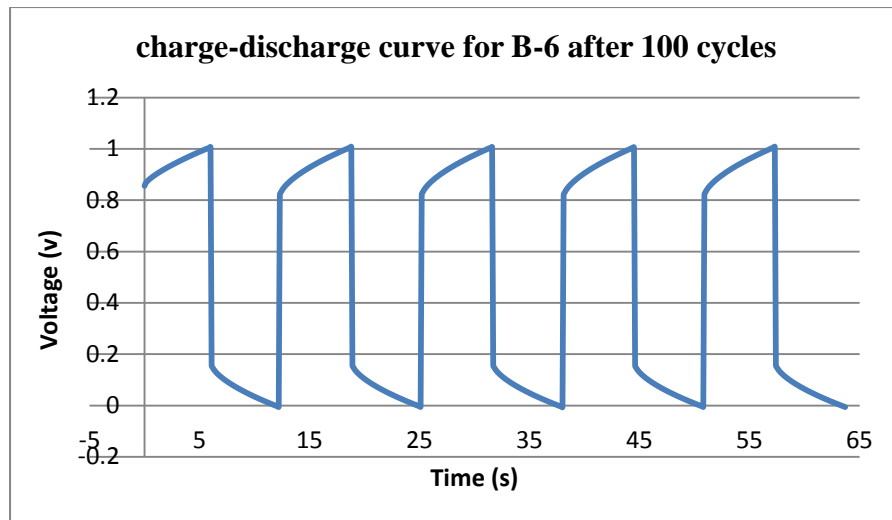


Figure 8-27 Charge-discharge for B-6 after 100 cycles

The new value for the capacitance was decreased to 1.538 F from 1.63 F, but the ESR was increased to 28.133 Ohms from 22.25 Ohms. Figure 8-28 shows the curve used to measure the capacitance of the B-6 prototype.

$$C = \frac{0.03}{0.0195} = 1.538 \text{ F}$$

$$ESR = \frac{1 - 0.156}{0.03} = 28.13 \text{ } \Omega$$

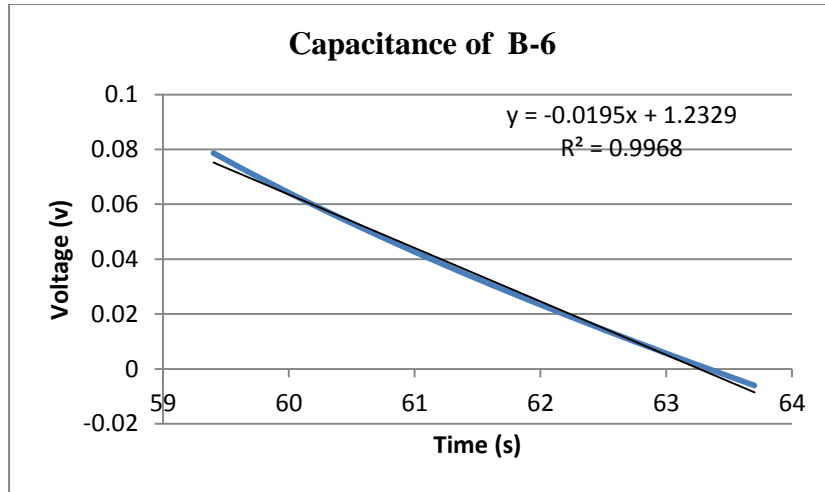


Figure 8-28 Capacitance of B-6

The CV curve after 100 cycles show a narrow curve that can be due to the small capacity or the high ESR for this prototype. Figure 8-29 shows the CV curve after 100 cycles.

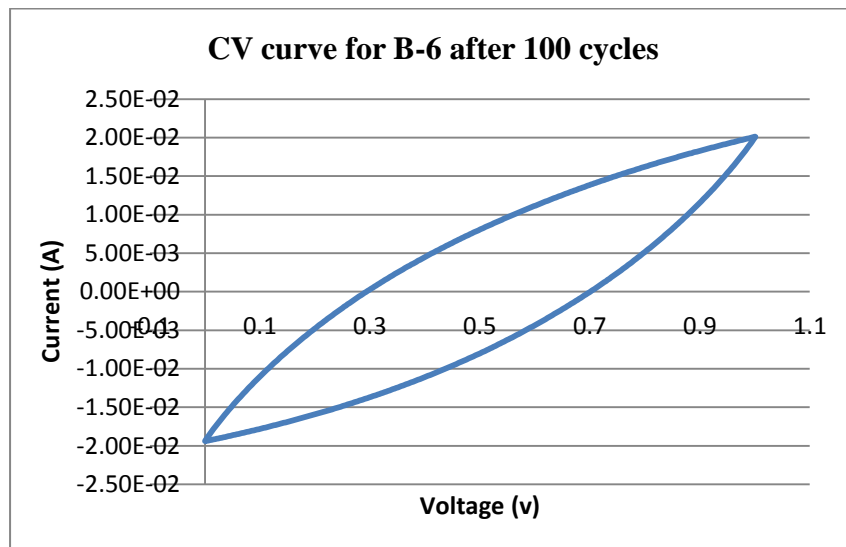


Figure 8-29 CV curve for B-6 after 100 cycles

8.6 Coin prototype B-7

The coin prototype B-7 was tested using the charge- discharge with 30 mA and 60 mA constant current. The first test was done at 10 cycles. Figure 8-30 shows the charge-discharge curve for B-7.

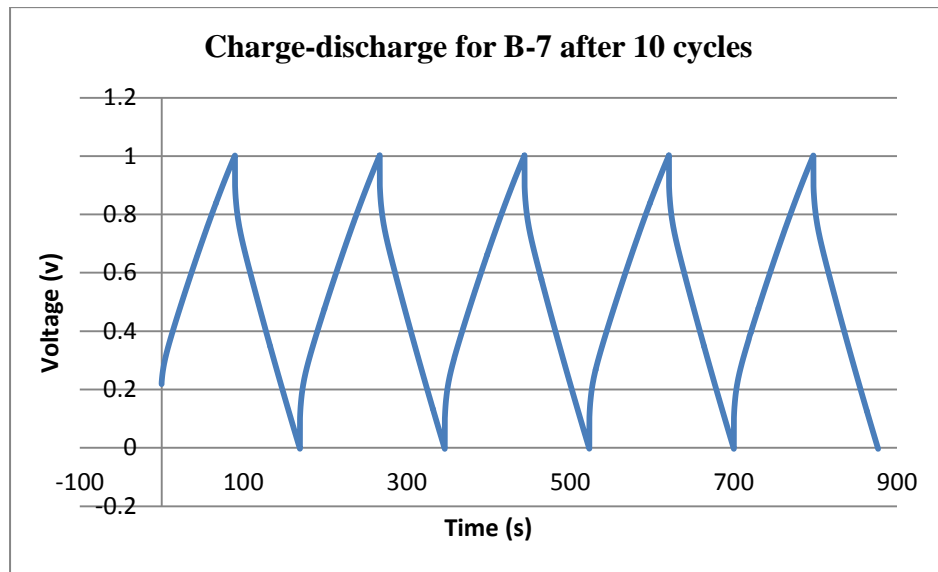


Figure 8-30 Charge-discharge for B-7 after 10 cycles

Portion of the charge-discharge curve is used to calculate the capacitance of the B-7 prototype, Figure 8-31 shows the curve used to measure the slope which was used to calculate the capacitance.

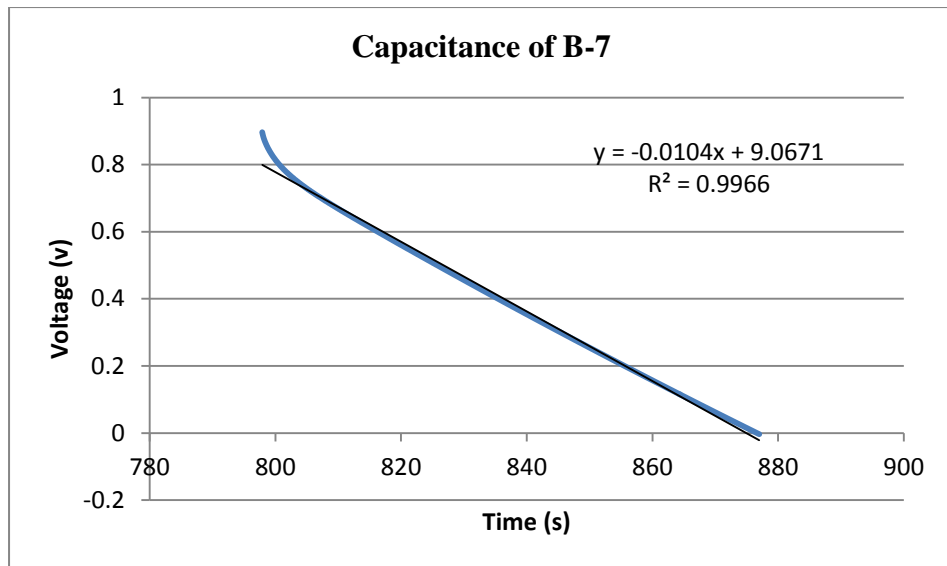


Figure 8-31 Capacitance of B-7

$$C = \frac{0.03}{0.0104} = 2.888 \text{ F}$$

$$ESR = \frac{1 - 0.897}{0.03} = 3.43 \text{ } \Omega$$

The B-7 prototype was tested using CV test to observe its behavior, Figure 8-32 shows the CV curve which closely resembles the ideal supercapacitor square shape curve.

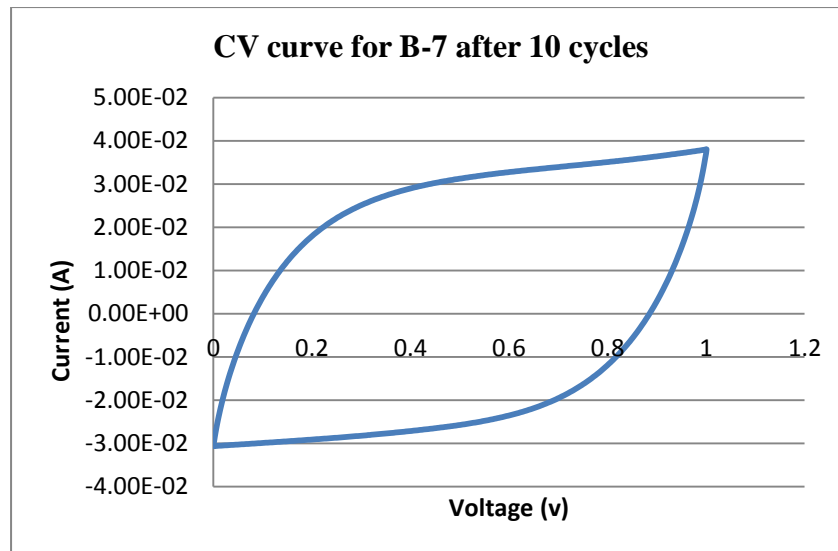


Figure 8-32 CV curve for B-7 after 10 cycles

The B-7 coin prototype was cycled for 100 cycles and tested again to observe the changes to the capacitance and the ESR values. Figure 8-33 shows the charge-discharge curve after 100 cycles.

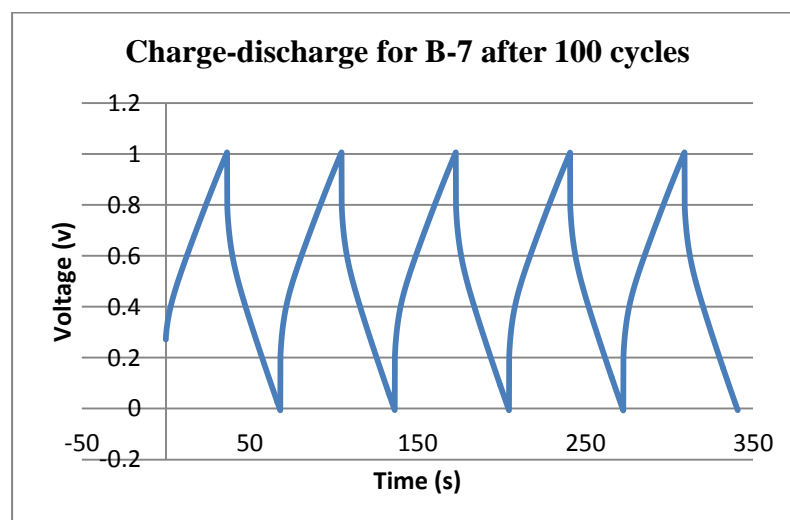


Figure 8-33 Charge-discharge for B-7 after 100 cycles

The new value for the capacitance was increased to 3.33 F from 2.88 F, and the ESR was decreased to 3.367 Ohms from 3.43 Ohms, the increase in the capacitance can be attributed to the electrolyte wetting and penetrating deeper into the active material. Figure 8-34 shows the curve used to measure the capacitance of the B-7 prototype.

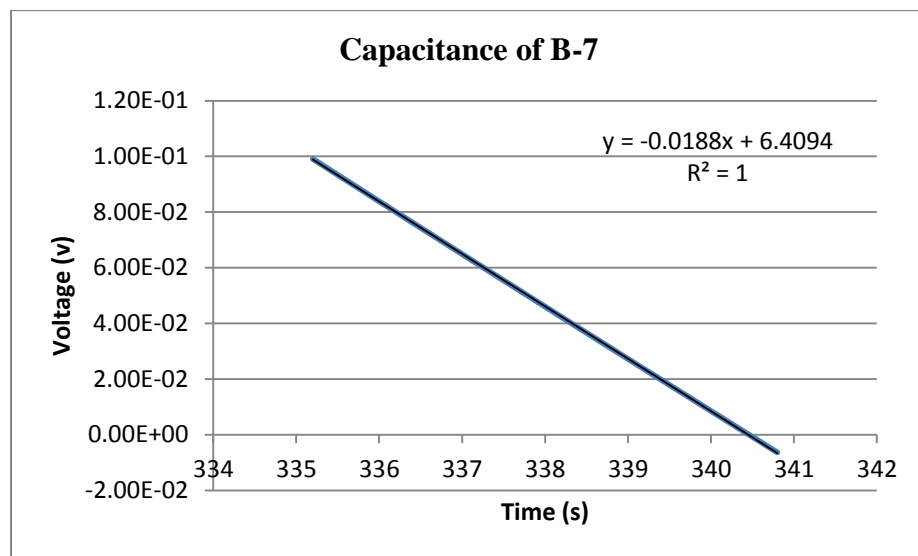


Figure 8-34 Capacitance of B-7

$$C = \frac{0.06}{0.018} = 3.33 \text{ F}$$

$$ESR = \frac{1 - 0.798}{0.06} = 3.36 \text{ } \Omega$$

The CV curve after 100 cycles reassembles the ideal supercapacitor curve. Figure 8-35 shows the CV curve after 100 cycles.

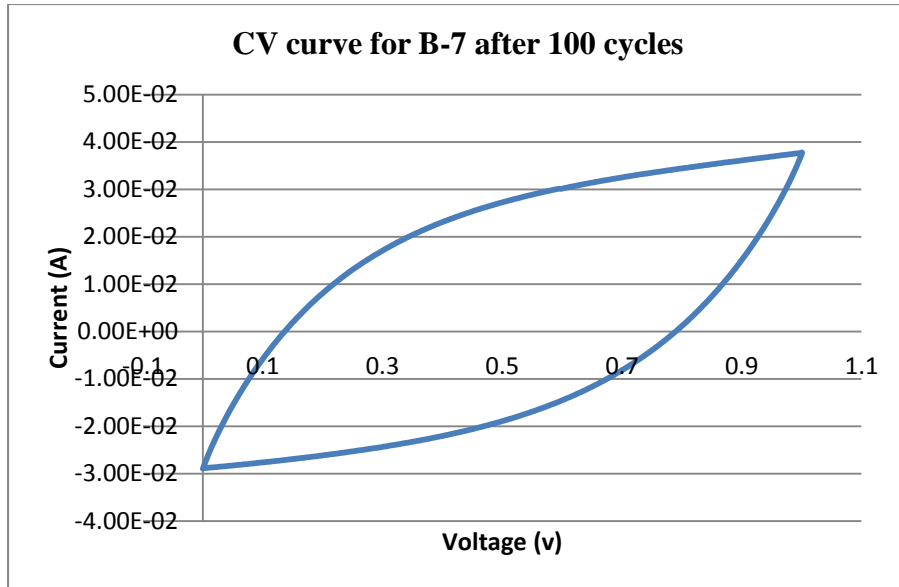


Figure 8-35 CV curve for B-7 after 100 cycles

8.7 Coin prototype B-8

The 8th coin prototype B-8 was tested using the charge-discharge with 30 mA constant current. The first test was done at 10 cycles. Figure 8-36 shows the charge-discharge curve for B-8.

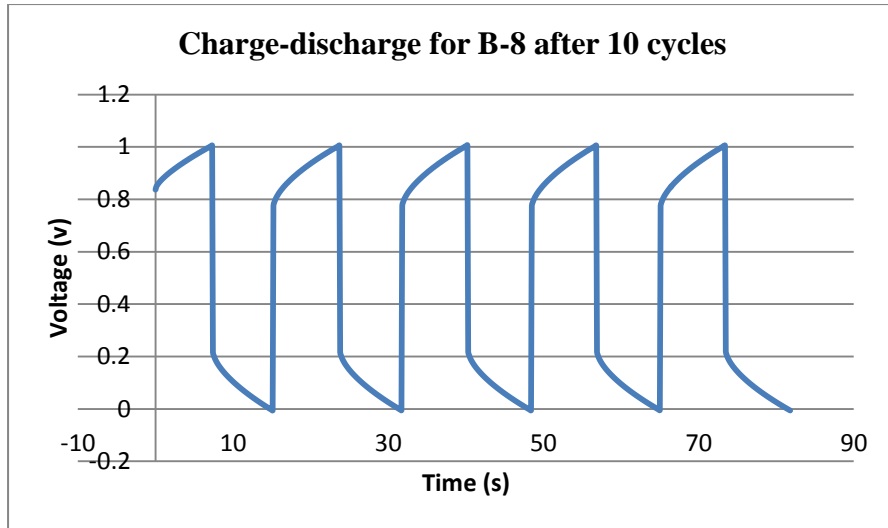


Figure 8-36 Charge-discharge for B-8 after 10 cycles

Portion of the charge-discharge curve was used to calculate the capacitance of the B-8 prototype, Figure 8-37 shows the curve used to measure the slope which then used to calculate the capacitance.

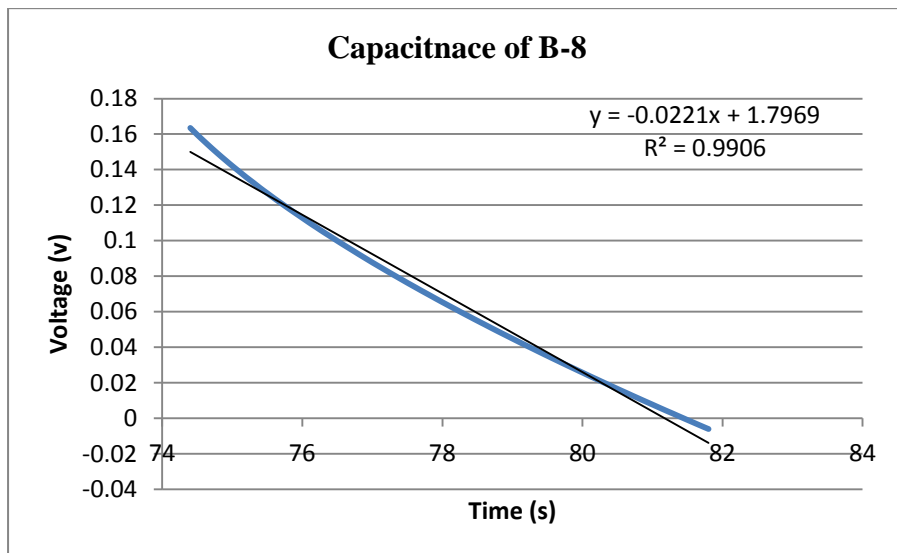


Figure 8-37 Capacitance of B-8

$$C = \frac{0.03}{0.0221} = 1.357 \text{ F}$$

$$ESR = \frac{1 - 0.217}{0.03} = 26.1 \Omega$$

The B-8 prototype was tested using CV test to observe its behavior, Figure 8-38 shows the CV curve, the narrow curve could be due to the high ESR value.

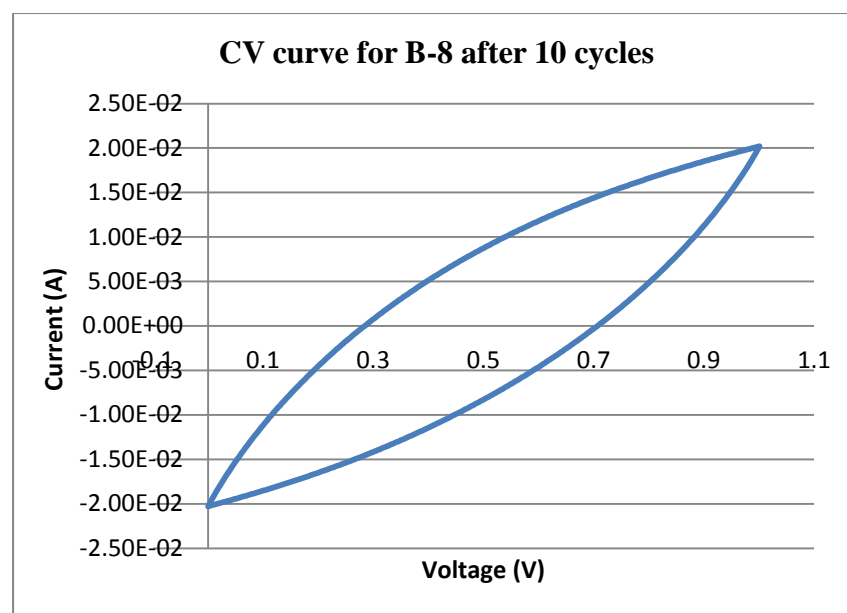


Figure 8-38 CV for B-8 after 10 cycles

The B-8 coin prototype was cycled for 100 cycles and tested again to observe the changes to the capacitance and the ESR values. Figure 8-39 shows the charge-discharge curve after 100 cycles.

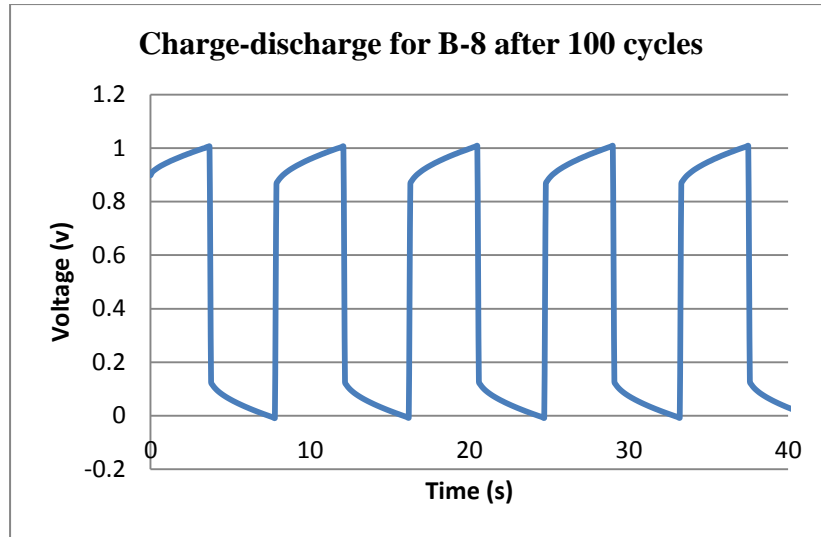


Figure 8-39 Charge-discharge for B-8 after 100 cycles

The new value for the capacitance was decreased to 1.162 F from 1.35 F, and the ESR was increased to 29.1 Ohms from 26.1 Ohms. Figure 8-40 shows the curve used to measure the capacitance of the B-8 prototype.

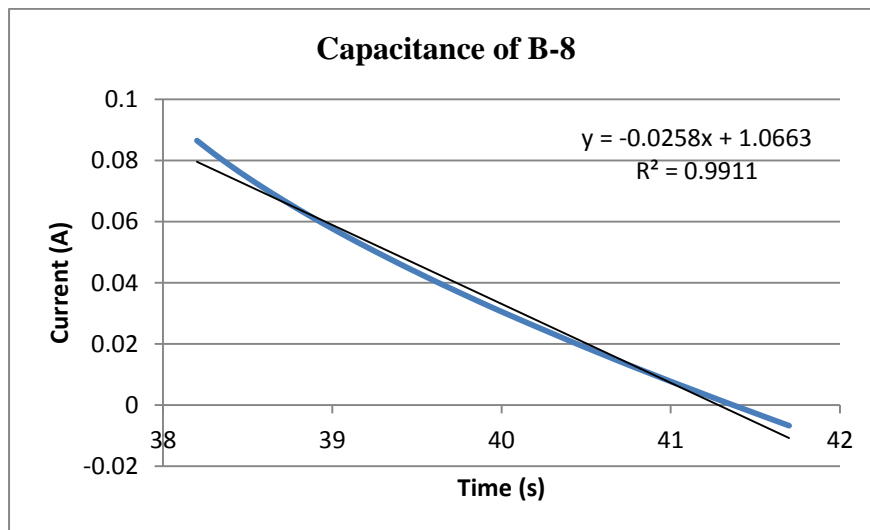


Figure 8-40 Capacitance of B-8

$$C = \frac{0.03}{0.0258} = 1.162 \text{ F}$$

$$ESR = \frac{1 - 0.127}{0.03} = 29.1 \Omega$$

After 100 cycles the CV curve show an even narrower curve due to the increase of the ESR value. Figure 8-41 shows the CV curve after 100 cycles.

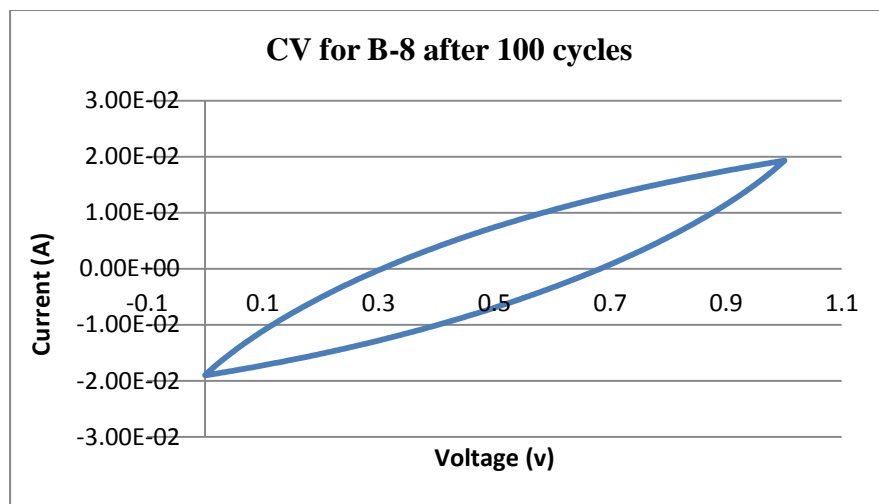


Figure 8-41 CV curve for B-8 after 100 cycles

8.8 Coin Prototype B-9

The 9th coin prototype B-9 was tested using the charge- discharge with 30 mA constant current. The first test was done at 10 cycles. Figure 8-42 shows the charge-discharge curve for B-9.

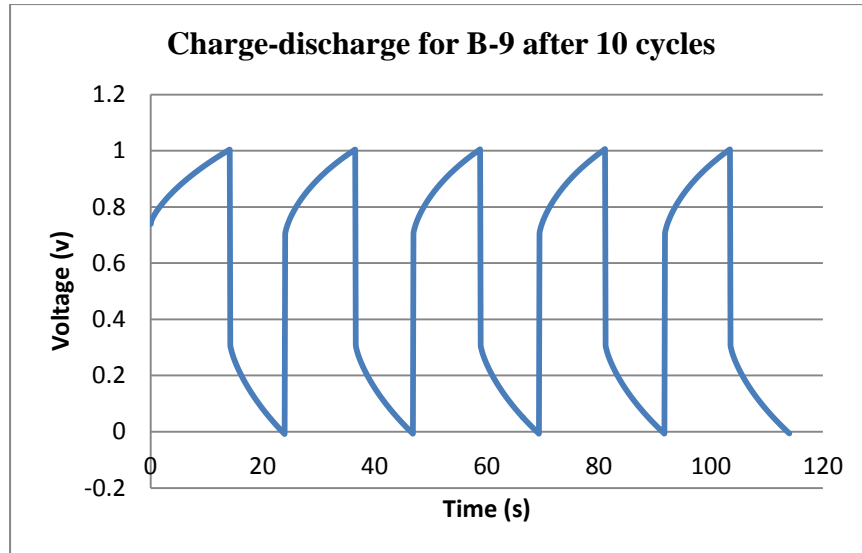


Figure 8-42 Charge-discharge for B-9 after 10 cycles

Portion of the charge-discharge curve is used to calculate the capacitance of the B-9 prototype, Figure 8-43 shows the curve used to measure the slope which was used to calculate the capacitance.

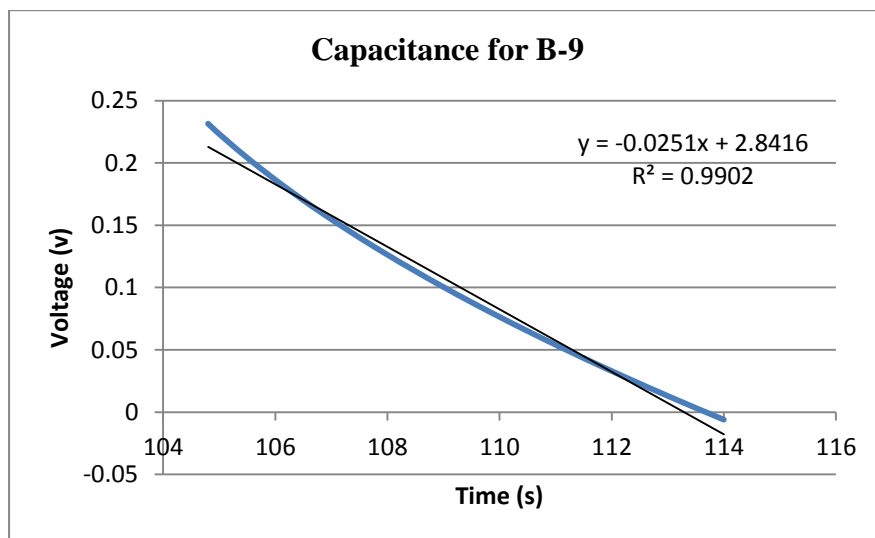


Figure 8-43 Capacitance for B-9

$$C = \frac{0.03}{0.0251} = 1.195 \text{ F}$$

$$ESR = \frac{1 - 0.308}{0.03} = 23.06 \text{ } \Omega$$

The B-9 prototype was tested using CV to observe its behavior, Figure 8-44 shows the CV curve which is narrow because of the high ESR value.

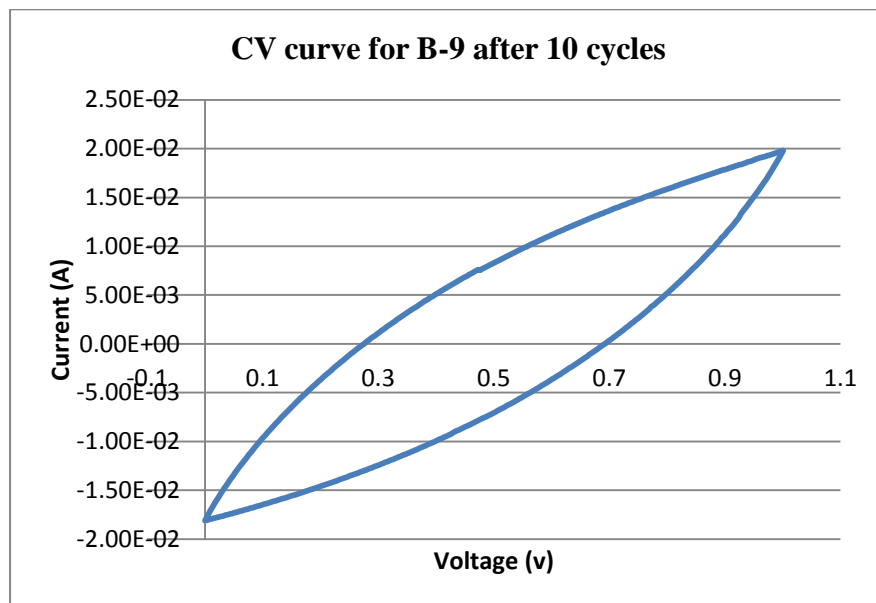


Figure 8-44 CV curve for B-9 after 10 cycles

The B-9 coin prototype was cycled for 100 cycles and tested again to observe the changes to the capacitance and the ESR values. Figure 8-45 shows the charge-discharge curve after 100 cycles.

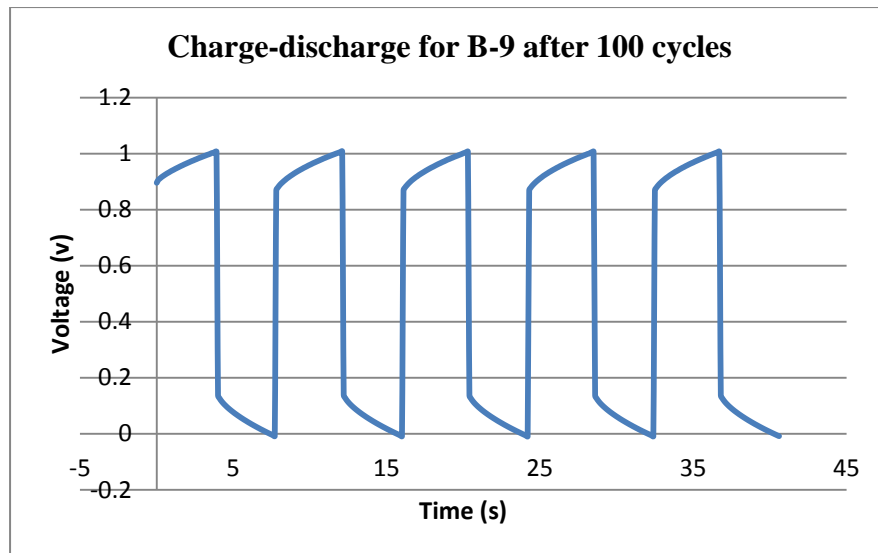


Figure 8-45 Charge-discharge for B-9 after 100 cycles

The new value for the capacitance was decreased to 1.034 F from 1.19 F, and the ESR was increased to 28.77 Ohms from 23.06 Ohms, the decreased capacitance can be due to the bad contact resistance between the active material and the current collector as the increase in ESR shows. Figure 8-46 shows the curve used to measure the capacitance of the B-9 prototype

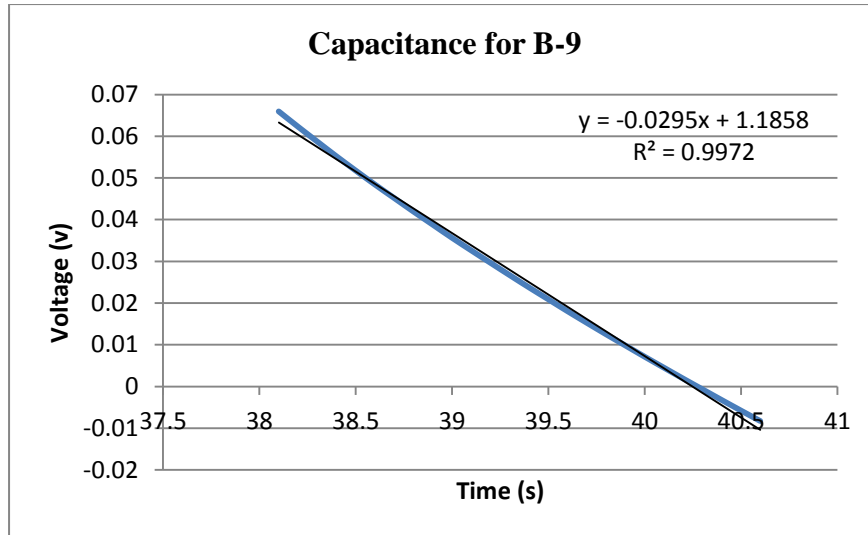


Figure 8-46 Capacitance of B-9

$$C = \frac{0.03}{0.029} = 1.034F$$

$$ESR = \frac{1 - 0.137}{0.03} = 28.77\Omega$$

The CV curve after 100 cycles became even narrower due to the increase of the ESR value. Figure 8-47 shows the CV curve after 100 cycles.

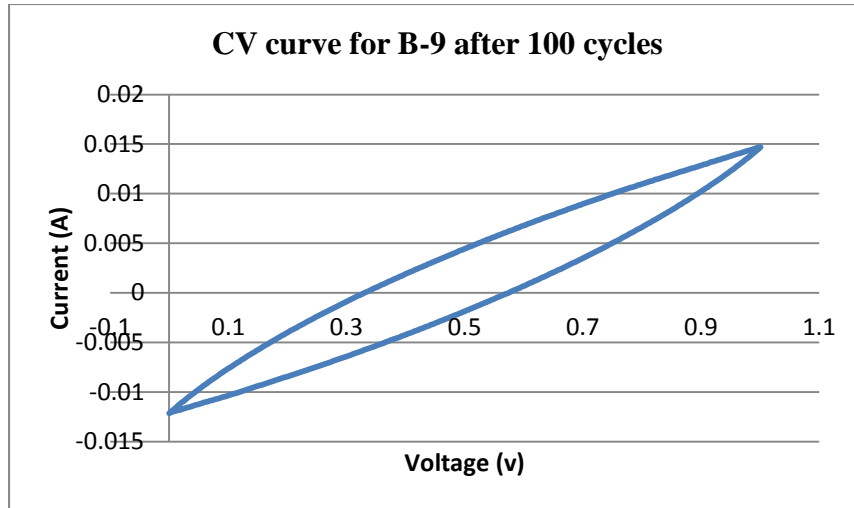


Figure 8-47 CV curve for B-9 after 100 cycles

8.9 Coin prototype B-10

The 10th coin prototype B-10 was tested using the charge-discharge with 30 mA and 60 mA constant current. The first test was done at 10 cycles. Figure 8-48 shows the charge-discharge curve for B-10.

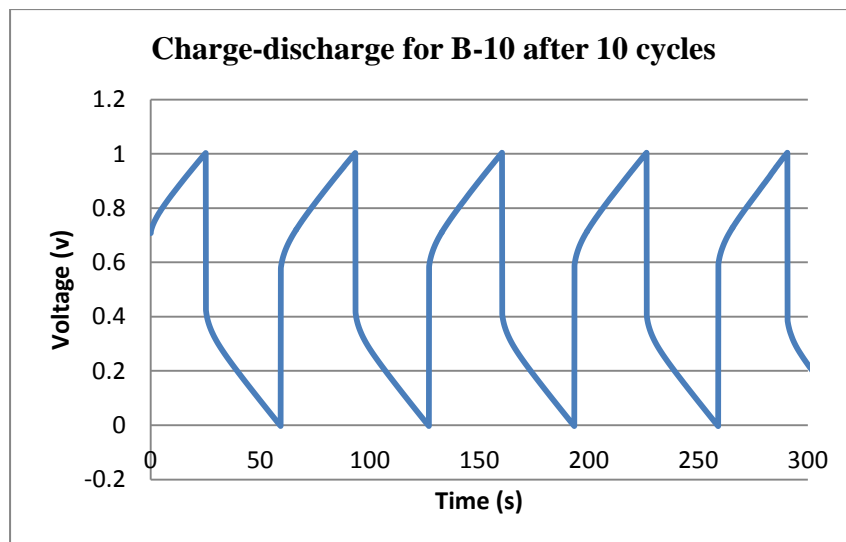


Figure 8-48 Charge-discharge for B-10 after 10 cycles

Portion of the charge-discharge curve is used to calculate the capacitance of the B-10 prototype, Figure 8-49 shows the curve used to measure the slope which was used to calculate the capacitance.

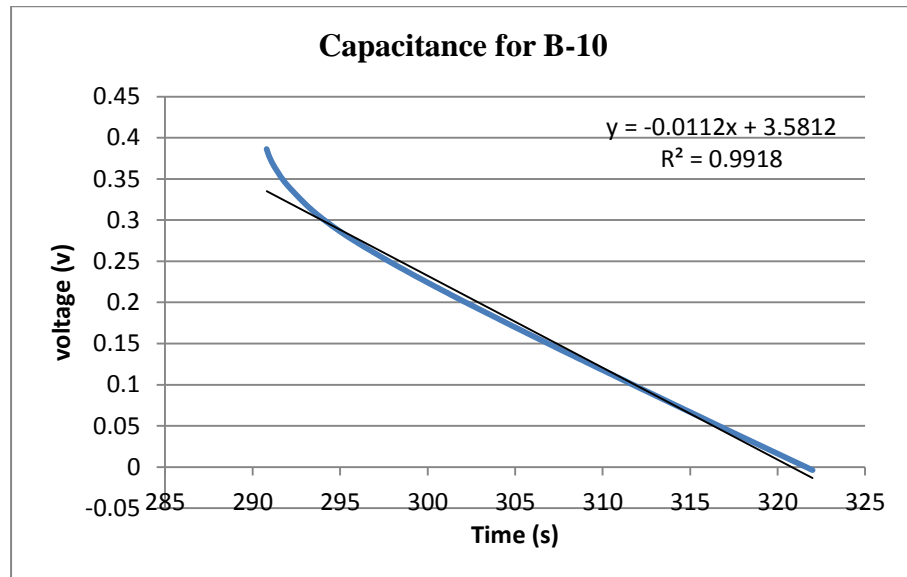


Figure 8-49 Capacitance for B-10 after 10 cycles

$$C = \frac{0.03}{0.0112} = 2.678 \text{ F}$$

$$ESR = \frac{1 - 0.4044}{0.03} = 19.85 \text{ } \Omega$$

The B-10 prototype was tested using CV to observe its behavior, Figure 8-50 shows the CV curve which ideally should resemble the ideal supercapacitor square shape curve.

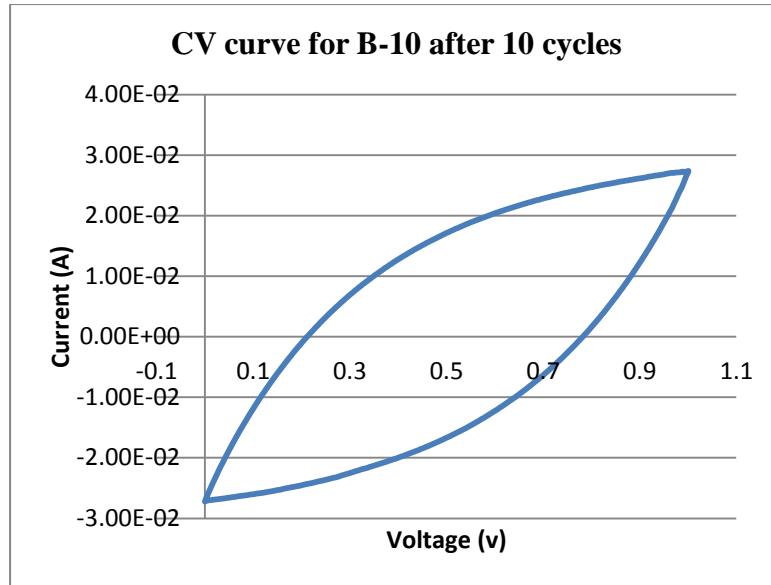


Figure 8-50 CV curve for B-10 after 10 cycles

The B-10 coin prototype was cycled for 100 cycles and tested again to observe the changes to the capacitance and the ESR values. Figure 8-51 shows the charge-discharge curve after 100 cycles.

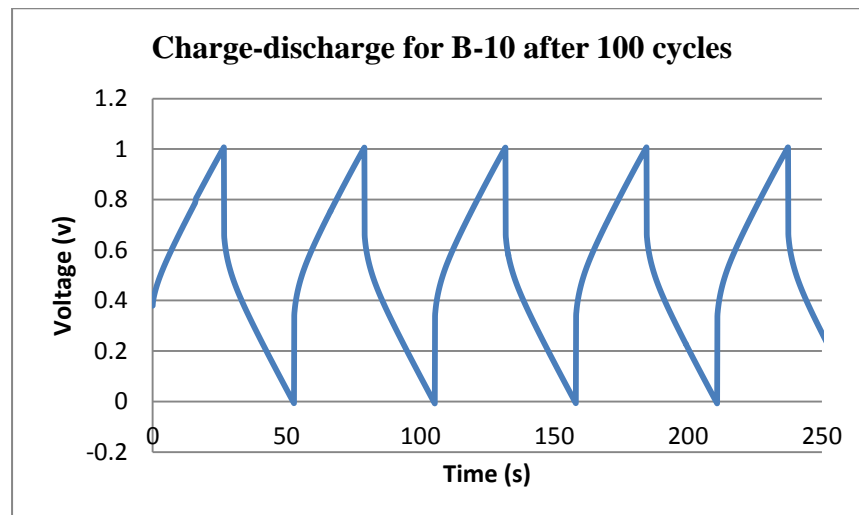


Figure 8-51 Charge-discharge for B-10 after 100 cycles

The new value for the capacitance was increased to 3.158 F from 2.67 F, and the ESR was decreased to 5.6 Ohms from 19.85 Ohms. Figure 8-52 shows the curve used to measure the capacitance of the B-10 prototype.

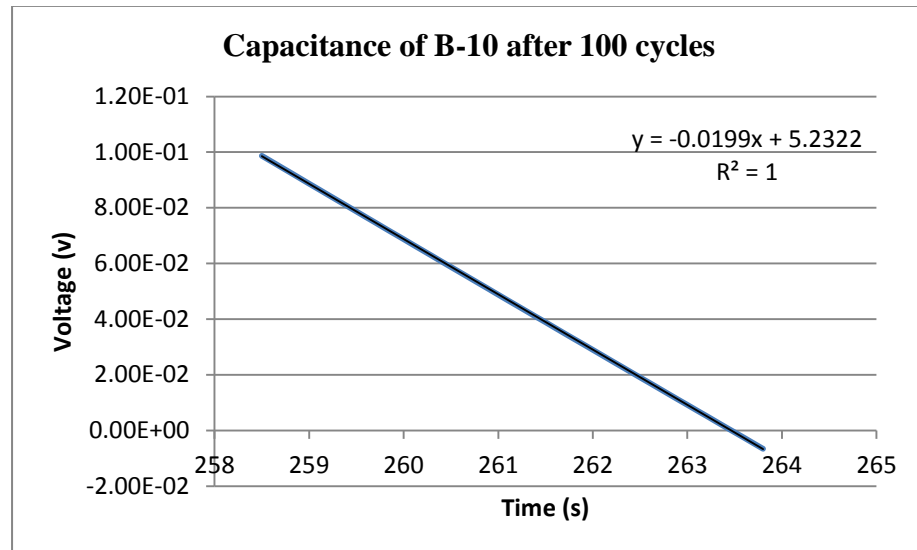


Figure 8-52 Capacitance of B-10 after 100 cycles

$$C = \frac{0.06}{0.019} = 3.158 \text{ F}$$

$$ESR = \frac{1 - 0.664}{0.06} = 5.6 \Omega$$

The CV curve after 100 cycles reassembles the ideal supercapacitor curve. Figure 8-53 shows the CV curve after 100 cycles.

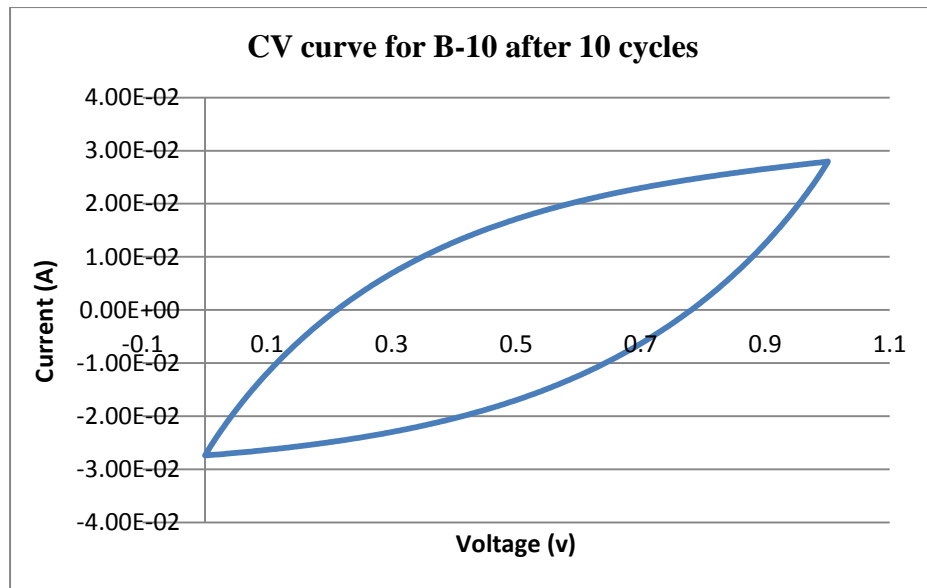


Figure 8-53 CV curve for B-10 after 100 cycles

8.10 Coin prototype B-11

The 11th coin prototype B-11 was tested using the charge-discharge with 50 mA constant current. The first test was done at 10 cycles. Figure 8-54 shows the charge-discharge curve for B-11.

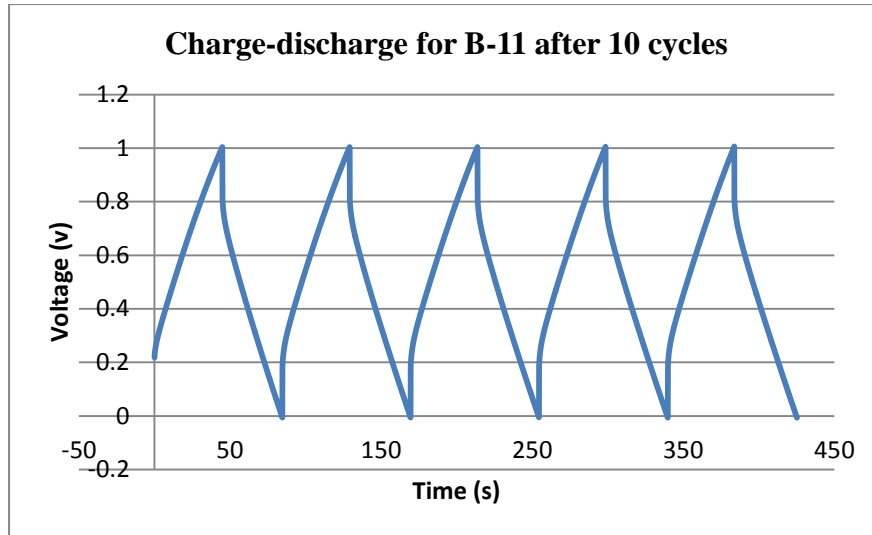


Figure 8-54 Charge-discharge for B-11 after 10 cycles

Portion of the charge-discharge curve is used to calculate the capacitance of the B-11 prototype, Figure 8-55 shows the curve used to measure the slope which was used to calculate the capacitance.

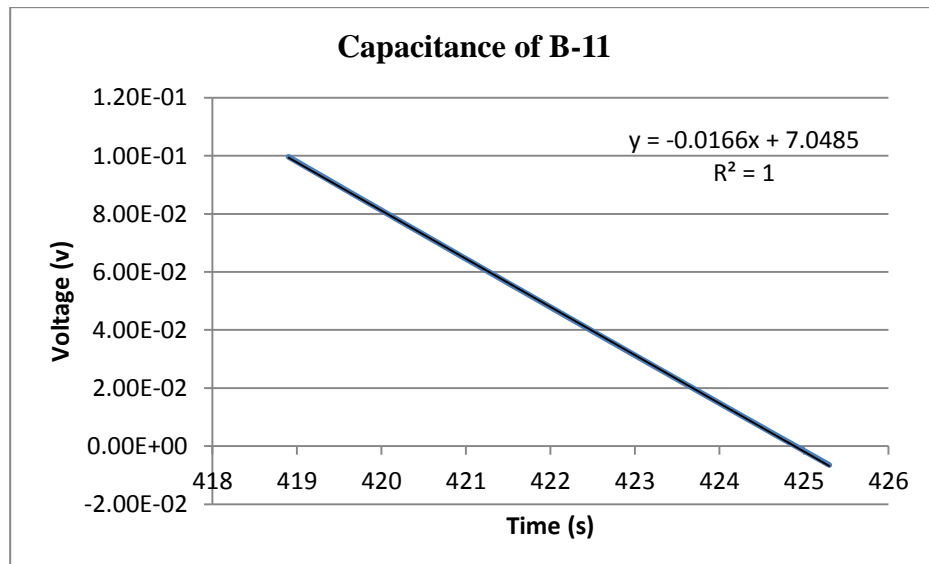


Figure 8-55 Capacitance of B-11

$$C = \frac{0.05}{0.0166} = 3.01 \text{ F}$$

$$ESR = \frac{1 - 0.812}{0.05} = 3.76 \text{ } \Omega$$

The B-11 coin prototype was cycled for 100 cycles and tested again to observe the changes to the capacitance and the ESR values. Figure 8-56 shows the charge-discharge curve after 100 cycles

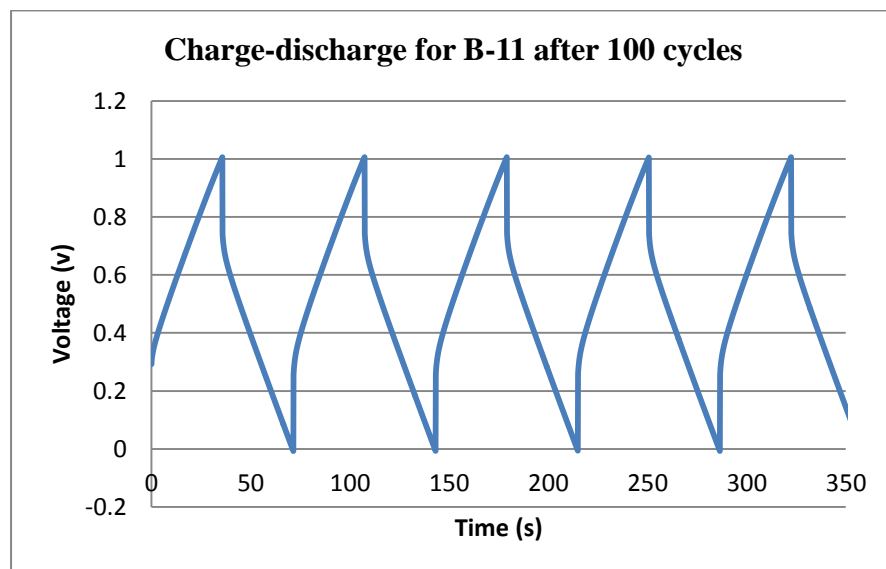


Figure 8-56 Charge-discharge for B-11 after 100 cycles

The new value for the capacitance was decreased to 2.777 F from 3.01 F, and the ESR was increased to 5.08 Ohms from 3.76 Ohms. Figure 8-57 shows the curve used to measure the capacitance of the B-11 prototype.

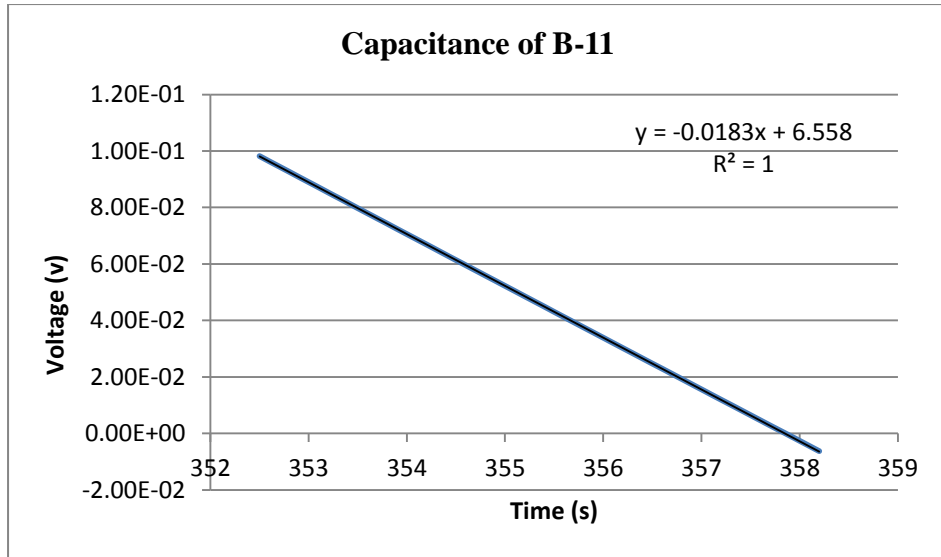


Figure 8-57 Capacitance of B-11

$$C = \frac{0.05}{0.018} = 2.777 \text{ F}$$

$$ESR = \frac{1 - 0.746}{0.05} = 5.08 \Omega$$

The CV curve after 100 cycles reassembles the ideal supercapacitor curve.

Figure 8-58 shows the CV curve after 100 cycles.

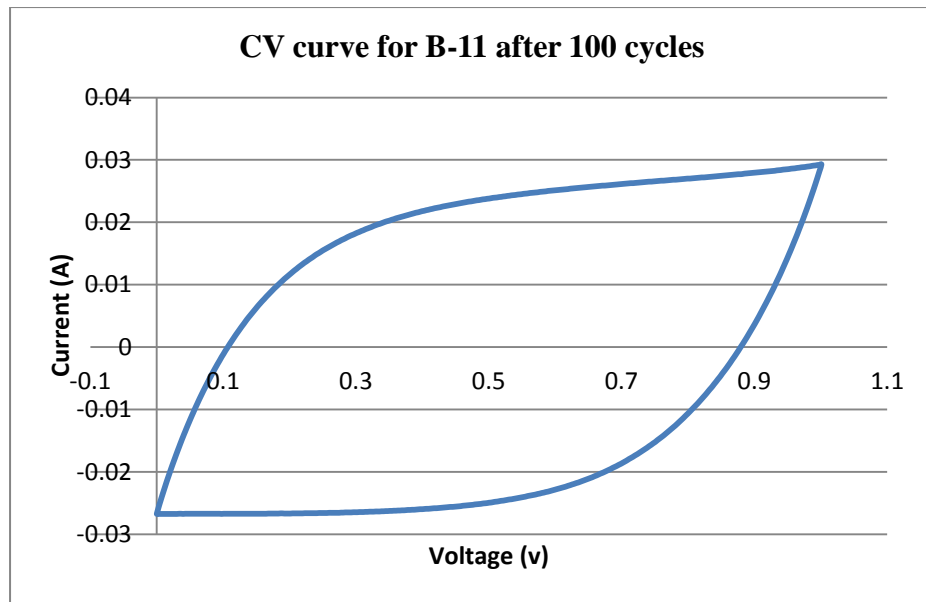


Figure 8-58 CV curve for B-11 after 100 cycles

8.11 Coin prototype B-12

The 12th coin prototype B-12 was tested using the charge-discharge with 50 mA constant current. The first test was done at 10 cycles. Figure 8-59 shows the charge-discharge curve for B-12.

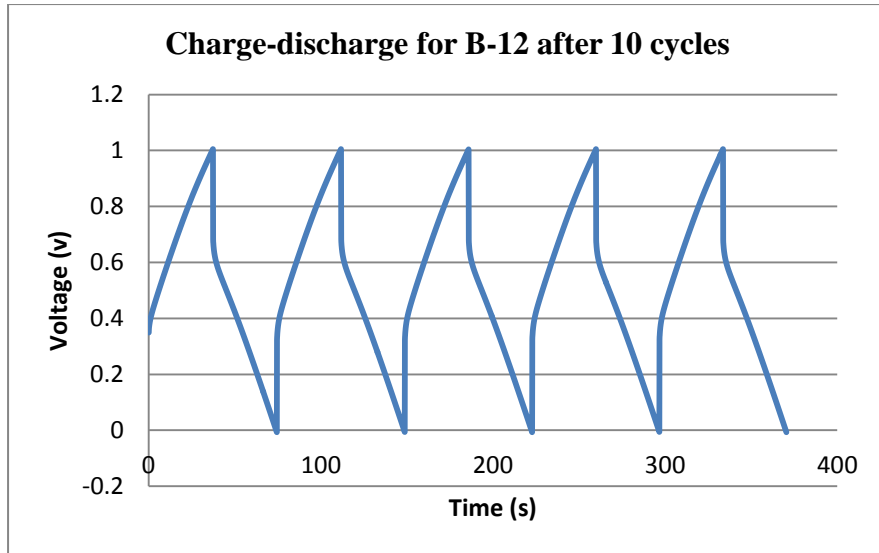


Figure 8-59 Charge-discharge for B-12 after 10 cycles

Portion of the charge-discharge curve is used to calculate the capacitance of the B-12 prototype, Figure 8-60 shows the curve used to measure the slope which was used to calculate the capacitance.

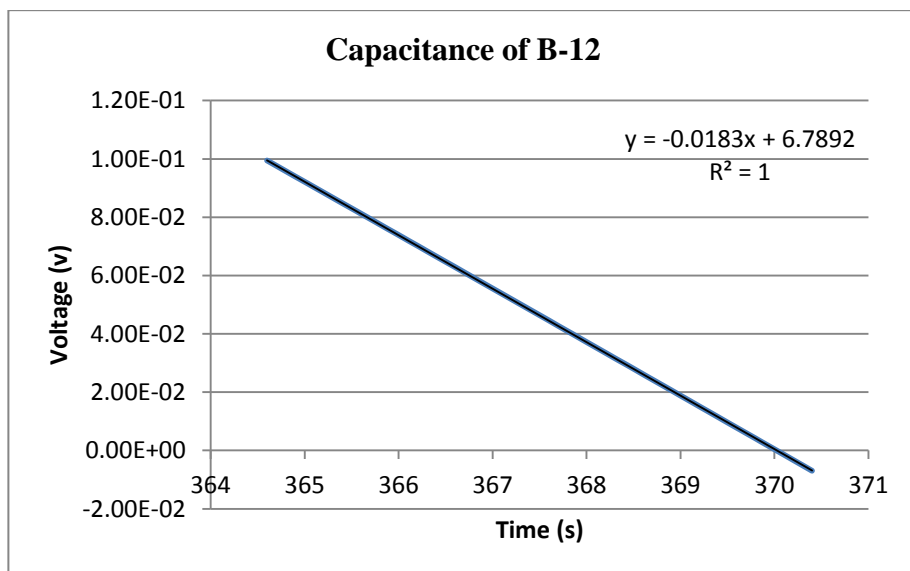


Figure 8-60 Capacitance of B-12

$$C = \frac{0.05}{0.0183} = 2.73 \text{ F}$$

$$ESR = \frac{1 - 0.681}{0.05} = 6.38 \text{ } \Omega$$

The B-12 coin prototype was cycled for 100 cycles and tested again to observe the changes to the capacitance and the ESR values. Figure 8-61 shows the charge-discharge curve after 100 cycles.

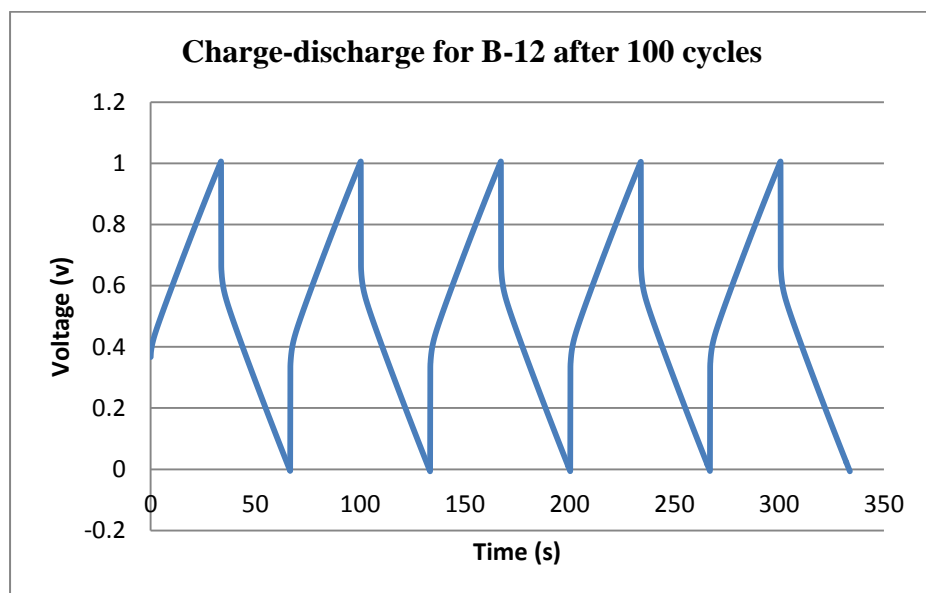


Figure 8-61 Charge-discharge for B-12 after 100 cycles

The new value for the capacitance was increased to 2.941 F from 2.73 F, similarly the ESR was increased to 6.72 Ohms from 6.38 Ohms. Figure 8-62 shows the curve used to measure the capacitance of the B-12 prototype.

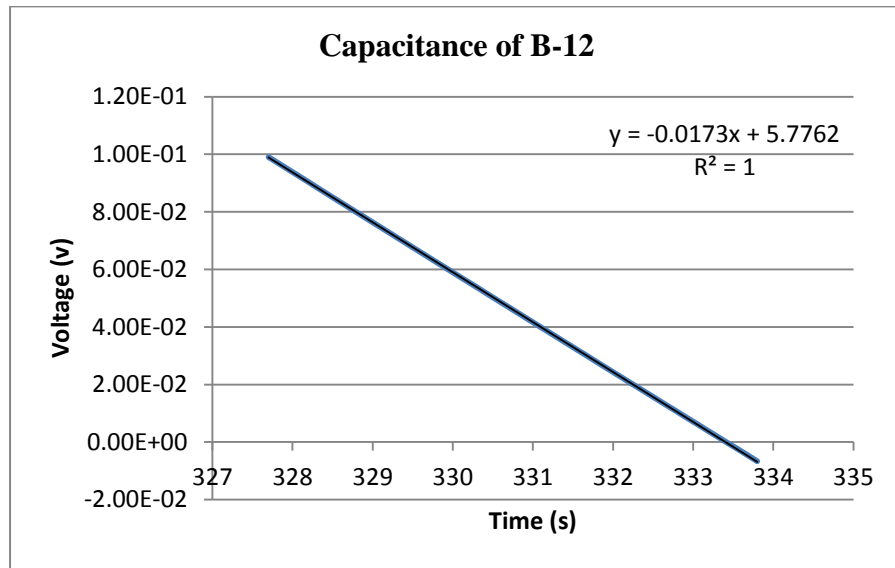


Figure 8-62 Capacitance of B-12

$$C = \frac{0.05}{0.017} = 2.941 F$$

$$ESR = \frac{1 - 0.664}{0.05} = 6.72 \Omega$$

The CV curve after 100 cycles reassembles the ideal supercapacitor curve. Figure 8-63 shows the CV curve after 100 cycles.

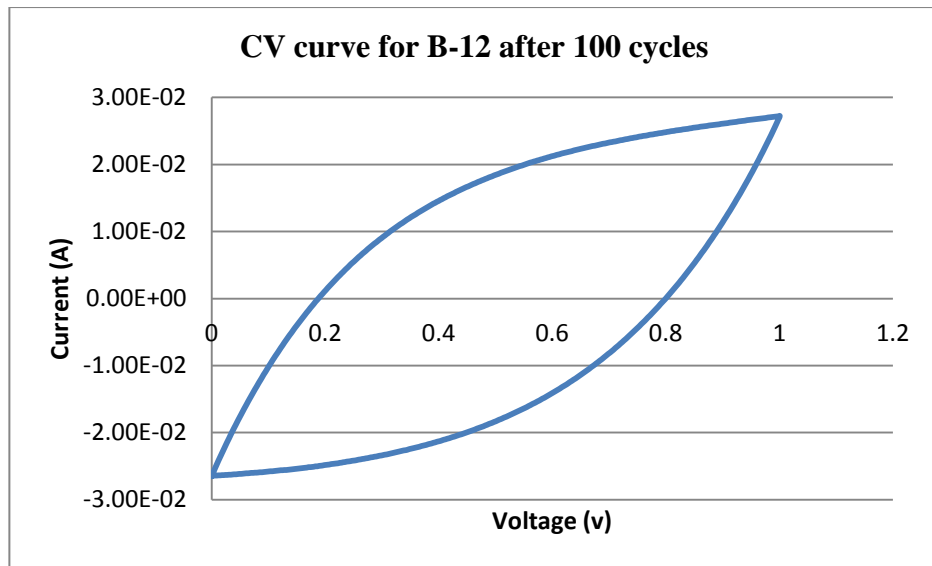


Figure 8-63 CV curve for B-12 after 100 cycles

8.12 Coin prototype B-13

The 13th coin prototype B-13 was tested using the charge-discharge with 50 mA constant current. The first test was done at 10 cycles. Figure 8-64 shows the charge-discharge curve for B-13.

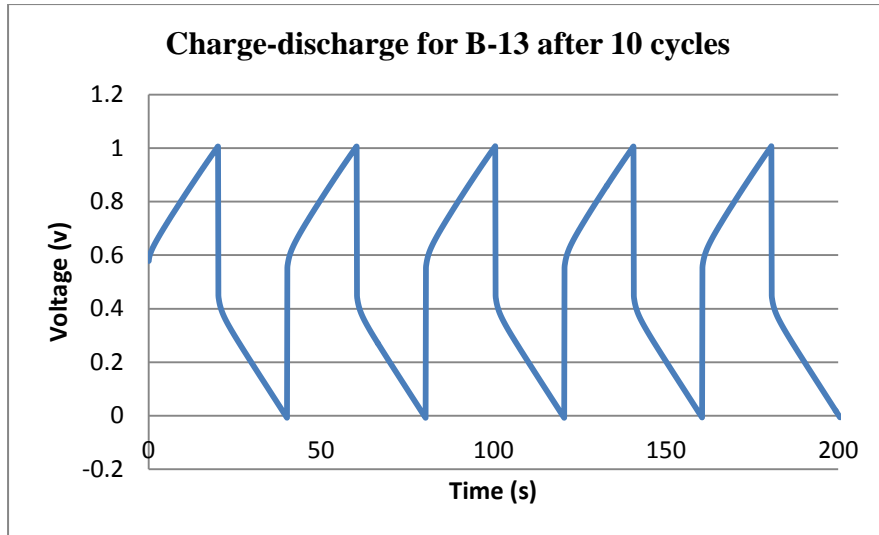


Figure 8-64 Charge-discharge for B-13 after 10 cycles

Portion of the charge-discharge curve is used to calculate the capacitance of the B-13 prototype, Figure 8-65 shows the curve used to measure the slope which was used to calculate the capacitance.

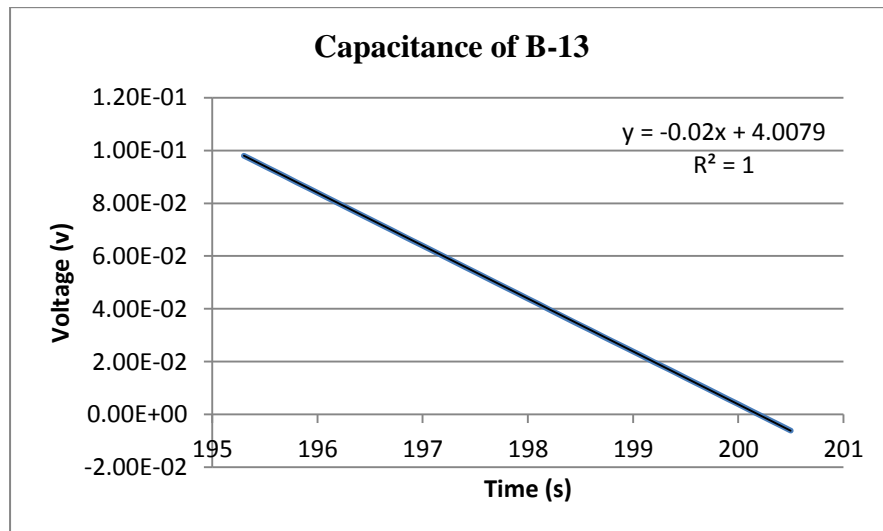


Figure 8-65 Capacitance of B-13

$$C = \frac{0.05}{0.02} = 2.5 \text{ F}$$

$$ESR = \frac{1 - 0.448}{0.05} = 11.04 \text{ } \Omega$$

The B-13 coin prototype was cycled for 100 cycles and tested again to observe the changes to the capacitance and the ESR values. Figure 8-66 shows the charge-discharge curve after 100 cycles

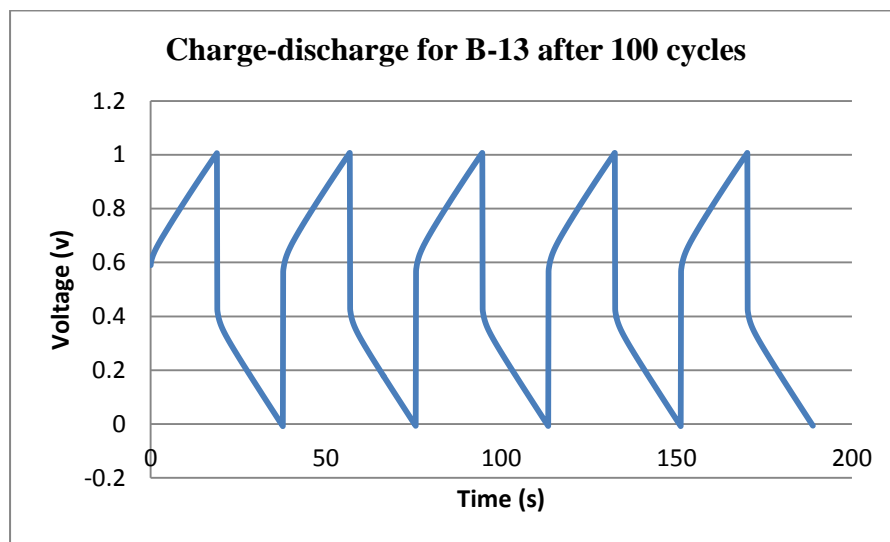


Figure 8-66 Charge-discharge for B-13 after 100 cycles

The new value for the capacitance was decreased to 2.478 F from 2.5 F, and the ESR was increased to 11.46 Ohms from 11.04 Ohms. Figure 8-67 shows the curve used to measure the capacitance of the B-13 prototype.

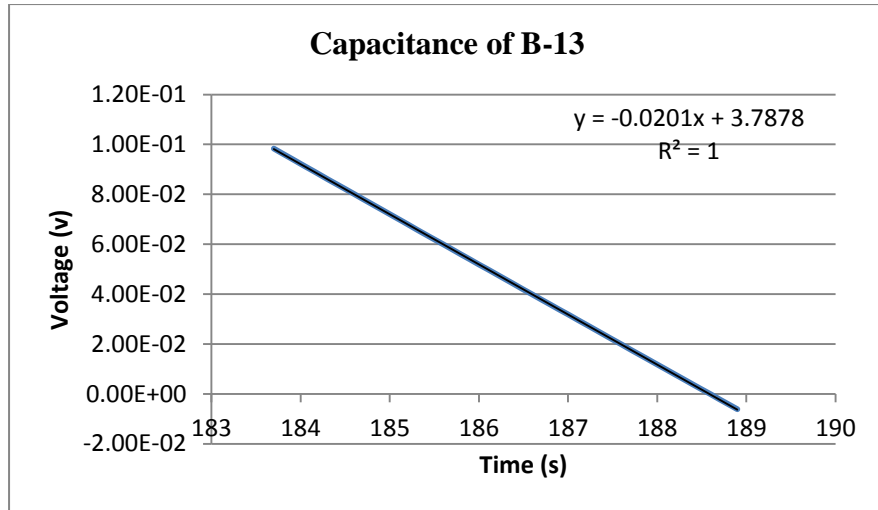


Figure 8-67 Capacitance of B-13

$$C = \frac{0.05}{0.0201} = 2.487 \text{ F}$$

$$ESR = \frac{1 - 0.427}{0.05} = 11.46 \text{ } \Omega$$

The CV curve after 100 cycles reassembles the ideal supercapacitor curve. Figure 8-68 shows the CV curve after 100 cycles.

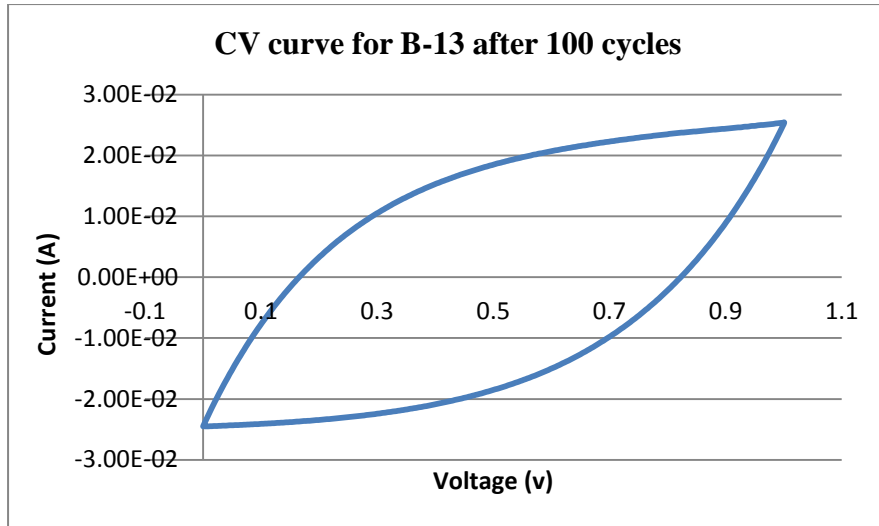


Figure 8-68 CV curve for B-13 after 100 cycles

8.13 Coin prototype B-14

The 14th coin prototype B-14 was tested using the charge-discharge with 50 mA constant current. The first test was done at 10 cycles. Figure 8-69 shows the charge-discharge curve for B-14.

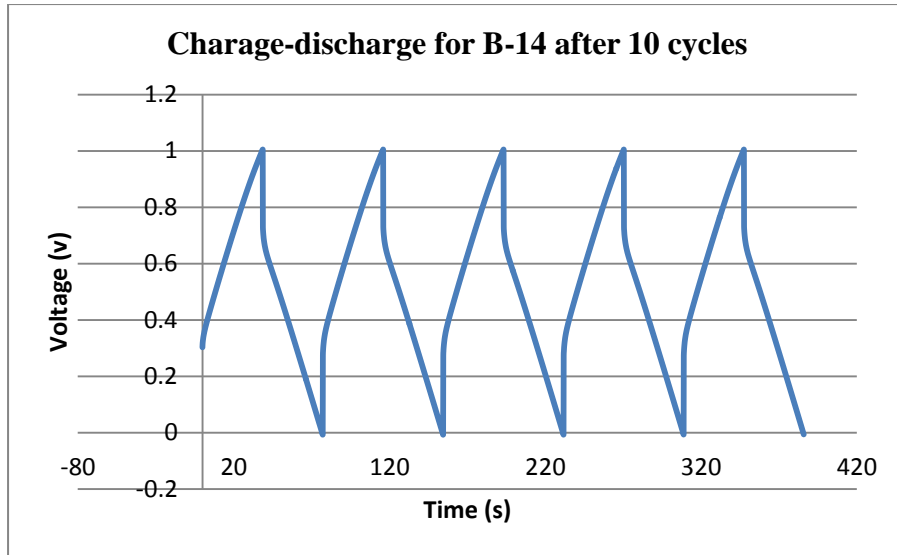


Figure 8-69 Charge-discharge for B-14 after 10 cycles

Portion of the charge-discharge curve is used to calculate the capacitance of the B-14 prototype, Figure 8-70 shows the curve used to measure the slope which was used to calculate the capacitance.

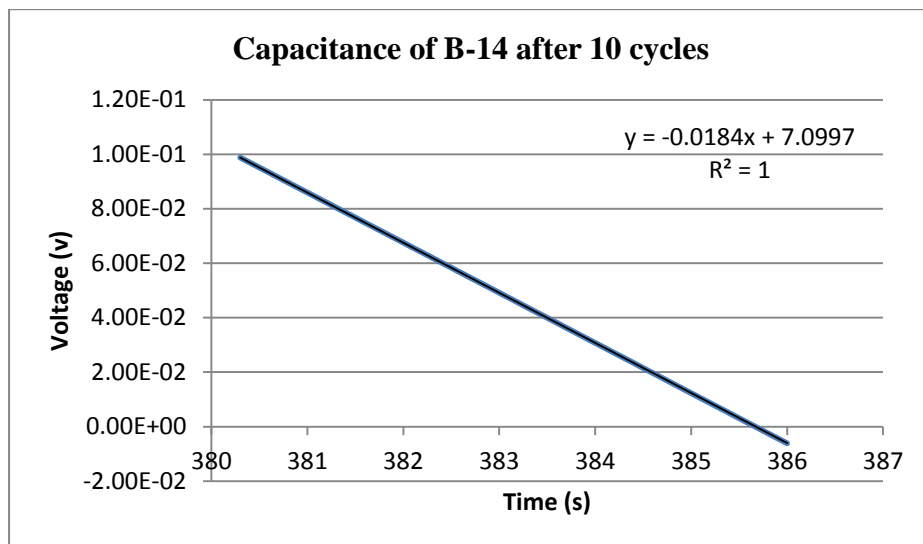


Figure 8-70 Capacitance for B-14

$$C = \frac{0.05}{0.0184} = 2.717 \text{ F}$$

$$ESR = \frac{1 - 0.730}{0.05} = 5.4 \text{ } \Omega$$

The B-14 prototype was tested using CV to observe its behavior, Figure 8-71 shows the CV curve which closely resembles the ideal supercapacitor square shape curve.

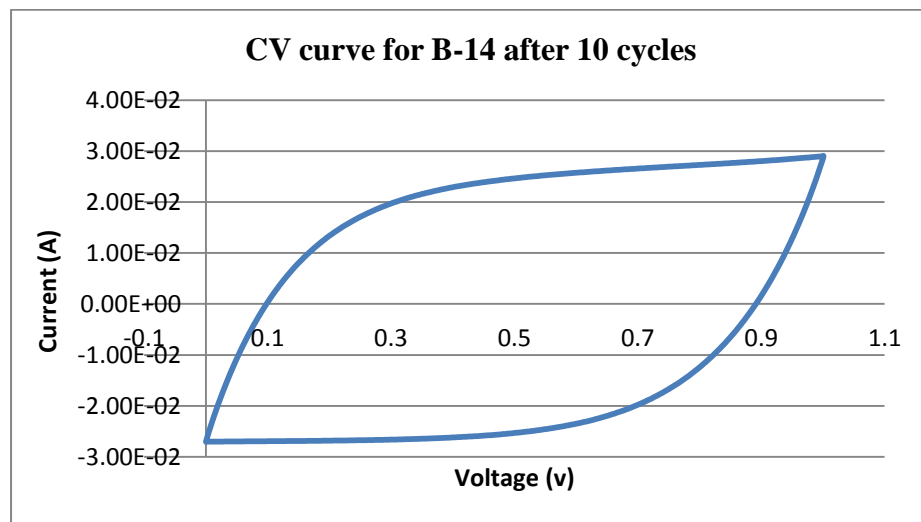


Figure 8-71 CV curve for B-14 after 10 cycles

The B-14 coin prototype was cycled for 100 cycles and tested again to observe the changes to the capacitance and the ESR values. Figure 8-72 shows the charge-discharge curve after 100 cycles

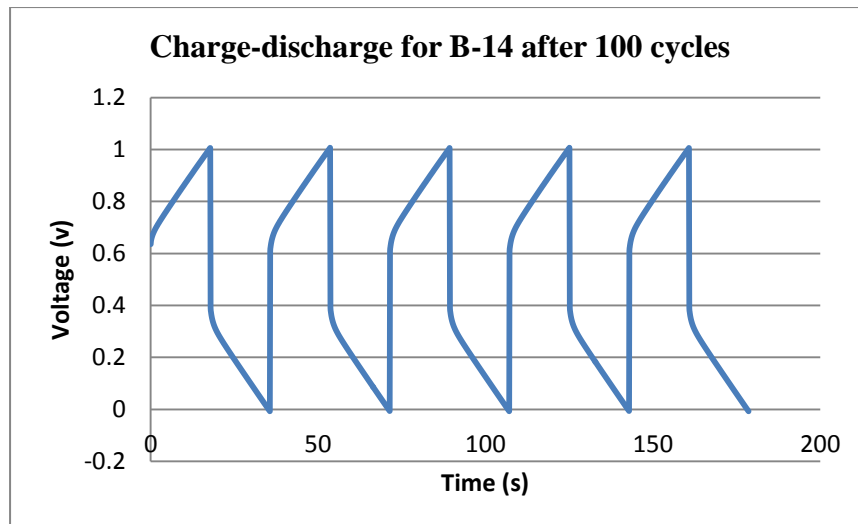


Figure 8-72 Charge-discharge for B-14 after 100 cycles

The new value for the capacitance was increased to 2.76 F from 2.717 F, similarly the ESR was increased to 12.2 Ohms from 5.4 Ohms. Figure 8-73 shows the curve used to measure the capacitance of the B-14 prototype.

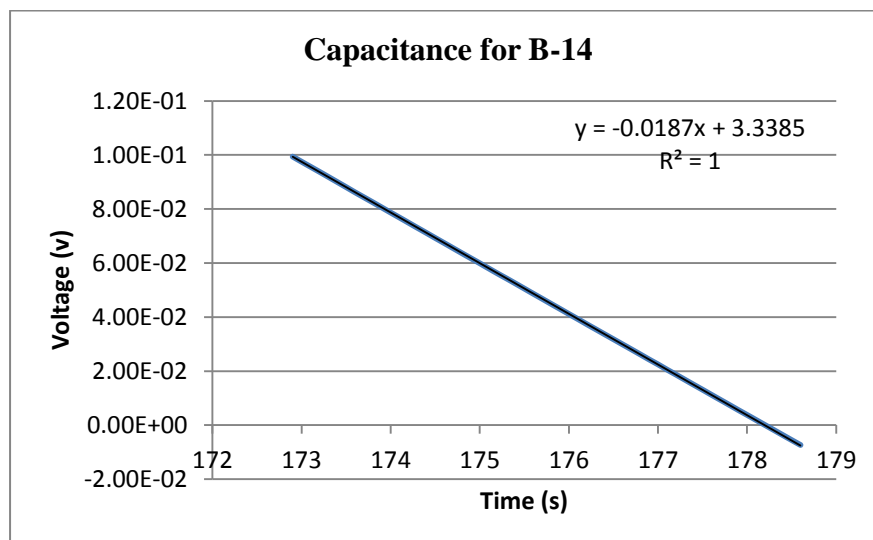


Figure 8-73 Capacitance for B-14

$$C = \frac{0.05}{0.0187} = 2.76 \text{ F}$$

$$ESR = \frac{1 - 0.39}{0.05} = 12.2 \text{ } \Omega$$

The CV curve after 100 cycles reassembles the ideal supercapacitor curve. Figure 8-74 shows the CV curve after 100 cycles.

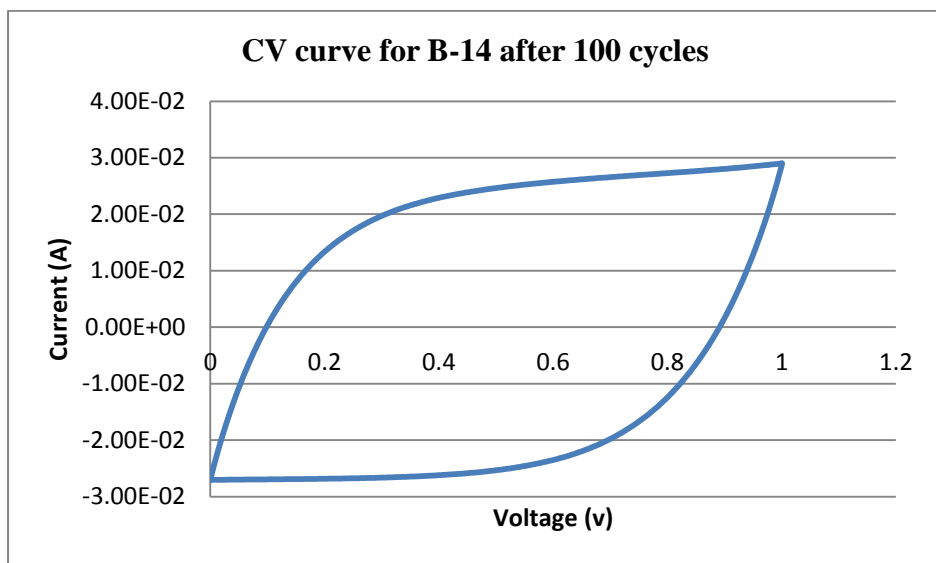


Figure 8-74 CV curve for B-14 after 100 cycles

8.14 Coin Prototype B-15

The 15th coin prototype B-15 was tested using the charge-discharge with 50 mA constant current. The first test was done at 10 cycles. Figure 8-75 shows the charge-discharge curve for B-15.

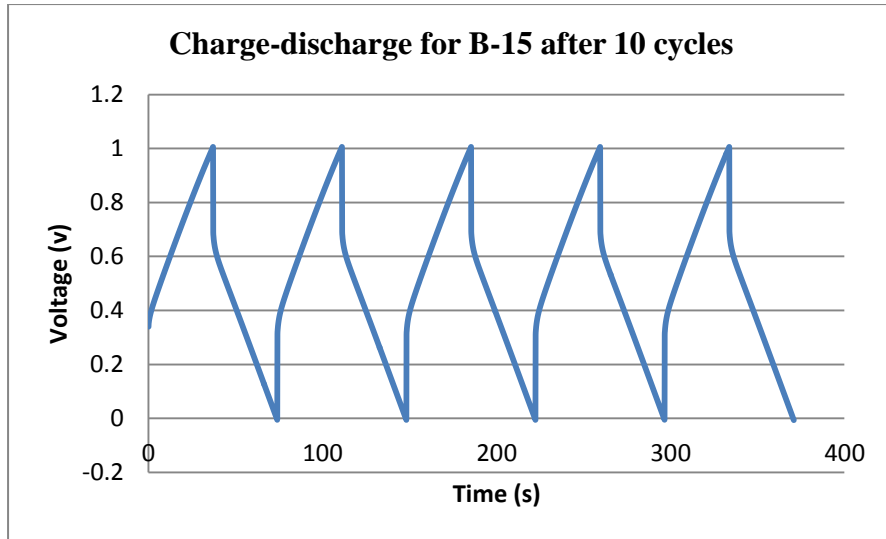


Figure 8-75 Charge-discharge for B-15 after 10 cycles

Portion of the charge-discharge curve is used to calculate the capacitance of the B-15 prototype, Figure 8-76 shows the curve used to measure the slope which was used to calculate the capacitance.

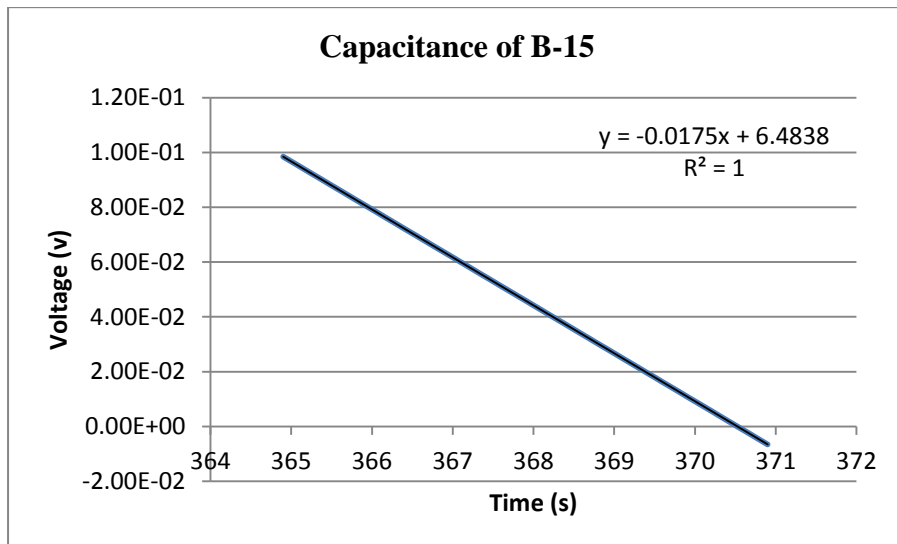


Figure 8-76 Capacitance of B-15

$$C = \frac{0.05}{0.0175} = 2.857 \text{ F}$$

$$ESR = \frac{1 - 0.692}{0.05} = 6.16 \text{ } \Omega$$

The B-15 coin prototype was cycled for 100 cycles and tested again to observe the changes to the capacitance and the ESR values. Figure 8-77 shows the charge-discharge curve after 100 cycles.

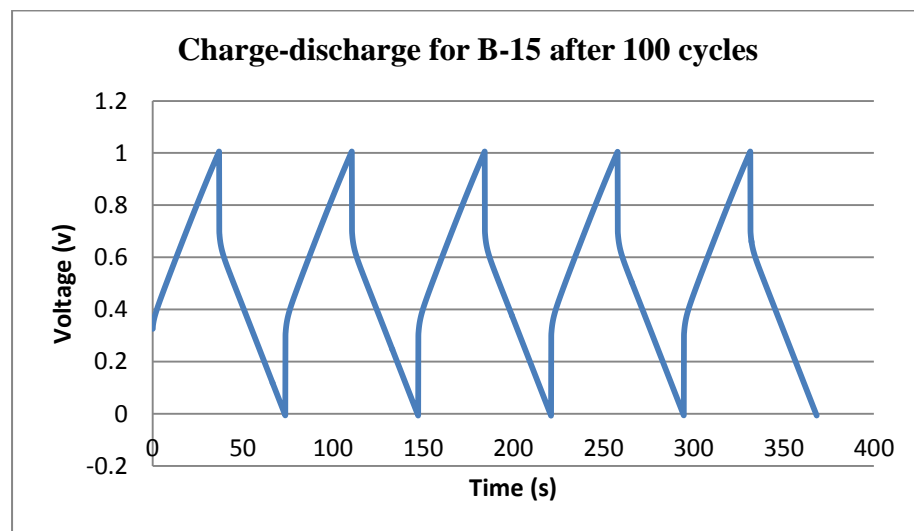


Figure 8-77 Charge-discharge after 100 cycles

The new value for the capacitance was decreased to 2.824 F from 2.857 F, similarly the ESR was decreased to 6 Ohms from 6.16 Ohms. Figure 8-78 shows the curve used to measure the capacitance of the B-15 prototype.

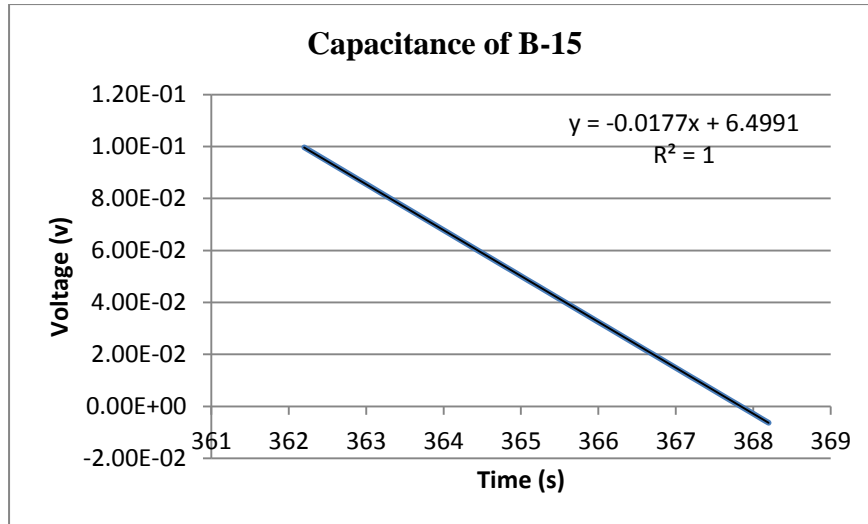


Figure 8-78 Capacitance of B-15

$$C = \frac{0.05}{0.0177} = 2.824 \text{ F}$$

$$ESR = \frac{1 - 0.700}{0.05} = 6. \Omega$$

The CV curve after 100 cycles reassembles the ideal supercapacitor curve, Figure 8-79 shows the CV curve after 100 cycles.

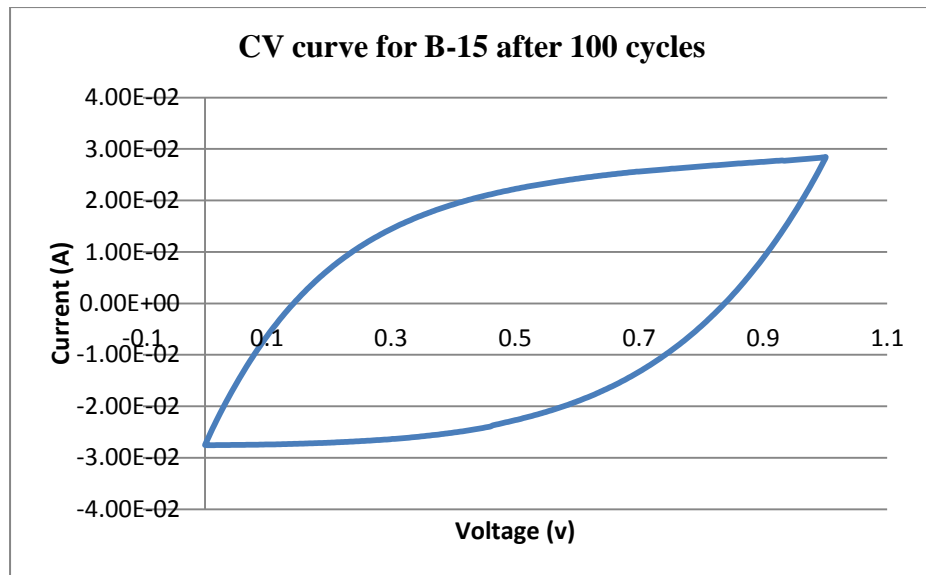


Figure 8-79 CV curve for B-15 after 100 cycles

8.15 Coin prototype B-16

The 16th coin prototype B-16 was tested using the charge-discharge with 50 mA constant current. The first test was done at 10 cycles. Figure 8-80 shows the charge-discharge curve for B-16.

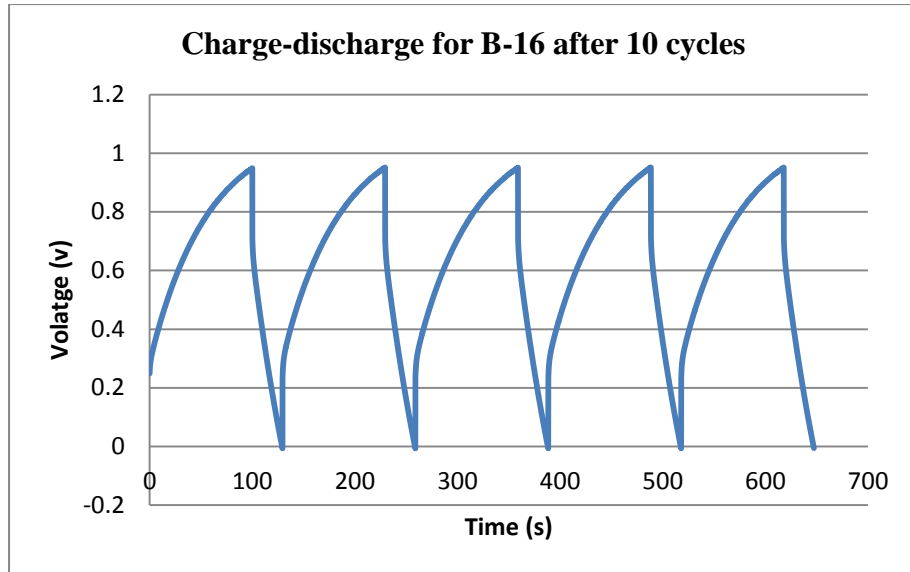


Figure 8-80 Charge-discharge for B-16 after 10 cycles

Portion of the charge-discharge curve is used to calculate the capacitance of the B-16 prototype, Figure 8-81 shows the curve used to measure the slope which was used to calculate the capacitance.

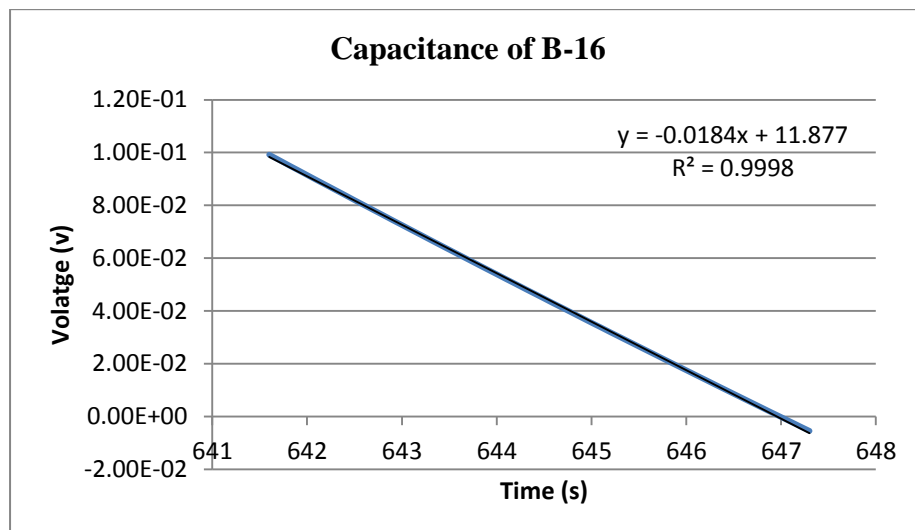


Figure 8-81 Capacitance of B-16

$$C = \frac{0.05}{0.0184} = 2.717 \text{ F}$$

$$ESR = \frac{1 - 0.488}{0.05} = 10.24 \text{ } \Omega$$

The B-16 coin prototype was cycled for 100 cycles and tested again to observe the changes to the capacitance and the ESR values. Figure 8-82 shows the charge-discharge curve after 100 cycles.

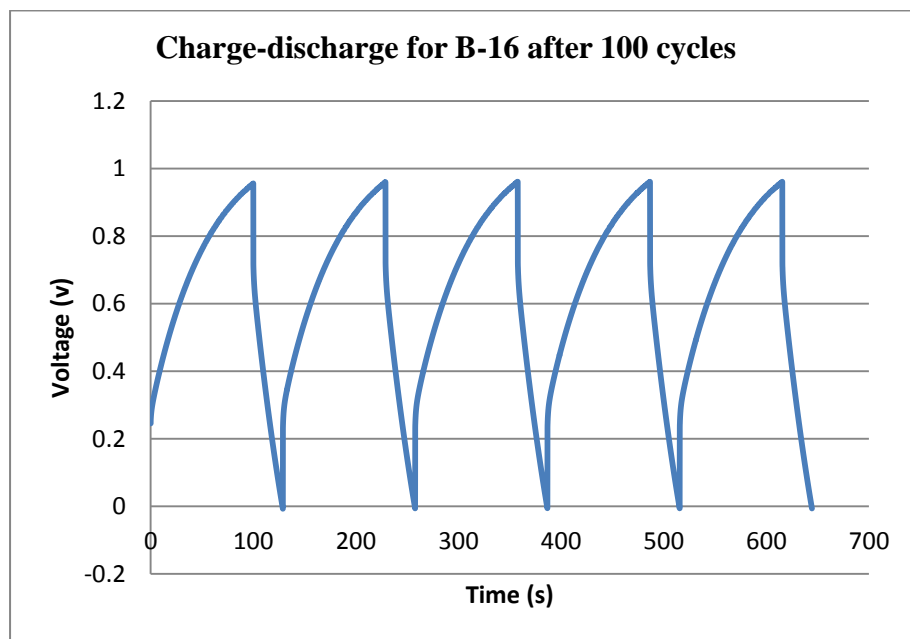


Figure 8-82 Charge-discharge for B-16 after 100 cycles

The new value for the capacitance was decreased to 2.659 F from 2.717 F, and the ESR was increased to 10.28 Ohms from 10.24 Ohms. Figure 8-83 shows the curve used to measure the capacitance of the B-16 prototype.

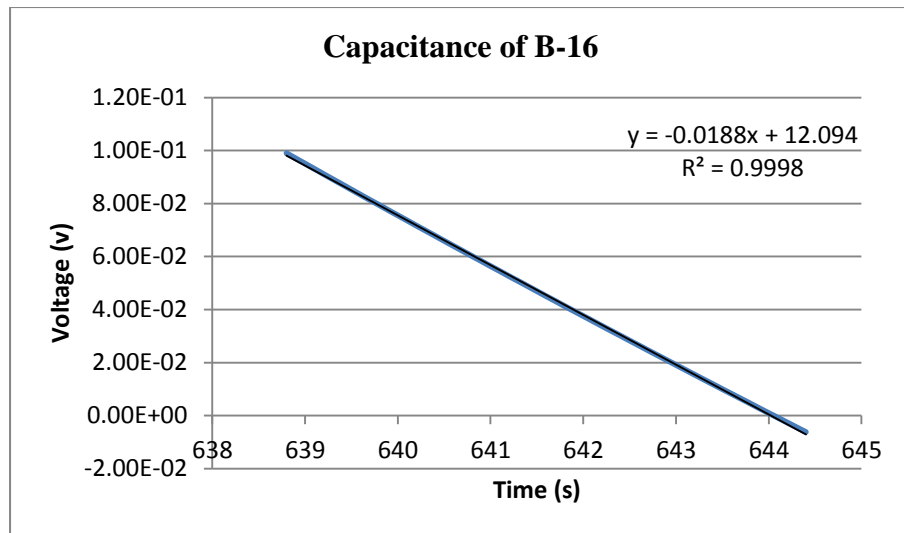


Figure 8-83 Capacitance of B-16

$$C = \frac{0.05}{0.0188} = 2.659 \text{ F}$$

$$ESR = \frac{1 - 0.486}{0.05} = 10.28 \Omega$$

The CV curve after 100 cycles reassembles the ideal supercapacitor curve. Figure 8-84 shows the CV curve after 100 cycles.

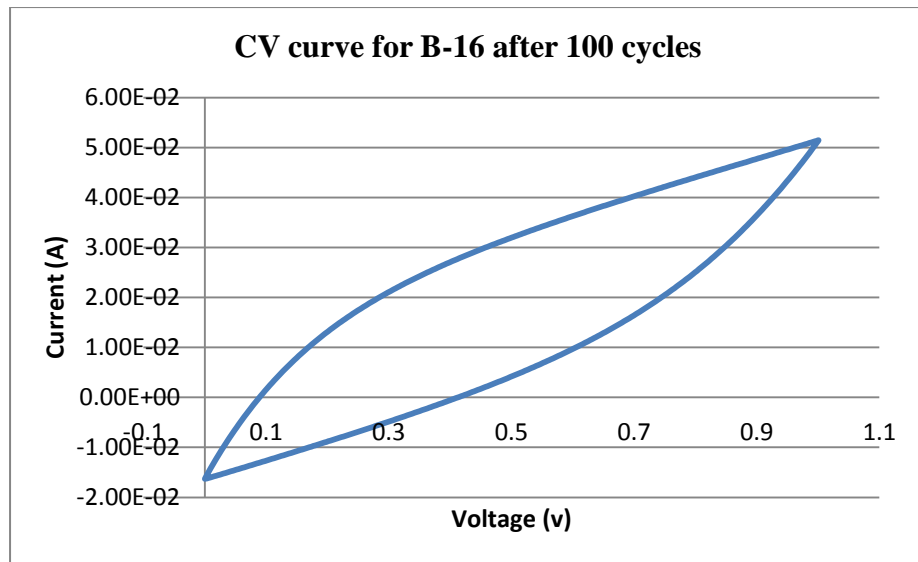


Figure 8-84 CV curve for B-16 after 100 cycles

8.16 Coin prototype B-17

The 17th coin prototype B-17 was tested using the charge-discharge with 50 mA constant current. The first test was done at 10 cycles. Figure 8-85 shows the charge-discharge curve for B-17.

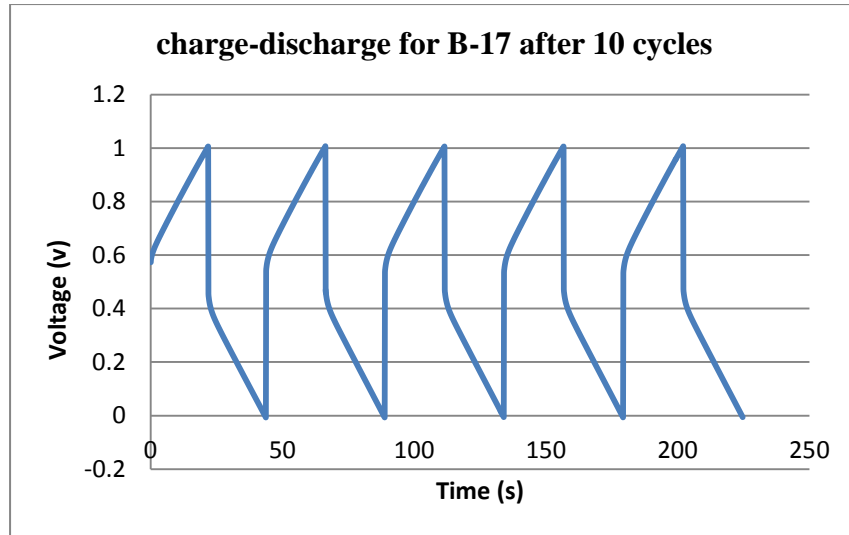


Figure 8-85 Charge-discharge for B-17 after 10 cycles

Portion of the charge-discharge curve is used to calculate the capacitance of the B-17 prototype, Figure 8-86 shows the curve used to measure the slope which was used to calculate the capacitance.

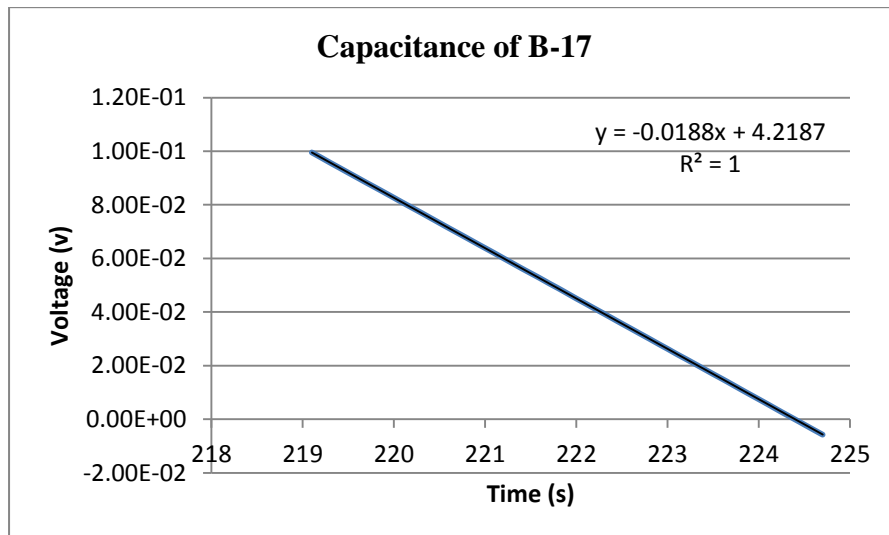


Figure 8-86 Capacitance of B-17

$$C = \frac{0.05}{0.0188} = 2.648 \text{ F}$$

$$ESR = \frac{1 - 0.471}{0.05} = 10.58 \text{ } \Omega$$

The B-17 coin prototype was cycled for 100 cycles and tested again to observe the changes to the capacitance and the ESR values. Figure 8-87 shows the charge-discharge curve after 100 cycles.

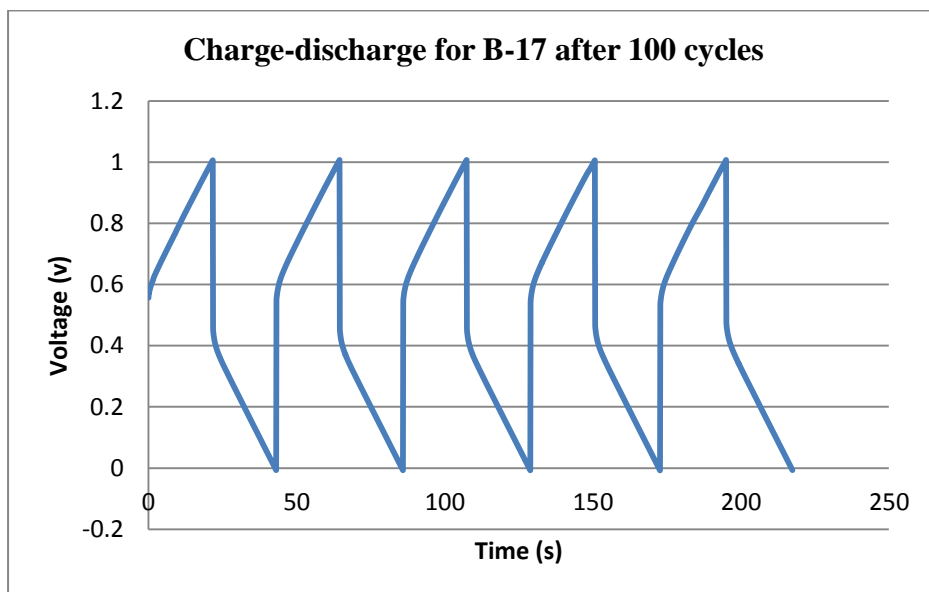


Figure 8-87 Charge-discharge for B-17 after 100 cycles

The new value for the capacitance was decreased to 2.617 F from 2.648 F, and the ESR was increased to 10.686 Ohms from 10.58 Ohms. Figure 8-88 shows the curve used to measure the capacitance of the B-17 prototype.

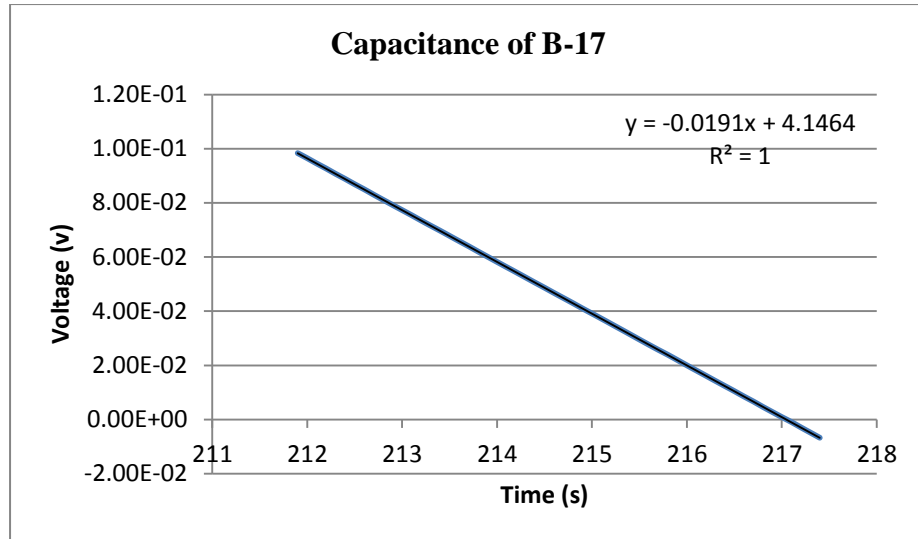


Figure 8-88 Capacitance of B-17

$$C = \frac{0.05}{0.0191} = 2.61748 F$$

$$ESR = \frac{1 - 0.466}{0.05} = 10.68 \Omega$$

The CV curve after 100 cycles reassembles a narrow ideal supercapacitor curve.

Figure 8-89 shows the CV curve after 100 cycles.

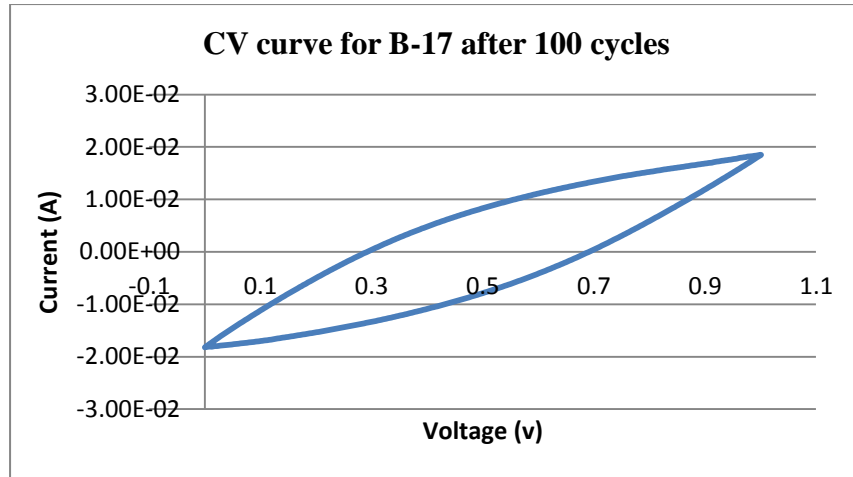


Figure 8-89 CV curve for B-17 after 100 cycles

8.17 Coin prototype B-18

The 18th coin prototype B-18 was tested using the charge-discharge with 50 mA constant current. The first test was done at 10 cycles. Figure 8-90 shows the charge-discharge curve for B-18.

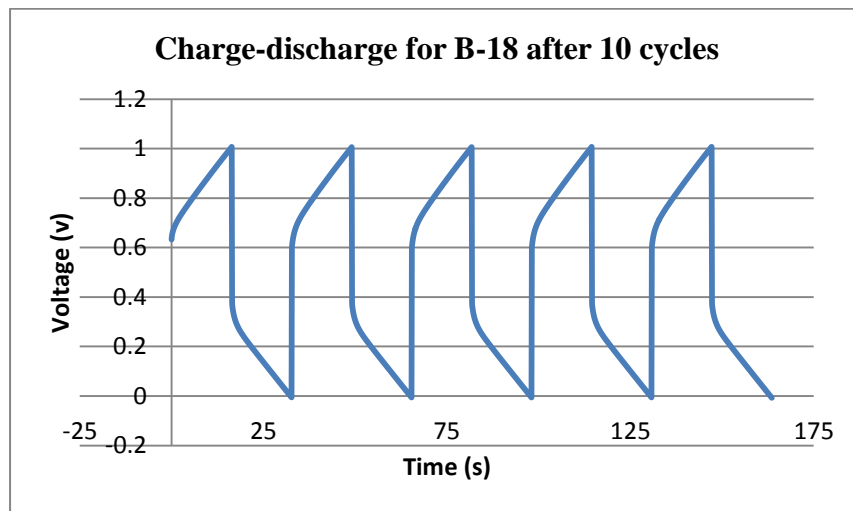


Figure 8-90 Charge-discharge for B-18 after 10 cycles

Portion of the charge-discharge curve is used to calculate the capacitance of the B-18 prototype, Figure 8-91 shows the curve used to measure the slope which was used to calculate the capacitance.

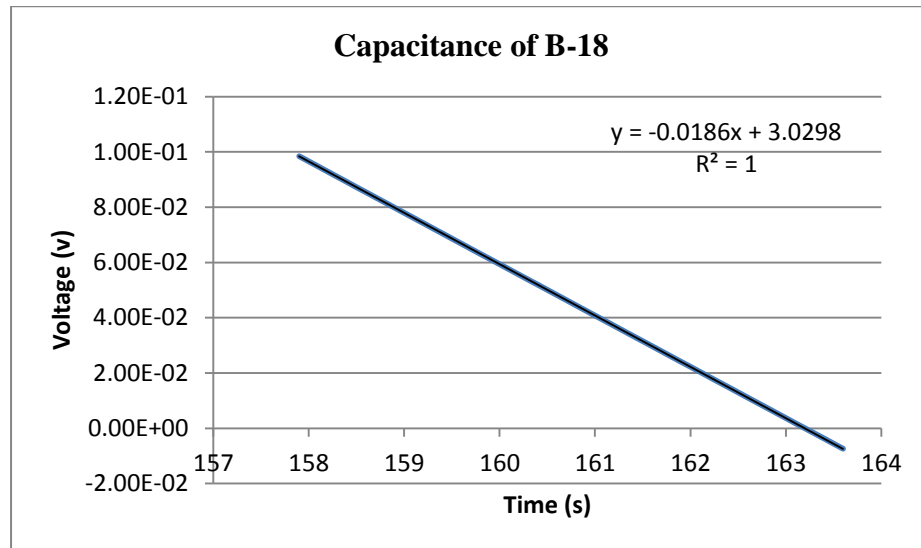


Figure 8-91 Capacitance of B-18

$$C = \frac{0.05}{0.0186} = 2.688 \text{ F}$$

$$ESR = \frac{1 - 0.375}{0.05} = 12.44 \text{ } \Omega$$

The B-18 coin prototype was cycled for 100 cycles and tested again to observe the changes to the capacitance and the ESR values. Figure 8-92 shows the charge-discharge curve after 100 cycles.

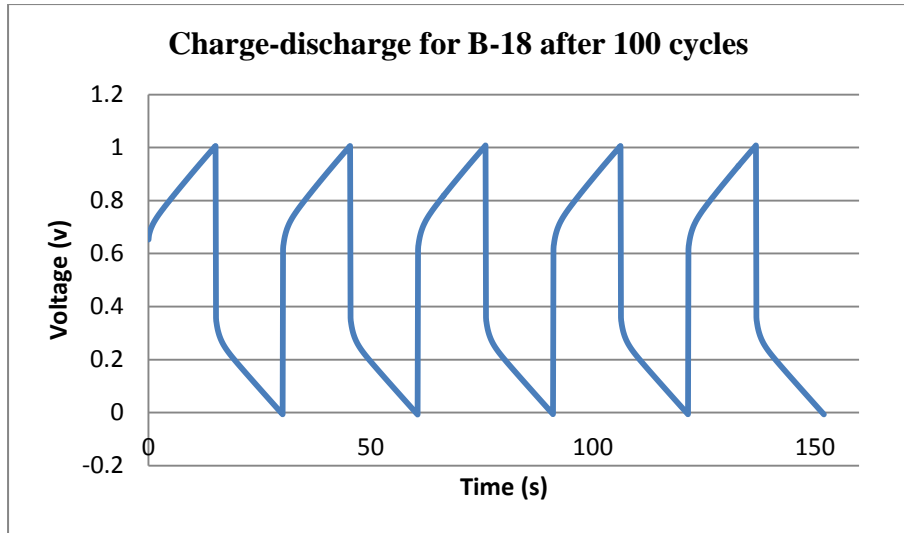


Figure 8-92 Charge-discharge for B-18 after 100 cycles

The new value for the capacitance was decreased to 2.673 F from 2.688 F, but the ESR was increased to 12.84 Ohms from 12.44 Ohms. Figure 8-93 shows the curve used to measure the capacitance of the B-18 prototype.

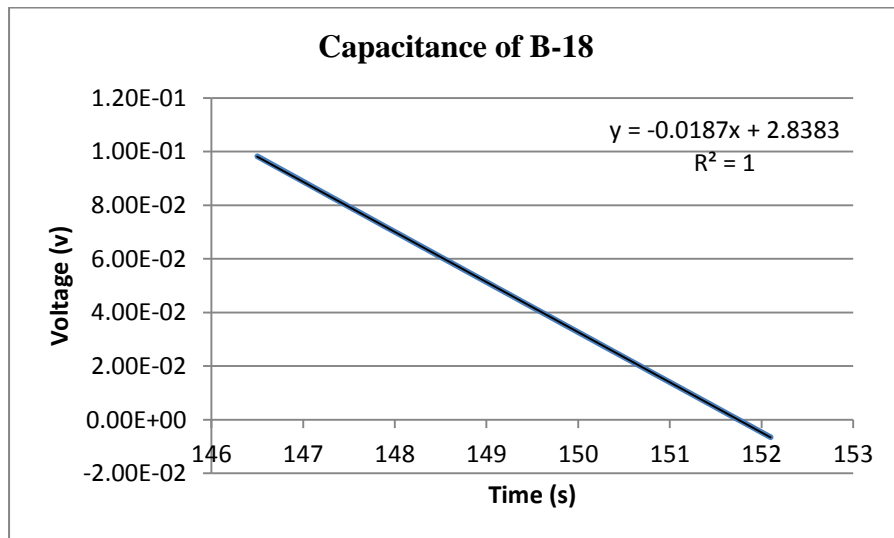


Figure 8-93 Capacitance of B-18

$$C = \frac{0.05}{0.0187} = 2.673 \text{ F}$$

$$ESR = \frac{1 - 0.358}{0.05} = 12.84 \text{ } \Omega$$

The CV curve after 100 cycles reassembles the ideal supercapacitor curve. Figure 8-94 shows the CV curve after 100 cycles.

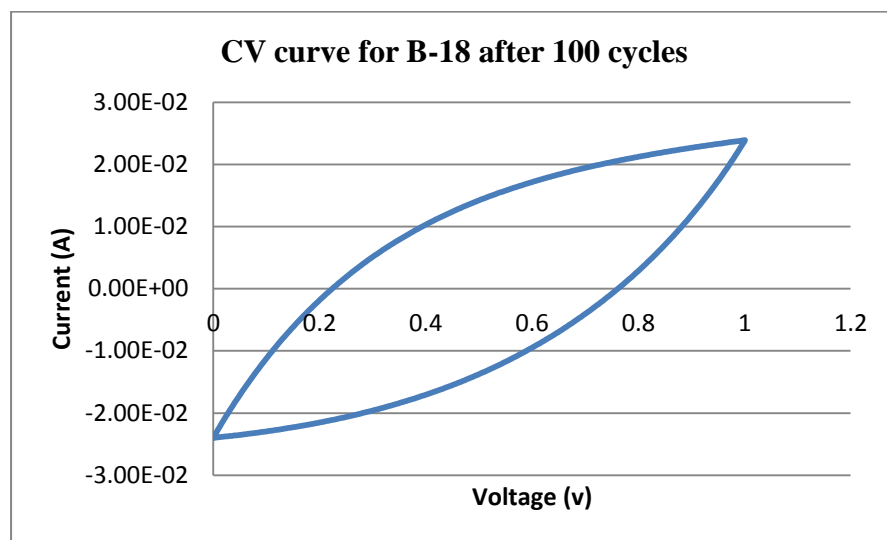


Figure 8-94 CV curve for B-18 after 100 cycles

9. Appendix C



ISSN: 2319-5967

ISO 9001:2008 Certified

International Journal of Engineering Science and Innovative Technology (IJESIT)

Volume 1, Issue 2, November 2012

Optimization of Process Factors in Super capacitor Fabrication Using the Genetic Algorithm to Optimize Taguchi Signal-to-Noise Ratios

Chia Yen Yee, Ridhuan Ahmad Samsuri, Dino Isa, Ahmida Ajina, Khiew Pooi Sim

keyx1cyy@nottingham.edu.my, kecx1ram@nottingham.edu.my, kezdi@nottingham.edu.my,

keyx7aaj@nottingham.edu.my, efzpsk@nottingham.edu.my

Department of Electrical and Electronic Engineering University of Nottingham Malaysia Campus,
Department of Electrical and Electronic Engineering University of Nottingham Malaysia Campus,
Department of Electrical and Electronic Engineering University of Nottingham Malaysia Campus,
Department of Electrical and Electronic Engineering University of Nottingham Malaysia Campus,
Foundation Studies in Engineering and Computer Science of University of Nottingham Malaysia Campus

Abstract— This paper proposes an approach which deals with the optimization of process factors for super capacitor fabrication. The methodology developed here is useful for solving multi response problems in a manufacturing environment. A way of implementing the proposed approach for fabrication of coin-type super-capacitors is presented. The Taguchi method is combined with a Genetic Algorithm (GA) in order to optimize a weighted signal-to-noise ratio (WSNR) which is essential in identifying the most robust process factors. Consequently, the GA is used to enhance the WSNR value and thus to maximize the strength of the signal over noise. Experimental result shows that the proposed approach has the potential and ability to solve multi response problem for this domain. A comparison of the results achieved using the GA and the result from the Overall Evaluation Criteria (OEC) is made based on the improvement of the SNR (in dB) and the standard deviation. Finally, variance analysis plays an important role in identifying the most statistically significant factors in the process. The main contribution of this approach is to effectively and efficiently tackle multi response problem involved in the fabrication of super-capacitors where the values of both Capacitance and Equivalent Series Resistance (ESR) are equally important.

Index Terms— Genetic Algorithm; Multi Response Problem; Process Optimization; Super Capacitors; Taguchi Method.

I. INTRODUCTION

Previous applications [1] – [4] indicate that the Taguchi method emphasizes the solution of single-response problems with the aid of knowledge gained from past experience. Thus, it is not capable of handling multi response problems without requiring some modifications in the application. The Taguchi method provides practitioners and designers with a systematic approach for conducting experiments to obtain near optimal settings of design factors for performance and cost [5] – [7]. The design (controllable) factors and noise (uncontrollable) factors, which influence the quality of the product, are considered together instead of individually [3] [4] [8]. The objective of implementing the Taguchi method is to obtain the best combination of factors and levels in order to achieve the most robust product. This means, the selected levels of the various design factors from the Taguchi method allows the performance of the product/process to be less sensitive to the noise factors. However, in today's manufacturing environment, many processes or products involve solving multi response problem to improve their product quality. One crucial fact is that the Taguchi method is incapable of performing well for multi-response optimization problem [5] [6]. In order to overcome this limitation, we have formulated a way to include a GA within the Taguchi method. A common method of solving the multi response problems is to assign each response with a weight, as mentioned in [5] [6] [9]. A normal question which arises is how to determine and define the weight for each response in a real case. The goal of this proposed strategy is to ensure that the performance characteristics (or the quality) have minimal variation while having its mean close to the desired target value.



ISSN: 2319-5967

ISO 9001:2008 Certified

International Journal of Engineering Science and Innovative Technology (JESIT)

Volume 1, Issue 2, November 2012

The idea underlying this integrated strategy is to convert the problem of optimizing a complicated multi process response into one that optimizes a single weight of the SNR. This means, the WSNR is used in the overall evaluation of experimental data in the multi response optimization problem. In this case, the GA strategy utilizes the normalized SNR (Z) from the Taguchi method to form its fitness function. The optimal level for each individual process factor is the level with the highest WSNR. This paper is organized as follows. Research methodology is presented in Section 2, which shows the background theories used in this research. Section 3 illustrates the proposed integrated strategy. The coin super capacitor fabrication process is the illustrative example given in this paper. Analysis of variance (ANOVA) is also applied to identify the most critical factors that influence WSNR. In Section 4, results and discussions are presented where a set of OEC based on the engineering judgment result is compared with the set of results obtained from the proposed integrated strategy. Confirmations of the results obtained from experiments are presented in Section 5. Section 6 concludes the paper.

II. RESEARCH METHODOLOGY

A. The Taguchi Method

Design of experiments (DOE) is a method that can be used to identify the critical areas that cause yield loss in a process. With proper application of DOE, design engineers or researchers are able to pinpoint the source of the yield problem and fix them to produce solid and robust designs with much higher yield [10]. In DOE, the three terms that need to be clearly defined are Factors, Levels and Replication. Factors or parameters are important variables that would affect the outcomes or output responses. However, all factors may not have equal importance as some factors may have a more prominent effect over other factors- "Levels" in the simplest terms are possible values for each factor identified thru gathered data (for this case the levels are "low" and "high"). For example, if two levels are assigned to each factor, one of the lower levels is a lower level and the other is a higher level. The values of these levels are assigned in reference to literature, consultation with experts or one can identify level values thru experimentation before the Taguchi method is carried out [1] [11]. A two-level factor assumes linear behavior while three-level factor best fits non-linear behavior but requires a larger number of trials while running experiments. Replication is necessary to address the concern on repeatability and also the spread of the variation in the experimental outcome. This is done in order to obtain adequately accurate statistical information of the process under study. This is done by producing several samples for each trial or by repeating the same trial several times.

The Taguchi method is famous for implementing robust (parameter and tolerance) design. Robust design is a result of determining the optimal factor combination/setting to reduce the response variation and brings the mean close to the target value consequently [12]. To implement the robust design, Taguchi employs an orthogonal array (OA) in order to reduce the number of experiments as compared to the full factorial DOE version. SNRs are used to evaluate the outcome of the experimental trials. The details of the SNR calculations are covered in section 3.1. It is common to include an ANOVA alongside SNR to study the percentage contribution made by each factor. Even though the Taguchi method has been successfully applied to processes in design and manufacturing, it has been criticized for its lack of efficiency because the method works well for single-objective optimization problems but not for multi-objective problems [1] [13]. Some modification on the existing method has to be made [6] [14] - [16] to make it work for some cases of multi objective problems. Similarly, the Taguchi method for multi-objective problems, as discussed by Phadke (1969) [15], is purely based on judgmental and subjective process knowledge [17].

When dealing with a multi-objective problem, one can use several techniques. The simplest way is by adopting the OEC (overall evaluation criteria) approach. This is done by assigning certain weighting to each of the output response criteria so as to normalize the two (or more) different response units. The weightings are arbitrarily chosen based on experience in order to make a response either dominate or have the same weight when compared to the other responses [10] [18] - [20]. Such judgments are not very accurate [17]. A way of overcoming this problem is by using the GA approach. In Section 2.2, the GA method will be further discussed specifically on how it was used with the Taguchi method to make solving the multi-objective problem possible. The GA will search for the optimal weights that maximize the SNR for each output response to improve its immunity to noise and thus make the product more robust. The hypothesis here is that the GA approach will result in a better SNR as compared to the OEC (initial method as stated table 9) method because the GA searches the entire solution space for the optimal point whereas the weights determined by experience does not. To proof this hypothesis, the percentage improvement of the SNR (if any) will be determined and then the process parameters will be implemented to confirm the increase in robustness of the product.



ISSN: 2319-5967

ISO 9001:2008 Certified

International Journal of Engineering Science and Innovative Technology (IJESIT)
Volume 1, Issue 2, November 2012

B. Genetic Algorithm (GA)

The main aim of integrating the GA into the Taguchi technique is to search for definite and optimal weights for each response (or performance characteristic and quality) in a multi-response system. As previously stated [1] [3] [4] [8] [9], the Taguchi method has been mostly utilized in optimizing single-response problems. One of the noted methods in tackling multi response systems is the problem of optimizing weights for signal to noise ratio as mentioned in the literature [1] [4]. In real multi-response cases as described in [1] [21], the weights are based on experience. For instance, in the OEC approach the relative weighting method is used to tackle problems with more than one objective [8]. The method of combining multi criteria of evaluation is truly based on the expertise and the experience gained in many experiments. However, in most real cases this does not result in a robust process or product. This might be due to a level of uncertainties in the decision-making stage especially when picking levels for the parameters. Furthermore, it is difficult for human experts to estimate the affect of the criteria used to evaluate a process as not all criteria have equal importance. As such, the key of obtaining a robust and practical process using this weighting method may be to eliminate the engineering judgment in deciding the weights (or the importance) of the criteria.

The GA is a powerful heuristic global search and optimization technique. It is an optimization technique which is built based on mimicking the evolutionary principles and chromosomal processing in natural selection and natural genetics [22] – [24]. It is a widely accepted approach to stochastic optimization, especially in dealing with a global optimization problems that consists of multi-modal search spaces. In a wider usage of the term, GA is any population-based model that uses selection and recombination operators to generate new sample points in a specific search space [25]. In his book [22], Goldberg demonstrated the possible domains where GA's can be applied. Moreover, many GA models have been introduced by researchers and are found to be effective from the experiment perspective [24] [25]. In addition, many of them are application oriented and have adopted GA's as optimization tools [6] [24] [25] [29]. The searching and selection of optimal weights for the process of fabrication of super-capacitors using the Taguchi method often involves problems related to constrained optimization which is similar to what is needed in manufacturing process optimization. Hence, it is appropriate that GA's are integrated with the Taguchi method to optimize the fabrication of coin-type super-capacitors. The capacitance and equivalent series resistance (ESR) of the device are adopted as the quantitative performance characteristic (quality) for evaluation in the current study.

GA's basically evolved from an idea of survival of the fittest and reproduction of new offspring to form a new population to create a novel and innovative search strategy [6] [25]. It implies that the genetic pool in GA of a given population potentially contains the solution, or a better solution, to a given adaptive problem [25] [26]. This makes the GA different as compared to other traditional point-to-point descending and ascending search techniques [28]. The GA initiates from a random set of solutions, known as the initial 'population'. Each individual solution in the population is known as a 'chromosome' (or string). At each generation, the GA works with genetic operators namely crossover and mutation, on the selected individuals which act as parents to recombine part of the strings (genes) and produce offspring (child) to create a new and hopefully fitter generation [22] [24] [26] [27]. During each generation, these chromosomes evolve to have better fitness. This is done by executing an operation known as selection. Eventually, the chromosomes in the population will converge from generation to generation. The aim is to select the best fit chromosome [6] [22] [26] [27]. By fulfilling the aim mentioned, GA utilizes the fitness function (or objective function) which will be used to create a new and conceivably better population of strings. The fitness function takes a chromosome and assigns a relative fitness value to the chromosome [22]. The fitness function evidently ranks the chromosome in some way by producing fitness values [26] [27]. The procedure for the application of Taguchi and GA to solve multi response problems is presented in section 3.

III. THE PROPOSED INTEGRATED STRATEGY – A CASE STUDY ON THE PROCESS FABRICATION OF COIN-TYPE SUPERCAPACITOR

In this particular case study, coin-type super capacitor is subjected for Taguchi-GA process optimization. The integrated approach is divided into several repeatable steps that could also be applied in other process/product multi-objective optimization problem accordingly. There are four steps outlined (Step 1-4) for the initial experimental factors and levels design, including the computation of SNRs from the experimental data. Next, the integration of GA approach for determining the optimal weights based on the normalized SNRs (Z) in the range between zero and one are conducted (Step 5-6). The WSNR is then computed by multiplying the weight with Z relates to each response. The final two steps (Step 7-8) will be the data analysis focusing on the main effect of each factor towards the WSNR values, which is essential for predicting the desired optimal setting. It continues with the



ISSN: 2319-5967

ISO 9001:2008 Certified

International Journal of Engineering Science and Innovative Technology (IJESIT)

Volume 1, Issue 2, November 2012

confirmation experiments. Consequently, further statistical data analysis includes the measure of variability between OEC and the proposed strategy is conducted using standard deviation and ANOVA, in order to determine the percentage improvement acquired (if any) and subsequently identify the dominant factors that influencing the capacitive performance of the device.

A. DOE (Steps of the method applied, the equation of SNR, Z)

The steps fall within the initial experimental design stage, are listed as follows:

Step 1: Assigning factors and levels for each of the main processes.

Table 1 provides the lists of control factors for process optimization of the mixing, calendaring, drying and electrolyte treatment process. All of the three factors (A, B and C) are assigned with two levels each for the experiment.

Table 1. Process Factors And Their Levels For The Super capacitors Fabricated

| Process | Factors | Level 1 | Level 2 | Output Response |
|-------------------------------|----------------------------|---------|---------------------------------|------------------------------------|
| 1 Mixing | A Mixing Speed (rpm) | 200 | 350 | 1. Capacitance (F). 2. ESR (Ω). |
| | B Mixing Time (min) | 15 | 30 | |
| | C Amount of AC (%) | 85 | 90 | |
| 2 Calendaring | A Calendaring time (min) | 15 | 30 | |
| | B Thickness (mm) | 0.65 | 0.85 | |
| | C Machine temp. (°C) | 23 | 30 | |
| 3 Drying | A Heating time (min) | 20 | 45 | |
| | B Heating temp. (°C) | 50 | 80 | |
| | C Vacuum | Yes | No | |
| 4 Electrolyte Treatment | A Electrolyte name | KCl | Na ₂ SO ₄ | |
| | B Electrolyte molarity (M) | 2 | 3 | |
| | C Electrolyte amount (ml) | 0.5 | 0.8 | |

Step 2: Determining the minimum number of experiments required and the selection of Taguchi orthogonal array. Here, the Taguchi multi-objective optimization begins with the selection of orthogonal array with specific number of levels (L) for A, B and C. The minimum number of experiments in the array is obtained by:

$$N = (L-1)F + 1 \quad (1)$$

where F= number of factors=3

Thus, L₄ orthogonal array is selected due to four numbers of trials required and outlined as in Table 2.

Table 2. 4 X L₄ Orthogonal Arrays for the Process Factors

| Process | Experiment, i | A | B | C |
|------------------|------------------|---|---|---|
| 1 Mixing | 1 | 1 | 1 | 1 |
| | 2 | 1 | 2 | 2 |
| | 3 | 2 | 1 | 2 |
| | 4 | 2 | 2 | 1 |
| 2 Calendaring | 1 | 1 | 1 | 1 |
| | 2 | 1 | 2 | 2 |
| | 3 | 2 | 1 | 2 |
| | 4 | 2 | 2 | 1 |
| 3 Drying | 1 | 1 | 1 | 1 |
| | 2 | 1 | 2 | 2 |
| | 3 | 2 | 1 | 2 |
| | 4 | 2 | 2 | 1 |



ISSN: 2319-5967

ISO 9001:2008 Certified

International Journal of Engineering Science and Innovative Technology (IJESIT)

Volume 1, Issue 2, November 2012

| | | | | |
|-------------|---|---|---|---|
| 4 | 1 | 1 | 1 | 1 |
| Electrolyte | 2 | 1 | 2 | 2 |
| Treatment | 3 | 2 | 1 | 2 |
| | 4 | 2 | 2 | 1 |

Step 3: Conducting all experiments outlined with three replications (samples) each.

Step 4: Computing SNR for every output responses.

The SNR values for the respective responses (SN_{IC} and SN_{IE}) are calculated from the raw data accordingly.

SNR for the capacitance response (larger-the-better);

$$SN_{IC} = -10 \log_{10} (1/n) \sum_{i=1}^n \frac{1}{y_i^2} \quad (2)$$

SNR for the ESR response (smaller-the-better);

$$SN_{IE} = -10 \log_{10} (1/n) \sum_{i=1}^n y_i^2 \quad (3)$$

where y_i is the experimental data at the i th sample and n is the number of samples.

B. The Integrated Taguchi method with GA

Step 5: Normalizing the SNRs so that all are in the range between 0-1.

Normalized y_{ij} as Z_{ij} [0, 1] by the corresponding formula to set the right effect of adopting different units:

Normalized SNR for the capacitance response (larger-the-better);

$$Z_{iC} = (Y_{avg.} - Y_{min.}) / (Y_{max.} - Y_{min.}) \quad (4)$$

Normalized SNR for the ESR response (smaller-the-better);

$$Z_{iE} = (Y_{max.} - Y_{avg.}) / (Y_{max.} - Y_{min.}) \quad (5)$$

where Y_{avg} is the average out of the n number of samples produced, Y_{min} and Y_{max} are the least and highest data value out of the n number of samples produced respectively.

Step 6: Searching for the exact/optimal weighting value w associated with each Z that would give the maximum WSNR by using GA approach.

The WSNR value is determined by using the weights (w_C and w_E) obtained from GA.

$$WSNR_i = w_C Z_{iC} + w_E Z_{iE} \quad (6)$$

In the GA approach of solving an optimization problem, the operation is summarized as follow:

Initialization

The algorithm is carried out randomly to create the solution space which is used for searching the optimal weights so as to maximize Z . In this coin super capacitor fabrication process, we have two output responses; hence there are only two weights which are considered as the gene. The initial population composes of 30 chromosomes. The 30 chromosomes in the initial population are generated subject to the feasibility condition, i.e. the sum of weights should always equal to one.

The Fitness Function

The total WSNR is used as the fitness function in GA strategy to calculate the fitness value. A fitness value in an objective function evaluates the performance level of an individual chromosome; therefore in this case, GA strategy utilizes Z from Taguchi method to form this fitness function. The particular fittest chromosome will be ranked against all other individual chromosomes. The fitness function is given as:

$$f(x) = \sum_{j=1}^k \sum_{i=1}^n (W_j Z_{ij}) \quad (7)$$

The above equation is written such that $f(x)$ is the total WSNR to be maximised, w_{ij} is the weight to each response, Z_{ij} is normalized SNR values, n is numbers of observation (experiments/runs) and k is the number of response.

Selection

Selection is also known as reproduction in the family of computational model inspired by evolution [24] [26] [27]. It allows individual string (chromosome) to be copied for possible inclusion in the next generation. The chance that a string will be copied is based on the string's fitness value which is calculated from the fitness function. For each generation, Selection chooses strings that are placed into the mating pool, which is used as the fundamental to create the next generation. Parent chromosomes are selected with a probability related to their fitness value. Therefore, highly fit strings possess the higher probability of being selected for mating [25]. In this supercapacitor fabrication process, the roulette wheel method is applied to the chromosome selection.

Crossover



ISSN: 2319-5967

ISO 9001:2008 Certified

International Journal of Engineering Science and Innovative Technology (IJESIT)

Volume 1, Issue 2, November 2012

Once the mating pool is created using Selection operator, the next operator is the crossover. The term 'Crossover' used in GA is analogous to reproduction and biological crossover. 'Crossover' is used to create a pair of offspring chromosome from the parent chromosome [25]. Crossover takes place by depending on the parameter known as the crossover probability, P_c [1]. If the crossover does not take place, two selected chromosomes are simply copied to the new population. The concept of this operator is the new chromosome may be better than both of the parent chromosomes as the offspring takes the goodness from each of the parents.

Mutation

One-gene mutation operation with a preset mutation probability P_m which indicates the frequency at which mutation occurs is applied to generate a new chromosome [1]. P_m should be preset at a very low value. In this case, mutation is performed during the crossover. Mutation occurs when a new gene's value is added to the new population pool. This is to avoid the population stagnating at any local optima [25].

Check for feasibility

This is an extra step to obtain reliable weights of the fitness function. In this case, this step is crucial to ensure that the sum of the weights is always equal to one. This step is to encounters 3 possible cases mentioned below.

Case 1 - the sum of the gene values of offspring is less than one.

For example,

If the sum of the gene values of offspring is 0.9; there is a shortage quantity of 0.1 (since $1 - 0.9 = 0.1$). The shortage quantity will be equally divided, and added equally to the gene values.

Case 2 - The sum of the gene values of offspring is more than one.

For example,

If the sum of the gene values of offspring is 1.2, there is an excess quantity of 0.2 (since $1.2 - 1.0 = 0.2$). The excess quantity will be equally divided, and added equally to the gene values.

Case 3 - The sum of the gene values of offspring equal to one, the gene values will remain the same.

Stopping Condition

The most usual and popular method – setting the maximum number of generation is used for the stopping condition. This can guarantee the convergence of a GA. In this case, the stopping condition is the total number of generations fixed at 10,000 [1] [22].

Step 7: Study the main effects on WSNR for each factor and level by plotting the Factor Effects on WSNR graphs. This will lead to our predicted optimal conditions.

WSNR is similar to the overall evaluation of experiment (OEC) data for a multi-response process but the weightings used are the main difference. The Table 6 depicts the main effect on the WSNR. The level with the highest WSNR is the optimal level of process factors. The computation of the main effect on WSNR is carried out by considering the average effect of each level with respect to each factor.

$$A_1 = (WSNR_{1+} + WSNR_{2-}) / 2 \tag{8}$$

$$A_2 = (WSNR_{3+} + WSNR_{4-}) / 2 \tag{9}$$

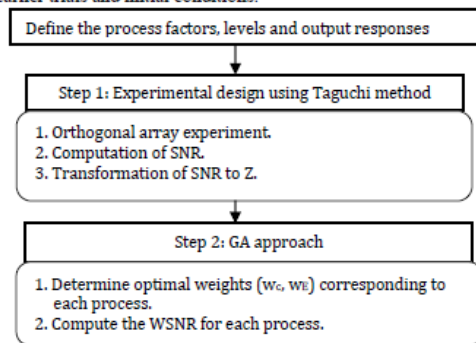
$$B_1 = (WSNR_{1+} + WSNR_{3-}) / 2 \tag{10}$$

$$B_2 = (WSNR_{2+} + WSNR_{4-}) / 2 \tag{11}$$

$$C_1 = (WSNR_{1+} + WSNR_{4-}) / 2 \tag{12}$$

$$C_2 = (WSNR_{2+} + WSNR_{3-}) / 2 \tag{13}$$

Step 8: Running the confirmation experiment and compare the results (Standard Deviation and SNR) with the earlier trials and initial conditions.





ISSN: 2319-5967

ISO 9001:2008 Certified

International Journal of Engineering Science and Innovative Technology (IJESIT)

Volume 1, Issue 2, November 2012

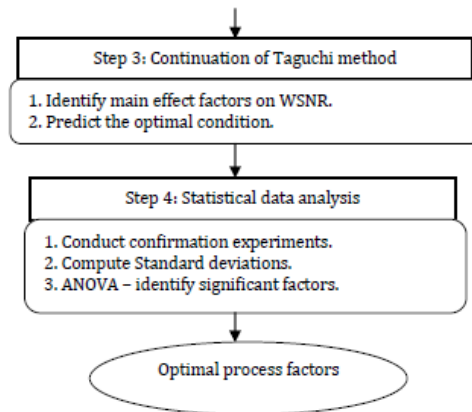


Fig. 1. The Proposed Integrated Approach

IV. RESULT AND DISCUSSION

According to L4 orthogonal array, all the trials were conducted and the results are shown in the Table 3. Three samples were produced for each run and their capacitance and ESR performance were tested using an Autolab Potentiostat (PGSTAT302N) under cyclic voltammetry and galvanostatic charge-discharge tests respectively. Table 4 summarizes the transformation values of raw data from the Table 3 into SNR and Z, before finally using the optimal weight of w_c and w_E found from GA method to determine the WSNR.

Table 3 .Experimental Output Data

| Process | Experiment, i | Response 1- Capacitance (F) | | | Response 2 - ESR (Ω) | | |
|-------------------------------|---------------|-----------------------------|-------|-------|-------------------------------|-------|-------|
| | | 1 | 2 | 3 | 1 | 2 | 3 |
| 1 Mixing | 1 | 0.989 | 1.074 | 1.105 | 12.15 | 19.05 | 18.45 |
| | 2 | 1.942 | 2.070 | 2.074 | 12.80 | 4.70 | 14.15 |
| | 3 | 2.231 | 2.441 | 2.399 | 3.20 | 6.60 | 2.00 |
| | 4 | 1.624 | 1.675 | 1.820 | 9.05 | 17.45 | 11.20 |
| 2 Calendering | 1 | 2.035 | 2.039 | 2.132 | 2.30 | 3.50 | 3.15 |
| | 2 | 2.583 | 2.440 | 2.654 | 2.35 | 2.05 | 3.20 |
| | 3 | 1.967 | 1.901 | 1.979 | 2.85 | 2.06 | 2.35 |
| | 4 | 2.140 | 2.173 | 2.406 | 2.25 | 3.00 | 2.95 |
| 3 Drying | 1 | 2.295 | 2.462 | 2.409 | 2.85 | 2.50 | 2.55 |
| | 2 | 2.558 | 2.317 | 2.680 | 2.30 | 2.90 | 2.75 |
| | 3 | 2.681 | 2.338 | 2.578 | 2.70 | 2.95 | 2.30 |
| | 4 | 2.448 | 2.581 | 2.459 | 2.45 | 2.50 | 2.70 |
| 4 Electrolyte Treatment | 1 | 1.757 | 1.901 | 1.653 | 3.35 | 2.85 | 3.00 |
| | 2 | 2.457 | 2.590 | 2.468 | 2.56 | 2.61 | 2.81 |
| | 3 | 1.622 | 1.598 | 1.605 | 5.10 | 6.45 | 4.25 |
| | 4 | 2.293 | 2.556 | 2.558 | 2.40 | 2.50 | 2.30 |

Table 4 .Weighted SNR (WSNR) Values



ISSN: 2319-5967

ISO 9001:2008 Certified

International Journal of Engineering Science and Innovative Technology (IJESIT)

Volume 1, Issue 2, November 2012

| Process | Experiment, i | $(SNR)_C$ | $(SNR)_E$ | Z_C | Z_E | $WSNR_i$ |
|-------------------------------|-----------------|-----------|-----------|--------|--------|----------|
| 1 Mixing | 1 | 10.03 | -24.53 | 0.578 | 0.362 | 0.5778 |
| | 2 | 15.69 | -21.22 | 0.656 | 0.393 | 0.6557 |
| | 3 | 16.99 | -12.85 | 0.600 | 0.580 | 0.5998 |
| | 4 | 14.19 | -22.32 | 0.420 | 0.581 | 0.4202 |
| 2 Calendering | 1 | 15.85 | -9.62 | 0.3471 | 0.4306 | 0.3484 |
| | 2 | 17.71 | -8.23 | 0.5561 | 0.3333 | 0.5526 |
| | 3 | 15.34 | -7.75 | 0.6154 | 0.5443 | 0.6143 |
| | 4 | 16.56 | -8.80 | 0.3747 | 0.3556 | 0.3744 |
| 3 Drying | 1 | 17.11 | -8.43 | 0.5609 | 0.6190 | 0.5612 |
| | 2 | 17.58 | -8.50 | 0.5546 | 0.4167 | 0.5539 |
| | 3 | 17.63 | -8.51 | 0.5666 | 0.4615 | 0.5661 |
| | 4 | 17.45 | -8.14 | 0.3609 | 0.6000 | 0.3621 |
| 4 Electrolyte Treatment | 1 | 14.52 | -9.75 | 0.4731 | 0.5667 | 0.5649 |
| | 2 | 17.52 | -8.50 | 0.3609 | 0.6000 | 0.5953 |
| | 3 | 13.67 | -14.55 | 0.4306 | 0.5379 | 0.5358 |
| | 4 | 16.34 | -7.61 | 0.6642 | 0.5000 | 0.5032 |

From GA, optimal weights for each response are obtained in order to maximize the values of SN ratio. For example, in Process 1 w_C and w_E were found to be 0.9990 and 0.0001 respectively. The following result was obtained as optimal weight corresponding to each response. The optimal weights are [0.9990, 0.0001]. Thus, the particular solution for WSNR from eq. 6 is given by;

$$WSNR_i = 0.999Z_{iC} + 0.0001Z_{iE} \quad (6)$$

The corresponding values of w_C and w_E for the rest of the other processes are shown in Table 5.

Table 5. Results Obtained From GA Approach

| Process | w_C | w_E |
|---------|--------|--------|
| 1 | 0.9990 | 0.0001 |
| 2 | 0.9844 | 0.0156 |
| 3 | 0.9951 | 0.0049 |
| 4 | 0.0196 | 0.9804 |

After all of the WSNR values for each trial and each fabrication process were computed (by substituting the w_C and w_E values into the WSNR formula) it was noticed that in Process 1 (mixing), Run 2 has the highest WSNR value. If we refer back to Table 2, it corresponds to A1, B2, C2 as the desired setting. However, this approach is less accurate as the interactions between factors and levels have not yet been taken into account. The same can be implied for the rest of the Processes (2, 3 and 4). A better approach is to evaluate the factor main effects on WSNR. The simple calculations of Equation (8-13) were performed to obtain the average WSNR that indicates the effect on the low and the high level for each factor. The higher the difference between the minimum (low level) and maximum (high level) is, the greater the effect it will have. Table 6 provides the details of the main effects on WSNR.

Figure 2 consists of four sets of the main effect plot for the respective process fabrication. This is a better way to illustrate the information obtained from Table 6. It provides the predicted optimal conditions for the process optimization. For Process 1, the optimal condition predicted is A_1, B_1, C_2 as for having higher WSNR values. Process 2 on the other hand is A_2, B_1, C_2 while Process 3 is A_1, B_1, C_2 and Process 4 is also A_1, B_1, C_2 . An observation that can be seen is that Factor C (machine temperature) in Process 2 (calendering) has the biggest margin with 0.2221 differences of its two levels. This tells us that such factor is quite sensitive if we change the level values thus it is a significant factor in producing a good quality of process or product. On the other hand, the



ISSN: 2319-5967

ISO 9001:2008 Certified

International Journal of Engineering Science and Innovative Technology (IJESIT)

Volume 1, Issue 2, November 2012

very small margin of 0.0011 obtained in Process 4 (electrolyte treatment) and Factor B (molarity) indicates that such factor does not have much effect on the outcome if we change the level values. In a later section, a more appropriate way for determining significant and insignificant factors using ANOVA will be discussed.

Table 6 .Main Effects On WSNR for Every Factor Investigated of the Respective Process

| Process | Factors | Low Level, L1 | High Level, L2 | WSNR _{max} - WSNR _{min} |
|----------------------------|------------------------|---------------|----------------|---|
| 1 Mixing | A Mixing Speed | 0.6167 | 0.5101 | 0.1066 |
| | B Mixing Time | 0.5889 | 0.5379 | 0.0509 |
| | C Amount of AC | 0.4990 | 0.6278 | 0.1288 |
| 2 Calendering | A Calendering time | 0.4505 | 0.4943 | 0.0438 |
| | B Thickness | 0.4813 | 0.4635 | 0.0178 |
| | C Machine temp. | 0.3614 | 0.5835 | 0.2221 |
| 3 Drying | A Heating time | 0.5575 | 0.4641 | 0.0934 |
| | B Heating temp. | 0.5636 | 0.4580 | 0.1057 |
| | C Vacuum | 0.4617 | 0.5600 | 0.0984 |
| 4 Electrolyte Treatment | A Electrolyte name | 0.5801 | 0.5195 | 0.0606 |
| | B Electrolyte molarity | 0.5504 | 0.5493 | 0.0011 |
| | C Electrolyte amount | 0.5340 | 0.5656 | 0.0315 |

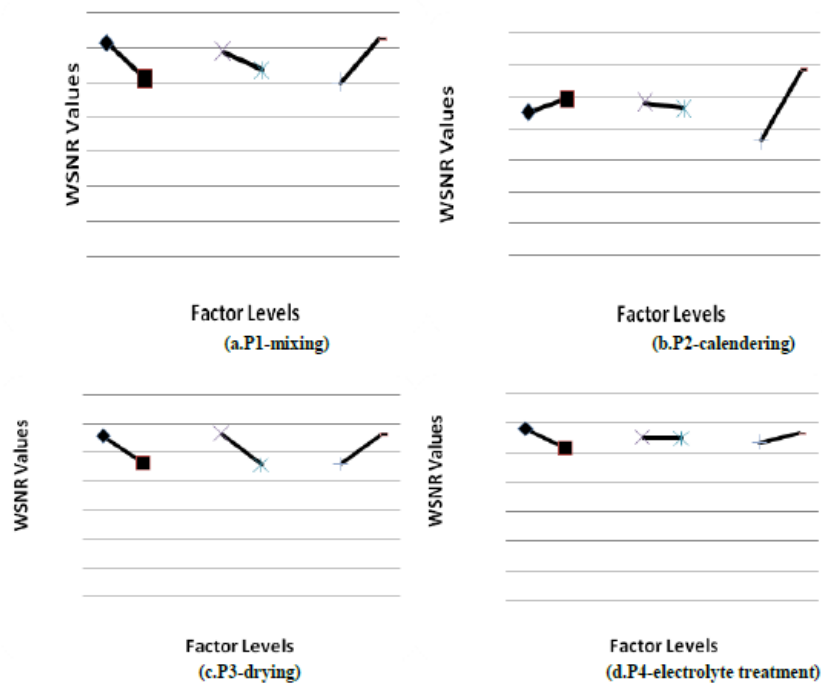


Fig. 2 .Factor Effects On WSNR.



ISSN: 2319-5967

ISO 9001:2008 Certified

International Journal of Engineering Science and Innovative Technology (IJESIT)

Volume 1, Issue 2, November 2012

V. CONFIRMATION EXPERIMENT

In confirmation of the predicted optimal settings obtained from the proposed Taguchi-GA approach, verification tests were conducted and another three samples were each produced and the results obtained are tabulated in Table 7. To evaluate the findings, a comparison of the standard deviation (SD) for all of the trials is conducted. The smaller value of SD implies the consistency of the samples and thus indicates that they are close to the target value. Consistency is related to process repeatability and robustness of product.

Table 7 .Experimental Output Data for Confirmation Experiments

| Process | Sample 1 | Sample 2 | Sample 3 |
|--|---------------------|---------------------|---------------------|
| 1 (A ₁ , B ₁ , C ₂) | 2.425 F; 1.602 Ω | 2.388 F; 3.691 Ω | 2.403 F; 2.925 Ω |
| 2 (A ₂ , B ₁ , C ₂) | 2.051 F; 1.811 Ω | 2.026 F; 2.008 Ω | 2.095 F; 1.760 Ω |
| 3 (A ₁ , B ₁ , C ₂) | 2.294 F; 2.571 Ω | 2.310 F; 2.529 Ω | 2.244 F; 2.708 Ω |
| 4 (A ₁ , B ₁ , C ₂) | 2.199 F; 1.98 Ω | 2.222 F; 1.85 Ω | 2.213 F; 2.00 Ω |

The standard deviations (SD) were obtained using the following formula;

$$SD = \sqrt{\frac{N \sum (X^2) - (\sum X)^2}{N(N-1)}} \quad (14)$$

where N is the number of replication and X is the experimental data.

Table 8 .SD for Each Experiment and under Optimal Conditions

| Process | Experiment, i | SD (cap) | SD (ESR) |
|---------|---|----------|----------|
| 1 | 1 | 0.0601 | 3.8223 |
| | 2 | 0.0751 | 5.1110 |
| | 3 | 0.1766 | 2.3861 |
| | 4 | 0.1111 | 4.3636 |
| | 5 (A ₁ , B ₁ , C ₂) | 0.0186 | 1.0568 |
| 2 | 1 | 0.0549 | 0.6171 |
| | 2 | 0.1090 | 0.5965 |
| | 3 | 0.0420 | 0.3996 |
| | 4 | 0.1445 | 0.4193 |
| | 5 (A ₂ , B ₁ , C ₂) | 0.0349 | 0.1310 |
| 3 | 1 | 0.0853 | 0.1893 |
| | 2 | 0.1847 | 0.3122 |
| | 3 | 0.1760 | 0.3279 |
| | 4 | 0.0738 | 0.1323 |
| | 5 (A ₁ , B ₁ , C ₂) | 0.0650 | 0.0936 |
| 4 | 1 | 0.1245 | 0.2566 |
| | 2 | 0.0738 | 0.1323 |
| | 3 | 0.0123 | 0.1094 |
| | 4 | 0.1524 | 0.1000 |
| | 5 (A ₁ , B ₁ , C ₂) | 0.0116 | 0.0814 |



ISSN: 2319-5967

ISO 9001:2008 Certified

International Journal of Engineering Science and Innovative Technology (IJESIT)

Volume 1, Issue 2, November 2012

Table 8 shows that the predicted condition in every process yields a certain extent of improvement (reduction) of capacitance and ESR standard deviation of values. Such findings proved that the GA results have successfully optimized the weightings and has thus maximized the values of SN ratio for both responses. The overall improvement percentage is determined as the ratio between sums of the improvement in values of all responses and the sum of the SNRs of initial responses for all responses [1]. The computations are presented in Table 9.

Table 9. Initial, Predicted and Actual Improvement Of SN Ratios

| Process | Responses | Initial condition (dB) | Predicted condition (GA) (dB) | Confirmation (dB) | Improvement (dB) |
|---------|-------------------------------|--|---|--|------------------|
| 1 | Capacitance | 16.99 | 15.69 | 17.166 | 0.176 |
| | ESR | -12.85 | -21.22 | -9.164 | 3.686 |
| | Optimal setting | A ₂ , B ₁ , C ₂ * | A ₁ , B ₂ , C ₂ ** A ₁ , B ₁ , C ₂ *** | A ₁ , B ₁ , C ₂ | |
| | Overall improvement in dB (%) | | | | 12.9 % |
| 2 | Capacitance | 15.34 | 15.34 | 15.340 | 0.000 |
| | ESR | -7.75 | -7.75 | -5.798 | 1.952 |
| | Optimal setting | A ₂ , B ₁ , C ₂ * | A ₂ , B ₁ , C ₂ ** | A ₂ , B ₁ , C ₂ | |
| | Overall improvement in dB (%) | | | | 8.4 % |
| 3 | Capacitance | 17.11 | 17.63 | 17.18 | 0.07 |
| | ESR | -8.43 | -8.51 | -8.31 | 0.12 |
| | Optimal setting | A ₁ , B ₁ , C ₁ * | A ₂ , B ₁ , C ₁ ** A ₁ , B ₁ , C ₂ *** | A ₁ , B ₁ , C ₂ | |
| | Overall improvement in dB (%) | | | | 0.7 % |
| 4 | Capacitance | 16.34 | 17.52 | 16.44 | 0.10 |
| | ESR | -7.61 | -8.50 | -5.78 | 1.83 |
| | Optimal setting | A ₂ , B ₂ , C ₁ * | A ₂ , B ₁ , C ₂ ** A ₁ , B ₁ , C ₂ *** | A ₁ , B ₁ , C ₂ | |
| | Overall improvement in dB (%) | | | | 8.1 % |

* Combination obtained from OEC computation (0.7:0.3).

** The highest WSNR given from Table 4.

*** Predicted condition from GA which is not in the L₄ Orthogonal array.

The SNRs for the initial condition are obtained by assigning 0.7 weighting for the capacitance response and 0.3 for the ESR response arbitrarily, based on the consensus that the capacitance performance should dominate the ESR response before conducting the GA approach. The GA method then searches for the optimal weightings that maximize the SNR for both responses to improve the performance of process factors. Different Capacitance to ESR ratio combinations (total=1) have also been tested - 0.6:0.4, 0.2:0.8 etc. It was found that after the capacitance ratio being altered gradually for example 0.2, 0.3, 0.4 etc, the outcome results in the same experimental run (e.g. Run 2) as the best run for the respective process. However, until at a certain ratio (e.g. 0.8:0.2) the results turn up to give a different experimental run (e.g. Run 3) as the best run. This shows that the weighting has certain impact on the optimal setting to be predicted. If that is so, there is a chance to fully optimise the SNR. This is can be done without using engineering judgment. For this case study, only one weighting ratio, 0.7:0.3, was used for the OEC computation. This is treated as the initial condition in which to compare WSNR results.



ISSN: 2319-5967

ISO 9001:2008 Certified

International Journal of Engineering Science and Innovative Technology (IJESIT)

Volume 1, Issue 2, November 2012

Table 10 .OEC Values to Determine the Optimal Setting for the Initial Condition

| Process | Experiment, i | Combination | OEC (0.7:0.3 weighting) |
|---------|------------------|--|-------------------------|
| 1 | 1 | A ₁ , B ₁ , C ₁ | 0.5125 |
| | 2 | A ₁ , B ₂ , C ₂ | 0.5756 |
| | 3 | A ₂ , B ₂ , C ₂ | 0.5940 |
| | 4 | A ₂ , B ₂ , C ₁ | 0.4669 |
| 2 | 1 | A ₁ , B ₁ , C ₁ | 0.3754 |
| | 2 | A ₁ , B ₂ , C ₂ | 0.5641 |
| | 3 | A ₂ , B ₂ , C ₂ | 0.5941 |
| | 4 | A ₂ , B ₂ , C ₁ | 0.3112 |
| 3 | 1 | A ₂ , B ₂ , C ₁ | 5.8250 |
| | 2 | A ₁ , B ₂ , C ₂ | 5.1260 |
| | 3 | A ₂ , B ₁ , C ₁ | 5.3430 |
| | 4 | A ₂ , B ₂ , C ₁ | 4.3260 |
| 4 | 1 | A ₁ , B ₁ , C ₁ | 0.5012 |
| | 2 | A ₁ , B ₂ , C ₂ | 0.2526 |
| | 3 | A ₂ , B ₁ , C ₂ | 0.4628 |
| | 4 | A ₂ , B ₂ , C ₁ | 0.6149 |

Table 10 presents how the combination of the initial condition is made by selecting the highest OEC values in every fabrication process. The SNRs of those experimental runs that based on the processing parameters as in Table 4 are compared with the SNRs of the confirmation experiments which use WSNR values. As in Table 9, it is observed that 12.9%, 8.4% and 8.1% improvement in dB was obtained for the mixing, calendaring and electrolyte treatment process respectively by using the proposed Taguchi-GA approach. These are quite impressive results. However, the drying process does not produce much improvement (0.7%). One possible reason for this small improvement is that the optimization has reached its certain limit for given factors and levels assigned. Unless different factors are added in to be investigated, this could be further improved.

The purpose of ANOVA in this study is to determine which of the process factors are significantly affect the performance characteristics [1] in the coin super capacitor fabrication. To achieve this, the total variability of the multi-objective WSNR measured by the sum of squared deviations is separated from the total mean of WSNR, before converting into percentage contribution for every individual factor. This part was implemented by utilizing the Qualitek-4 software. Some of the factors are pooled to avoid calling something significant when it is not. This is to maximize the percentage contribution of the dominant and significant factors. Table 11 displays the ANOVA results.

Table 11 .Results of ANOVA Analysis on WSNR

| Process | Factor | DOF | Sum of Squares | % Contribution |
|---------|--------|-----|----------------|----------------|
| 1 | A | 1 | 0.011 | 37.181 |
| | B | 1 | 0.002 | 8.360 |
| | C | 1 | 0.016 | 54.130 |
| | Error | 0 | | |
| | Total | 3 | 0.030 | 100 % |
| 2 | A | 1 | 0.001 | 3.16 |
| | B | (1) | (0) | POOLED |
| | C | 1 | 0.049 | 96.00 |
| | Error | 1 | -0.01 | 0.84 |
| | Total | 3 | 0.051 | 100 % |



ISSN: 2319-5967

ISO 9001:2008 Certified

International Journal of Engineering Science and Innovative Technology (IJESIT)

Volume 1, Issue 2, November 2012

| | | | | |
|---|-------|-----|--------|---------|
| 3 | A | 1 | 0.008 | 29.230 |
| | B | 1 | 0.011 | 37.973 |
| | C | 1 | 0.009 | 32.458 |
| | Error | 0 | | |
| | Total | 3 | 0.029 | 100 % |
| 4 | A | 1 | 0.003 | 91.503 |
| | B | (1) | (0) | POOLED |
| | C | 1 | 0.001 | 24.803 |
| | Error | 1 | -0.001 | -16.306 |
| | Total | 3 | 0.004 | 100 % |

Consequently, optimal conditions for every process can be set as A₁, B₁, C₂ for the mixing process, A₂, B₁, C₂ for the calendaring process, A₁, B₁, C₂ for the drying process, and A₁, B₁, C₂ for the electrolyte process. It is found that the most significant process factor for the respective process is in the sequence of machine temperature (96%) in the calendaring process, followed by the KCl electrolyte (91.503%) in the electrolyte treatment process, the amount of activated carbon (54.13%) in the mixing process, and finally the heating temperature (37.97%) in the drying process. Such process factors with a high percentage contribution obtained statistically are believed to have a huge impact towards the performance of the supercapacitor fabricated.

As part of this effort we also wanted to determine the physical effect of an “optimized” process factor on the material itself. Referring to the SEM pictures below, we observe a difference in the homogeneity and structure of the electrode material after adding the binder and the mixing process for different parameters i.e. before and after optimization.

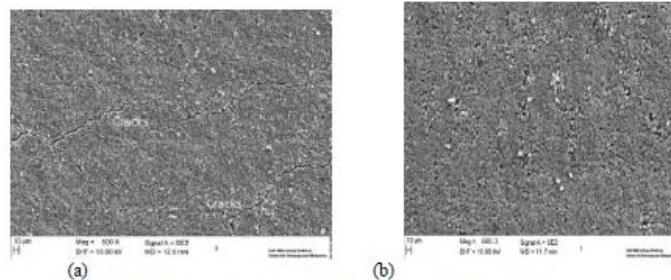


Fig. 3: Optimizing AC % A) Before Optimizing (Cracks), B) After Optimizing (Cracks Free).

Figure 3, shows the effect of optimizing AC and binder percentages on the cracks formed on the surface of the electrode.

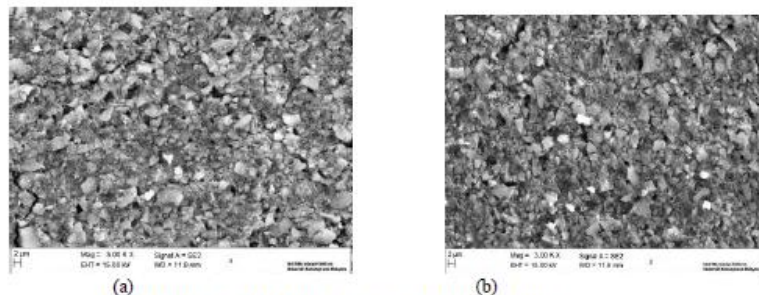


Fig. 4: Optimizing the Mixing Process A) Before B) After



ISSN: 2319-5967

ISO 9001:2008 Certified

International Journal of Engineering Science and Innovative Technology (IJESIT)

Volume 1, Issue 2, November 2012

Optimizing the mixing process can result in more homogenise structure, resulting in smaller gaps between the particles, which can improve the ESR and the capacitance of the supercapacitor.

VI. CONCLUSION

The super capacitor fabrication process dealing with a multi response problem has been presented in this paper. From the experimental and analytical results, the conclusions are as follows:

1. Taguchi method has successfully minimized the cost and time span of the experimental procedure consisting of three factors and two-level each. Only four trials are required when using the orthogonal array experiment.
2. The proposed integrated approach has improved the SNR (dB). Hence, optimal conditions have great influences on the design factors with less sensitivity to the noise factors.
3. The proposed Taguchi-GA integrated strategy provides a robust design in the sense of reproducibility and reliability. This could not be achieved by the OEC approach alone as this approach is dependent on engineering judgment (that has higher variation), a mean value that is far from the desired target value if those judgments were inaccurately made.

ACKNOWLEDGMENT

The authors would like to acknowledge funding support under Sahz Holdings Sdn. Bhd.

REFERENCES

- [1] R. Jeyapaul, P. Shahabudeen, K. Krishnaiah, Simultaneous optimization of multi response problems in the Taguchi method using genetic algorithm, *Int J Adv Manuf Technol* (2006) 30: 870-78.
- [2] Abbas Al-Refaie, Tai-Hsi Wu and Ming-Hsien Li (2009). Data development analysis approaches for solving the multiresponse problem in the Taguchi method. *Artificial Intelligence for Engineering Design, Analysis and Manufacturing (AI EDAM)*, 23, pp 159-173 doi: 10.1017/S0890060409000043.
- [3] Tung-Hsu Hou, Chi-Hung Su, Wang-Lin Liu, Parameters optimization of a nano-particle wet milling process using the Taguchi method, response surface method and genetic algorithm, *Powder Technology* 173 (2007) 153-162.
- [4] Ranjit K. Roy, *Design of Experiments using the Taguchi Approach*, A Wiley Interscience Publication (2001), 10 -26.
- [5] Hung-Chung Liao, Multi-response optimization using weighted principal component, *Int J Adv Manuf Technol* (2006) 27, 720 – 725.
- [6] R. Ramakrishna · L. Karumamoorthy, Multi response optimization of wire EDM operations using robust design of experiments, *Int J Adv Manuf Technol* (2006): 29, 105 -112.
- [7] Phadke, M. S. (1989). *Quality engineering using robust design*, New Jersey: AT&T Bells Laboratory/Prentice-Hall.
- [8] W.H. Yang, Y.S. Tang, Design optimization of cutting parameters for turning operations based on the Taguchi method, *Journal of Materials Processing Technology* 84 (1998) 122-129.
- [9] Antony J , Simultaneous optimization of multi quality characteristics in manufacturing processes using Taguchi's quality loss function, *Int J Manuf Technol* 17 (2001) 134.
- [10] Jack Sifri, Recent advancements in RFIC simulation technology for analyzing large RFICs, Agilent Technologies, USA.
- [11] Tatjana V. Sibalija, Vidosav D. Majstorovic, Novel Approach to Multi-Response Optimization for Correlated Responses, *FME Transactions* (2010) 38, 39-48.
- [12] Jami Kovach, Byung Rae Cho, Constrained robust design experiments and optimization with the consideration of uncontrollable factors, *The Int Journal of Adv Manuf Tech*, Vol 38, Numbers 1-2, 7-18.
- [13] A. Kumar Dubey, V. Yadava, Multi-objective optimization of laser beam cutting process, *Optics & Laser Technology* 40 (2008) 562-570.
- [14] Gabriella Dellino, Jack P.C. Kleijnen, Carlo Meloni, Robust Simulation-Optimization using metamodels, *Proceedings of the 2009 Winter Simulation Conference*.
- [15] V. N. Gaitonde, S. R. Kamik, B. T. Achyutha, Methodology of Taguchi for multi-drilling problem to minimize burr size, *Int. J. Adv. Manuf. Technol.* (2007) 34: 1-8.
- [16] Chang-Yuan Tang, Yi-Leh Wu, Chien-Chin peng, Fundamental matrix estimation by multiobjective genetic algorithm with Taguchi's method, *Applied Soft Computing* 12 (2011) 553-558.



ISSN: 2319-5967

ISO 9001:2008 Certified

International Journal of Engineering Science and Innovative Technology (IJESIT)

Volume 1, Issue 2, November 2012

- [17] I. Mukherjee, P. K. Ray, A review of optimization techniques in metal cutting process, *Computer & Industrial Engineering* 50 (2006) 15-34.
- [18] Morris H. DeGroot, Reaching Consensus, *Journal of The American Statistical Association*, Vol. 69, No. 345 (Mar., 1974), pp. 118-121.
- [19] Nathaniel C. Bantayan, Ian D. Bishop, Linking objective and subjective modelling land use decision-making, *Landscape and Urban Planning* 43 (1988) 35-48.
- [20] Pierre A. Balthazard, William R. Ferrell, Dorothy L. Aguilar, Influence allocation methods in group decision support systems, *Group Decision and Negotiation*, Vol. 7, No. 4, 347-362.
- [21] Tong I-I, Su C-T, The optimization of multi response problems in Taguchi method, *Int J Qual Reliab Manage* (1997) 14:4:367-380.
- [22] David E. Goldberg, *Genetic algorithms in search, optimization and machine learning*, Addison-Wesley Pub. Co.1989.
- [23] J. H. Holland, "Adaptation in Natural and Artificial Systems". University of Michigan Press, Ann Arbor, 1975.
- [24] Randy L. Haupt, S. E. Haupt, "Practical genetic algorithms", 2nd Edition, Wiley-IEEE, 2004.
- [25] Franci Cus*, Jozse Balic, Optimization of cutting process by GA approach, *Robotics and Computer Integrated Manufacturing* 19 (2003) 113-121.
- [26] K. F. Man, K.S. Tang, S. Kwong, genetic Algorithm: Concepts and Applications, *IEEE Transactions on industrial Electronics* Vol. 43, No.5 (1996), 519 – 534.
- [27] Srinivas, M., Patnaik, L.M, *Genetic Algorithms: A Survey*, *Computer*, Vol 27, Issue 6, 17 – 26.
- [28] Tung-Hsu (tony) Hou, Chi-Hung Su, Hung-Zhi Chang, Using neural networks and immune algorithms to find the optimal parameters for an IC wire bonding process, *Expert System with Applications*, Volume 34, Issue 1, January 2008, Pages 427-436.
- [29] David Eby, R.C. Averill, William F. Punch, Erik D. Goodman (1999). Optimal design of flywheels using an injection island genetic algorithm. *AI EDAM*, 13 , pp 327-340.